Function of the purinergic receptor P2X7 in MVA-infected feeder cells during MVA cross-presentation

Inaugural dissertation

for the attainment of the title of doctor in the
Faculty of Mathematics and Natural Sciences
at the Heinrich Heine University Düsseldorf

presented by

Ylenia Longo

from Partinico

Düsseldorf, January 2025

from the Institute of Virology

at the Heinrich Heine University Düsseldorf

Published by permission of the
Faculty of Mathematics and Natural Sciences at
Heinrich Heine University Düsseldorf

Supervisor: Prof. Dr. Ingo Drexler

Co-Supervisor: Prof. Dr. Julia Frunzke

Date of oral examination: 12.05.2025

The results of this thesis contributed to the following publication:

Longo Y, Mascaraque SM, Andreacchio G, Werner J, Katahira I, De Marchi E, Pegoraro A, Lebbink RJ, Köhrer K, Petzsch P, Tao R, Di Virgilio F, Adinolfi E, Drexler I. The purinergic receptor P2X7 as a modulator of viral vector-mediated antigen cross-presentation. Front Immunol 2024;15. https://doi.org/10.3389/FIMMU.2024.1360140.*

*Detailed contributions are listed in the publication above. Briefly, the doctoral researcher, Longo Y, contributed to the majority of the manuscript's raw data and performed most of the experiments. Longo Y has written the initial draft of the manuscript and was involved in all aspects of its further processing until finalization. The co-authors were involved in manuscript writing/review/editing, experimental design, data curation, analysis, methodology, investigation, supervision and funding acquisition.

Table of contents

1. Summary/Zusammenfassung

Modified vaccinia virus Ankara (MVA) is currently being used as a safe vaccine candidate, inducing strong innate and adaptive immune responses. However, not much is known about how these are initiated or regulated. One mechanism, by which strong and long-lived $CD8^+$ T cell responses upon MVA infection are accounted is the cross-presentation of MVA-derived antigens. In general, there is little research on how this process is triggered by feeder cells, hence, cells that are not antigen-presenting cells. We have recently discovered, that the stimulus for the initiation of these adaptive immune responses, derived from the MVA-infected feeder cells. In the process of analyzing members of the innate immune system in Cloudman (CM) feeder cells, we have discovered the possible importance of the receptor P2X7 (P2RX7). This surface receptor was long thought to be part of the initiator complex of the inflammasome pathway. Recent studies have demonstrated that it might be involved in the kickoff of a variety of downstream signaling routes. Therefore, we aimed to analyze the involvement of a P2RX7-dependent pathway in MVA-infected feeder cells and to investigate how these mechanisms potentially affected cross-presentation by dendritic cells. We first generated a CM cell line harboring the functional P2RX7 receptor from BALB/c mice. We confirmed imminent P2RX7 functions in these cells, hence membrane blebbing, calcium influx, and effects on mitochondrial metabolism upon MVA infection. We further analyzed the impact of the active P2X7 receptor variant in MVA-infected CM feeder cells upon co-culture with bone marrow-derived dendritic cells (BMDCs) and $CD8^+$ T cells. The presence of an active P2RX7 in feeder cells led to a significantly improved MVA-mediated antigen cross-presentation by BMDCs, resulting in increased IFNγ and TNFα production by $CD8^+$ T cells, as well as an increased surface expression of the SIINFEKL peptide on the H2-K^b of BMDCs. These effects were shown to be P2RX7-dependent and could be associated to different P2RX7-specific functions. We assume that P2RX7-dependent extracellular vesicle release, containing important regulatory structures as well as antigens in the form of mRNA might be involved in improving the adaptive immune responses. We additionally assume, that secreted inflammatory cytokines as well as a delayed viral gene expression in CM P2RX7 could trap antigens in viral factories, which were shown to be present in MVA-infected CM P2RX7 cells, might be beneficial for improved antigen cross-presentation. We were not able to corroborate these results using a CRISPR/Cas9 mediated *P2rx7* knockout model, possibly accounting for the gene similarity of *P2rx7* with its family member *P2rx4* and possibly observed an off-target effect of the CRISPR endonuclease Cas9. However, we have successfully demonstrated that P2RX7 as an innate trigger in CM feeder cells plays a crucial role in regulating adaptive immune responses. This is a first-time study of the role of P2RX7 during MVA infection and in the context of cross-presentation, unfolding its function for further improvements of the MVA viral

vector. Further studies are required to elucidate the exact mechanisms of how P2RX7 alters antigen-generation processes in CM feeder cells and subsequently in antigen-presenting cells.

Das Modifizierte Vaccinia Virus Ankara (MVA) wird derzeit als sicherer Impfstoffkandidat eingesetzt, der starke angeborene und adaptive Immunreaktionen auslöst. Es ist jedoch nicht viel darüber bekannt, wie diese initiiert oder reguliert werden. Ein Mechanismus, auf den starke und langlebige $CD8^+$ T-Zell-Antworten nach einer MVA-Infektion zurückzuführen sind, ist die Kreuzpräsentation von MVA-Antigenen. Im Allgemeinen gibt es nur wenig Forschung darüber, wie dieser Prozess durch „Feeder Zellen“ ausgelöst wird, also Zellen, die nicht Antigen-präsentierende Zellen sind. Wir haben kürzlich entdeckt, dass der Stimulus für die Auslösung dieser auf Kreuzpräsentation beruhenden adaptiven Immunantworten, anders als bisher angenommen, von den MVA-infizierten „Feeder Zellen“ ausgeht. Bei der Analyse des angeborenen Immunsystems in Cloudman (CM) „Feeder Zellen“ haben wir die mögliche Bedeutung des Rezeptors P2X7 (P2RX7) entdeckt. Dieser Oberflächenrezeptor wurde lange Zeit für einen Teil des Initiatorkomplexes zur Aktivierung des Inflammasoms gehalten. Erst jüngste Studien haben gezeigt, dass er an der Aktivierung einer Vielzahl von nachgeschalteten Signalwegen beteiligt sein könnte. Daher war es unser Ziel, die Beteiligung der P2RX7-abhängigen Signalwege in MVA-infizierten „Feeder Zellen“ zu analysieren und zu untersuchen, wie diese Mechanismen möglicherweise die Kreuzpräsentation durch dendritische Zellen beeinflussen. Zunächst erzeugten wir eine CM-Zelllinie, die den funktionellen P2RX7-Rezeptor von BALB/c Mäusen beherbergt. Wir bestätigten die P2RX7-spezifischen Funktionen dieser Zellen, d. h. Membran-Blebbing, Kalziumeinstrom und Auswirkungen auf den mitochondrialen Stoffwechsel nach MVA-Infektion. Darüber hinaus analysierten wir die Auswirkungen der aktiven P2X7-Rezeptorvariante in CM „Feeder Zellen“ bei der Co-Kultur mit Knochenmark abgeleiteten dendritische Zellen -(BMDCs) und $CD8^+$ T-Zellen. Das Vorhandensein eines aktiven P2RX7 in „Feeder Zellen“ führte zu einer signifikant verbesserten MVA-vermittelten Antigen-Kreuzpräsentation durch BMDCs, was zu einer erhöhten IFNγ- und TNFα-Produktion von $CD8^+$ T-Zellen sowie zu einer erhöhten Oberflächenexpression des SIINFEKL-Peptids auf dem H2-K^b von BMDCs führte. Es konnte gezeigt werden, dass diese Effekte P2RX7-abhängig waren und durch verschiedene P2RX7-spezifische Funktionen verursacht wurden. Wir vermuten, dass die P2RX7-abhängige Freisetzung extrazellulärer Vesikel, die wichtige regulatorische Strukturen sowie Antigene in Form von mRNA enthalten, an der Verbesserung der adaptiven Immunantwort beteiligt sein könnte. Wir nehmen an, dass sezernierte inflammatorische Zytokine, sowie eine verzögerte virale Genexpression, die nachweislich in MVA-infizierten CM P2RX7 Zellen vorhanden sind, dazu führen können, Antigene in viralen Replikationskomplexen einzufangen. Das könnte für eine verbesserte Kreuzpräsentation von Vorteil sein. Wir waren nicht in der Lage, diese Ergebnisse mit einem CRISPR/Cas9-vermittelten *P2rx7*-Knockout-Modell zu bestätigen, was möglicherweise auf die Genähnlichkeit von *P2rx7* mit seinem Familienmitglied *P2rx4* zurückzuführen ist, und beobachteten womöglich einen Off-Target-Effekt der CRISPR-Endonuklease Cas9. Wir haben jedoch erfolgreich nachgewiesen, dass P2RX7 als Teil der

angeborenen Immunantwort in CM „Feeder Zellen“ eine entscheidende Rolle bei der Regulierung adaptiver Immunantworten spielt. In dieser Arbeit wurde zum ersten Mal die Rolle von P2RX7 während einer MVA-Infektion und für die Kreuzpräsentation von Antigenen untersucht. Die Erkenntnisse dieser Arbeit sind wesentlich für die weitere Optimierung von MVA-Vektorvakzinen. Weitere Studien sind jedoch erforderlich, um die genauen Mechanismen aufzuklären, wie P2RX7 die Antigengenerierungsprozesse in CM „Feeder Zellen“ und anschließend in Antigen-kreuzpräsentierenden Zellen verändert.

2. List of abbreviations

Adenosine triphosphate	**ATP**
Absent in melanoma 2	**AIM2**
Acid sphingomyelinase	**A-SMase**
Amino acid	**aa**
Amino acid terminus	**A-terminus**
Antigen-presenting cells	**APCs**
Apoptotic bodies	**ApoBDs**
Associated speck-like complex	**ASC**
B-cell lymphoma protein 2	**Bcl-2**
Bovine serum albumin	**BSA**
Brefeldin A	**BFA**
Bone marrow-derived dendritic cells	**BMDCs**
Calcium	**Ca^{2+}**
Calcium chloride	**$CaCl_2$**
Carboxyl-terminus	**C-terminus**
Chicken embryo fibroblasts	**CEF**
Chorioallantois Vaccinia virus	**CVA**
Cloudman S91 melanoma cells	**CM**
Cowpox virus	**CPVX**
Clustered regularly interspaced short palindromic repeats/CRISPR-associated protein 9	**CRISPR/Cas9**
Cyclic guanosine monophosphate adenonsine monophosphate	**cGAMP**
Cyclic GMP-AMP synthase	**cGAS**
Cytopathic effect	**CPE**
Cytotoxic T lymphocytes	**CTLs**
Danger-associated molecular patterns	**DAMPs**
Dendritic cells	**DCs**
Dimethyl sulfoxide	**DMSO**
Double-stranded DNA	**dsDNA**
Endoplasmic reticulum	**ER**
ER aminopeptidase-1	**ERAP1**
Escherischia coli	***E.coli***
Ethidium bromide	**EtBr**
Exosome	**Exos**
Extracellular acidification rate	**ECAR**
Extracellular ATP	**eATP**

Extracellular vesicles	**EVs**
Granulocyte-macrophage colony-stimulating factor	**GM-CSF**
Green fluorescent protein	**GFP**
Guide ribonucleic acid	**gRNA**
Hours post infection	**hpi**
Human immunodeficiency virus	**HIV**
Infectious units	**IU**
Insertion-deletion mutation	**INDEL**
Interferon regulatory transcription factor 3	**IRF3**
Interferon	**IFN**
Interferon α/β receptor	**IFNAR**
Interferon gamma	**IFNγ**
Interferon gamma inducible protein 16	**IFI16**
Interleukin	**IL**
Intracellular ATP	**iATP**
Intracellular calcium concentration	**$[Ca^{2+}]_i$**
Intracellular cytokine staining	**ICS**
Knockout	**KO**
Lysogeny broth	**LB**
Major histocompatibility complex	**MHC**
Melanoma differentiation-associated protein 5	**MDA5**
Micro RNA	**miRNA**
Microvesicles	**MVs**
Modified Vaccinia virus ankara	**MVA**
Mean fluorescent intensity	**MFI**
Multiplicity of infection	**MOI**
Next generation sequencing	**NGS**
Nuclear factor kappa-light chain enhancer of activated B cells	**NF-κβ**
Nucleotide-binding oligomerization domain, Leucine-rich repeat and pyrin domain containing	**NLRP**
Oxygen consumption rate	**OCR**
Pathogen-associated molecular patterns	**PAMPs**
Pattern recognition receptors	**PRR**
Potassium	**K^+**
Psoralen-UV-A	**PUVA**
P2X purinoreceptor 7	**P2RX7**
Reactive oxygen species	**ROS**
Real-time polymerase chain reaction	**RT-PCR**

Relative light units	**RLU**
Retinoic acid-inducible gene 1	**RIG1**
Room temperature	**RT**
Single nucleotide polymorphisms	**SNPs**
Sodium	**Na^+**
Standard deviation	**SD**
Standard error of the mean	**SEM**
Stimulator of interferon genes	**STING**
TANK-binding kinase 1	**TBK1**
Tissue culture infectious dose 50	**$TCID_{50}$**
Toll-like receptors	**TLRs**
Transporter associated with antigen processing	**TAP**
Tricarboxylic acid	**TCA**
Tumor necrosis factor	**TNF**
T cell receptor	**TCR**
T cell stimulating factor	**TCGF**
Vaccinia virus	**VACV**
Variola virus	**VARV**
Western blot	**WB**
World health organization	**WHO**
Zentrale Einrichtung für Tierversuchsanstalt	**ZETT**
2’ (3’)-O-(4-benzoylbenzoyl)adenosine-5’-triphosphate	**Bz-ATP**

3. Introduction

4. Modified Vaccinia virus Ankara

Modified Vaccinia virus Ankara (MVA) belongs to the family of *Poxviridiae* and the genus Orthopoxvirus [1]. Members of this family have a linear double-stranded DNA (dsDNA), replicate inside the cell's cytoplasm and are described to be brick- or oval-shaped [2–4]. Widely known representatives of this family are the Vaccinia virus (VACV) and the Variola virus (VARV), the causative agent of smallpox (or also called variola major), one of the most contagious and deadly diseases worldwide [5,6].

4.1.1 Historical background

Smallpox was one of the most devastating diseases in human history, affecting millions of people and causing death in 3 out of 10 infected individuals [7]. The origin of variola major is remote, and appears to have occurred as soon as 10.000 BC [6,8]. In an attempt to create a vaccination procedure for the population's protection against smallpox, Edward Jenner used the substance from a cowpox virus (CPVX, also a member of the Orthopoxvirus genus) lesion of a dairymaid to inoculate an infant. After the first administration, the child only developed mild symptoms. However, at a later time point, the child was given a substance from a smallpox lesion and did not encounter any disease manifestations [9,10]. Vaccination with cowpox virus material was later substituted with material from Vaccinia virus, a related strain from a possibly unknown origin but inducing less adverse effects to induce cross-protection against VARV [10,11].

As part of the World Health Organization (WHO) smallpox eradication campaign, a safer vaccine option was required. Therefore, next to other attenuated VACV strains, MVA was generated by passaging the related strain Chorioallantois Vaccinia virus Ankara (CVA) in chicken embryo fibroblasts (CEFs) over 570 times and used as a vaccination vector for the eradication of smallpox [12,13]. Serial passaging of CVA led to the loss of genetic information, leaving MVA with a genome size of 178 kbp [14]. This strain was then used in the 1970s as a primary vaccination vector against smallpox, resulting in no serious adverse events in over 120.000 patients [13,15,16].

4.1.2 MVA as a vaccine vector

The serial passaging of MVA has resulted in the deletion of six major genomic regions, making it unable to replicate in most mammalian cells and, therefore, less capable of inducing disease. The deletions also caused the loss of several immunomodulatory proteins, such as the decoy

receptors for interferon gamma (IFNγ) or tumor necrosis factor (TNF), improving MVA's suitability as a viral vaccine vector [14,17–19].

MVA as a viral vector allows insertion of foreign genes, promoting the generation of multivalent vaccines for the prevention of multiple diseases. Various antigens can be expressed under the control of poxviral promoters in the host cell, without viral replication in most mammalian cells, as previously stated. Furthermore, its easy manipulation allows for the vaccine vector to be quickly developed, allowing the search to swiftly adapt to emerging infectious diseases, which plays a crucial role in the control of current pandemics, such as the recent COVID-19 outbreak [20–24]. These characteristics not only make MVA a promising candidate for the prevention of infectious diseases, such as human immunodeficiency virus (HIV), Ebola, malaria or tuberculosis, but also render MVA a potent vaccine vector that is tested in cancer immunotherapy [25–29].

In particular, MVA was demonstrated to induce both strong cellular and humoral immune responses, comparable to or stronger than the original VACV strain, ranking MVA as a powerful vaccine vector with extensive applications, which will be further elucidated in the next chapters [30–35].

4.2 Immune responses upon MVA infection

Professional antigen-presenting cells (APCs), such as dendritic cells (DCs), are a prerequisite for initiating cellular-mediated and humoral adaptive immune responses. In brief, during viral infection of DCs, antigens can either be processed directly by the infected cell, loaded on their major histocompatibility complex (MHC) and presented to T cells, triggering their activation. Alternatively, extracellular antigens can be released by infected cells, subsequently internalized by APCs, loaded on their MHC and presented to T cells to induce T cell responses [36,37].

MVA infection can lead to the activation of cytotoxic T lymphocytes (CTLs) via both, direct and cross-presentation processes, as was previously demonstrated, playing an important role in regulating immune responses [30,38,39].

Generally, the focus of basic MVA research lies in understanding how MVA infection triggers adaptive immune responses and how these can be regulated to achieve an improved MVA vaccine vector. Different stimuli immediately trigger an innate immune response by endogenous triggers called danger- or pathogen-derived stimuli named danger or- pathogen-associated molecular patterns (DAMPs or PAMPs, respectively) [40]. This is precisely why it

is important to acknowledge the function of DNA sensing pathways upon MVA infection, since innate signaling occurs as the first line of defense.

4.2.1 Direct-presentation

Activation of $CD8^+$ T cells was originally assumed to occur only via the direct-presentation pathway, referring to the infection of the DC and the presentation of the endogenous viral antigen to the CTLs, hence the classical MHCI pathway. Upon viral infection, the proteasome degrades viral antigens in the cytosol into small oligopeptides, which are transported to the endoplasmic reticulum (ER) via the transporter associated with antigen processing (TAP). Further processing by the ER aminopeptidase-1 (ERAP1) in the ER allows the breakdown of these peptides into 8-11mers, which fit in the MHCI groove and transferred to the cell surface for the activation of CTLs (classical cytosolic pathway). The classical MHCI does not only display epitopes from viral proteins for the activation of $CD8^+$ T cells but also from exogenous antigens taken up by APCs. Direct presentation is known as the process by which $CD8^+$ T cells are activated by endogenous antigens; antigens that have been produced in the cell that presents [39,41]. For MVA, it was shown that depending on the vector design and route of immunization and the translation process of antigens, $CD8^+$ T cells can be efficiently activated by direct antigen-presentation [31,42–44].

4.2.2 Cross-presentation

However, studies have shown that cross-presentation might be more efficient in activating CTLs, as rapid apoptosis of MVA-infected DCs could result in premature degradation of antigens, evading the classical MHCI presentation pathway [45–47]. Multiple researchers described this alternative pathway to occur regularly and predominantly taking place during the activation of $CD8^+$ T cells, especially in regards to MVA infection [44,45,48–50]. Indeed, cross-presentation plays a crucial role in situations where the APC cannot be infected by a virus (e.g. due to host cell restrictions). In addition to this, cross-presentation is essential in the presentation of tumor-derived antigens, which do not necessarily derive from APCs but can be from parenchymal cells that had undergone a mutation [37,48,51,52].

Cross-presentation describes the mechanism by which exogenously generated antigens are taken up by APCs, processed and loaded on MHCI and presented for the activation of CTLs. Exogenous antigens were long believed to be only presented via the MHCII pathway to CD4 T cells, as they would not be able to enter the cytosol. Different mechanisms have been described as how exogenous antigens are internalized to be cross-presented. Larger particles (>1mm) are taken up by phagocytosis, whilst smaller molecules (<1mm) by micropinocytosis,

both of these mechanisms being unique for both macrophages and dendritic cells [39,52]. In addition to this, antigens can also be acquired via direct cell-to-cell contact, such as gap junctions [53]. Antigenic sources for cross-presentation were also described to derive from necrotic, intact tumor or autophagic cells [54,55]. In regards to MVA, it is assumed that most of the antigens involved in cross-presentation derive from dying cells due to the MVA infection and are consequently used by APCs as an antigenic source [56,57].

The constitution of the antigen to be cross-presented has been a long debate throughout the years. Up to now, there has been a common agreement that the antigen source has to be cell-associated to be efficiently cross-presented [48,51,58–60]. However, alternative forms of antigens have also been acknowledged to play a possible role for the cross-presentation and activation of CTLs, such as exogenous RNA and DNA coding sequences [39].

Once the antigen is internalized, two distinct pathways are described to occur for the MHCI presentation. On the one hand, the antigen can undergo the classical cytosolic pathway for the final loading on the MHCI. On the other hand, however, internalized antigens are processed and degraded within vacuolar compartments. The loading of the peptide on the MHCI occurs within these enclosed structures and the MHCI-peptide complex is immediately transferred to the cell surface [61–63].

Surface exposure of the MHCI-peptide complex leads to the activation of CTL by binding to its T cell receptor (TCR) and simultaneous stimulation with CD80, CD40, and CD86 maturation markers of DCs to the receptor family proteins present on activated T cells. In turn, T cells get activated and generate anti- or pro-inflammatory immune signals [37,64].

4.2.3 Current approaches to cross-presentation *in vitro*

In literature, cross-presentation is studied with a variety of methods, including the infection of TAP-deficient cells with MVA and subsequent vaccination of mice, as well as the use of soluble ova protein as antigenic source for DCs [45,65].

However, another method that has been recently described from this laboratory, resembles the *in vivo* situation more closely [66]. Hence, we use Cloudman S91 (CM) melanoma cells as feeder cells. These cells are infected with MVA-Ova, a recombinant MVA vector containing an expression cassette encoding for the model antigen ovalbumin, co-cultured with granulocyte-macrophage colony-stimulating factor (GM-CSF; a cytokine promoting differentiation of cells) generated BMDCs and then with MVA-specific $CD8^+$ T cells. To be more precise, either B8 (a dominant native antigen of MVA) or Ova (ovalbumin, a classic model antigen)-specific T cells are used to elucidate the MVA-specific antigen transfer from donor cell (CM) to the APC (BMDCs) for subsequent presentation to $CD8^+$- specific T cells. Due to the different MHCI

background of CM cells (DBA mouse strain) and BMDCs/T cells (C57BL/6 mouse strain) we ensure exclusive presentation of the antigen from BMDCs to T cells and not accidental presentation of CM to T cells (Figure 1).

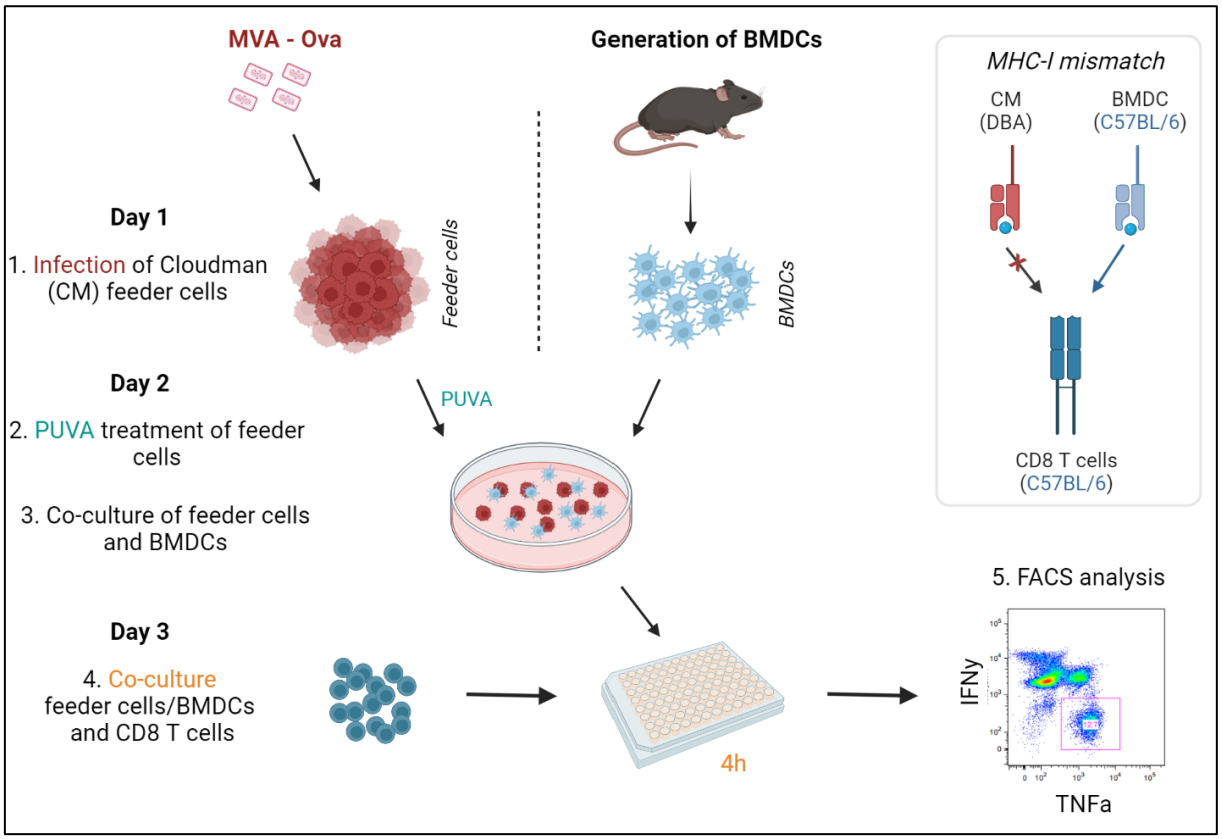

Figure 1: Antigen cross-presentation - experimental setting. CM cells (DBA mouse strain) are infected with MVA-Ova and the next day inactivated with psoralen UV-A (PUVA) treatment. These cells are subsequently co-cultured with previously generated immature BMDCs (Day 7) and on the next day further co-cultured with antigen-specific $CD8^+$ T cells in the presence of Brefeldin A (BFA) for 4h. Cells are stained for intracellular cytokines and analyzed for IFNγ or TNFα production by flow cytometry. The figure was created using Biorender.com.

4.2.4 MVA and innate sensing pathways

Different DAMPs, including adenosine triphosphate (ATP), uric acid or interleukin- (IL) 2 or PAMPs, such as bacterial/viral nucleic acids or bacterial/fungal cell wall components are known to activate a diverse number of pattern recognition receptors (PRR). In this regard, Toll-like receptors (TLR) are able to recognize bacterial or viral PAMPs in extracellular or endolysosomal compartments and, as a consequence, initiate MyD88 or Trif-dependent activation of type I interferon (IFN) signaling and synthesis of inflammatory cytokines. Other PRRs such as RIG1 (retinoic acid-inducible gene 1) or MDA5 (melanoma differentiation-associated protein 5) also contribute to the activation of the type I IFN response. The cGAS/STING signaling pathway has gained importance in recent years as one of the main inducers of type I IFNs. Upon DNA sensing by cGAS (cyclic GMP-AMP synthase), STING (stimulator of interferon genes), the adaptor molecule is activated by 2´3´- cyclic guanosine

monophosphate adenonsine monophosphate (cGAMP) and as a consequence activates the downstream targets TBK1 (TANK-binding kinase 1) and IRF3 (interferon regulatory transcription factor3), leading to the activation of the NF-κβ (nuclear factor kappa-light chain enhancer of activated B cells) pathway and the synthesis of type I IFNs [40,67]. Type I IFNs in return can exert their antiviral functions, binding on interferon α/β receptors (IFNAR) and activating intracellular signaling pathways or even initiating a positive feedback loop [68].

The canonical inflammasome is a multiprotein complex of the innate signaling system that is also activated upon viral infection and consists of the sensor molecule, the apoptosis-associated speck-like complex (ASC) and the Caspase-1 protein. Upon sensing of the trigger by a sensor molecule, such as AIM2 (absent in melanoma 2), IFI16 (interferon gamma inducible protein 16) or NLRP1/3/6 (Nucleotide-binding oligomerization domain, Leucine-rich repeat and pyrin domain containing), a complex formation between the sensor molecule, ASC and Caspase-1 is initiated, leading to its activation and to the maturation of inflammatory cytokines, such as IL-1ß and IL-18, eventually concluding in pyroptosis [67]. The P2X purinergic receptor 7 (P2RX7) is described to be involved in the activation of the canonical inflammasome, which will be discussed in more detail in the next sections [69–71]. Unpublished next generation sequencing (NGS) data from this group has additionally shown significant regulation of inflammasome members, including *P2rx7* expression upon MVA infection in Cloudman melanoma cells.

Recent studies have demonstrated that MVA is frequently involved in inducing cGAS/STING-mediated immune responses in innate immune cells as well as in DCs, and MVA has also been shown to activate the inflammasome [72–76]. In addition to this, Barnowski and colleagues have further elucidated the importance of STING absence in CM feeder cells for improved MVA-mediated antigen cross-presentation [66]. In summary, many of the innate sensing pathways do not take place exclusively upon viral infection but can occur simultaneously. There is limited information known as to what extent innate stimulation is achieved in regards to MVA. This demands the detailed investigation of innate host-viral vector interactions not only in antigen-presenting cells but also in antigen-donor cells such as feeder cells during cross-presentation.

4.3 The P2X7 receptor

ATP does not only serve as an energy source and signaling molecule in multiple pathways but is also referred to as a DAMP, promoting inflammation upon infection by different pathogens [77,78]. One of the most researched binding site for ATP is the P2X7 receptor, a bifunctional receptor that is present on immune cells, epithelial and endothelial cells and leads to the

formation of a selective cation channel or a large non-selective pore [78–82]. P2RX7 belongs to the P2-receptor family, which is subdivided into the P2Y and P2X subsets. The P2Y members are G-protein coupled receptors, being involved in the activation of ion channels, adenylyl cyclase, and phospholipase C. In contrast to this, P2X receptors (P2RX1 to 7) belong to the group of transmitter-gated ion channels that upon ligand binding lead to the influx of calcium and sodium (Ca^{2+} and Na^{+}), respectively, and the efflux of potassium (K^{+}) [78,83].

4.3.1 P2RX7 characteristics

The P2RX7 gene is located on chromosome 5 in mice or chromosome 12 in humans and the full-length variants consist of 11-13 exons, translating into 595 amino acids (aa) proteins and being the largest of its family, sharing between 77-85% of its identity sequence between each other. Each subunit of this trimeric protein consists of two hydrophobic membrane-spanning regions (transmembrane domains) between which the ATP binding segment can be found. The intracellular domain contains short amino- (N) and long carboxyl- (C) termini. In this regard, the C-terminus of P2RX7 has many binding sites for Src-kinase proteins and is crucial for the opening of the large conductance pore. In addition to this, all subunits contain consensus sequences for glycosylation [77,82,84,85].

Multiple alternative splice variants of the P2X7 receptor have been described, where for example a novel Exon 1 or C-terminal truncations at the P2RX7 can occur, potentially leading to a proliferative advantage [77,82]. Furthermore, many single nucleotide polymorphisms (SNPs) in the *P2rx7* gene, leading to an up- or downregulation of the receptor function, have been outlined in humans [82]. In mice, one of the most frequently characterized non-synonymous SNP in the *P2rx7* gene is the P451L mutation, where a proline at position 451 (cytoplasmic tail) has been exchanged with a leucine molecule, rendering the P2X7 receptor less sensitive to ATP stimuli [86].

Most commonly, P2RX7 has been described to be a surface receptor that is activated by extracellular ATP before initiating its downstream signaling [87,88]. However, a recent study proposes that functional P2RX7 is not only found on the plasma membrane, but also in intracellular compartments. Sarti and colleagues have characterized the effects of P2RX7 molecules on mitochondrial surfaces and their importance for the regulation of cellular metabolism [89]. Additionally, Atkinson and co-workers identified P2X7 receptors and their impact on gene transcription on nuclear envelopes of neurons [90].

Many features render P2RX7 unique in the P2- receptor family. Besides the activation with ATP, 2’ (3’)-O-(4-benzoylbenzoyl)adenosine-5’-triphosphate (Bz-ATP) can also potently stimulate P2RX7. Unlike other receptors, P2RX7 activity and permeability are progressive and

do not decrease over time and stimulus, but can be rather potentiated, therefore the P2X7 receptor is often described as a non-desensitizing receptor, unlike its family members P2X1 and P2X3 [77]. Under physiological conditions, P2RX7 activity can be regulated by the presence of surface ectonucleotidases, which can degrade extracellular ATP (eATP) detracting the P2RX7 antagonist [91].

Typically, upon P2RX7 activation, the cation-selective pore opens, leading to the intracellular increase in calcium. Upon longer agonist exposure, however, a non-selective pore is opened, allowing entry of large molecules. This pore is often referred to as the ethidium bromide (EtBr) pore, because large molecules of up to 900 Da, such as EtBr, can permeate and are used in fluorometric assays to establish pore function [77,83,85,92]. Due to the implication of P2RX7 in many signaling pathways and diseases, various P2RX7 antagonists have been developed and described, ranging from ions to monoclonal antibodies. However, currently, A740003, a potent P2RX7 competitive inhibitor, seems to be promising in P2RX7 inhibition and is frequently used in *in vitro* studies [77,93]

4.3.2 Function of P2RX7 in different signaling pathways

P2RX7 has been described to have multiple functions that are dependent on cell type, the availability of ATP or extracellular conditions [94]. As previously described, P2RX7 is involved in the stimulation of the NLRP3 inflammasome, which is activated by a variety of pathogenic or cellular triggers [95,96]. Another major function of P2RX7 is its involvement in apoptotic processes, unlike other members of the P2X family. Interestingly, it was demonstrated that increased cellular energy stores are P2RX7-dependent and grant a proliferation advantage to the cell. However, excessive P2RX7 stimulation can also turn P2RX7 into a pro-apoptotic receptor, inducing cell death [77,81]. Additionally, P2RX7 activity can also lead to reversible phosphatidylserine flip to the cell surface [97].

The activity of P2RX7 impels an intracellular calcium increase, which in turn activates calcineurin, causing the dephosphorylation of the NFAT transcription factors and their translocation to the nucleus [98,99]. Activation of these transcription factors is associated with cell cycle progression and subsequent cell development, as well as cell differentiation and tumor progression [100,101].

Besides these functions, P2RX7 is also involved in the activation of different metalloproteases, which leads to the shedding of surface molecules, such as CXCL16, IL-6, CD62L, CD23, CD27 and CD44 [102–106]. P2RX7 has also been linked to the induction of lysosome exocytosis, cell fusion, plasma membrane blebbing and the release of extracellular vesicles (EVs), which will be discussed in more detail in the next chapter [82,107]. In regards to this, Costa-Junior

and colleagues also proposed the correlation between P2RX7 activity and lipid metabolism [108].

Since ATP is also known as a neurotransmitter, most descriptions of P2RX7 focus on the nervous system and neuroinflammation [92]. Only a few studies describe the involvement of P2RX7 in other immunological processes. One study associates P2RX7 activity to be involved in dendritic cell migration upon an endogenous danger signal [109]. Another research focused on the transfer of pre-formed MHCI-SIINFEKL peptide complexes from P2RX7 bearing cells to the cell membrane of antigen-presenting cells. This mechanism, termed “cross-dressing” led to the activation of T cells, conferring the crucial role of P2RX7 in this non-conventional antigen presentation pathway [110].

In summary, P2RX7 is not exclusively involved in the mediation of neurological information by the neurotransmitter ATP, but also aids in the reprogramming of cellular metabolism in stress situations by altering gene expression and other signaling pathways.

4.3.3 P2RX7 in extracellular vesicle release

The P2RX7 activity, unlike initially believed, does not exclusively lead to the opening of the cation channel and the large pore but is associated with the initiation of several downstream signaling pathways, as previously shown. Indeed, the P2X7 receptor has been demonstrated to form complexes with other target proteins, forming the so-called “P2X7 receptor signaling complex”. These proteins, with whom P2RX7 has been shown to associate, vary from being different structural proteins to signaling proteins [111,112].

As reported before, P2RX7 activity is associated with the release of extracellular vesicles [78,113,114]. Signaling proteins at the C-terminus of the P2X7 receptor were demonstrated to be directly involved in cytoskeleton rearrangement by activating various enzymes, such as acid sphingomyelinase (A-SMase) and inducing the hydrolysis of sphingomyelin, abundant in the plasma membrane, to ceramide, thereby promoting the generation of EVs [115,116]. Extracellular vesicles can be subdivided into three subclasses, hence exosomes (Exos; 30-150nm), microvesicles (MVs; 50-1000nm) and apoptotic bodies (ApoBD; 1000-5000nm). Besides varying in size, these vesicles can also be distinguished by their content and cellular origin. Whilst ApoBD are generated upon disassembly of an apoptotic cell and might contain degraded proteins or even entire organelles, the formation of Exos and MVs undergoes a more controlled process. Exos originate from endosomal compartments and are secreted upon fusion with the plasma membrane. Similarly, MVs originate from the outward budding of the plasma membrane itself and contain cytoplasmic material as well [117–120].

The analysis of extracellular vesicles has gained researchers´ interest in recent years, since the content of EVs, especially Exos, varies depending on the pathological condition, making them potential markers for early disease detection. Additionally, EVs have been demonstrated to be carriers of many signaling molecules, showing both protective and pathological roles in the different setups. For instance, P2RX7-dependent EV generation results in EVs loaded with ATP, Caspase-1, IL-18, IL-1ß, IL-6 and other cytokines [120–124]. Their properties vary from the regulation of adaptive immune responses to mediating tumor progression [120,124–126]. In fact, EVs are intercellular mediators, involved in phagocytosis processes as they expose phosphatidylserine on the cell surface invoking “eat-me” signals for APCs or even participate in antigen transfer, e.g. for cross-presentation [118,127,128]. Besides this, EVs contain other proteins, such as MHC molecules, chemoattractive or adhesion molecules, DNA sequences and small regulatory RNAs, such as micro RNA (miRNA) [113,124,129].

4.3.4 Pathogenesis of P2RX7

Following up on the topic of P2RX7 in cell proliferation mentioned earlier, tumor transformation is associated with uncontrolled cell division [81]. Additionally, as shown before, P2RX7 is involved in various cellular pathways, not surprisingly participating in tumorigenesis and inflammation.

Indeed, in humans, some *P2rx7* SNPs or haplotypes are linked to either increased or decreased P2X7 receptor function, leading to cardiovascular, musculoskeletal, inflammatory or even psychiatric disorders. Diseases as multiple sclerosis, Alzheimer's disease, ischemia, pulmonary fibrosis and Huntington’ are described to be associated with P2RX7 abnormal function [82]. Many cancer types, such as prostate and breast cancer, as well as squamous cell carcinoma, pancreatic tumor and neuroblastoma, are also coupled to impaired P2RX7 activity [107].

Besides this, a study from Amores-Iniesta and co-workers suggests P2RX7-dependent allograft rejection in patients. Indeed P2RX7-specific blockade led to increased graft durability coupled to a lower extracellular ATP concentration [95].

4.4 Importance and aim of the thesis

Due to recent infectious outbreaks, it has become crucial to act rapidly and efficiently, especially when in need of a vaccination strategy [24]. MVA is one of the frequently used candidates for the development of novel vaccines, as it is safe and induces robust immune responses [17]. However, many of the mechanisms eliciting these immune responses in the context of MVA infection are poorly understood. In this field, the importance of cross-presentation for MVA-mediated immunity has not attracted enough attention. In fact, optimal $CD8^+$ T cell activation in the MVA infection context has been shown to occur by allowing cross-presentation of antigens [45]. The precise processes involved in the successful generation and transfer of antigen from the donor feeder cells, however, are barely characterized and remain remote.

It has been believed that only antigen-presenting cells play the leading role in cross-presentation, as they are the mediators for the activation of $CD8^+$ T cells [36,37]. Yet, a recent study published by the members of this group has demonstrated that the trigger involved in coordinating adaptive immune responses, lies in the regulation of innate immune components in feeder cells [66]. We wanted to further investigate these innate stimuli and focused our study on the role of the P2RX7. This receptor gained our attention once we analyzed NGS data (unpublished data, Cornelia Barnowski) obtained from MVA-infected Cloudman cells (DBA mouse background). Interestingly, this receptor is described to be less sensitive to ATP stimulation in cells from DBA mice [86], therefore picking our curiosity even more about the importance of this channel during MVA infection and cross-presentation.

As stated before, P2RX7 is involved in a multitude of immune pathways, showing the versatility of effects that a simple surface receptor might have. Many of the pathways described might play a crucial role in the regulation of immune responses, most importantly for us, in the cross-presentation pathway. Therefore, we used an active P2RX7 variant from BALB/c mice [86] to transfect our Cloudman cells (CM P2RX7) and investigate the role of this functional receptor in feeder cells during MVA antigen cross-presentation. Once we know the effect of this variant in feeder cells for cross-presentation of MVA antigens, we aim to understand how different processes required for antigen generation in feeder cells are affected by the presence of BALB/c P2RX7. Moreover, we will focus on the analysis of different P2RX7-dependent pathways, such as apoptosis, mitochondrial metabolism and the secretome of CM P2RX7 cells. In regards to this, we will analyze more closely the potentially altered extracellular vesicle fraction as well as the supernatant fraction of CM P2RX7 cells infected with MVA. As a final attempt to investigate P2RX7 function in feeder cells, we aim to delete *P2rx7* via CRISPR/Cas9-mediated knockout (Clustered regularly interspaced short palindromic repeats/CRISPR associated protein 9) in CM cells (CM P2RX7 xKO). The focus will lie on

comparing the pathways affected by altered P2RX7 phenotype in the different cell lines (CM P2RX7 and CM P2RX7 xKO) upon MVA infection. Based on this, it will be able to draw conclusions about how MVA infection affects antigen processing and how cross-presentation of antigens is regulated by feeder cells.

This research will highlight the importance of studying cross-presentation in more detail, as it has a strong impact on the vector design area, e.g. for vaccination against infectious diseases and tumor antigens. Currently, the feeder cells are not fairly recognized for their pivotal role as initiators of cross-presentation by being infected with MVA. P2RX7 research is mainly centered in the pathological context and only a few studies describe the involvement of P2RX7 during antigen presentation. Currently there are no studies describing the role of P2RX7 during MVA-mediated immunity or, in general, portraying P2RX7 in the MVA infection model. We therefore aim to challenge this lack of research and want to illustrate the importance of the different P2RX7-dependent pathways for MVA-mediated antigen cross-presentation in feeder cells. Understanding the interplay of these pathway will refine our knowledge of the immune responses elicited by MVA and advance future research on MVA.

5. Materials and Methods

6. Materials

6.1.1 Eukaryotic cells

Cell line	Reference
Cloudman S91 melanoma (Clone M-3)	ATCC CCL-53.1
CM pcDNA3	This study; CM transfected with empty vector plasmid pcDNA3
CM P2RX7	This study; CM transfected with P2RX7 plasmid
HEK293	Elena Adinolfi, University of Ferrara [130]
HEK293 hP2RX7	Elena Adinolfi, University of Ferrara [130]
B8-specific CD8 T cells	Ronny Tao, University of Düsseldorf
Ova-specific CD8 T cells	Ronny Tao, University of Düsseldorf
UMNSAH-DF1	ATCC CRL-12203
EL4	ATCC TIB-39
HEK293T	ATCC CRL-3216

6.1.2 Bacterial cells

Strain	Reference
***Escherichia coli (E.coli)* XL-1 blue cells**	Agilent technologies

6.1.3 Viruses

All recombinant MVA were generated by Ronny Tao (University of Düsseldorf) by homologous recombination as described in [21]. MVA stocks were kept at -80°C and working stocks were freeze/thawed for a maximum of three times for usage. Upon thawing, virus was sonicated for 1min at full speed to ensure homogenous distribution of viral particles.

Strain	Description
MVA-PK1L-OVA	MVA expressing ovalbumin under the control of the early PK1L promoter
MVA-P7.5-GFP	MVA expressing GFP under the control of the intermediate/late P7.5 promoter
MVA-PK1L-mCherry-Ova	MVA expressing mCherry-ovalbumin fusion protein under the control of the early PK1L promoter
MVA-P11-OVA	MVA expressing ovalbumin under the control of the late P11 promoter
MVA-P7.5-OVA	MVA expressing OVA under the control of the intermediate/late P7.5 promoter

6.1.4 Mice strains

All animals were maintained at the Zentrale Einrichtung für Tierversuchsanstalt (ZETT) in Düsseldorf under specific pathogen-free conditions. Animals were left to acclimate for at least a week before sacrifice. All procedures involving animals were approved by the regional authorities (North Rhine-Westphalia State Environment Agency - LUA NRW, Germany) and the animal use committee at the University of Düsseldorf (Reg. No O119/11). All animal procedures performed by the colleagues at the University of Ferrara were approved by the University of Ferrara Ethics Committee and the Italian Ministry of Health (Italian D. Lgs 26/204).

Experimental model	Application	Reference
C57BL/6N	Bone marrow isolation for generation of dendritic cells (12-16 weeks, female); Isolation of splenocytes for T cell stimulation (different ages and both sexes)	Janvier
BALB/c	Bone marrow isolation for generation of dendritic cells, 12-16 weeks, female	Janvier
BALB/c *P2rx7-/-*	Bone marrow isolation for generation of dendritic cells, 12-16 weeks, female. (Prepared bone marrow was received from the University of Ferrara)	Francesco Di Virgilio, University of Ferrara

6.1.5 Antibodies

6.1.5.1 Western Blot antibodies

Antibody	Clone	Conjugate	Host	Dilution/diluent	Source
Anti-ovalbumin	n/d	No	rabbit	1:20 000	Rockland
Anti-Cleaved-Caspase8	D5B2	No	rabbit	1:1000 in BSA	Cell signaling
Anti-ß-Actin	AC-74	No	mouse	1:50 000	Sigma-Aldrich
Anti-P2RX7	n/d	No	rabbit	1:300 in 3% skimmed milk and 0.5% BSA	Sigma-Aldrich
Anti-Myosin II A	n/d	No	rabbit	1:100 in 5% skimmed milk and 0.5% BSA	Sigma-Aldrich
Anti-Mouse, IgG	n/d	Horse radish peroxidase	---	1:3000	Jackson Laboratories
Anti-Rabbit, IgG	n/d	Horse radish peroxidase	---	1:3000	Jackson Laboratories
Anti-Caspase9	n/d	No	rabbit	1:1000 in BSA	Cell signaling
Anti-STING	D2P2F	No	rabbit	1:1000 in BSA	Cell signaling
Anti-pSTING	S365	No	rabbit	1:1000 in BSA	Cell signaling

Anti-TBK1	D1B4	No	rabbit	1:1000 in BSA	Cell signaling
Anti-pTBK1	S172-D52C2	No	rabbit	1:1000 in BSA	Cell signaling
Anti-IRF3	D83B9	No	rabbit	1:1000 in BSA	Cell signaling
Anti-pIRF3	S396-4D4G	No	rabbit	1:1000 in BSA	Cell signaling

6.1.5.2 FACS antibodies

Antibody	Conjugate	Clone	Dilution/diluent	Source
Anti-IFNγ	APC	XMG1.2	1:400 in 1:10 BD PermWash	Invitrogen
Anti-TNFα	PE-Cy7	Mp6-XT22	1:300 in BD Perm/Wash	Invitrogen
Anti-CD11c	PE	N418	1:300 in FACS buffer	Invitrogen
Anti-SIINFEKL/H2K^b	PE-Cy7	eBio25-D1.16	1:300 in FACS buffer	eBioscience
Anti-CD8a	eFluor 450	53-6.7	1:300 in FACS buffer	eBioscience
Apotracker-Green	FITC	n/d	1:10 in FACS buffer, then 5µl of this to 100µl cells in FACS buffer	Biolegend
Fixable viability dye	eFluor 506	n/d	1:600 in PBS	Invitrogen
Fixable viability dye	eFluor 660	n/d	1:2000 in PBS	Invitrogen
Anti-H2K^b	FITC	AF6-88.5	1:300 in FACS buffer	Biolegend
Anti-CD16/CD32	---	93	1:200 in FACS buffer	eBioscience
R-Phycoerythrin AffiniPure F(ab')$_2$ Fragment Goat Anti-Mouse IgG, Fcγ fragment specific (Anti-PE-IgG)	---	n/d	1:200 in FACS buffer	Jackson Laboratories
Anti-CD11c	APC-Cy7	HL3	1:300 in FACS buffer	BD Pharmingen
Anti-CD86	APC	GL1	1:300 in FACS buffer	BD Pharmingen
Anti-CD40	PB	3/23	1:300 in FACS buffer	Biolegend
Anti-MHCII	PE	AF6-120.1	1:300 in FACS buffer	eBioscience
Anti-P2RX7	n/d	n/d	1:200 in BD Perm/Wash	Sigma-Aldrich

6.1.5.3 Confocal microscopy dyes

Dye	Dilution/diluent	Source
PKH26 Red fluorescent cell membrane labeling	2µM in saline saccharose solution	Sigma-Aldrich
Quinacrine dihydrochloride	2µM in saline saccharose solution	Sigma-Aldrich
NucBlue Fixed cell stain ready probes TM reagent Dapi special formulation	Manufacturer's instructions	Life technologies
Goat anti-Rabbit IgG (H+L) Cross-Adsorbed Secondary Antibody, Alexa Fluor™ 488	1:500 in 1% BSA/0.05% saponin	Invitrogen
Anti-P2RX7	1:500 in 1%BSA/0.05% saponin	Sigma-Aldrich

6.1.6 Buffers

Buffer	Application	Constituents
Lysis buffer	*In vitro* toxicity assay	10% SDS 0.01M HCl
10x Running buffer	SDS PAGE/Western Blot	250mM Tris-base 2M Glycine 1% (w/v) SDS
10x Blotting buffer (+CH_3OH in 1x Blotting buffer)	SDS PAGE/Western Blot	0.5M Tris-base 0.4M Glycine
BD Perm/Wash working solution	FACS	1:10 of Perm/Wash in dH20
10x saline solution	Ca^{2+} fluorometric analysis	125mM NaCl 5mM KCl 1mM $MgSO_4$ 1mM NaH_2PO_4 20mM HEPES 5.5mM Glucose 5mM $NaHCO_3$ 1mM $CaCl_2$ pH 7.4
Saline saccharose solution	Live confocal microscopy Ethidium bromide pore measurements	300mM Sucrose 1mM K_2HPO_4 1mM $MgSO_4$ 5mM D-glucose 20mM HEPES pH7.4 1mM $CaCl_2$
FACS buffer	FACS staining	1% BSA 0.02% sodium azide PBS
Annealing buffer	CRISPR/Cas9 cloning	10mM Tris pH 8.0 50mM NaCl 1mM EDTA

6.1.7 Oligonucleotides

6.1.7.1 Plasmids

Plasmid	Description	Reference
pcDNA3	Empty vector plasmid carrying the Geneticin resistance gene	Elena Adinolfi, University of Ferrara
mP2RX7	Plasmid expressing the murine P2RX7 from BALB/c mice and carrying the geneticin resistance gene	Elena Adinolfi, University of Ferrara [131]
RP-557	Transfer plasmid for CRISPR/Cas9 cloning carrying the puromycin resistance gene	Robert Jan Lebbink, University of Utrecht
RP-557_P2RX7_KO	Transfer plasmid RP-557 containing the gRNA sequencing for the knockout of P2XR7	This study
pMD2.G	VSV-G envelope expressing plasmid for CRISPR/Cas9 cloning	Robert Jan Lebbink, University of Utrecht
psPAX2	Packaging plasmid for CRISPR/Cas9 cloning	Robert Jan Lebbink, University of Utrecht

6.1.7.2 Primer

All primers were diluted to a final concentration of 10µM before usage and stored at -20°C.

Primer	Sequence (5´-3´)	Application	Source
***P2rx7*_fw**	CAC ACC AAG GTC AAA GGC AT	RT-PCR	This study
***P2rx7*_rev**	CAC TTG GCC TTC TGA CTT GAC	RT-PCR	This study
***18s rRNA*_fw**	AAA CGG CTA CCA CAT CCA AG	RT-PCR	[132]
***18s rRNA*_rev**	CCT CCA ATG GAT CCT CGT TA	RT-PCR	[132]
***Ova*_fw**	CAC AAG CAA TGC CTT TCA GA	RT-PCR	[132]
***Ova*_rev**	GAC TTC ATC AGG CAA CAG CA	RT-PCR	[132]
***B8*_fw**	ATC CGC ATT TCC AAA GAA TG	RT-PCR	[132]
***B8*_rev**	ACA TGT CAC CGC GTT TGT AA	RT-PCR	[132]
A19L_fw	GCA TGA CGT GTT CTG CCT	RT-PCR	[132]

***A19L*_rev**	GGC CAG TGT ATT ACC CCT CA	RT-PCR	[132]
Sting_fw	TCC CCA TTC AGA AGC CAC TT	RT-PCR	This study
Sting_rev	CAA AGG ATC ATC AGG CTG GC	RT-PCR	This study
***CMW*_fw**	CGC AAA TGG GCG GTA GGC GTG	Sequencing	https://www.addgene.org/browse/sequence/2097/giraffe-analyze_vdb/
Bgh_rev	CCT CGA CTG TGC CTT CTA	Sequencing	https://www.addgene.org/browse/sequence/2097/giraffe-analyze_vdb/
P2RX7_gRNA_fw	ACC GAA TTA TGG CAC CGT CAA G	CRISPR/Cas9 KO	This study
P2RX7_gRNA_rev	AAACCTTGACGGTGCCATA ATT	CRISPR/Cas9 KO	This study
RP-557_seq	TGC AGG GGA AAG AAT AGT AGA C	Sequencing	Cornelia Barnowski, Institute of Virology, Düsseldorf
P2RX7_cDNA_gRNA	GGG AAG GTG TAG TCT GCA GT	Sequencing	This study
P2RX7_xKO_fw	TTC CAC TCA CAT TCA GGG CA	Sequencing	This study
P2RX7_xKO_rev	ACC CAC ATA GAA TCC AGC CA	Sequencing	This study
P2RX7_seq1	GGG TTG TCC GGA AAA CAA AGG GA	Sequencing	This study
P2RX7_seq2	GGG GGT GGG GAG GGG GAA TTT T	Sequencing	This study
P2RX7_seq3	AAG GCA TGC ACC ACC ACA CTG G	Sequencing	This study
P2RX7_seq4	AAA TGA TAC CCT TGT GGG ACA AAG	Sequencing	This study
P2RX7_seq5	AGA TGG CTC AGT CGT TAA TTG AAC	Sequencing	This study

6.1.7.3 gRNA

To generate a P2RX7 CRISPR/Cas9 mediated knockout (KO), the following guide RNA (gRNA) (PAM sequence in italics) for P2RX7 was used:

CGAATTATGGCACCGTCAAG *TGG*

6.1.8 Synthetic peptides

All peptide stocks were 1mg/ml and were stored at -80°C. All peptide working solutions (0.1mg/ml in DMSO) were stored at -20°C and were used for a maximum of three months.

Peptide	Sequence	MHC-I restriction	Function	Reference
$B8_{20-27}$	TSYKFESV	H2-K^b	Virulence factor	[133]
$Ova_{257-264}$	SIINFEKL	H2-K^b	Model antigen	[134]

6.1.9 Commercial kits

Kit name	Source
RNAse-free DNAse Set	Qiagen
Revert Aid H Minus First strand cDNA synthesis kit	Thermo Fisher Scientific
RNeasy Mini Kit	Qiagen
LumiKine Xpress mIFN-ß 2.0	Invivogen
LumiKine Xpress mIFN-α 2.0	Invivogen
QIAmp DNA Mini Kit	Qiagen
Pierce BCA Protein Assay Kit	Thermo Fisher Scientific
Mouse IL-18 ELISA Kit	MBL
Legendplex MU Anti-Virus response panel 13-plex	Biolegend
Seahorse XF Cell Mito Stress test kit	Agilent technologies
Extracellular Flux Assay Kit	Agilent technologies
BD Cytofix/cytoperm Fixation/Permeabilization kit	BD Biosciences
BD Perm/Wash	BD Biosciences
HALT Protease & Phosphatase Inhibitor cocktail, EDTA-free (100x)	Thermo Fisher Scientific
Luminescent ATP detection Assay Kit	abcam
Abc anti-Rat/Anti-Hamster Bead Kit	Invitrogen
Caspase-Glo1 Inflammasome assay	Promega
Pierce ECL substrate kit	Thermo Fisher Scientific
RealTime-Glo Extracellular ATP assay	Promega
NucleoSpin® Gel and PCR Clean-up	Macherey Nagel

6.1.10 Chemicals and reagents

Material name	Source
UltraPure TM Distilled Water DNase/RNase free	Invitrogen
RPMI Medium 1640 (1X) + GlutaMax TM -I	Gibco
DMEM high glucose, Glutamax TM, pyruvate	Gibco
Opti-MEM	Thermo Fisher Scientific
0.05% Trypsin-EDTA (1X)	Gibco
Dimethylsulfoxide (DMSO)	Sigma-Aldrich
Geneticin selective antibiotic	Gibco
GM-CSF	Harvested from supernatant of B16-GM-CSF producing cells, Molecular Virology, Düsseldorf
TCGF	Harvested from rat spleen supernatant stimulated with Concatenin A and a-D-Mannopyranoside, Molecular Virology, Düsseldorf
Trypan Blue Stain (0.4%)	Gibco
DPBS (1X)	Gibco
Hexadimethrinbromide	Sigma-Aldrich
4′-Aminomethyltrioxsalen –hydrochlorid (Psoralene)	Sigma-Aldrich
FBS Supreme	Pan-Biotech
Thiazolyl Blue Tetrazolium Bromide	Merck
Glacial acid	Merck
BD Pharm Lyse buffer	BD Biosciences
Brefeldin A	Sigma-Aldrich
Lipofectamine LTX Reagent	Invitrogen
ProLong Antifade mountant	Invitrogen
RIPA buffer	Thermo Fisher Scientific
A740003	Tocris
PowerUP SYBR Green Master Mix	Applied Biosystems
XFCalibrant pH7.4	Agilent technologies
Apyrase	Sigma-Aldrich
TEMED	VWR

Paraformaldehyde	Merck
Tween 20	Merck
PageRuler Prestained protein ladder	Thermo Fisher Scientific
SDS	Roth
Rotiphorese Gel (37.5:1)	Roth
Albumin Fraction V	Roth
Enliten Luciferase/luciferin reagent	Promega
Firezyme Diluent buffer	Firezyme
Calcium chloride	Merck
Glycine	Roth
Milk powder	Roth
Methanol	Merck
Magnesium chloride	Merck
Hydrochloric acid (32%)	Roth
D(+) Saccharose	VRW
Ethanol, absolute	Merck
Isopropanol	Merck
Sodium Chloride	Roth
2- ß- mercaptoethanol	Roth
Triton X-100	Sigma-Aldrich
FURA-2 AM	Life technologies
Bz-ATP	Sigma-Aldrich
ATP	Sigma-Aldrich
Ionomycin	Invitrogen
Digitonin	Sigma-Aldrich
NaH_2PO_4	Roth
KCl	Merck
Ethidium bromide	Sigma-Aldrich
$MgSO_4$-$7H_20$	Merck
Glucose	Merck
$NaHCO_3$	Sigma-Aldrich

Saponin	Sigma-Aldrich
HEPES	Sigma-Aldrich
Sodium Azide	Roth
Sulfinpyrazone	Sigma-Aldrich
Dithiothreitol (DTT)	Invitrogen
10x Buffer Tango	Thermo Fisher Scientific
Quick ligase	NEB
2x Quick ligase reaction buffer	NEB
Gel loading dye purple (6x)	NEB
Esp3I	Thermo Fisher Scientific
Ampicillin	Sigma-Aldrich
Biozym LE Agarose	Biozym
LB Agar	Invitrogen
LB Broth	Roth
Polyethyleneimine (PEI)	Sigma-Aldrich
Hexadimethrine bromide	Sigma-Aldrich
Puromycin dihydrochloride	Sigma-Aldrich
TBE,10x Liquid concentrate, ultra pure	VWR

6.1.11 Consumables

Material name	**Source**
Seahorse XF96 Cell culture microplate	Agilent technologies
96 flat well chimney base plate non sterile	Thermo Fisher Scientific
Pluristrainer mini 20µM	Pluriselect
Cell culture plate 96K, F-form, black	Greiner BioOne
Tissue culture 96-well plate	TPP
Cell strainer 70µm	VWR
10µl filter tip	Starlab
20µl filter tip	Starlab
100µl filter tip	Starlab
1000µl filter tip	Starlab

6cm tissue culture dish	VWR
10cm tissue culture dish	TPP
T25 tissue culture flask	VWR
T75 tissue culture flask	Thermo Fisher Scientific
T182.5 tissue culture flask	VWR
6-well tissue culture plate	VWR
12-well tissue culture plate	VWR
24-well tissue culture plate	VWR
1ml Sub-Q syringe	BD Plastipaq
0.2ml 8-strip PCR tubes	Starlab
Discardid II Syringe 5ml	BD
50mL falcon	Greiner BioOne
15mL falcon	Greiner BioOne
5mL stripette	Costar
10mL stripette	Falcon
25mL stripette	Greiner BioOne
Nitrocellulose blotting membrane 0.45µm	GE Healthcare Life sciences
Chromatography paper	GE Healthcare Life sciences
Safe lock 2.0ml tubes	Eppendorf
Safe seak 1.5ml tube	Sarstedt
Cell scraper S	TPP
Cell scraper M	TPP
FACS titer micro test tube	Bio-Rad
Freezing tubes	Thermo Fisher Scientific
Freezing box	Biozym
Cover glass 24mm	BDH
0.45µm filter	GE Healthcare Life sciences

6.1.12 Technical equipment

Tool	Source
Heraeus Megafuge 16R centrifuge	Thermo Fisher Scientific
Centrifuge 5810R	Eppendorf
Rotor 75003624	Thermo Fisher Scientific
Rotor 75003629	Thermo Fisher Scientific
Rotor A-4-81	Eppendorf
MP-3AP power supply	MS Major Science
Gammacell 1000 Elite Irradiation machine	Nordion International
Vortex Genie 2	Scientific Industries
neoBlock1 2-25-03	Neolab
ABI7500 Real-time PCR System	Applied Biosystems
TrisStar Multimode reader LB942	Berthold technologies
Cary Eclipse Fluorescence Spectrophotometer	Cary Eclipse
Victor3 1420 Multiwell counter	Perkin Elmer
FACS Canto II	BD Biosciences
Professional Trio Thermocycler	Biometra
ECL Chemostar	Intas
Sonopuls	Bandelin
NanoDrop2000	Thermo Fisher Scientific
UV-Crosslinker	Vilber
ZEISS LSM880	Zeiss
Seahorse XFe96 Analyzer	Agilent technologies
Spark plate reader	Tecan
Leica microscope	Leica
Olympus Fluoview FV3000	Olympus

6.1.13 Software

Software	Source
Cary Eclipse Ratio application software version 1.2 [146]	Agilent technologies
Cary Eclipse Kinetics application software version 1.2 [146]	Agilent technologies

Wave 2.4.3	Agilent technologies
BD FACS Diva II	BD
GraphPad Prism 5/8	Graphpad
MS Office	Microsoft
Flowjo 9.4.10	Treestar
7500 Software v2.3	Applied Biosystems
Mikrowin 2000	Mikrotech
Morpheus	Broad Institute
Benchling	Benchling
Biolegend LEGENDplex Data analysis software	Biolegend
BioRender	BioRender
ImageJ	US National Institute of Health
Zeiss Zen microscopy software	Zeiss
OMERO	Open microscopy environment
The Sequence manipulation suite	Stothard Paul

6.2 Methods

6.2.1 Cytological methods

6.2.1.1 Cell maintenance

The cells were cultured in either RPMI or DMEM containing 10% heat-inactivated FBS and maintained at 37°C and 5% CO_2. The medium of primary cells or $CD8^+$ T cells was supplemented further with 50µM 2-ß-mercaptoethanol (M2). The cells were split every three to four days, depending on their confluency. If the cells were adherent, the vessel was first washed with PBS and then cells were harvested after trypsinization with 0.05% trypsin-EDTA solution. If the cells were semi-adherent or in suspension, cells were harvested and centrifuged at 319g for 5min, split accordingly and then transferred to a new vessel. Cells were counted using a Neubauer cell counting chamber. Unless otherwise stated, cells were centrifuged in a falcon at 319g for 5min.

6.2.1.2 Generation of dendritic cells from bone marrow

The mouse was sacrificed using cervical dislocation. The skin around the legs was disinfected with 70% ethanol and then removed by cutting. The legs were then detached by cutting the

femur at the hip joint. The muscle tissue surrounding the bone was removed and each leg was separated at the knee joint. The tibiae and the femur were cut at each end to expose the bone marrow. The bone marrow was flushed out with M2 several times to collect the bone marrow cells. Red blood cells were lysed using 5ml of diluted BD Pharm Lyse buffer for 1min at room temperature (RT), filtered through a 70µm strainer to retain bone fragments or unwanted tissue and adjusted to $5x10^6$ cells/ml. A total of $5x10^6$ cells in 10ml of M2 supplemented with 100ng granulocyte-macrophage colony-stimulating factor (GM-CSF) (obtained from the supernatant of GM-CSF expressing B16 cells) were seeded in a 10cm dish (Day 0). On Day 3, 10ml M2 supplemented with 100ng GM-CSF were added to the dish. On Day 6, 10ml were aspirated from the dish and fresh 10ml M2 with GM-CSF were added. Bone marrow-derived dendritic cells were harvested and used on Day 7 by scraping.

6.2.1.3 $CD8^+$ T cell culture maintenance

$CD8^+$ specific T cells required a weekly restimulation with the respective cognate peptide. $CD8^+$ T cells which were shown to be specifically activated after at least two restimulations (see 4.2.1.3.3) were frozen on Day 3 or 4 post-restimulation. Cells were used from Day 5 on.

6.2.1.3.1 Isolation of splenocytes

The mouse was sacrificed by cervical dislocation. The skin was disinfected with 70% ethanol and the spleen was removed. The spleen was homogenized on a 70µm filter placed on a 6cm dish containing 5ml M2 with the back of a syringe plug. The solution containing the splenocytes was poured through a 70µm filter and the remaining cells on the 6cm dish were collected in a falcon as well. The dish was washed with fresh medium to take the remaining cells. After centrifugation cells are lysed with 5ml of diluted BD Pharm Lyse buffer for 1min at room temperature and then resuspended in M2 to dilute the lysis buffer and prevent excessive cell damage. Isolated splenocytes were irradiated at 3000cGy in the Gammacell 1000 Elite. Subsequently, cells were counted (1. dilution: 1:10 with M2 medium; 2. dilution: 1:4 with acetic acid and trypan blue in a ratio of 1:2:1, respectively; final dilution 1:40) and adjusted to a final cell number of $12x10^6$ cells/ml.

6.2.1.3.2 Restimulation of $CD8^+$ T cells

$CD8^+$ T cells were previously generated by the members of the working group and its generation has been described in [66]. EL4 cells were scraped, collected in a falcon and irradiated with 10 000 cGy. After the irradiation, cells were washed with only medium (not

supplemented) and separated into two falcons, for the available cell lines, B8 and Ova. The EL4 cells were centrifuged, supernatant discarded and pellet resuspended in a final volume of one milliliter and incubated with 1ng/ml of the specific peptide ($B8_{20-27}$ TSYKFESV or $Ova_{257-264}$ SIINFEKL) for 30min at 37°C and 5% CO_2. Peptide-loaded EL4 cells were washed in M2 to discard excessive unbound peptide and adjusted to $1x10^6$ cells/ml. In each well of a 24-well plate, 500µl of $12x10^6$ cells/ml splenocytes, 500µL specific peptide-loaded (either B8 or Ova) EL4 cells, 500µl of $CD8^+$ T cells (either B8 or Ova) (final dilution 1:4) and 500µl of 20% T cell growth factor (TCGF) (medium from rat splenocytes stimulated with Concanavalin A) were mixed and incubated for one week.

6.2.1.3.3 Peptide activation assay

$CD8^+$ T cells were kept in culture at least for two restimulations and tested for their specificity and functionality before usage. For testing DC2.4 cells were harvested and adjusted to $4x10^6$ cells/ml. One milliliter of DC2.4 cells was plated in a 96-well dish and loaded with different concentrations of either B8/Ova peptide (from 1000ng/ml to 0.1ng/ml) or negative control group (either the non-cognate peptide (NC) or medium (Ø)). DC2.4 cells were incubated with the corresponding peptides for 30min at 37°C and 5% CO_2. To discard the medium, the plate was centrifuged at 300g for 2min. $CD8^+$ T cells were harvested and adjusted to $4x10^6$ cells/ml (1:40 dilution with trypan blue, acetic acid and medium). $CD8^+$ T cells at a density of $4x10^5$ (either B8 or Ova) were co-incubated with the peptide or control peptide-loaded DC2.4 cells and 1.25µg/ml brefeldin A at 37°C and 5% CO_2 for four hours. Cells were stained according to the $CD8^+$ T cell staining protocol described in 4.2.4.1.1.

6.2.1.4 Transfection of CM cells for gene expression

The day prior to transfection, 1.5×10^5 cells were seeded in a well of a 6-well plate. The plasmid DNA (either 3µg P2RX7 or pcDNA3) was dissolved in 150µL Opti-MEM and mixed with 1µl of PlusReagent. The solution was then incubated at RT for 5min. Lipofectamine (3µl) was added and the DNA-Lipofectamine mix was further incubated for 30min at RT. The medium of the cells was changed to OptiMEM and the DNA-Lipofectamine mix was added dropwise to the cells for incubation overnight. The next day, the medium was changed to the regular cell culture protocol and two days post-transfection selection with 0.2mg/ml geneticin was started. After selection, successful transfection was tested by expression analysis, western blot (WB) analysis and calcium measurements assays.

6.2.1.5 Transfection of HEK293 cells for generation of lentivirus

The day prior to transfection, $3.8x10^6$ HEK293 cells in (DMEM 10% FBS) were seeded in a 10cm dish and incubated at 37°C and 5% CO_2. The next day, 500µl serum-free DMEM was mixed with 5µg pMD2.G, 5µg psPAX2, 10µg of the RP-557_P2RX7_KO transfer plasmid and 60µg PEI, thoroughly mixed and incubated at RT for 15min. Meanwhile, the medium of the HEK293 cells was changed to serum-free medium and then the DNA-PEI mix was carefully added to the cells for incubation at 37°C and 5% CO2 for 8h. The medium was then changed to complete DMEM and the cells incubated for a total of two days. Thereafter, the supernatant was harvested, passed through a 0.45µm filter, aliquoted and frozen at -80°C or immediately used for lentiviral transduction.

6.2.1.6 Lentiviral transduction

The day prior to transduction $1.5x\ 10^5$ CM cells were seeded in a 12-well plate and incubated at 37°C and 5% CO_2. The next day, the medium was replaced with lentiviral supernatant supplemented with 8µg/ml polybrene and centrifuged at 380g at 37°C for 1h. The cells were then immediately incubated at 37°C. Fresh medium was added the next day to dilute down the polybrene and cells were further incubated for three days. Puromycin selection (0.5µg/ml) was started four days post-transduction.

6.2.1.7 *In vitro* toxicity assay

The assay used allows determination of the toxicity of a substance based on the cleavage of the tetrazolium ring in MTT by dehydrogenases in the mitochondria of living cells. On the day prior to the assay, 7500 cells/well of a 96-well plate were seeded (in 100µl final volume). The next day, the medium was aspirated and 90µl fresh medium was added to each well. Different concentrations of A740003 and DMSO were prepared in such a way that by the addition of 10µl of the sample, the desired concentration was achieved in the respective well. In total, 10µl of substrate to be tested were added to each well and incubated for 24h at 37°C and 5% CO_2. 10µl of a 5mg/ml stock solution of MTT were added to each well and the plate was further incubated for 4h. Then 100µl of *in vitro* toxicity assay lysis buffer were added and the plate was incubated overnight. The next day the absorbance at 570nm was measured and the survival rate relative to the control was calculated.

6.2.1.8 MVA infection

In general, MVA infection was performed in a 15ml falcon, unless otherwise stated. For this, a maximum of $2x10^6$ cells was harvested in 200µl in a falcon and the desired amounts of MVA were added to the cell pellet and the mixture was dissolved. Infected cells were incubated at 37°C and 5% CO_2 for two hours, with intermittent shaking every 15min. After incubation, cells were washed twice with medium and then plated for the indicated time points. For titration analyses or infection for subsequent isolation of RNA, cells were first seeded in a 6-well plate and let adhere prior to infection. For titration analyses or RNA expression analyses, cells were infected one hour at RT (0h time point) or one hour at 4°C (0h time point), respectively, prior to harvesting or incubation for extended time points.

6.2.1.9 Isolation of different fractions

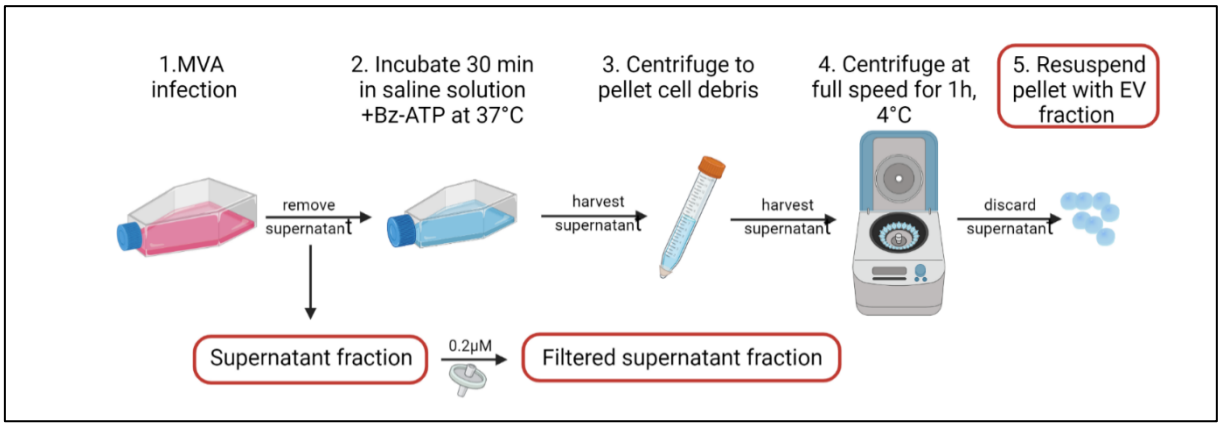

Figure 2: Workflow for the isolation of different subcellular fractions. CM cells were MVA-infected and incubated for 20h. The supernatant was taken and either immediately used for assays or passed through a 0.2µm filter. The cells were further incubated with saline solution and Bz-ATP at 37°C for 30min. The supernatant was harvested and centrifuged to discard cell debris. The obtained supernatant was further centrifuged at full speed at 4°C in a tabletop centrifuge for 1h and the resulting pellet with the extracellular vesicle (EV) fraction was used for downstream assays. The figure was created using Biorender.com.

6.2.1.9.1 Isolation of extracellular vesicles (EVs)

To isolate extracellular vesicles from cells, a high number of cells in culture was required. The protocol suggested by the working group of Elena Adinolfi (University of Ferrara, Italy) was adapted to our MVA infection conditions. The day prior to MVA infection cells were seeded in five T75 flasks for each condition to obtain a confluent cell monolayer. On the day of infection, the cells of one of each flask were counted to estimate the cell number and maintain the MOI similarly throughout all conditions and biological replicates. To ensure the isolation of comparable amounts of cells, only as many flasks were used that allowed to obtain approximately $3x10^7$ total cells. The medium was aspirated and cells were washed once. Three

milliliter medium was added and the cells were infected with a multiplicity of infection (MOI) of 1.5 with MVA-PK1L-Ova. For isolation of RNA, cells were incubated for 1h at 4°C (0h time point) while shaking every 15min. Afterwards, cells were harvested (for the 0h time point) or washed and further incubated for the desired time point (Isolation of RNA). For the isolation of extracellular vesicles for protein extraction or cross-presentation assay, cells were washed after the two hour infection and new medium was added to the T75 for 18 more hours.

For isolation of the vesicles, the medium was aspirated and the cells were washed with PBS. Three milliliter saline solution per T75 was added and cells were stimulated with 200µM Bz-ATP for 30min at 37°C and 5% CO_2. The saline solution was harvested in a 15ml falcon and centrifuged at 230g for 5min to remove cell debris. The supernatant could be used for cross-presentation. For this purpose, the virus was inactivated via PUVA treatment, aliquoted in 1.5ml Eppendorf tubes and centrifuged at full speed for one hour at 4°C. The supernatant could also be directly aliquoted and centrifuged (for protein or RNA isolation). After centrifugation the supernatant was discarded and the pellet containing the extracellular vesicle fraction (EV-fraction) was resuspended in either lysis buffer (protein isolation, RNA isolation) or PBS (Cross-presentation). With this method, only the bigger fraction of vesicles, hence the apoptotic bodies and the microvesicles were isolated.

6.2.1.9.2 Isolation of supernatant and filtered supernatant fraction

After 20h infection with MVA-PK1L-OVA (as described above), $2x10^6$ cells were harvested, centrifuged at 230g for 5min to pellet the cells and the supernatant was either immediately used for protein extraction or the viral particles inactivated via PUVA treatment for the cross-presentation assay (sup-fraction). This supernatant was further passed through a 0.2µm filter to remove apoptotic bodies (fil sup-fraction).

6.2.1.10 Cross-presentation assay

For cross-presentation assays, Cloudman (S91 melanoma) cells were used as MHCI mismatched feeder cells. This ensured antigen presentation only from the BMDCs to the $CD8^+$ T cells. $2x10^6$ cells were either mock or MVA-PK1L-Ova infected at MOI 1 as described above and incubated overnight (≈20h) at 37°C and 5% CO_2. The next day, the cells were first incubated with 1µg/ml psoralene at 37°C and 5% CO_2 for 15min and then further irradiated with UV-A for 15min. The cells were then harvested, washed twice with M2 medium to discard any remaining viral particles and co-incubated with previously generated BMDCs (4.2.1.2) at a ratio of 1:1 for 20h. As a control for the functionality of the BMDCs, dendritic cells were

infected (MOI1, MVA-PK1L-Ova) in parallel to check their activation the next day. On the third day, $2x10^5$ of the respective $CD8^+$ T cell line was co-incubated for 4h in the presence of 1µg/ml BFA and 100µl of the CM/BMDC mixture (containing $2x10^5$ BMDCs), which had been previously harvested and resuspended in 1ml final volume. Subsequently, the cells were stained for activation markers of $CD8^+$ T cells as described above. In addition to this, the CM/BMDC mixture was also stained with fluorochrome-labelled antibodies to check for activation markers of dendritic cells or the surface expression of the SIINFEKL peptide on the MHCI of the dendritic cells.

6.2.1.10.1 Adjusted assay for A740003 treatment

A740003 is a potent and competitive P2RX7 antagonist. In order to block P2RX7 activity, CM cells were treated with 20µM A740003 inhibitor in a shaking incubator for one hour prior to MVA infection. The infection was then performed as described above and the CM cells were incubated for 20h in the presence of the A740003 inhibitor. The next day, CM cells were first PUVA inactivated and the assay continued as described above.

Apyrase treatment

Apyrase is an ATP-diphosphohydrolase and catalyzes the hydrolysis of ATP. To understand whether ATP played a role during the co-culture period of CM and BMDCs, 1U/ml of apyrase was added to the co-culture of mock or MVA-infected CM cells and BMDCs for 20h. The next day, apyrase was washed away prior to the addition of $CD8^+$ T cells. The assay was then performed as described above.

Addition of extracellular vesicles/supernatant/filtered-supernatant

The fractions were isolated as described in 4.2.1.9 and were added to the co-culture of CM cells and BMDCs (Day 2). For the extracellular vesicle fraction, the isolated sample was split in two to add one half to either mock-infected or MVA-infected CM cells with BMDCs. In the assay with the supernatants, the supernatant of $2x10^6$ CM cells (MVA-infected CM pcDNA3 or CM P2RX7 cells) was used. On the third day, the cells were washed and the experiment was continued as described above.

6.2.1.11 Titration assay

CM cells ($1x10^6$) were seeded in a 6-well plate and were allowed to adhere for 2h. For the infection, the medium was replaced with one milliliter of fresh medium and MVA-P7.5-GFP

(MOI5) was directly added to the well. Cells were incubated at RT for one hour with intermittent shaking every 15min. After one hour, the supernatant was replaced with fresh medium and for the 0h time point cells were harvested by scraping. For the remaining time points, the medium was replaced and the cells were further incubated at 37°C and 5% CO_2 until the harvesting time point, washed and collected. The collected samples were vortexed harshly, frozen and thawed three times (-80°C/water bath) and subsequently sonicated for 3min. These samples were used to titrate the viral particles on MVA-permissive DF-1 cells [135]. For this, $1.5x10^4$ DF-1 cells in 100µl final volume (5% FBS in RPMI) were seeded in each well of a 96-well plate the day prior to titration. To assess the viral titer, 100µl of a serial dilution (performed in 2% FBS in RPMI) of the sample was added to DF-1 cells. After one week of the addition of the infected sample to calculate the tissue culture infectious dose 50 ($TCID_{50}$), the fluorescent signal or cytopathic effect (CPE) could be monitored.

6.2.2 Molecular Methods

6.2.2.1 Isolation of DNA

DNA isolation was performed according to the QIAmp DNA Mini Kit. Briefly, $2x10^6$ cells were harvested and resuspended in 200µl PBS, 20µl Qiagen proteinase K and 200µl AL buffer for incubation at 56°C for 10min. After the addition of 200µl absolute ethanol, to allow DNA binding to the column, the sample was applied to a QIAmp spin column. Different centrifugation steps and washing steps were performed prior to the elution of DNA into AE buffer.

6.2.2.2 Isolation of DNA from gel fragments

The desired band was excised from an agarose gel by cutting with a sharp scalpel. The DNA from the gel piece was extracted using the NucleoSpin® Gel and PCR Clean-up Kit according to the manufacturer's instructions. Briefly, the gel piece was weighted, dissolved in NT1 buffer at 50°C and then loaded onto the NucleoSpin Gel and PCR Clean-up column, washed and eluted using Buffer NE.

6.2.2.3 DNA sequencing

DNA (100ng), 2µl of 10µM primer (forward or reverse primer) in a final volume of 17µl in a 1.5ml Eppendorf tube was sent to sequencing at Eurofins Genomics.

6.2.2.4 RNA extraction

RNA was isolated according to the RNeasy Mini Kit of Qiagen. Briefly, cells were resuspended in 350µl RLT buffer supplemented with 2-ß-mercaptoethanol, one volume of 70% ethanol was added and transferred to an RNeasy Mini spin column. The flow-through was discarded and the column was treated with DNaseI and incubated at RT for 15min. After subsequent washing steps, the RNA was eluted in RNase-free water. To increase RNA yields, the sample was placed again on the column and repeatedly eluted.

6.2.2.5 cDNA synthesis

Reverse transcription of RNA was done according to the Revert Aid H Minus First strand cDNA synthesis kit of Thermo Fisher Scientific. For this, 2µg of total RNA was mixed with 1µl random hexamer primer, 4µl 5x reaction buffer, 1µl RiboBlock RNase inhibitor (20U/µl), 2µl 10mM dNTP mix, 1µl of Revert Aid H Minus M-MuLV reverse transciptase (200U/µl) and nuclease free water up to 20µl. The sample was incubated at 25°C for 5min, followed by a reaction at 42°C for 60min and the termination of the reaction at 70°C for 5min. The final product was diluted 1:50 for subsequent use for RT-PCR (real-time polymerase chain reaction).

6.2.2.6 RT-PCT

For expression analyses, 10µl of SYBR Select Master Mix were mixed with 1µl of each (forward/reverse) primer (10µM), 2µl of diluted cDNA and 6µl of RNase-free water. As a housekeeping gene and relative expression analyses the *18s rRNA* was used.

The DNA polymerase was activated in the first step at 95°C for 2min and subsequently 40 rounds of denaturation at 95°C for 15s and annealing/extension at 60°C for 1min steps were performed. After each run, the melting curves of all the samples were manually inspected to exclude unspecific primer binding and amplification.

6.2.2.7 Protein isolation

The cells were harvested, pelleted and washed with PBS. The pelleted cells were lysed using RIPA buffer supplemented with protease inhibitor (1:100) and further isolated by three rounds of freeze-thaw cycles and 3min of sonication. The samples were then centrifuged at full speed for 5min in a pre-cooled (4°C) tabletop centrifuge and the supernatant was used for protein analyses.

6.2.2.8 Protein quantification

The amount of protein in a sample was quantified using the Pierce BCA protein assay kit. For this, 50 parts of Reagent A were mixed with one part of Reagent B and 200µl of this solution were added per sample. 20µl of protein sample or 20µl of the serial dilution of bovine serum albumin (BSA) standards was added to each well with A+B solution and the 96-well plate was incubated at 37°C for 30min and then at RT for 20min. The absorbance at 562nm (precision mode) was measured and used to calculate protein amounts based on the BSA standard curve.

6.2.2.9 SDS-PAGE and Western Blot

In total, 15µg protein were mixed with 5x Lämmli buffer and boiled at 95°C for 5min. The sample was applied on a 10% polyacrylamide gel and let run at 80V for 10min and then at 100V for ≈2.5h. The gel was blotted using a semi-dry blotting device. Then the membrane was first incubated for 1h with a blocking agent (either 5% BSA or 5% skimmed milk in 1x TBST) and then with primary antibody at 4°C overnight with moderate shaking. The next day, the membranes were washed with 1x TBST (three cycles of 10min) and then incubated with a secondary antibody. Prior to detection, membranes were repeatedly washed and then incubated with a 1:1 dilution of the reagents in the Pierce ECL substrate kit for under dimmed light conditions for 1min. If the membrane was used for the detection of more than one protein, washing steps were extended to 15min each.

6.2.2.10 CRISPR/Cas9 cloning

6.2.2.10.1 Design of gRNA

For the design of a gRNA, a suitable genomic region without single nucleotide polymorphisms and untranslated regions at an early exon was searched in the UCLC Genome Browser (Santa Cruz, USA). This region was then used to design the gRNA on CRISPOR (Santa Cruz, USA) specific for the C57BL/6 strain (UCSC Dec. 2011 (mm10=C57BL/6J) + SNPs: C57BL/10)…) and the protospacer adjacent motif (20bp, NGG-SpCas9, SpCas9-HF1, espCas9 1.1). One suggested gRNA with characteristics for a successful knockout (such as a high “specific score” [depicting specificity], a high “Doench´16” [depicting efficiency] value and a low off-target number) was chosen [136].

6.2.2.10.2 Design of primers for CRISPR/Cas9

To incorporate the gRNA sequence into the RP-557 transfer plasmid, two annealing primers with sequences at each end for cloning into the RP-557 plasmid were designed. The forward primer was constituted of the gRNA itself, without the PAM sequence and with 5' ACC overlaps. For the reverse primer, the reverse complement of the gRNA (without PAM sequence) was designed using the website (https://www.bioinformatics.org/sms/rev_comp.html) and 5' AAAC overhangs were attached. Primers were ordered at Eurofins Genomics, dissolved to a final concentration of 100pmol/µl, and used for the subsequent cloning steps.

6.2.2.10.3 Cloning for CRISPR/Cas9

Vector digestion

Generally, 5µg of RP-557 were incubated with 0.3µl of DTT (100mM), 3µl of Tango yellow buffer (10x), 1µl *Esp3*I and water up to 30µl at 37°C overnight. The next day, the digested vector was mixed with gel-loading purple dye (6x) and loaded on a 1% agarose gel (1x TBST). The gel was run at 100V for approximately one hour and the upper band (11557 bp) was excised for gel elution as described above.

Annealing of oligonucleotides

In total, 1µl of *P2RX7_gRNA_fw* and 1µl of *P2RX7_gRNA_rev* primer were mixed with 23µl of annealing buffer and incubated in a thermocycler as follows:

95°C – 5min
85°C – 5min
75°C – 5min
65°C – 5min
55°C – 5min
35°C – 5min
25°C – 5min
15°C – ∞

Ligation reaction

In total, 50µg of gel-eluted RP-557 vector were incubated with 10µl Quick ligase buffer (2x), 1µl of quick ligase, 1µl of annealed oligonucleotides (1:10 dilution) and up to 20µl ddH_2O in a 1.5ml Eppendorf tube at RT for 10min.

Bacterial transformation

Competent *E.coli* XL-1 blue cells were transformed by a 10min thawing step on ice and subsequent addition of 3µl ligation reaction. Cells were incubated on ice for 10min and then heat-shocked at 42°C for 45s . Bacteria were placed on ice for 2min and then incubated with 400µl lysogeny broth (LB) medium at 37°C in a shaking incubator. Transformed bacteria were plated on a LB- agar plate supplemented with 100µg/ml ampicillin and incubated at 37°C overnight. The next day, single clones were picked and grown in LB-medium (supplemented with 100µg/ml ampicillin). Plasmids were isolated from cultures grown from single colonies as described below.

Plasmid isolation

Plasmids were isolated using the Plasmid DNA purification protocol of the QIAprep Spin Miniprep Kit according to the manufacturer's instructions. Briefly, bacterial cells were pelleted and resuspended in 250µl Buffer P1. After the addition of Buffer P2, cells were mixed by inverting the tube multiple times and then buffer N3 was added and the cells centrifuged at full speed in a table-top centrifuge. The resulting supernatant was added to a QIAprep 2.0 spin column, the sample was centrifuged and the flow-through discarded. The column was washed multiple times with Buffer PB and Buffer PE and the plasmid was finally eluted in 50µl Buffer EB. The isolated plasmid was sent to sequencing with the primer *RP-557_seq* to confirm the insertion of gRNA and the absence of mutations.

6.2.3 Spectrofluorometric analysis

6.2.3.1 Calcium measurements assay

A maximum of $2x10^6$ cells were harvested, transferred to a 15ml falcon and resuspended in 200µl 1x saline solution supplemented with 250µM sulfinpyrazone and 1mM calcium chloride ($CaCl_2$). Then 4µM of the fluorescent indicator FURA-2 AM were added and incubated at 37°C in a water bath for 20min. The cells were then pelleted, resuspended in 2ml 1x saline solution (+ sulfinpyrazone and $CaCl_2$) and transferred to a 1ml thermostat quartz cuvette with a magnetic stirrer. Different Bz-ATP or ATP stimuli were added at 2min post-measurement start. As a control for FURA-2 AM loading cells were treated with 1mM ionomycin after 6min. If measurements should be performed without $CaCl_2$, 0.5mM EDTA was used to bind available calcium residues during the measurement. The excitation was set to 340/380nm and the emission at 505nm and intracellular calcium was determined by recalculation of values using a calcium standard curve.

6.2.3.2 Ethidium bromide pore opening assay

A maximum of $1x10^6$ cells were pelleted, resuspended in 2ml 1x saline saccharose solution (+ 1mM $CaCl_2$) and transferred to a thermostat quartz cuvette with a magnetic stirrer. 2µl of ethidium bromide were added and the recording was started. The cells were stimulated with Bz-ATP after 2min and then with 100µM digitonin after at least 7min of measurement. The samples were excited at 360nm and the emission recorded at 580nm.

6.2.4 Immunological methods

6.2.4.1 Flow cytometry staining protocols

The cells were transferred into a V-bottom 96-well plate prior to the staining. All incubation steps were performed on ice and in dimmed light conditions. All centrifugation steps were done at 300g in a pre-cooled centrifuge at 4°C. Unless otherwise stated, fixed samples were stable for up to five days at 4°C until analysis using FACS Canto II.

6.2.4.1.1 Intracellular $CD8^+$ T cell staining (ICS)

In total, 200µl ($4x10^5$) of cells were washed with PBS and first stained with the viability dye 506 for 20min. Subsequently, cells were washed with FACS buffer and then incubated with anti-CD8 eFluor 450 for 30min. Then cells were permeabilized with 100µl BD Cytofix/cytoperm and incubated for 15min. Thereafter cells were stained with anti-IFNγ FITC and anti-TNFα PE-Cy7 for 30min. Finally, cells were washed and resuspended in 1% PFA in PBS.

6.2.4.1.2 SIINFEKL/H2-Kb staining

For this staining, 200µl ($2x10^5$) of cells were washed and stained with the viability dye 660 for 20min. Cells were washed and incubated with anti-CD16/CD32 for 20min. The cells were then stained for anti-CD11c PE, anti-$H2K^b$ FITC and anti-SIINFEKL/$H2K^b$ PE-Cy7 for 30min. The samples were then washed and resuspended in 1% PFA in PBS.

6.2.4.1.3 Maturation staining

To analyze the maturation of BMDCS, 200µl ($2x10^5$) of cells were washed and stained with the viability dye 506 for 20min. Then cells were washed and incubated with anti-CD16/CD32 for 20min. The cells were then stained with anti-CD11c APC-Cy7, anti-CD86 APC, anti-CD40 PB

and anti-MHCII PE for 30min. After incubation, the samples were washed and resuspended in 1% PFA in PBS.

6.2.4.1.4 Intracellular P2RX7 staining

To detect intracellular P2RX7, $2x10^5$ cells were washed with FACS buffer and then permeabilized with 100µl of BD Cytofix/cytoperm solution for 15min. Cells were washed with 1x solution of BD PermWash solution and incubated with anti-P2RX7 for 1h. After a washing step, cells were further incubated with Goat anti-Rabbit IgG (H+L) cross-adsorbed secondary antibody, Alexa Fluor™ 488 rabbit for 40min and then fixed with 1% PFA in PBS.

6.2.4.1.5 Phosphatidylserine surface exposure staining

The staining for phosphatidylserine surface exposure was done according to the Apotracker-Green FITC manufacturer's instructions. Briefly, $2x10^5$ cells were incubated in 5µl of the diluted (1:10) Apotracker dye at RT for 20min. Additionally, cells were stained with the viability dye 660 as described above and immediately analyzed.

6.2.4.1.6 Legendplex assay

The Legendplex Multi-Analyte Flow assay Kit (Mouse Anti-Virus Response panel 13-plex) was used to determine presence of multiple cytokines in the supernatants extracted as described above. The standards were prepared by reconstitution with assay buffer and performance of a serial dilution as described in the kit. The supernatant samples were not diluted. In total, 25µl of assay buffer, 25µl of standards or supernatant sample and 15µl of mixed beads were mixed in a V-bottom plate and incubated at RT on a plate shaker for 2h. The plate was then centrifuged at 250g for 5min and the supernatant discarded. The plate was subsequently washed two times with 1x wash buffer and incubated for 1min. After addition of 25µl of detection antibody, the plate was sealed and placed on a plate shaker at RT for 1h. Immediately after, 25µl of Streptavidin-PE were added and the plate further incubated for 30min. After incubation, samples were washed and the beads resuspended in 1x wash buffer for detection. The data was analyzed using the Biolegend LEGENDplex Data analysis software following the step by step instructions of the program.

6.2.4.2 Confocal microscopy stainings

6.2.4.2.1 Live confocal microscopy staining

In total, $5x10^5$ CM cells were infected in a falcon with MVA-PK1L-OVA (MOI1) under shaking conditions for 1h. The cells were then plated in a well of a 6-well plate with a round cover dish for approximately 20h. The next day, cells were washed with 1x saline saccharose solution (+ 1mM $CaCl_2$) and then incubated with 2µM PKH26 and 2µM quinacrine dihydrochloride at 37°C for 15min. After incubation, the samples were washed and then the cover dish was placed in the appropriate confocal microscopy holder with 500µl 1x saline saccharose solution (+ 1mM $CaCl_2$) containing 0.5µM PKH26 and 2µM quinacrine dihydrochloride. The samples were then visualized using Olympus Fluoview FV3000 in live recording mode (40x magnification), acquiring an image every 10s. After acquisition of the first images, 200µM Bz-ATP dissolved in 500µl 1x saline saccharose (+ 1mM $CaCl_2$) were carefully added without disturbing the acquisition beam. The images were taken for a total time of approximately 20min.

6.2.4.2.2 Staining for infection with fluorescent MVA

In total, $5x10^5$ CM cells were infected in a falcon with MVA-PK1L-mCherry-OVA (MOI1) in shaking conditions for 1h and then plated in a 6 cm well with a round cover dish for approximately 20h. The next day, cells were washed with 1x saline saccharose solution (+ 1mM $CaCl_2$) and incubated with 2µM quinacrine dihydrochloride at 37°C for 15min. The samples were then washed with 1x saline saccharose solution (+ 1mM $CaCl_2$) and the cover dish was placed in the confocal microscopy holder with 1ml 1x saline saccharose solution (+ 1mM $CaCl_2$) containing 2µM quinacrine dihydrochloride. Images were acquired at 40x magnification using Olympus Fluoview FV3000.

6.2.4.2.3 Intracellular P2RX7 staining

In total, $5x10^5$ CM cells were infected in a falcon with MVA-PK1L-mCherry (MOI5) with intermittent shaking every 10min at 37°C and 5% CO_2 for 1h and then transferred onto a well of a 6-well plate with a cover dish inside. Cells were incubated at 37°C and 5% CO_2 for a total of 6h and then fixed with 4% PFA at RT for 15min. After a washing step with PBS, cells were permeabilized with 0.1% saponin (in PBS) at RT for 15min. Afterwards, cells were incubated with anti-P2RX7 at RT for 1h, washed and then further incubated with Alexa Fluor™ 488 Goat anti-Rabbit IgG secondary antibody at RT for 1h. Cells were washed with PBS, resuspended in 1mL PBS and stained with two drops of Nucblue fixed cell dye to stain the nuclear fractions. The cover glass with the stained cells was glued with ProLong Antifade mountant to a microscope slide for visualization using ZEISS LSM880 (40x magnification).

6.2.4.3 ELISA

6.2.4.3.1 IL-18

Detection of IL-18 was performed according to the instructions provided by the manufacturer (Mouse IL-18 ELISA Kit – MBL) and was done with the supernatants prepared in 4.2.1.9.2. For this, 100µl of supernatant or standard sample were pipetted in an IL-18 antibody coated 96-well plate and incubated at RT for 1h. The wells were then washed for a total of four times with wash solution. Then 100µl of conjugate were added to each well and incubated for another hour. After four rounds of washing steps, the plate was incubated with 100µl of substrate reagent for 30min. The reaction was aborted by addition of a stopping solution and the absorbance was read at 450nm. IL-18 amounts were calculated based on the absorbances of the IL-18 standard curve measured.

6.2.4.3.2 mIFN-α2/mIFN-ß

mIFN-α2 or mIFN-ß were detected using the bioluminescent LumiKine Xpress mIFN-α2 or mIFN-ß 2.0 kits with the supernatants prepared in 4.2.1.9.2. The white flat-bottom MaxiSorp 96-well plate was first coated with 50µl of anti-mIFN antibody at RT overnight. The next day, excess antibody was removed and the plate was incubated with 200µl blocking buffer (3%BSA and 0.05% Tween 20 in PBS) at 37°C for 2h. After removal of the blocking buffer, 50µl of supernatant sample or diluted standard solutions were added to the wells. Then 50µl of Lucia-conjugated detection antibody were added to each well and incubated at 37°C for 2h. The plate was then washed three times and 200µl of QUANTI-Luc detection solution were immediately added for acquisition of luminescence at the TrisStar Multimode reader LB942. The luminometer reading time was set to 0.1s.

6.2.4.4 Hoechst staining

Hoechst staining was performed to assess cell density in the Seahorse XF96 Cell culture microplate after performance of the Mitostress test (4.2.5.2). For this the medium of each well was replaced with fresh medium supplemented with 5µg/ml Hoechst dye and incubated at RT for 10min. The Hoechst stain was then detected using the Spark plate reader (Ex:358nm; Em:461nm).

6.2.5 Biochemical methods

6.2.5.1 ATP measurements

6.2.5.1.1 Intracellular ATP measurement

The day prior to infection, $5x10^4$ cells in 100µl final volume were seeded per well in white, flat bottom 96-well plate. The next day, the cells were infected by adding MVA-PK1L-Ova directly to each well and the plate was incubated at 37°C and 5% CO_2 and shaken every 10min for 1h. After a total of 6h, the assay to detect intracellular ATP was performed according to the Luminescent ATP detection Assay Kit manual. Briefly, 50µl of cell suspension or standard solution were added to each well and the plate was shaken for 5min. Then 50µl of substrate solution are added to each well and the plate was shaken and incubated for further 5min. The plate was placed in the dark for 10min and then the luminescence was measured using the Spark plate reader.

This assay was performed with the support of Julia Werner of the working group of Phillip Lang (University of Düsseldorf).

6.2.5.1.2 Extracellular ATP measurement

Extracellular ATP was assessed using the supernatants from $1x10^6$ cells as described above. In total, 50µl of Firezyme diluent buffer were mixed with either 50µl of supernatant or 50µl of diluted standard solution in a black 96-well plate. The plate was placed into the Victor3 1420 Multiwell counter and luminescence was measured upon automated addition of 100µL of Enliten Luciferase/luciferin reagent.

6.2.5.1.3 Apyrase testing

To test whether the apyrase was working as expected, the supernatant sample of CM P2RX7 cells was used for apyrase activity analyses. For this, 100µl of supernatant or different dilutions of ATP standards were mixed with 50µl of M2 medium and 50µl of 4x RealTime-Glo eATP assay reagent and incubated under shaking conditions for 1min. The luminescence was then measured using the TrisStar Multimode reader LB942.

6.2.5.2 Mitochondrial activity test

To assess the mitochondrial activity of the different CM cell lines under mock- or MVA infected conditions, $2x10^4$ cells in 80µl final volume were seeded in a Seahorse XF96 Cell culture microplate and let stand for 1h at RT prior to incubation overnight at 37°C and 5% CO_2. The

experimental procedures described above were in accordance with the Seahorse XF Cell Mito Stress test kit . One day prior to experiment, 20mlML of XF Calibrant were placed in a non-CO_2 37°C incubator and the sensors of the cartridge were hydrated by placing into water.

The next day, cells were infected in the plate by direct addition of MVA-PK1L-OVA (MOI5) for a total of 6h. The cartridge sensors were submerged into calibrant and placed in a non-CO_2 37°C incubator for 1h. The cells were washed with XF Assay medium and then 60µl medium was removed from the cells, replaced with 200µl assay medium and incubated in a non-CO_2 37°C incubator for 1h. Afterwards, cells were repeatedly washed and resuspended in 180µl final fresh medium volume. The different compounds were injected into the sensor cartridge to obtain the final concentrations of 15µM oligomycin, 5µM of FCCP and 5µM of Antimycin A + Rotenone. The plate was placed in the Seahorse XFe96 Analyzer to determine mitochondrial activity. This assay was done with the support of Ichiro Katahira from the working group of Philipp Lang at the University of Düsseldorf.

6.2.6 Statistical analysis

All statistical analyses were performed using GraphPad Prism 8. The statistical significance of two groups was calculated using the unpaired, two-tailed Student's t-test. The results are either depicted as mean ± standard deviation (SD) or the standard error of the mean (SEM). Data represented is from at least three (n=3) independent experiments (unless differently specified). The statistical significance (P) is shown as $P \leq 0.05$ (*), $P \leq 0.01$ (**), $P \leq 0.001$ (***) and $P \leq 0.0001$ (****).

7. Results

7.1 The P2X7 receptor in Cloudman cells and MVA infection

The surface P2X7 receptor was inactive in Cloudman wildtype cells

P2X7 receptor activity was reported to be monitored by measurements of the calcium flux in cells using fluorometric analysis [86].The fluorescent indicator FURA-2-AM binds free calcium within the cells and leads to the shift of the excitation to 340nm, which can be measured [137]. We investigated activity of the P2X7 receptor in CM cells either mock (CM) or MVA-infected with MOI 1 for 20h upon stimulus with the P2RX7 specific activator Bz-ATP [138]. Despite the stimulus, there was not a visible increase in intracellular calcium neither in mock nor in MVA-infected cells (Figure 3A). To confirm loading of the cells with FURA-2-AM, ionomycin was added to cells, which instantly led to an increase in intracellular calcium [139]. Bz-ATP is a potent activator of P2RX7 and has been shown to function when present in small amounts [140]. To exclude that the 200µM Bz-ATP, the standard concentration used in cells transfected with P2RX7 [121], is insufficient, we also stimulated CM cells with higher concentrations of Bz-ATP, hence 400µM and 800µM. However, independently of the Bz-ATP concentration used, we were not able to observe a peak for the increase of intracellular calcium (Figure 3B). We further investigated the activity of P2RX7 under more harsh stress conditions, hence by first infecting the cells with MOI of either 5 or 10 for 20h and then stimulating with Bz-ATP. There was no visible increase in intracellular calcium in neither of the conditions (Figure 3C). It was published that cells deriving from the DBA or C57BL/6 strain harbor the P451L mutation, rendering the P2X7 receptor activity less sensitive to ATP stimuli [86]. Indeed we confirmed this mutation in our CM cells, which is a melanoma cell line deriving from the DBA mouse strain (Figure 3D).

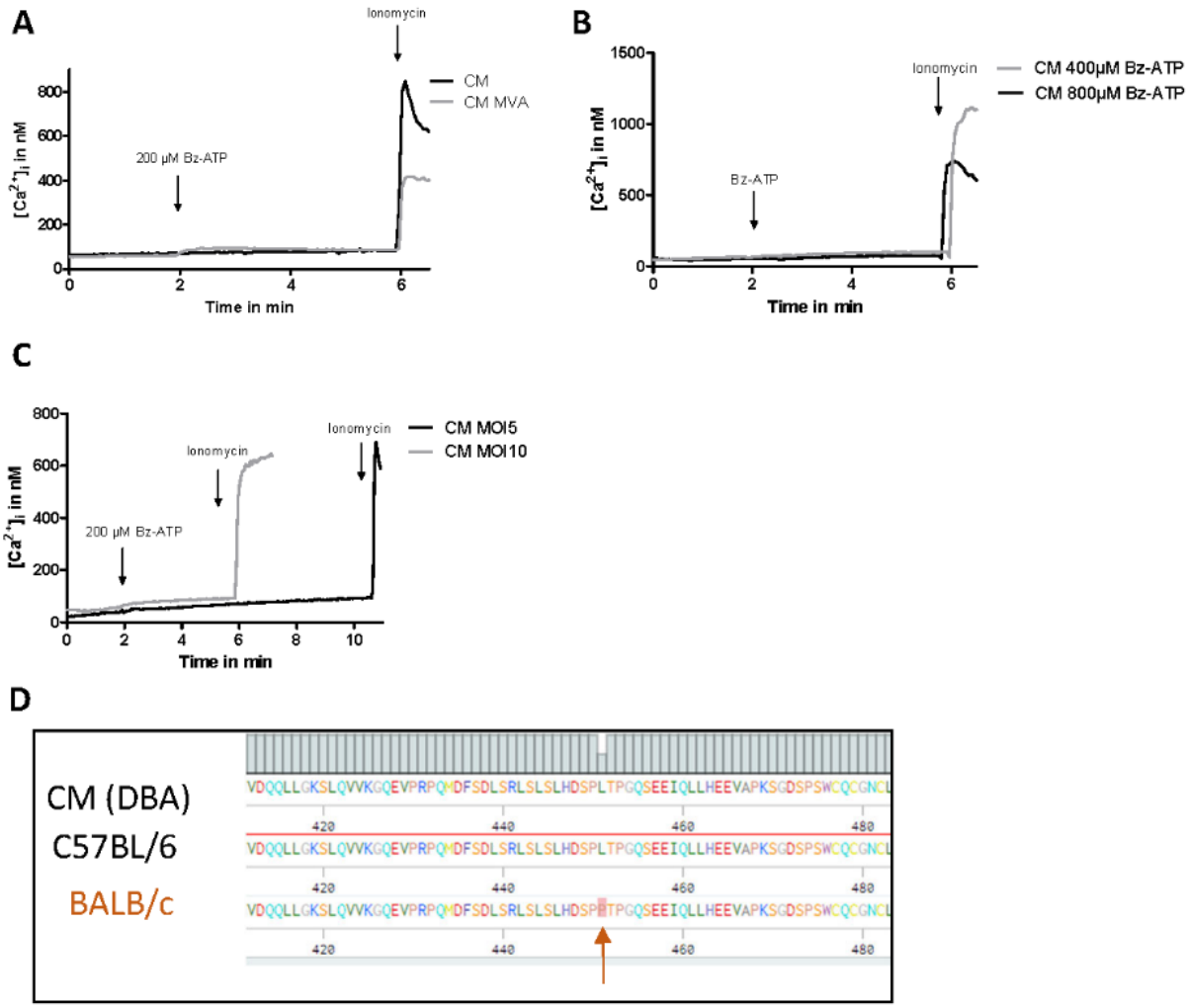

Figure 3: The surface P2X7 receptor in CM (DBA background) cells is not active. (A) MVA-PK1L-Ova (MOI1, 20hpi) or mock-infected CM cells were harvested and loaded with the fluorescent indicator FURA-2-AM (4µM). Cells were then stimulated first with 200µM Bz-ATP and then with ionomycin (1mM) before intracellular calcium concentrations were fluorometrically determined. (B) CM cells were harvested, loaded with FURA-2-AM (4µM) and stimulated with either 400µM (CM 400µM Bz-ATP) or 800µM (CM 800µM Bz-ATP) before analyzing intracellular Ca^{2+} concentration $[Ca^{2+}]_i$. (C) CM cells were infected with MVA-PK1L-Ova with either MOI5 (CM MOI5) or MOI10 (CM MOI10) for 20h. Cells were harvested, loaded with FURA2-AM for subsequent stimulation with 200µM Bz-ATP and ionomycin (1mM) and subsequently intracellular Ca^{2+} concentrations were determined. (D) Sequencing analysis of the locus leading to the P451L mutation in *P2rx7* (depicted by the red arrow) in CM cells (CM DBA) and the comparison to the complementary sequence in C57BL/6 and BALB/c mice. Data are pooled from n=3 independent experiments and shown as means (A-C).Sequencing results shown in D was a single experiment (n=1).

Stimuli with ATP led to increased intracellular calcium in CM cells

ATP is known as the main activator of members of the P2-family. Therefore, we used ATP at different concentrations, which is known to activate other the members of the P2-family, and measured intracellular calcium increase in CM cells [141]. We showed that a stimulus with ATP (both 3mM and 5mM) led to the increase of intracellular Ca^{2+}. The peak size and therefore the intracellular calcium was increasing with higher ATP stimuli, as expected (Figure 4A). In addition, the appearance of the peak can be described as desensitizing, hinting the presence

of other active P2- family members as well [142]. To prove that the increase in intracellular calcium was indeed caused by the presence of members of the P2- family and not by the release of intracellular calcium stores, the experiment was performed in the absence of $CaCl_2$. As shown in Figure 4B, there was no increase in intracellular calcium upon stimulus with ATP when there were no outside sources of calcium.

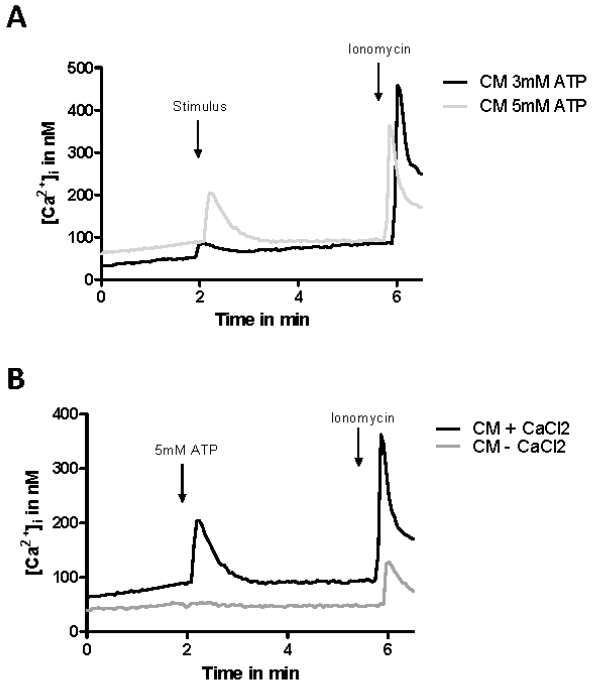

Figure 4: Other surface receptors of the P2- family are active in CM cells. (A) CM cells were harvested and loaded with the fluorescent indicator FURA-2-AM (4µM). Cells were either stimulated with 3mM ATP (CM 3mM ATP) or 5mM ATP (CM 5mM ATP) at the indicated time point and then subsequently treated with ionomycin (1mM) to measure intracellular calcium concentration. (B) Cells were harvested and loaded with FURA-2-AM (4µM) either in the presence of 1mM $CaCl_2$ (CM + CaCl2) or in the absence of $CaCl_2$ (CM – CaCl2) and then stimulated with 5mM ATP and ionomycin (1mM). Data are pooled from n=2 independent experiments and shown as means.

Transfection of CM cells with functional P2RX7 from BALB/c mice led to increased expression of *P2rx7* and increased intracellular Ca^{2+}

Different from C57BL/6 or DBA mice, cells deriving from BALB/c mice harbor an active variant of P2RX7 [86]. We transfected CM cells with this functional variant from BALB/c mice and with the pcDNA3 empty vector control, carrying the same antibiotic resistance as the P2RX7 transfer vector plasmid. Upon P2RX7 transfection we showed an increase in intracellular calcium upon Bz-ATP stimulus which was significant compared to the absent peak in CM cells (Figure 5A right). This effect was reversible upon A740003 treatment, a P2RX7-specific inhibitor. In contrast, CM WT or CM pcDNA3 cells did not show increased intracellular calcium upon stimulus (Figure 5A left). In addition to this, we also measured the expression of *P2rx7* in our CM, CM pcDNA3 and CM P2RX7 cells and in infected cells (from 0hpi to 24hpi).

Expression of *P2rx7* in CM P2RX7 cells significantly increased when compared to CM or CM pcDNA3 cells. In general, it seemed that infection with MVA led to increase in *P2rx7* expression in all the analyzed cell lines with a peak at 8hpi (Figure 5B). However it has to be mentioned, that the selected primers did not target all the P2RX7 variants.

We further performed an *in vitro* toxicity assay to ensure that the used P2RX7 inhibitor A740003 was not harmful for the cells (Figure 5C). Indeed, we showed that even at higher concentrations other than the used 20µM, A740003 had low toxicity as shown by the rather comparable survival rate to the DMSO control. Exception were CM P2RX7 cells at 100µM.

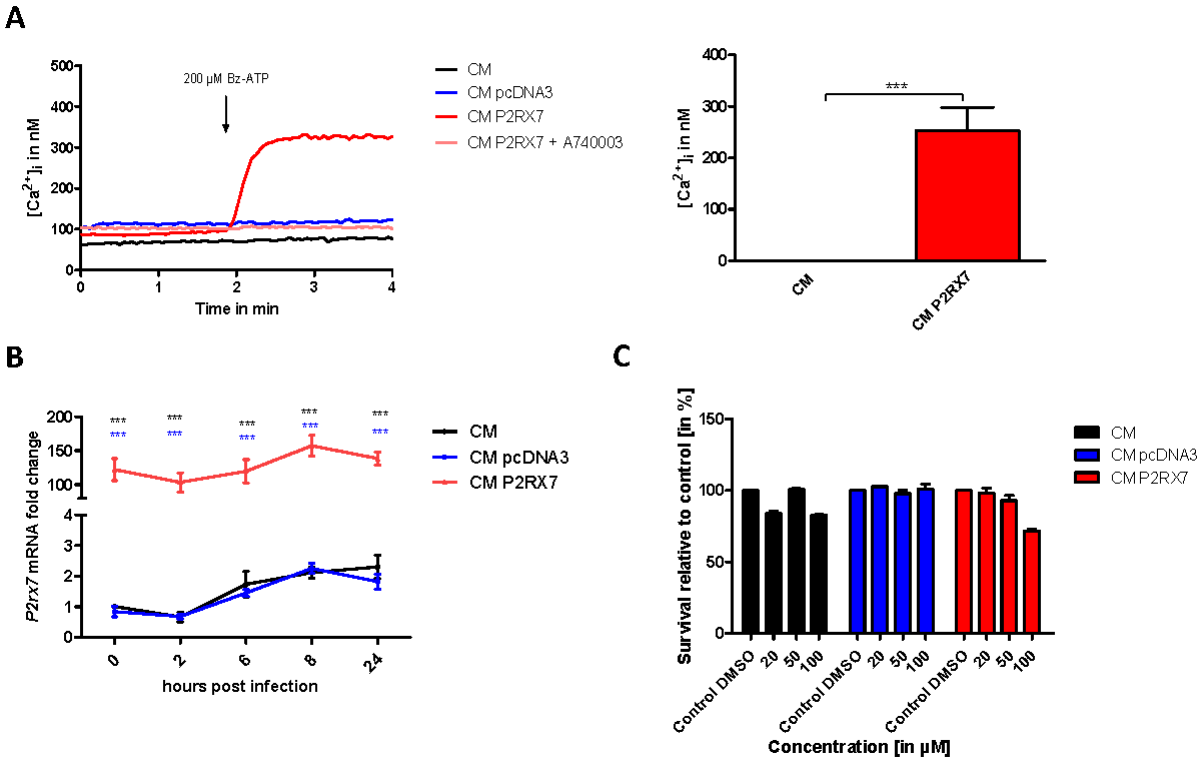

Figure 5: Transfection of CM cells with a functional P2RX7 variant from BALB/c mice restores P2RX7-specific functions. (A) (left) CM cells were either transfected with empty vector (CM pcDNA3) or P2RX7 containing plasmid DNA (CM P2RX7). CM P2RX7 were further pre-treated with 20µM A740003 (CM P2RX7 + A740003), loaded with fluorescent indicator FURA-2-AM (4µM) to assess intracellular Ca^{2+} concentration. (Right) Difference between the maximum concentration of intracellular Ca^{2+} and the basal concentration of CM and CM P2RX7 cells upon Bz-ATP stimulus. (B) CM, CM pcDNA3 and CM P2RX7 cells were infected with MVA-PK1L-Ova (MOI1) and harvested at the indicated time points post-infection to assess the expression of *P2rx7*. mRNA fold change is shown as the expression of the respective gene at each time point compared to the 0h time point of CM cells. (C) CM cells (WT, pcDNA3 or P2RX7 transfected) were incubated with the indicated concentrations of A740003 or control DMSO for 20h and then the survival rate was calculated relative to DMSO-treated cells. Data are pooled from n=3 independent experiments and are shown as means ± SD. P values indicate statistical significance (P) with ***P ≤ 0.001.

Early MVA infection led to increased intracellular calcium concentrations in CM P2RX7 cells

To further investigate the role of the P2X7 receptor in transfected cells, we infected cells with MVA for a short 4h (Figure 6A) or long 20h period of time (Figure 6B) and then stimulated with Bz-ATP. Interestingly, only after 4hpi we could observe a significant increase in intracellular calcium as when compared to uninfected CM P2RX7 cells (Figure 6A right). As previously described, strong P2RX7 activation can also lead to the so-called pore formation [83]. This opening allows large molecules, such as ethidium bromide to enter the cell [143]. We used ethidium bromide, which intercalates with DNA and becomes fluorescent once internalized, and stimulated CM, empty vector- or P2RX7 transfected cells (either mock- or MVA-infected) with Bz-ATP [77]. There was no difference in fluorescence intensity in neither the CM cells (WT or pcDNA3-transfected) nor the CM P2RX7 cells, concluding that there was no pore formation in these cells. As a positive control for the assay, digitonin was added to the cells (Figure 6C).

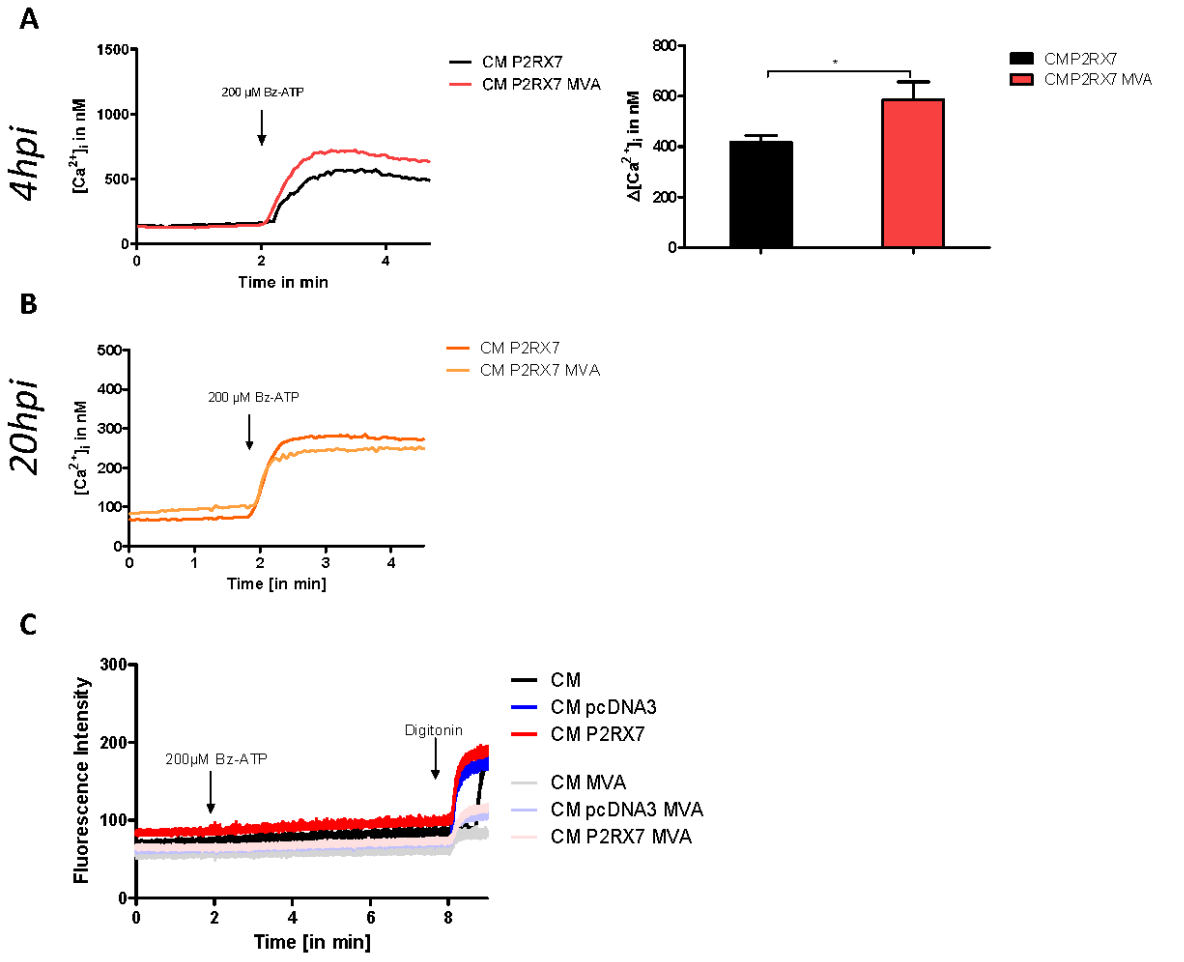

Figure 6: Early MVA infection enhances P2RX7 activity in CM P2RX7 cells but does not alter pore formation capacities of P2RX7 late in infection. (A) (left) CM cells transfected with P2RX7 containing plasmid DNA (CM P2RX7) were either mock- or MVA-PK1L-Ova-infected for 4h (MOI1). CM P2RX7 were loaded with the fluorescent indicator FURA-2-AM (4µM) to assess intracellular Ca^{2+} concentration.

(Right) Difference between maximum concentration of intracellular Ca^{2+} and basal concentration of CM P2RX7 and CM P2RX7 MVA cells upon Bz-ATP stimulus (200µM). (B) CM P2RX7 cells were either mock- or MVA-infected for 20h (MOI1). CM P2RX7 were loaded with fluorescent indicator FURA-2-AM (4µM) to assess intracellular Ca^{2+} concentration. (C) CM cells (WT, pcDNA3 or P2RX7 transfected) were incubated with EtBr (2µl) and then stimulated with 200µM Bz-ATP and 100µM digitonin (disrupts cell membrane, acting as a positive control for the assay) to measure fluorescence intensity. Data are pooled from n=3 independent experiments and are shown as means ± SD. P values indicate statistical significance (P) with *P ≤ 0.05.

MVA infected CM P2RX7 exhibited membrane blebbing characteristics

We wanted to investigate whether membrane blebbing would occur as P2RX7 activity is also associated with changes in membrane morphology [144]. Therefore, we infected our cells with MVA and analyzed their morphology under the microscope. As can be seen in Figure 7, cells appeared with distinct roundish forms. When infected, cell borders seemed to loosen, indicating a possible ongoing apoptosis process. Interestingly, stimulation with Bz-ATP in CM or CM pcDNA3 cells (mock- or MVA-infected) did not alter the appearance of the cells. However, when infected with MVA, CM P2RX7 cells exhibited a change in morphology, resembling the well-described P2RX7-dependent membrane blebbing [144]. It is noteworthy that besides the Bz-ATP stimulus, MVA infection was a pre-requisite for CM P2RX7 cells to rearrange the membrane.

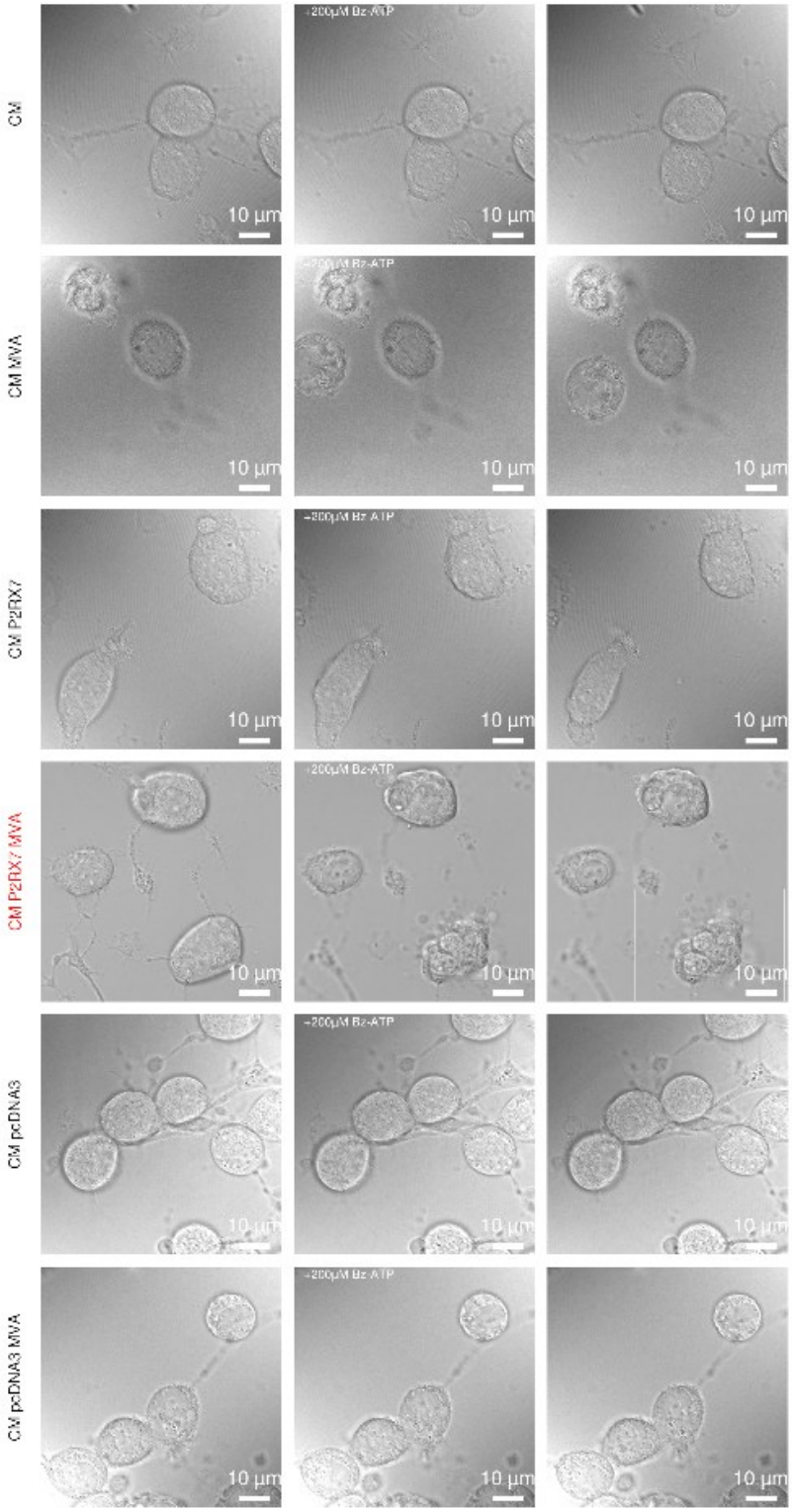

Figure 7: MVA infection in CM P2RX7 cells leads to P2RX7-dependent membrane blebbing. Various CM (CM, pcDND3 empty vector- or P2RX7-transfected) cells were either mock- or MVA-PK1L-Ova infected for 20h (MOI1). CM cells were imaged using 40x magnification at the Olympus Fluoview FV3000 with live imaging settings for a total time frame of 20min. The first row images represent the untreated time points (1min post recording), After 2min cells were stimulated with 200µM Bz-ATP as indicated (second row images). The third row images represent the indicated cells at 20min post-recording. Data are from n=1 experiment.

7.2 Role of P2RX7 in feeder cells during MVA infection and cross-presentation

Antigen cross-presentation was enhanced when using CM P2RX7 cells as feeders

One of the main objectives of this study was to analyze the role of P2RX7 in feeder cells during MVA cross-presentation. As previously stated, besides the importance of dendritic cells during cross-presentation, we speculated that feeder cells as source for the antigen play a crucial role for successful cross-presentation as well. For this purpose, we used CM cells (WT or transfected with pcDNA3 or P2RX7), infected them with or without MVA. These cells were first co-cultured with antigen-presenting cells overnight and lastly $CD8^+$ T cells were added for antigen recognition. We demonstrate that in the presence of a functional P2RX7 in MVA-infected CM feeder cells, antigen cross-presentation by APCs led to significantly higher $CD8^+$ T cell activation, as shown by increased IFNγ and TNFα production in $CD8^+$ T cells. This effect was evident in B8 and Ova- specific $CD8^+$ T cell lines in regards to the TNFα production. Additionally, the B8-specific $CD8^+$ T cell showed an increased IFNγ production (Figure 8A). In addition to the activation of $CD8^+$ T cells, we also analyzed the SIINFEKL/H2-K^b expression on the surface of BMDCs as another indicator of antigen cross-presentation. Consistent with the previous result, we demonstrated that cells harboring an active P2RX7 led to a significantly higher SIINFEKL/H2-K^b expression on the surface of BMDCs (Figure 8B left). The mean fluorescent intensity (MFI), hence the amount of SIINFEKL/H2-K^b complexes on the surface membrane per cell, reflects the SIINFEKL/H2-K^b expression on the surface of BMDCs (Figure 8B right). In order for the dendritic cells to present the peptide epitope to $CD8^+$ T cells, DCs must exhibit a distinct MHC phenotype to be recognized by $CD8^+$ T cells [145]. One of these molecules is the MHCI which is loaded with the antigen to be presented. We analyzed the production of this cell surface molecule on dendritic cells that were co-cultured with mock- or MVA-infected feeder cells and showed that dendritic cells in co-culture with mock-infected CM P2RX7 exhibited a significantly higher MHCI synthesis than DCs co-cultured with CM or CM pcDNA3 cells (Figure 8C left). The MFI of the MHCI on dendritic cells mimicked this effect (Figure 8C right). It seemed that the mere presence of P2RX7 in CM cells altered production of MHCI of dendritic cells.

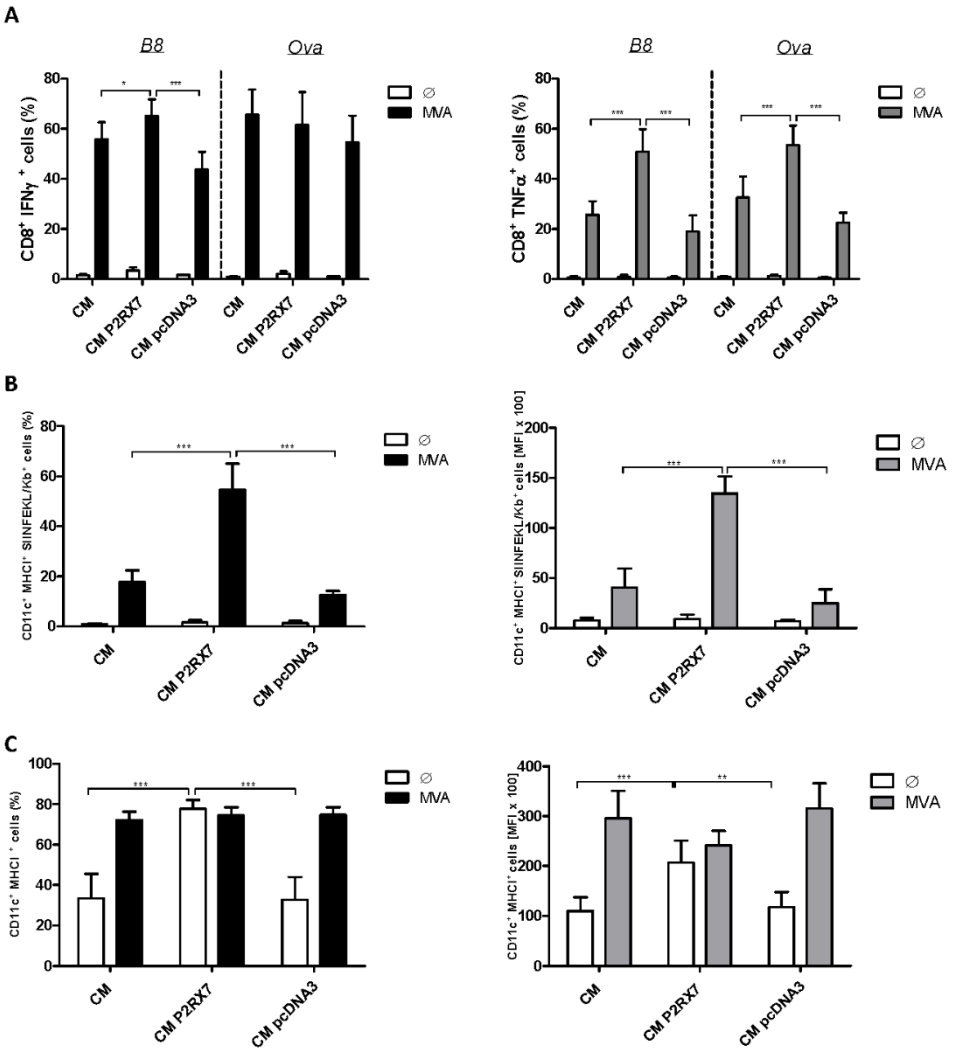

Figure 8: Presence of active P2RX7 in feeder cells enhances antigen cross-presentation capacity in dendritic cells. CM WT (CM) cells were either transfected with empty vector (CM pcDNA3) or P2RX7 containing plasmid DNA (CM P2RX7). Cells were infected with MVA-PK1L-Ova (MOI1) for 20h, harvested, PUVA inactivated and co-cultured with GM-CSF-treated bone marrow-derived dendritic cells (BMDCs) for 20h. (A) Cells were further co-cultured with B8-or Ova-specific $CD8^+$ T cells for 4h to assess IFNγ (left) or TNFα (right) production via flow cytometry (FACS). (B) Frequency (in %) (left) of SIINFEKL/H2-K^b expression on BMDCs and the respective mean fluorescent intensity (right) was measured. (C) Surface analysis of MHCI molecules on BMDCs and the respective mean fluorescent intensity (right) was measured. Data are pooled from at least n=3 independent experiments and are shown as means ± SD. P values indicate statistical significance (P) with *P ≤ 0.05; **P ≤ 0.01; P***P ≤ 0.001.

Specific inhibition of P2RX7 in CM P2RX7 cells mostly restored CM feeder cell phenotype during MVA antigen cross-presentation

Besides the empty vector control cell line (CM pcDNA3) we also wanted to confirm P2RX7-specific functions using a competitive inhibitor for the P2X7 receptor. A740003 is a strong antagonist used in various studies that specifically inhibits P2RX7 [93]. We used this inhibitor to pre-treat our CM feeder cells prior to MVA infection and then continued with the inhibition during the time frame of MVA infection. To prevent that the inhibitor affected the dendritic cells

and the $CD8^+$ T cells at later time points in the co-culture, the cells were thoroughly washed and the antagonist was completely removed for subsequent cross-presentation assays. We showed that pre-treatment of MVA-infected CM P2RX7 cells with A740003 significantly reduced TNFα synthesis in B8- and Ova-specific $CD8^+$ T cells when co-cultured with dendritic cells. However, IFNγ production remained unaltered in both, B8- and Ova-specific $CD8^+$ T cells, presumably due to the immediate synthesis of this cytokines in these cells when being minimally activated (Figure 9A). We further investigated the SIINFEKL/H2-K^b expression on the surface of BMDCs and noticed a significant reduction of SIINFEKL/H2-K^b complexes when MVA-infected CM P2RX7 cells were pre-treated with A740003 and then co-cultured with BMDCs (Figure 9B). Interestingly, pre-treatment of CM P2RX7 cells (mock- or MVA-infected) did not alter MHCI synthesis in BMDCs as compared to untreated cells (Figure 9C), hinting to a different trigger in CM P2RX7 cells, other than the surface P2RX7, being responsible for the stimulation of BMDCs and production of MHCI. The synthesis of other maturation markers, such as CD40 or CD86 on BMDCs was either not altered or even reduced, respectively, when CM cells harbored a functional P2X7 receptor. Inhibition with A740003 did not alter this phenotype (Supplementary Figure S1).

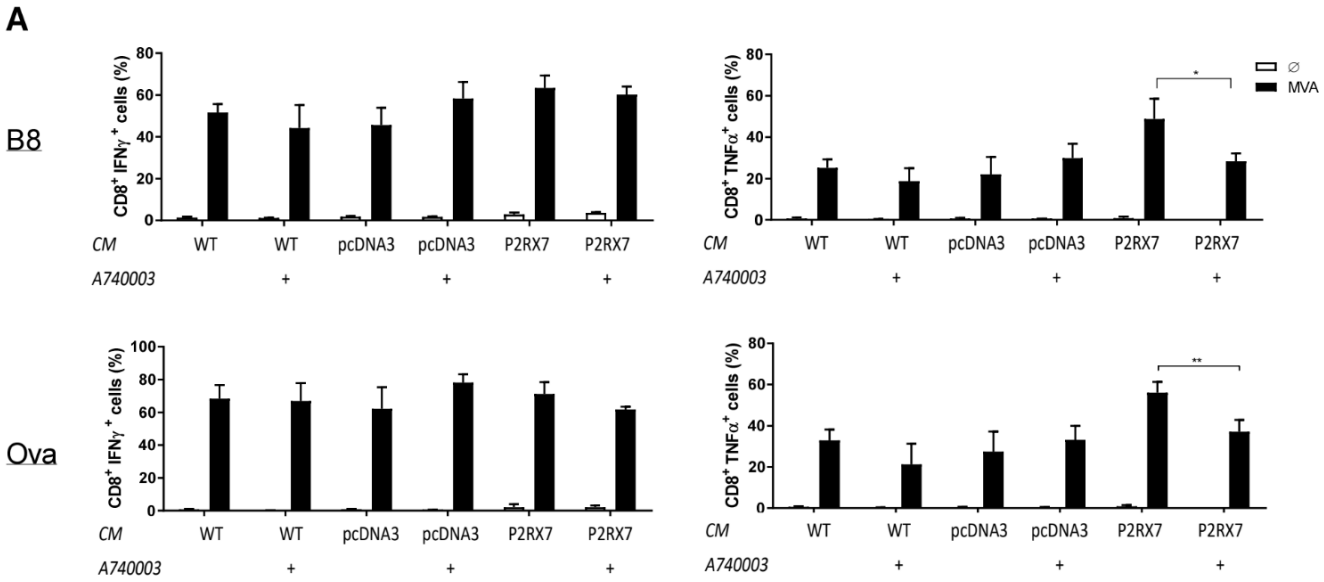

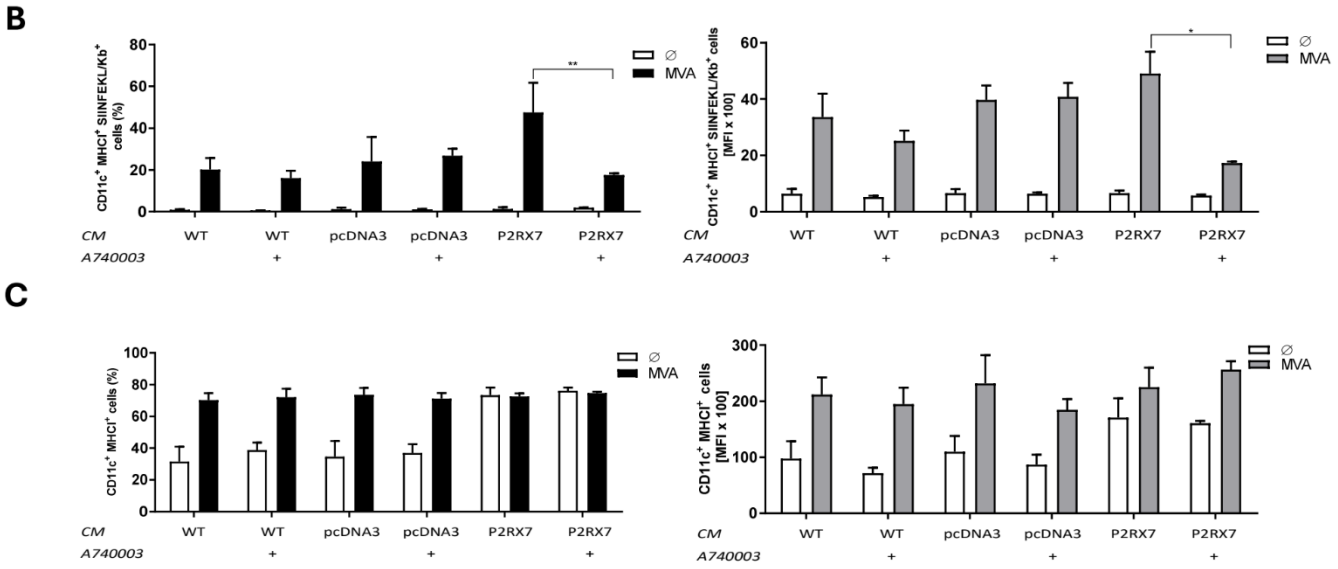

Figure 9: A740003 inhibition in MVA-infected CM P2RX7 cells reduces BMDCs mediated antigen-cross-presentation. CM cells (WT, pcDNA3- or P2RX7-transfected) were pre-treated with 20µM A740003 for 1h and then infected with MVA-PK1L-Ova for 20h. Cells were harvested, washed, PUVA inactivated and co-cultured with BMDCs for 20h. (A) CM/BMDCs co-culture was further incubated with B8- or Ova-specific $CD8^+$ T cells for 4h and IFNγ (left) or TNFα (right) production was assessed by flow cytometry. (B) CM/BMDC co-culture was used to determine SIINFEKL/H2-K^b expression on the surface of BMDCs (left image depicts the frequency in %, right image depicts the MFI). (C) MHCI expression on the surface of BMDCs in co-culture with mock-or MVA infected CM cells (untreated or A740003 pre-treated) (left image depicts the frequency in %, right image depicts the MFI). Data are pooled from at least n=3 independent experiments and are shown as means ± SD. P values indicate statistical significance (P) with *P ≤ 0.05; **P ≤ 0.01.

Viral entry is delayed, but replication is not altered in CM cells harboring a functional P2RX7

Due to our previous results in cross-presentation assays, we speculated whether the improved cross-presentation capacity of dendritic cells by the presence of P2RX7 in feeder cells was due to a better infectivity of the latter cells with MVA. For this scope, we infected our CM cells with MVA at different time points and determined the titer using DF-1 cells, an MVA permissive cell line to establish the $TCID_{50}$ [146]. Using a very high viral infectious dose (so-called one-step growth experiment), we observed a significant increase in $TCID_{50}$ at 0h (virus input bound to cells) when CM cells had a functional P2X7 receptor, hinting to a possible role of this receptor in virus entry. However, at later time points (4h-24h) the viral titer in CM P2RX7 cells was comparable to CM or CM pcDNA3 cells (Figure 10A). We wanted to further exclude an altered viral infection in these cells and therefore calculated the delta between the 24h time point and the 0h time point, but we could not detect a significant difference between the cell lines (Figure 10B), indicating that the viral particle amount were similar between all the cell lines tested at 24hpi. Similarly, preliminary results from a confocal image experiment, in which

the indicated cell lines were infected with MVA-PK1L-mCherry-Ova (20hpi) confirmed comparable permissivity for MVA in all cell lines. (Supplementary Figure S2).

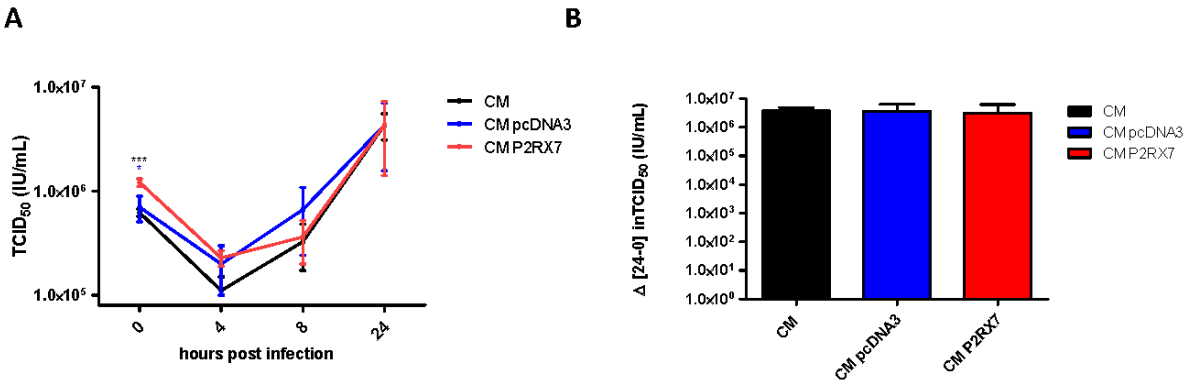

Figure 10: P2RX7 in CM cells leads to an improved attachment of MVA but not to an overall increase in viral output. (A) CM cells (WT, pcDNA3- or P2RX7-transfected) were infected with MVA-P7.5-GFP (MOI5) (MVA synthetizing green fluorescent protein (GFP) under the control of the viral early/late promoter P7.5). At the indicated time points (0h=1h at RT), cells were harvested and prepared for titration on DF-1 cells to determine viral replication. Cytopathic effect on DF-1 was determined one-week after infection and the tissue culture infectious dose ($TCID_{50}$) (infectious units (IU) per milliliter) was calculated. (B) Final viral production (the difference between $TCID_{50}$ of 24h (viral output) and 0h (viral input)) in the indicated cell lines. Data are pooled from n=3 independent experiments and are shown as means ± SD. P values indicate statistical significance (P) with *P ≤ 0.05; ***P ≤ 0.001.

MVA gene expression was delayed in active P2RX7 harboring cells

Prior results have shown that presence of an active P2RX7 in feeder cells increased antigen-presentation capacity of BMDCs. We excluded that this was due to increased antigen production because of viral replication in these cells. Therefore, we wanted to analyze whether the viral gene expression in CM P2RX7 cells was altered. We therefore analyzed the two virus expressed genes, *B8R* (Figure 11A), a non-functional IFNγ resistance gene as well as *Ova* (Figure 11B), a model antigen expressed under the control of the early PK1L MVA promoter and *A19L,* a late expressed viral gene (Figure 11C) [133,134,147]. We infected CM WT (CM), CM pcDNA3 and CM P2RX7 cells with MVA and harvested the samples at different time points to determine viral gene expression. Data analysis was performed either by comparing the dCT to the 0h time point of the analyzed cell line (left column) or by comparing the dCT to the 0h time point of the CM cell line (right column). Hence, we wanted to analyze the viral expression pattern on its own, but also the expression trend compared to the WT or pcDNA3 transfected cells, anticipating a P2RX7-specific phenotype.

Indeed, we observed that *B8R* gene expression was significantly lower in CM P2RX7 cells when compared to the untransfected CM cells until 8hpi, however at 24hpi fold change expression significantly increased. Whilst we detected an increasing expression of *B8R* in CM P2RX7 at 24hpi, CM or CM pcDNA3 *B8R* gene expression reached its peak at 6hpi and

decreased afterwards. In contrast to this, when the dCT was compared to the 0h time point of the respective cell line, we noted that *B8R* expression was initially low, but then rapidly increased to reach its maximum at 24hpi in CM P2RX7 cells. *B8R* expression remained also significantly higher as compared to either CM or CM pcDNA3 cells. Future results should include a more in-depth analysis between 8hpi and 24hpi to corroborate these findings.

Expression of *Ova* and *A19L* resembled *B8R* expression when the dCTs were compared to the 0h time point of the respective cells. However, when comparing the fold change calculated for CM P2RX7 cells to the one calculated for the 0h time point in CM cells, it remained lower than CM or CM pcDNA3 cells at most time points (right images). At 24hpi, we observed a significantly higher *Ova* or *A19L* expression in CM P2RX7 cells compared to CM or CM pcDNA3 cells. Overall we speculate that the observed pattern was due to a delayed start of viral gene expression in CM P2RX7 as compared to CM/CM pcDNA3 cells.

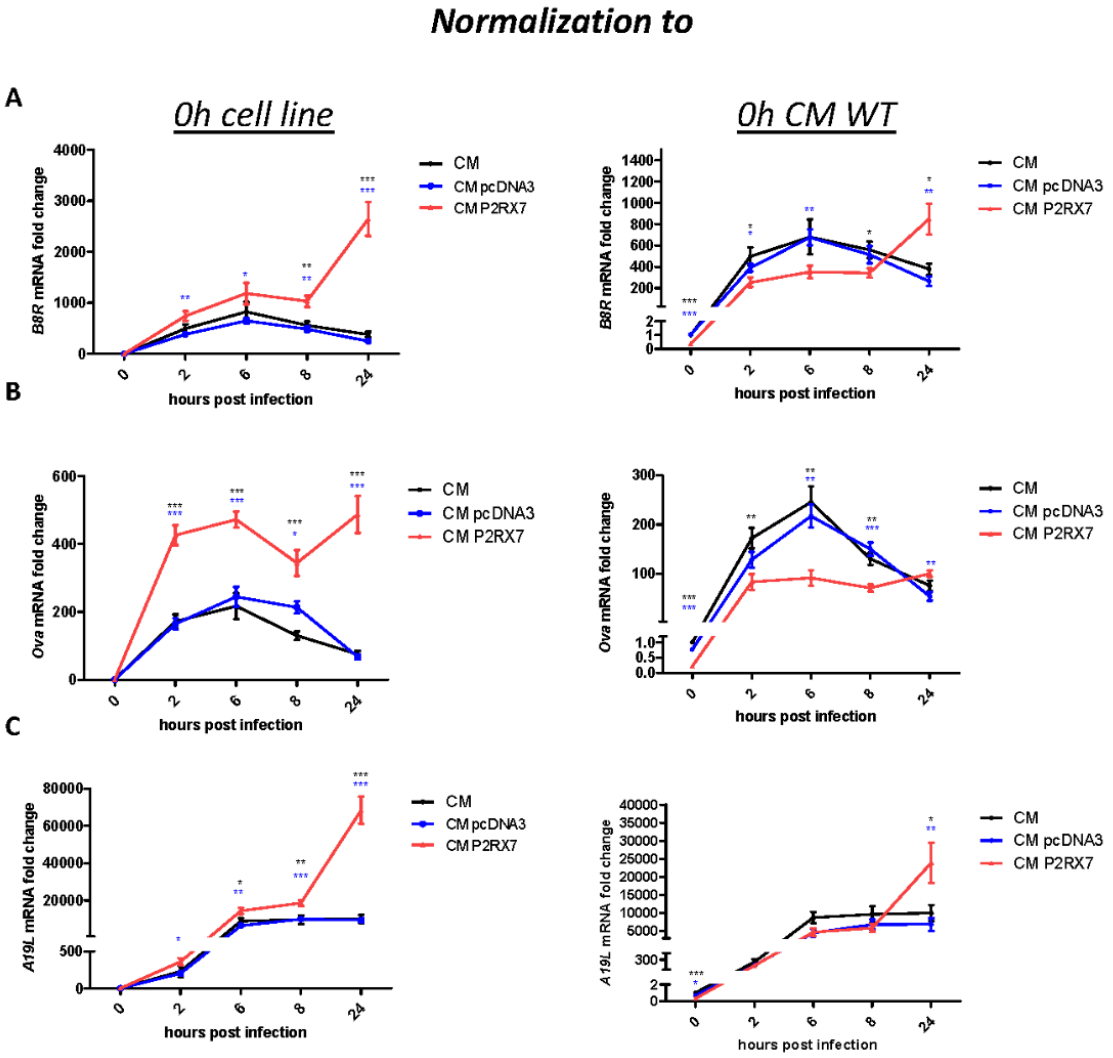

Figure 11: Onset of viral gene expression is delayed in CM P2RX7 cells. CM, empty vector pcDNA3- (CM pcDNA3) or P2RX7-transfetced (CM P2RX7) cells were infected with MVA-PK1L-Ova (MOI1) and harvested at different time points (0h (1h at 4°C) to 24hpi) mRNA fold change of (A) *B8R*, (B) *Ova* or (C) *A19L* is shown as expression of the respective gene at each time point first compared to the *18s* housekeeping gene and then either to the 0h time point of the analyzed cell line (left column) or to the 0h time point of the CM control cell line (right column). Data are pooled from at least n=3 independent

experiments and shown as means ± SEM. P values indicate statistical significance (P) with *P ≤ 0.05; **P ≤ 0.01; ***P ≤ 0.001.

OVA protein amounts in CM P2RX7 cells were comparable to WT CM cells after MVA infection

Since it has been assumed that the availability of protein antigen is a pre-requisite for antigen take-up by dendritic cells for subsequent cross-presentation, we wanted to analyze protein turnover in CM cells [52,148]. We had previously observed a delayed viral gene expression pattern in CM P2RX7 cells compared to CM or CM pcDNA3 cells and speculated that this turned into an increased protein load at 20hpi, potentially favoring subsequent cross-presentation processes.

We therefore mock- or recombinant MVA-infected our CM cells (WT, pcDNA3 or P2RX7) for either 8h or 20h and performed a western blot analysis (Figure 12) to detect the model antigen OVA. We then compared both, the presence of P2RX7 and OVA in the mock-transfected (CM), pcDNA3 or P2RX7-transfected cells to the ß-ACTIN loading control (Figure 12B/C). As expected, the P2RX7-transfected cells showed a significantly higher P2XR7 load than CM or CM pcDNA3 cells (Figure 12B) at 8hpi. Production of OVA at 8hpi seemed lower in CM P2RX7 cells compared to CM cells. However, at 20hpi OVA synthesis in CM P2RX7 cells was similar to CM or CM pcDNA3 cells in CM (Figure 12C).

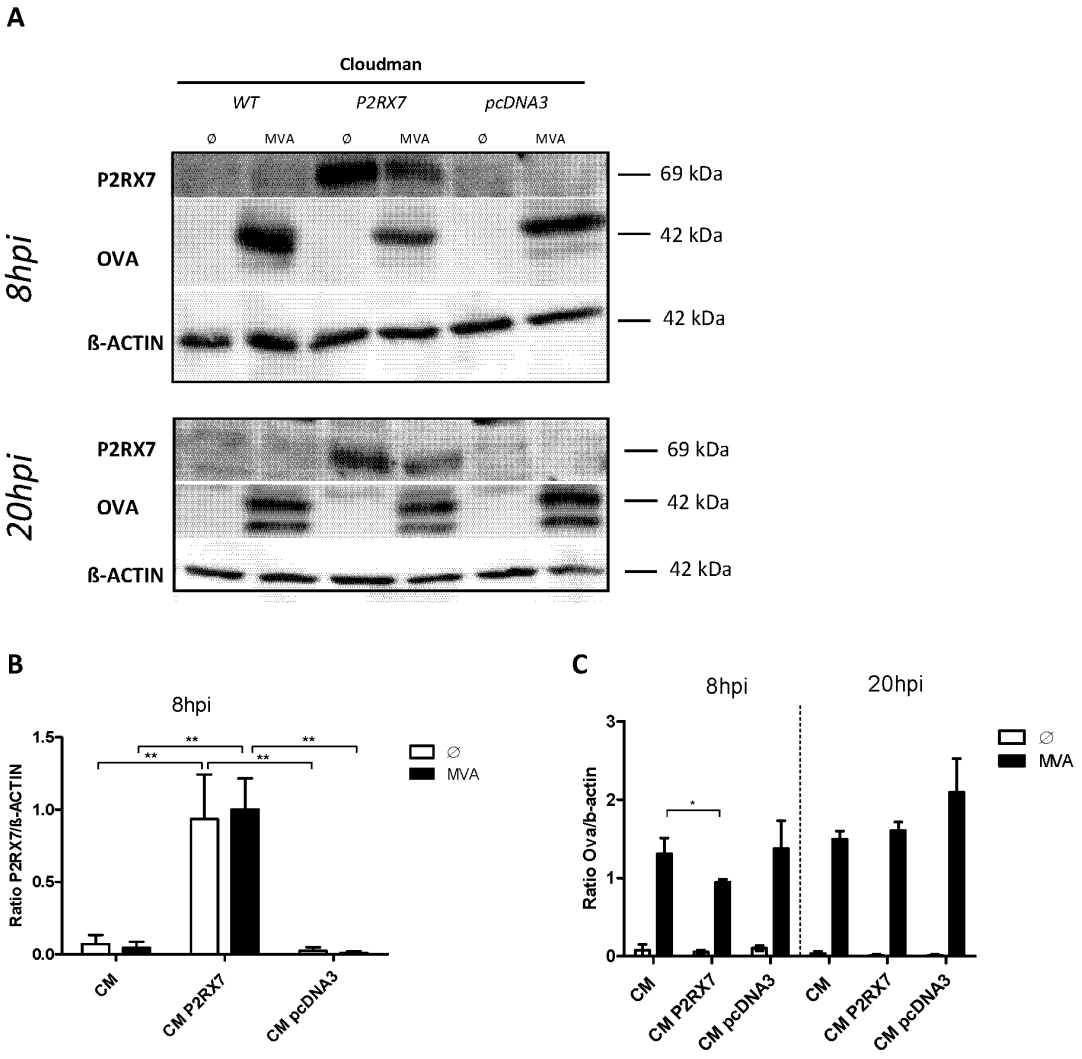

Figure 12: OVA protein availability is comparable in CM P2RX7 cells at 24hpi compared to CM or CM pcDNA3 cells. (A) CM, empty vector pcDNA3- (CM pcDNA3) or P2RX7-transfetced (CM P2RX7) cells were mock (Ø) or MVA-PK1L-Ova-infected (MOI1) and harvested at different time points (8h and 20h) to isolate proteins. Proteins were loaded on SDS-gel and western blot analysis was performed to detect P2RX7, OVA and ß-ACTIN. (B) Ratio of P2RX7 to ß-ACTIN control at 8hpi. (C) Ratio of OVA to ß-ACTIN control at 8hpi or 20hpi. The western blot shown (A) is a representative of a total of n=3 western blots. Data are pooled from n=3 independent experiments (B/C) and are shown as means ± SD. P values indicate statistical significance (P) with *P ≤ 0.05; **P ≤ 0.01.

CM P2RX7 cells exhibited characteristics indicating the activation of apoptosis

Antigen-presenting cells require antigen to phagocytose in order to cross-present it to $CD8^+$ T cells. We therefore hypothesized that CM P2RX7 allowed easier access to the antigen to be cross-presented by DCs via different mechanisms. Apoptosis is a form of programmed cell death that is known to occur upon MVA infection [47]. We postulated that a higher cross-presentation capacity by DCs co-cultured with MVA-infected CM P2RX7 feeder cells might be due to increased apoptosis since antigen amounts remain unaltered. Therefore, we performed western blot analysis and detected significantly more active Caspase-8 in CM P2RX7 cells, independently of MVA infection (20h) as compared to CM or CM pcDNA3 cells (Figure 13A/B).

Exposure of phosphatidylserine to the outer leaflet of the membrane is a characteristic of apoptotic cells and is often seen as an “eat-me” signal for antigen-presenting cells [149]. We further assessed the flip of the phosphatidylserine by flow cytometry analysis (Figure 13C/D). Dying cells that have an intact plasma membrane (and are therefore APC^-) and expose phosphatidylserine residues on the surface are characterized as early apoptotic cells. However, once the plasma membrane becomes permeabilized (APC^+), cells are defined as late apoptotic cells [150]. Interestingly we observed that mock- and MVA-infected (6h) CM P2RX7 cells had significantly higher amounts of late apoptotic cells as compared to mock-infected CM or CM pcDNA3 cells. In contrast to this, the frequencies of early apoptotic CM P2RX7 (Figure 13C) cells were low and comparable to CM or CM pcDNA3 cells in mock- and 6h MVA-infected cells. Even though western blot analysis had shown that CM P2RX7 cells produced higher amounts of active Caspase-8, we did not see this phenomenon in the phosphatidylserine assay, as early apoptotic cells were even less in CM P2RX7 cells at 20hpi and frequencies of late apoptotic cells were comparable to CM or CM pcDNA3 cells (around 25%). Additionally, when visualizing MVA-infected CM P2RX7 cells, they seemed to handle infection better as more cells were presented compared to MVA-infected CM or CM pcDNA3 cells (Supplementary Figure S3).

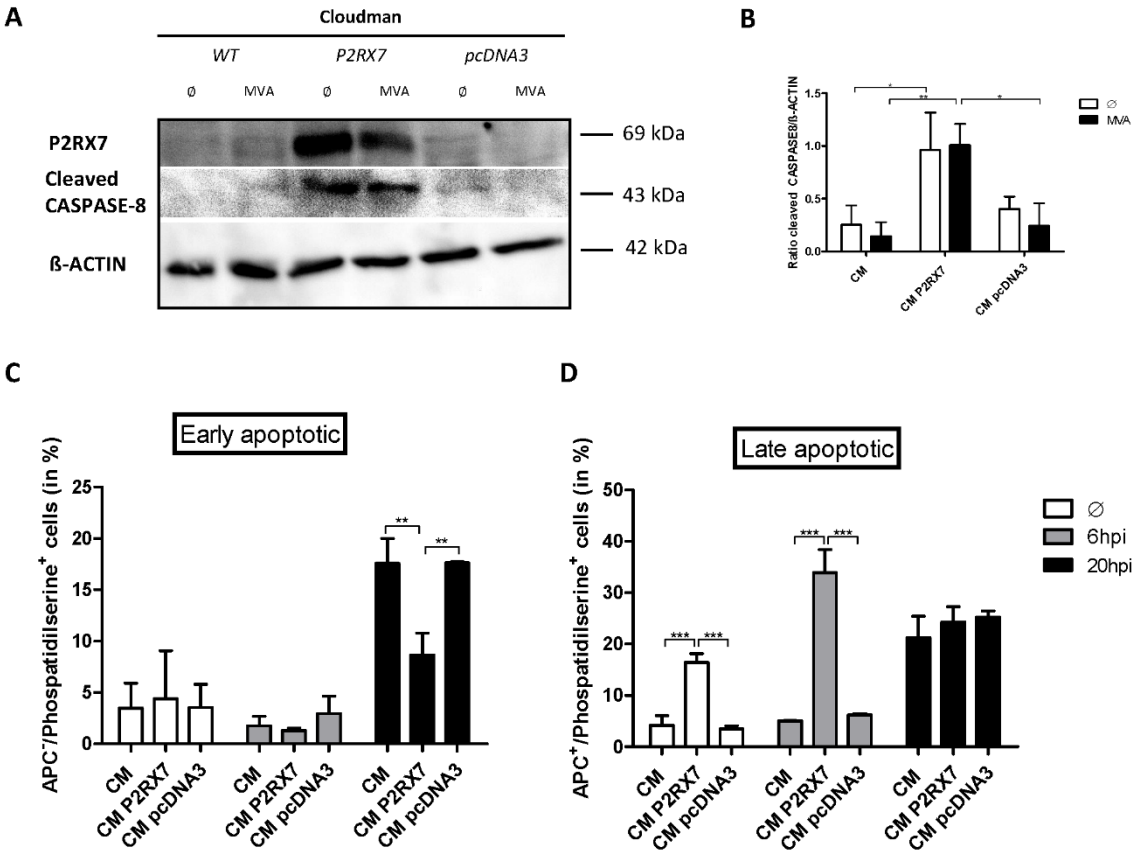

Figure 13: The apoptosis signaling pathway is altered in CM P2RX7 cells marked by increased activeCASPASE-8 and high frequency of late apoptotic cells. (A) CM, empty vector pcDNA3- (CM pcDNA3) or P2RX7-transfected (CM P2RX7) cells were mock (Ø) or MVA-PK1L-Ova infected (MOI1) and harvested at 20hpi to isolate proteins. Proteins were loaded on an SDS-gel and western blot analysis was performed to detect P2RX7, cleaved Caspase-8 and ß-ACTIN. (B) Ratio of cleaved Caspase-8 to ß-ACTIN control at 8hpi. (C) The different CM cells were either mock- or MVA-infected (MOI1) and harvested at 6h or 20hpi. The cells were stained for a live/dead (APC) and for phosphatidylserine exposure (Apotracker green marker). They were either selected for (C) APC^- (dye non-permissive; alive) and $phosphatidylserine^+$ cells or (D) APC^+ (dye permissive; dead) and $phosphatidylserine^+$ cells, depicting either early or late apoptotic cells, respectively. The western blot shown is a representative of at least n=3 western blots performed (A). Data are pooled from n=3 independent experiments and are shown as means ± SD (B-D). P values indicate statistical significance (P) with *P ≤ 0.05; **P ≤ 0.01; ***P ≤ 0.001.

Caspase-9-dependent apoptosis was not affected by the presence of an active P2RX7 in CM cells

Intrinsic apoptosis is another mode of programmed cell death that a cell can undergo when cell-dependent factors, such as Caspase-9 or B-cell lymphoma protein 2 (Bcl-2) initiate the process [151]. Since we have demonstrated that presence of P2RX7 itself causes alteration of cellular signaling pathways, we thought that Caspase-9-dependent apoptosis might be affected as well. Therefore, we investigated the pattern of Caspase-9 cleavage in CM P2RX7 cells by western blot analysis and compared it to CM/CM pcDNA3 cells. We were not able to detect the presence of cleaved Caspase-9 in mock- or MVA-infected (20hpi) CM P2RX7 cells and therefore concluded that Caspase-9 dependent apoptosis was not affected in these cells at the 20hpi time point (Figure 14).

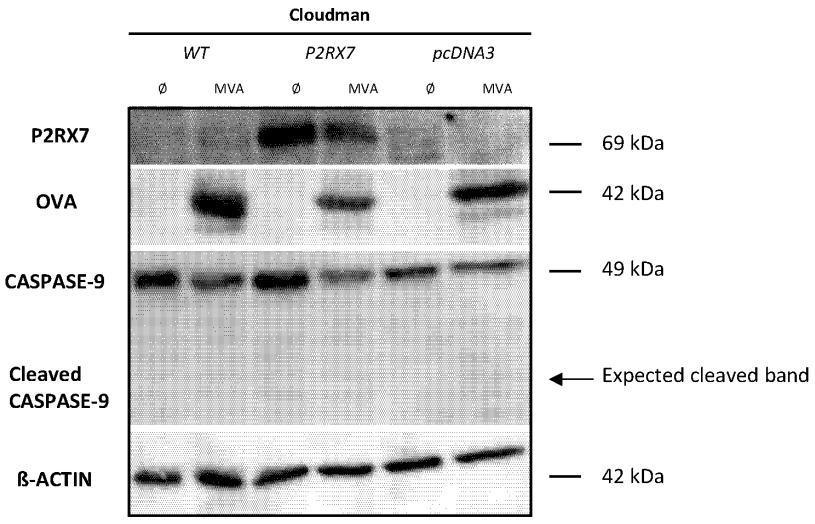

Figure 14: Intrinsic apoptosis is not altered in CM P2RX7 cells. (A) CM, empty vector pcDNA3- (CM pcDNA3) or P2RX7-transfected (CM P2RX7) cells were mock (Ø) or MVA-PK1L-Ova-infected (MOI1) and harvested at 20hpi to isolate proteins. Proteins were loaded on an SDS-gel and western blot analysis was performed to detect P2RX7, cleaved Caspase-9 and ß-ACTIN. The western blot shown is representative for n=3 independent experiments.

7.3 P2RX7 localization and its effects on cellular metabolism upon MVA infection

Energy metabolism in CM P2RX7 cells has been significantly altered

It has been previously shown that active P2RX7 affects cellular metabolism in different ways. The altered metabolism is also attributed to the presence of P2RX7 on the surface of mitochondria, affecting energy metabolism significantly [89,152]. Mitochondrial respiration is an important cellular metabolic process that is measured by the so-called oxygen consumption rate (OCR) in the Mitostress Seahorse assay. It detects the flux of oxygen in the medium surrounding the cells after addition of certain activators or inhibitors of the respiratory chain [153]. We wanted to further investigate the impact of active P2RX7 on cellular metabolism, as we have already established its role during viral gene expression and apoptosis signaling. Therefore, we mock- (Figure 15A left) or MVA-infected (6h) (Figure 15A right) our CM cells and used the Mitostress Seahorse assay to analyze the respiratory pathways. We observed that mere presence of P2RX7 led to a significant increase in basal respiration, the energy needs of the cell under normal conditions as shown by OCR values [154]. However, the basal respiration rate of MVA-infected CM P2RX7 cells was comparable to infected CM/CM pcDNA3 cells. When P2RX7 was active in CM cells, maximal respiration and spare capacity were significantly increased as well, independently of MVA infection (Figure 15B). Maximal respiration analysis was detected by adding the uncoupler FCCP, mimicking an increased energy demand and stimulating the cell to operate at maximum capacity. In contrast, the spare capacity, the difference between the maximal respiration and the basal respiration of the cells, determines the ability of the cell to react under stressful conditions [154].

The Mitostress Seahorse assay kit used in this study also allowed the determination of the extracellular acidification rate (ECAR), an approximate indicator of glycolysis, measuring the protons mainly generated during the breakdown of glucose to pyruvate and ATP [153,155]. However, it must be considered that the protons measured may also derive from the TCA (tricarboxylic acid) cycle [156]. Interestingly, in the mock- as well as MVA-infected P2RX7 cells, ECAR values were three times higher, as compared to CM or CM pcDNA3 cells (Figure 15C). The ECAR values in the control groups CM and CM pcDNA3 were comparable and remained unchanged after MVA infection. In summary, we confirmed that mitochondrial respiration as well as glycolysis are significantly enhanced in CM P2RX7 bearing cells.

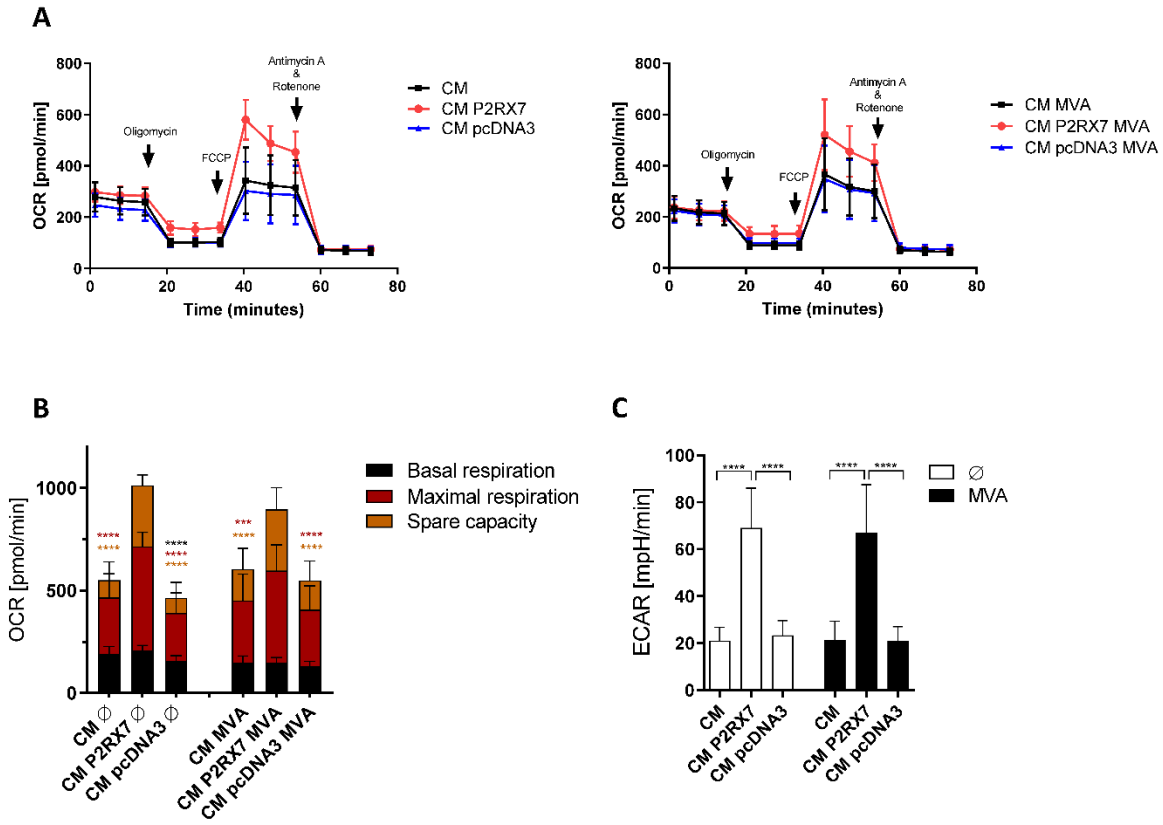

Figure 15: Mitochondrial respiration and glycolysis are significantly increased by the presence of functional P2RX7. (A) CM, empty vector pcDNA3- (CM pcDNA3) or P2RX7-transfected (CM P2RX7) cells were mock (Ø) or MVA-PK1L-Ova-infected (MOI5) and used at 6hpi to perform the Mitostress Seahorse assay. Cells were treated with modulators of the electron transport chain, Oligomycin (15µM), FCCP (5µM) and with a mix of Antimycin A and Rotenone (5µM) at the indicated time points to calculate the oxygen consumption rate (OCR). (B) Basal respiration, maximal respiration and spare capacity of these cells were calculated based on the OCR. (C) Comparable conditions were used to determine the extracellular acidification rate (ECAR) of CM, CM pcDNA3 and CM P2RX7 under mock- or MVA-infected conditions. Data are pooled from n=3 independent experiments and are shown as means ± SD. P values indicate statistical significance (P) with ***P ≤ 0.001; **** P ≤ 0.0001.

P2RX7 localized at viral factories in CM P2RX7 cells after infection with MVA

Previous studies have proven that P2RX7, does not solely localize to the cell membrane, but can also be found on mitochondrial or nuclear areas [89,90]. Since we have observed an altered viral expression pattern in MVA-infected cells, we suspected an altered localization of active P2RX7. Therefore, we stained DNA-rich regions with DAPI and P2RX7 with the respective primary antibody and detected it using an Alexa Fluor 488-conjugated secondary antibody, as described before. Interestingly we predominantly detected P2RX7 in MVA-infected cells (Figure 16B, white arrows) compared to mock-infected cells (Figure 16A). We were also able to detect enrichment of P2RX7 around distinct DNA-rich round areas in which viral gene expression takes place, called viral factories [132], anticipating a direct involvement of P2RX7 at these sites. These P2RX7-positive structures, as they appear as bright spots were

assumed to be P2RX7 complexes rather than single molecules. However, these results should still be interpreted carefully. As the background was relatively high, it was difficult to identify the P2RX7 clearly. More P2X7 receptors were expected on the cell surface, especially in the mock-infected cells. Therefore, for future studies, an improved staining and detection protocol is required.

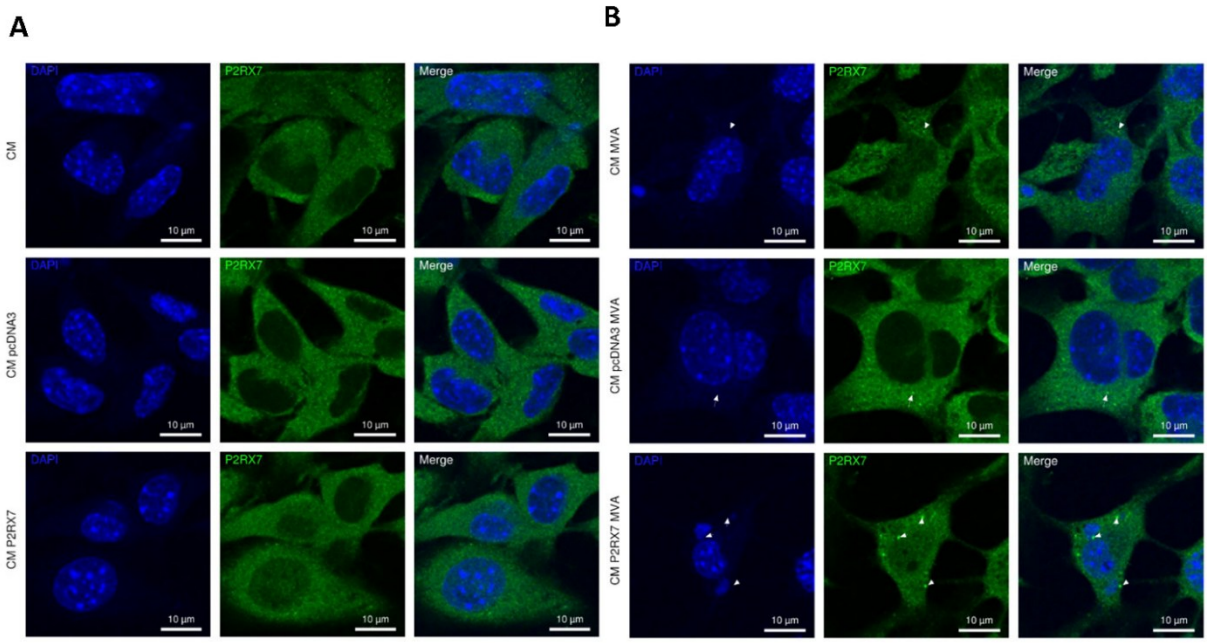

Figure 16: P2RX7 localizes close to DNA rich regions in MVA-infected CM P2RX7 cells (A) CM, empty vector pcDNA3- (CM pcDNA3) or P2RX7-transfected (CM P2RX7) cells were mock (Ø) or (B) MVA-PK1L-Ova infected (MOI5) and used at 6hpi for DAPI (blue) and P2RX7 (green) staining. Cells were imaged at 40x magnification and further zoomed in to improve visualization. The shown images are representatives of n=3 independent experiments.

Functional P2RX7 led to altered ATP levels

It is a well-known fact that P2RX7 is a purinergic receptor, activated by ATP [157]. Recent studies have also shown that the presence of P2XR7 alters ATP levels in cells [158]. We thought to analyze whether in our setup ATP amounts would also differ, especially in the context of MVA infection. We mock- or MVA-infected (MOI5, 6h) our CM cells (Figure 17A) and first analyzed the intracellular ATP (iATP) levels. We demonstrated that intracellular ATP levels significantly increased exclusively in MVA-infected CM P2RX7 cells as compared to MVA-infected CM or CM pcDNA3 cells. In addition, we showed a significant difference in iATP levels in mock-infected CM P2RX7 cells when compared to control transfected CM pcDNA3 cells, but not to the CM wildtype cells.

Since our CM feeder cells were co-cultured with antigen-presenting cells to cross-present MVA antigens to $CD8^+$ T cells, we assumed that ATP is crucial in the supernatant as well, especially after various studies were published promoting the role of ATP during antigen presentation [158–160]. Therefore, we infected our CM cells with a low MOI of 1 for a short time frame

(Figure 17B) and observed that only mock-infected CM P2RX7 cells exhibited significantly higher eATP levels as compared to CM/CM pcDNA3 cells. eATP values in MVA-infected cells remained comparable within the different cell groups. This changed when CM cells were infected with a higher MOI (MOI5), as eATP in CM and CM pcDNA3 cells significantly increased (Figure 17C). CM and CM pcDNA3 cells exhibited a similar phenotype when infected for a longer time period (20h, MOI1) (Figure 17D), whilst eATP in CM P2RX7 cells remained stable at all tested conditions. It has to be considered that MVA infection leads to the initiation of apoptosis and as a consequence the release of ATP due to death, affecting the assay results. Therefore, the presence of active P2RX7 seemed to stabilize eATP levels, not fluctuating as in CM/CM pcDNA3 cells.

The next experimental step aimed to test whether ATP during co-culture affected cross-presentation abilities of BMDCs. In anticipation to this next experiment, we performed an assay to test whether apyrase, an enzyme catalyzing the hydrolysis of ATP to AMP and phosphate, was working in our setup [161]. Therefore, we used the supernatant of our CM P2RX7 cells and treated it with 1U/mL apyrase. We confirmed that apyrase used in the tested concentration does work as expected, as eATP values significantly decreased in the apyrase-treated group (Figure 17E).

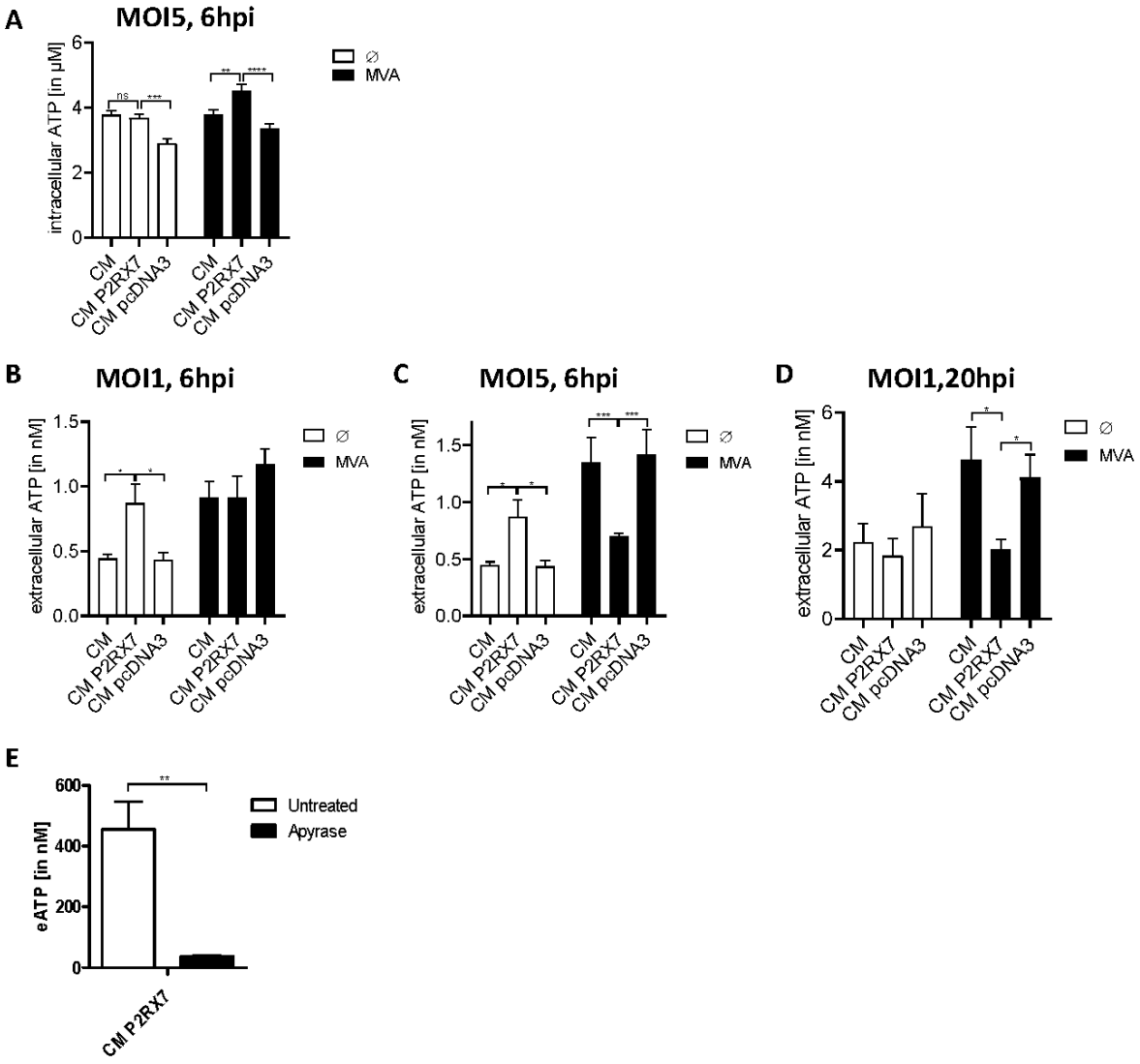

Figure 17: Active P2RX7 alters extracellular and intracellular ATP levels in CM cells. (A) CM, empty vector pcDNA3- (CM pcDNA3) or P2RX7-transfected (CM P2RX7) cells were mock (Ø) or MVA-PK1L-Ova-infected (MOI5) and used at 6hpi to measure intracellular ATP levels. (B-D) Extracellular ATP was assessed by harvesting the medium and measuring its ATP levels using the Enliten Luciferase/luciferin reagent in mock- or MVA-infected CM, CM pcDNA3 and CM P2RX7 cells at (B) MOI1 for 6h (C) at MOI5 for 6h (D) at MOI1 for 20h (E) CM P2RX7 cells were cultured for 6h. The medium was harvested and was either treated with apyrase (1U/mL) or left untreated. The extracellular ATP levels of these supernatants were then measured using the Enliten Luciferase/luciferin reagent. Data are pooled from n=3 independent experiments and are shown as means ± SEM (A-D) or ± SD (E). P values indicate statistical significance (P) with *P ≤ 0.05; **P ≤ 0.01; ***P ≤ 0.001.

Apyrase treatment of CM/BMDCs co-cultures did not affect the antigen cross-presentation capacity of APCs

There are many studies reporting the importance of ATP during antigen presentation [158–160]. We have already established that the extracellular and intracellular availability of ATP is altered in the presence of functional P2RX7 and wanted to analyze whether subtraction of available ATP in CM, CM pcDNA3 and CM P2RX7 affected subsequent cross-presentation by DCs. Therefore, on the second day of the experiment, we co-cultured our mock- or MVA-infected CM cells with bone marrow-derived dendritic cells in the presence of apyrase. On the

third day of the experiment, the apyrase was removed and $CD8^+$ T cells were added, as described above to measure their activation (cytokine production) via flow cytometry. We did not observe a significant difference in $CD8^+$ T cell activation, as depicted by IFNγ (Figure 18A left) or TNFα (Figure 18A right) synthesis in none of the cells when apyrase was present. This observation was independent of the $CD8^+$ specific T cell line used (B8 or Ova, Figure 18A upper graphs, or Figure 18A bottom graphs, respectively). As expected, the frequency of SIINFEKL/H2-K^b complexes on the surface of the BMDCs as well as the SIINFEKL/H2-K^b complexes per cell (MFI) were also not affected when CM cells were co-cultured with BMDCs in the presence of apyrase (Figure 18B). This suggests, that during the co-culture period, ATP was not responsible for the previously reported improved cross-presentation capacity of BMDCs when seeded with MVA-infected CM P2RX7 cells.

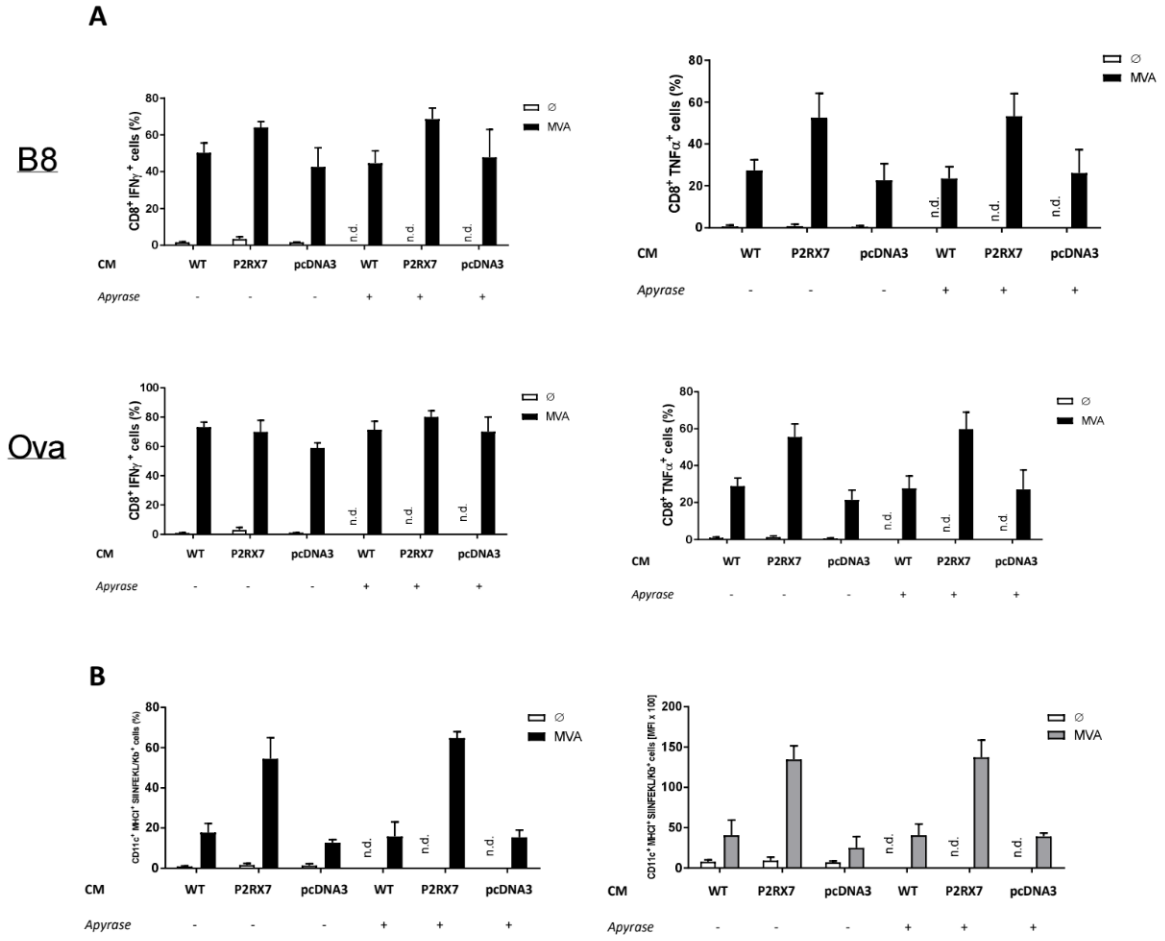

Figure 18: ATP depletion in CM/BMDCs co-cultures did not affect MVA-mediated antigen cross-presentation by BMDCs. (A) CM, empty vector pcDNA3- (CM pcDNA3) or P2RX7-transfected (CM P2RX7) cells were mock (Ø) or MVA-PK1L-Ova-infected (MOI1, 20h). MVA-infected CM cells were PUVA inactivated and co-cultured with BMDCs and additionally treated or not with 1U/mL apyrase (±) for 20h, whilst mock-infected cells were not treated as indicated by the not determined abbreviation (n.d). CM/BMDCs co-culture was then co-seeded with $CD8^+$ specific T cells (B8 or Ova) and incubated in the presence of BFA to detect production of IFNγ or TNFα for 4h. (B) SIINFEKL/H2-K^b complexes on the surface of BMDCs after co-culture of APCs with mock-or MVA-infected (MOI1, 20hpi) CM cell lines in the presence or absence of apyrase (left) and the corresponding MFI (right). Data are pooled from n=3 independent experiments and are shown as means ± SD.

7.4 Differences of CM P2RX7 feeder cell secretome and its impact on MVA cross-presentation

MVA infection resulted in release of extracellular vesicles in CM P2RX7 cells

The presence of an active P2X7 receptor is directly associated with rearrangement of the cellular membrane structures and release of extracellular vesicles. As previously described, there are many types of EVs and the secretion can be easily stimulated with the P2RX7-specific activator Bz-ATP and monitored through live confocal microscopy [118,121]. We therefore wanted to corroborate this feature in our MVA-setup and used the CM, CM pcDNA3 and CM P2RX7 cells to infect with MVA and visualized the release of EVs upon Bz-ATP stimulation. Indeed, we demonstrated the secretion of EVs only in CM P2RX7 cells infected with MVA. These EVs were visualized by the red color, as they derive from the cell membrane and therefore stain similarly. CM and CM pcDNA3 or mock-infected CM P2RX7 cells seemed to release roundish membrane structures upon Bz-ATP stimulus that we, however, classified as apoptotic bodies, generated by dying cells. Interestingly, mock-infected CM P2RX7 cells stimulated with Bz-ATP did not actively release EVs, showing that the release was dependent on both, the presence of a functional P2RX7 and MVA infection (Figure 19A). We tried to quantify the release of these EVs by manually counting the secreted membrane structures and normalized them to the cell numbers determined in the frame. As expected, we found a significantly higher number of extracellular vesicles in MVA-infected CM P2RX7 cells compared to the MVA-infected CM or CM pcDNA3 counterpart (Figure 19B).

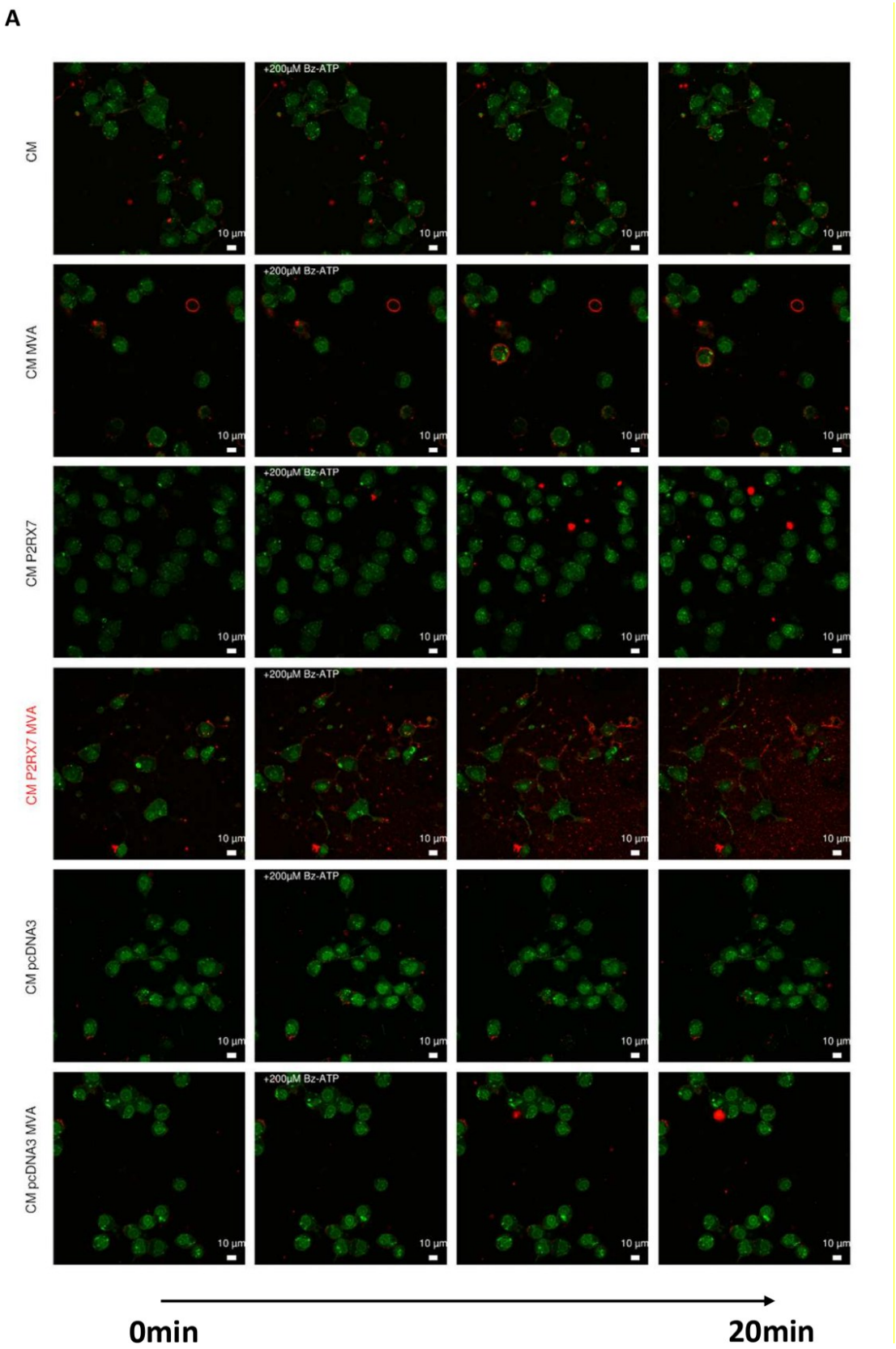
A
CM
CM MVA
CM P2RX7
CM P2RX7 MVA
CM pcDNA3
CM pcDNA3 MVA
+200μM Bz-ATP
10 μm
0min
20min

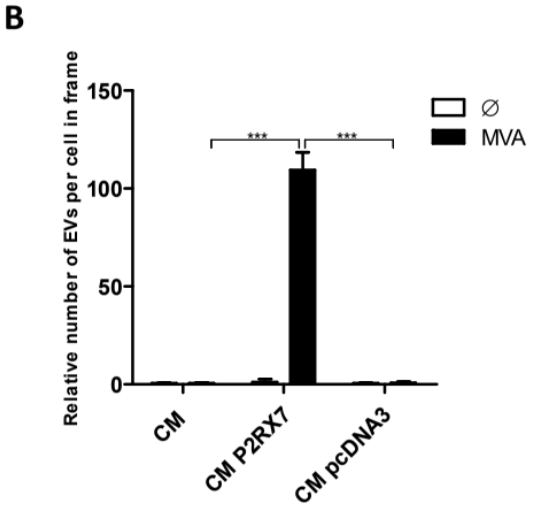

Figure 19: Functional P2RX7 in CM results in EV release upon MVA infection. (A) CM, empty vector pcDNA3- (CM pcDNA3) or P2RX7-transfected (CM P2RX7) cells were mock or MVA-PK1L-Ova infected (MOI1, 20hpi) and stained with quinacrine (for detection of nucleic acids) and PKH-26 (membrane dye) for live confocal imaging recording at 40x magnification. After 2min of the record start, cells were stimulated with 200µM Bz-ATP and EV release was visualized for a total of 20min. (B) EVs were quantified after stimulation with Bz-ATP by counting 5 subsequent frames. EVs were normalized to the cell number per frame. The images shown are representatives of n=3 independent experiments (for A) and the data pooled and are shown as means ± SD (B). P values indicate statistical significance (P) with ***P ≤ 0.001.

EVs were characterized by an altered viral gene expression in CM P2RX7 cells, However, OVA protein amounts were comparable and independent of P2RX7 expression

Extracellular vesicle content has been long debated and studied in regards to its composition and role. Many researchers postulate that these small membrane-embedded structures contain more than just cell debris. Indeed, it has been demonstrated that these structures carry a large variety of regulatory RNAs as well as molecules necessary for cell-to-cell communication [113]. The extraction method used in this study focused on the bigger fraction of EVs, hence the apoptotic bodies and exosomes. A smaller fraction of EVs could have been obtained by ultracentrifugation of the supernatant fraction and should be considered for future studies.

Nonetheless, we detected significantly higher *B8R* expression in CM P2RX7 at 0hpi (1h at 4°C) as compared to CM or CM pcDNA3 cells in EVs. Expression of *B8R* at 24h in CM P2RX7-derived EVs was comparable to CM/CM pcDNA3-derived EVs (Figure 20A). The higher *B8R* mRNA content in EVs in CM P2XR7 might explain the lower presence in cellular extracts, at 0hpi, as shown in the Figure above. In contrast to this, *Ova* (Figure 20B) or *A19L* (Figure 20C) expression in EVs derived from the respective cells was comparable.

Western blot analysis of OVA protein in CM cells (WT, CM pcDNA3 and CM P2RX7) showed lower amounts of OVA in CM P2RX7 MVA-infected cells (Figure 20D), however, when

quantifying the results to the ß-ACTIN loading control, the difference was not significant to MVA-infected CM or CM pcDNA3 counterparts (Figure 20E).

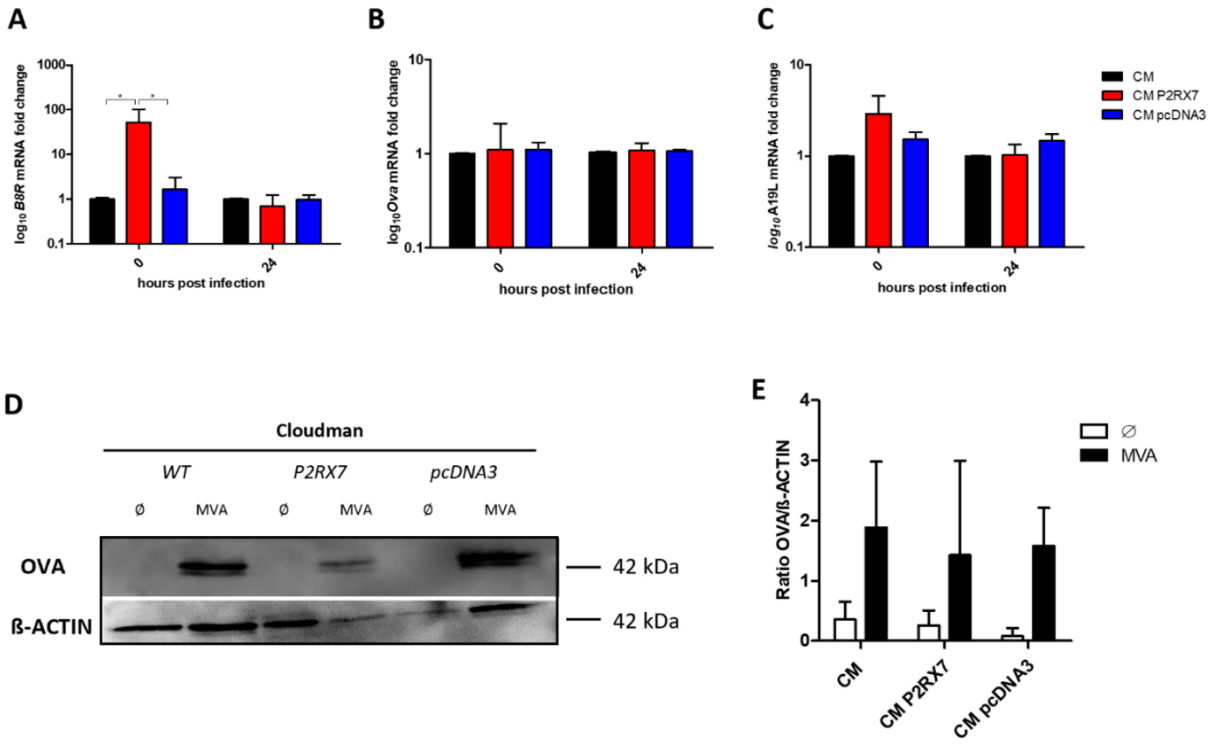

Figure 20: Functional P2RX7 in CM cells alters MVA gene expression and viral protein synthesis. CM, empty vector pcDNA3- (CM pcDNA3) or P2RX7-transfected (CM P2RX7) cells were MVA-PK1L-Ova-infected (MOI1.5) and harvested at 0hpi (1h at 4°C) or at 24hpi to isolate EVs by differential centrifugation. Upon EV isolation, RNA was isolated and cDNA reverse-transcribed to analyze expression of (A) *B8R*, (B) *Ova* and (C) *A19L* using real-time RNA expression analyses. The ddCT was calculated first by comparison of the CT-value to the *18s* housekeeping gene and then to the 0h time point of CM cells. (D) Indicated CM cells were either mock- or MVA-infected (MOI1.5, 20hpi) and the supernatant harvested to isolate EVs and subsequently proteins from the isolated EVs. Western blot analysis was done to detect OVA and ß-ACTIN protein. (E) OVA protein was quantified using ß-ACTIN loading control. Data are pooled from n=3 independent experiments and are shown as means ± SD. P values indicate statistical significance (P) with *P ≤ 0.05.

The supernatant of CM P2RX7 cells contained a highly inflammatory cytokine and chemokine cocktail

Until now we have analyzed cellular pathways in CM cells upon P2RX7 transfection and had a more detailed view on the viral antigen expression in P2RX7-dependent extracellular vesicles. However, many studies report that the presence of an active P2RX7 also alters the cells´ secretome [110,119,162].

Firstly, we analyzed the synthesis of the OVA protein in mock- or MVA-infected cells and established that presence of OVA in CM P2RX7 cells after infection was comparable to CM/CM pcDNA3 cells (Figure 21 A/B).

We also wanted to get a first idea of RNA release and did a simple spectrometry analysis, measuring the A260/280 ratio, used to assess the purity of DNA and RNA, in the supernatant of mock- or MVA-infected CM cells. We observed that MVA-infected CM P2RX7 cells exhibited higher A260/280 ratio values in the range of 1.8-2.0, being indicative of higher amounts of DNA and RNA molecules in the sample, as compared to CM or CM pcDNA3 supernatants (Figure 21C).

Since we know that inflammatory cytokines play a crucial role during antigen presentation, we anticipated an altered secretome in CM P2RX7 cells, especially in regards to the secretion of cytokines [112,163]. We analyzed different cytokines using the Legendplex Mouse Anti-Virus Response panel 13-plex and determined the inflammatory molecules that were significantly altered in the supernatant of CM P2RX7 cells as compared to CM and CM pcDNA3 supernatants in mock- or MVA-infected cells at 8hpi (Figure 21D left) and 20hpi (Figure 21D right). Under mock- or MVA-infected conditions, the inflammatory cytokines (KC, MCP-1, RANTES, IP-10, IL6) were abundant in the supernatant of CM P2RX7 cells. Infection with MVA led a lower synthesis and release of some cytokines in CM P2RX7 supernatants as compared to the mock-infected CM P2RX7 supernatant. The supernatants of the controls CM or CM pcDNA3 had barely a changed chemokine profile upon MVA infection and in general, as compared to CM P2RX7 supernatants, moderate amounts of the indicated chemokines. Only minor changes could be detected for RANTES, IP-10 and IL-6 in CM or CM pcDNA3-derived supernatants. The values for each chemokine listed in these heat maps can be found in Supplementary Figure S4 A/B. These include statistical significances, indicating the highly significant difference between chemokines in the supernatant of CM P2RX7 cells to CM and CM pcDNA3 supernatants. Furthermore, cells were treated with the P2RX7-specific inhibitor A740003 for the chemokine analysis as described above (Supplementary Figure S4 C). We were not able to detect a significant change in the release of the tested chemokines for the A740003 treated CM P2RX7 group as compared to the untreated group, emphasizing the possible importance of intracellular P2X7 receptors, which were not targeted by A740003 as it does not permeate the cells and acts only on the cellular surface receptors. We also tested the cytokine secretion in mock- or MVA-infected BMDCs (Supplementary Figure S5).

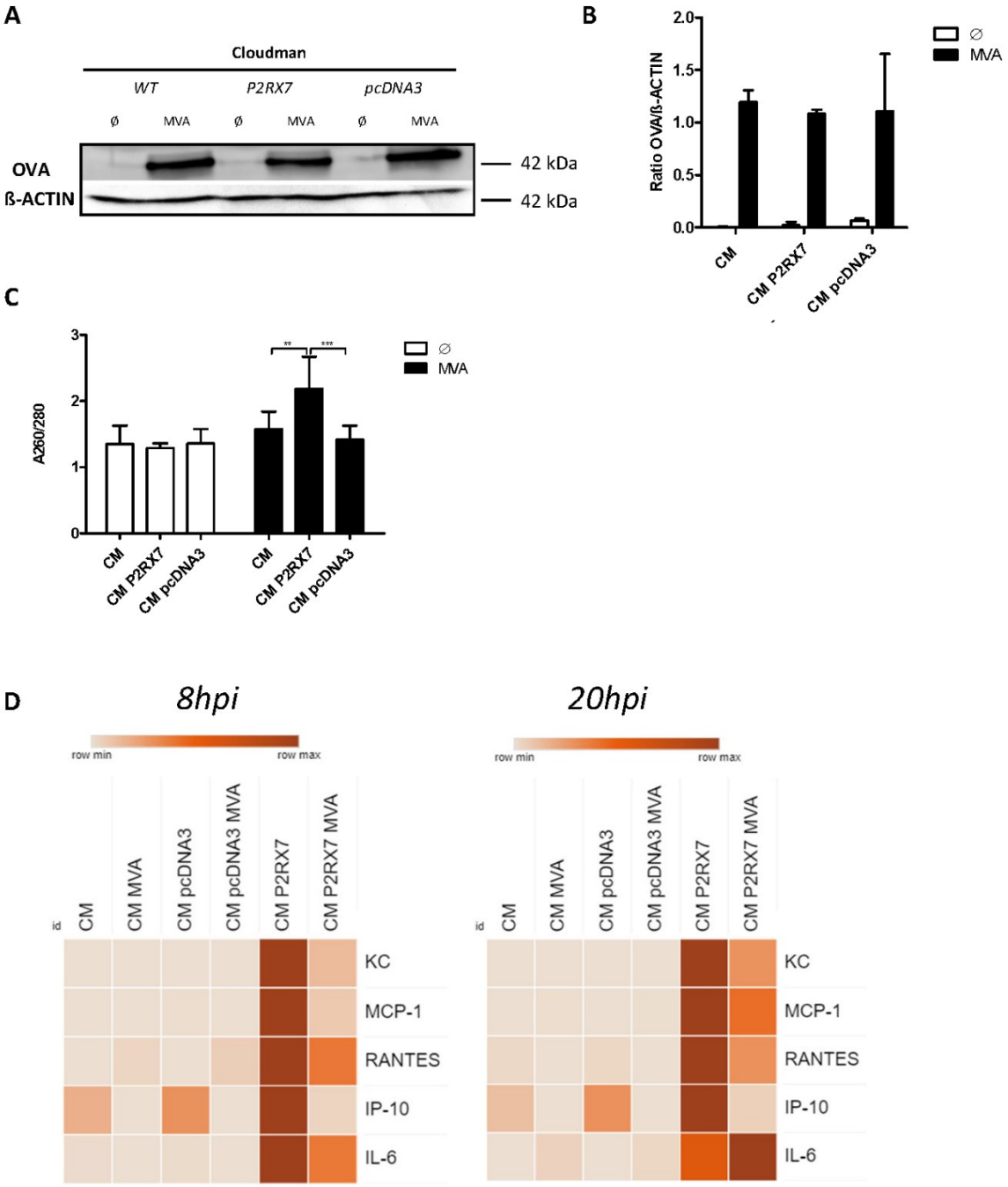

Figure 21: Chemokine but not OVA protein secretion in CM P2RX7 is significantly altered. (A) CM, empty vector pcDNA3- (CM pcDNA3) or P2RX7-transfected cells (CM P2RX7) were mock (Ø) or MVA-PK1L-Ova-infected (MOI1, 20hpi), the supernatant harvested and used for western blot analysis to detect OVA and ß-ACTIN. (B) Quantification of OVA to ß-ACTIN loading control. (C) The supernatant of CM, CM pCDNA3 and CM P2RX7 mock-or MVA-infected (MOI1, 20hpi) was used to calculate the A260/280 ratio, to assess the purity of DNA and RNA in a sample, using a spectrofluorometer. (D) The supernatants of CM, CM pcDNA3 and CM P2RX7 cells either mock- or MVA-infected (MOI1, 8hpi or 20hpi) were used to detect the presence of chemokines using the Legendplex Mouse Anti-Virus Response panel 13-plex. Data are pooled from at least n=3 independent experiments and are shown as means ± SD. P values indicate statistical significance (P) with **P ≤ 0.01; ***P ≤ 0.001.

EV-fraction and supernatant fraction played a role during MVA-mediated antigen cross-presentation by BMDCs

We have characterized the content of the extracellular vesicle fraction (EV-fraction) of CM cells (WT, pcDNA3 and P2RX7 transfected) as well as the supernatant fraction (sup-fraction) of these cells more in detail. Our main focus was to understand how the presence of functional P2RX7 in CM feeder cells enhanced BMDCs mediated antigen cross-presentation of MVA. We therefore thought to use both isolated fractions of MVA-infected CM pcDNA3 or CM P2RX7 cells and add them in a second step to the co-culture of mock-infected CM cells and BMDCs to assess cross-presentation capacity to B8- or Ova- specific $CD8^+$ T cells (Figure 22A/B). We were not able to detect a significant difference in IFNγ or TNFα production by $CD8^+$ T cells when BMDCs were co-cultured with CM cells either in the presence of CM pcDNA3 EV-fraction or CM P2RX7 EV-fraction (Figure 22A). However, when using the supernatant fraction of CM P2RX7 cells, we observed a significant difference in IFNγ (only B8 $CD8^+$ T cells) and TNFα synthesis in both B8- and Ova-specific $CD8^+$ T cells (Figure 22B) as compared to the supernatant fraction from CM pcDNA3 cells. Interestingly, even though to a lower extent, $CD8^+$ T cells were activated when the co-culture contained the EV-fraction or the supernatant fraction from MVA-infected CM pcDNA3 cells, indicating that also in the control transduced cells, the supernatant and the EV-fraction might play a role for antigen cross-presentation, by e.g. improving the cytokine milieu or the antigen source.

Besides the activation of $CD8^+$ T cells, we assessed the loading of the SIINFEKL peptide on the H2-K^b of BMDCs, as an additional more sensitive indicator of the cross-presentation capacity of DCs. We used mock-infected CM cells and added the MVA-infected CM P2RX7 or CM pcDNA3 derived supernatant- or EV-fractions (Figure 22C). Additionally, we infected CM cells with MVA and further added the fractions of MVA-infected CM P2RX7 or CM pcDNA3 cells (Figure 22D). Unlike the $CD8^+$ T cell assay, we observed a significant increase in SIINFEKL/H2-K^b surface expression in BMDCs upon addition of the MVA-infected CM P2RX7 EV-fraction when added to mock-infected CM cells and then co-cultured with BMDCs and compared to the CM pcDNA3 control group (Figure 22C). This effect was not as prominent when CM cells were additionally infected with MVA. When comparing infected CM cells to comparable cells supplemented with the EV- or sup-fraction from CM P2RX7 cells, we showed a slight significant difference (Figure 22D). Expression of maturation markers on BMDCs was not significantly altered when comparing the P2RX7 group to the pcDNA3 control group, possibly because of the quick activation of BMDCs independently of the trigger source (Supplementary Figure S6).

Overall, we can conclude that both EV- and supernatant fractions of CM P2RX7 feeder cells, contributed to the activation of $CD8^+$ T cells upon BMDCs cross-presentation.

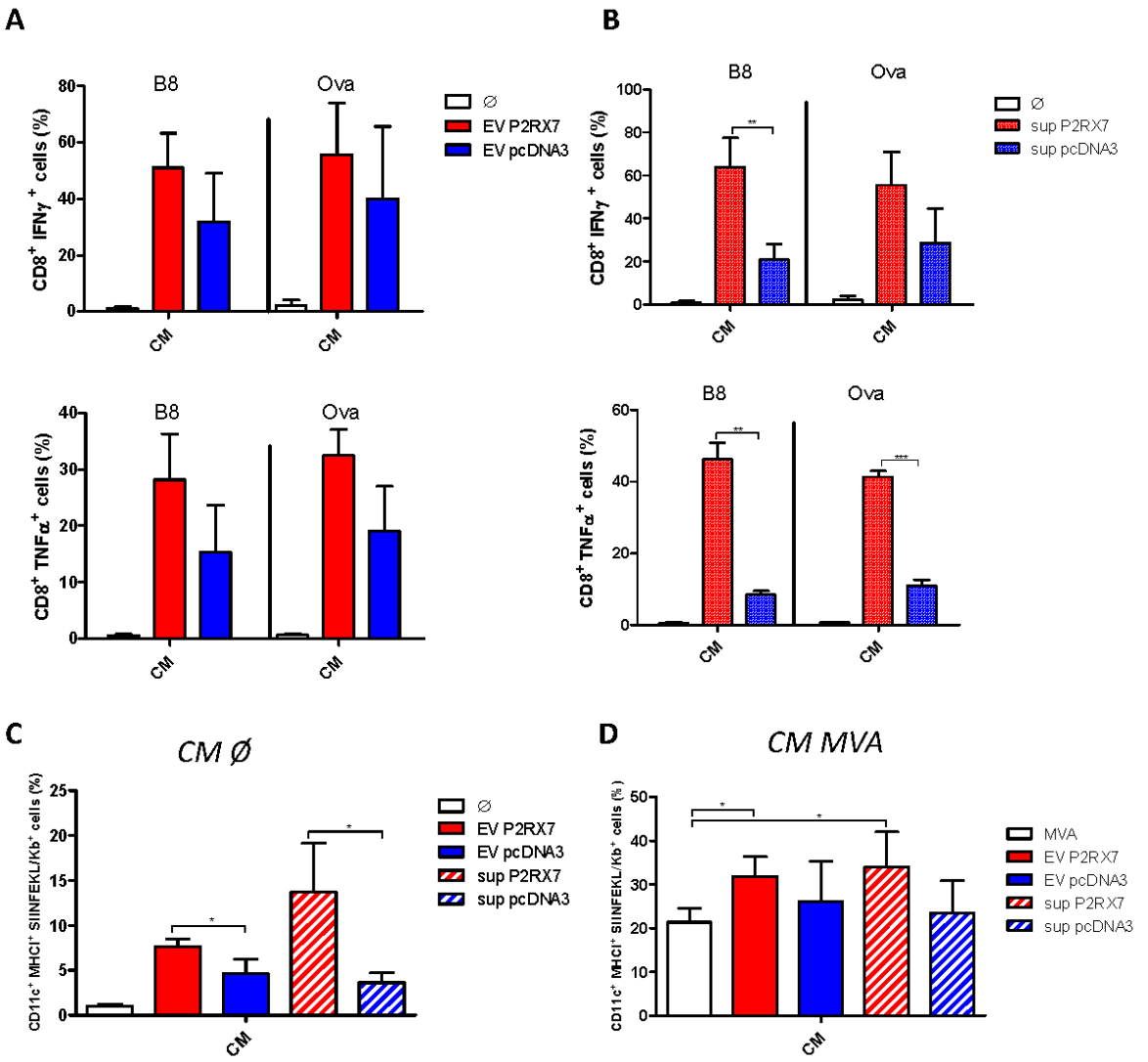

Figure 22: EVs and supernatants from CM P2RX7 cells have an impact on BMDCs´ cross-presentation capacity. (A) EV-fraction or (B) sup-fraction of MVA-PK1L-Ova-infected (MOI1.5 for EV, MOI1 for sup, 20hpi) CM pcDNA3 or CM P2RX7 cells were PUVA inactivated and added to mock-infected (Ø) CM cells in co-culture with BMDCs for 20h. Thereafter $CD8^+$ T cells (B8- or Ova-specific) were added for 4h. Intracellular cytokine staining of IFNγ (upper graphs) or TNFα was done to measure their synthesis via FACS (bottom graphs). (C) The MVA-infected (MOI1.5, 20hpi) EV-fraction or sup-fraction (MOI1, 20hpi) of CM pcDNA3 or CM P2RX7 cells were PUVA inactivated and added to the co-culture with mock-infected CM cells and BMDCs for 20h. Surface staining of SIINFEKL/H2-K^b on BMDCs was done and analyzed via FACS. (D) The MVA-infected (20hpi) EV-fraction (MOI1.5) or sup-fraction (MOI1, 20hpi) of CM pcDNA3 or CM P2RX7 cells was PUVA inactivated and added to the co-culture with MVA-infected (20h) CM cells and BMDCs for a total of 20h. SIINFEKL/H2-K^b complexes were stained on the surface of BMDCs and analyzed via FACS. Data are pooled from n=3 independent experiments and are shown as means ± SD. P values indicate statistical significance (P) with *P ≤ 0.05; **P ≤ 0.01; ***P ≤ 0.001.

The filtered supernatant fraction of CM P2RX7-cells significantly increased SIINFEKL/H2-K^b surface expression when added to CM/BMDCs´ co-culture

The supernatant of infected cells might not only contain inflammatory cytokines but also cellular debris, such as apoptotic bodies that will not be retained in the pellet after centrifugation. Apoptotic bodies of CM feeder cells, a side product during MVA infection, might also contain

factors leading to the stimulation of antigen-presenting cells and subsequent activation of $CD8^+$ T cells [47,54,118]. Therefore, we thought to filter the supernatant of MVA-infected CM pcDNA3 or CM P2RX7 cells in order to retain the bigger fraction of apoptotic bodies. These filtered portions were added to the co-culture of mock- or MVA-infected CM cells and BMDCs. We showed that the filtered supernatant of CM P2RX7 cells added to the mock- as well as MVA-infected CM /BMDCs co-culture significantly increased SIINFEKL/H2-K^b expression on the surface of BMDCs. When the CM/BMDCs co-culture was supplemented with supernatants from MVA infected CM P2RX7 cells, the SIINFEKL/H2-K^b complexes per BMDC were also increased (MFI). The filtered supernatant of CM pcDNA3 cells only slightly increased the SIINFEKL/H2-K^b expression in BMDCs (Figure 23A). Analysis of MHCI (Figure 23B), MHCII (Figure 23C) and CD86 (Figure 23D) did not result in significant differences between the filtered supernatant of CM P2RX7 and CM pcDNA3 cells as when compared to CM cells. However, CD40 surface expression on BMDCs significantly increased when the mock-infected CM/BMDCs co-culture received the filtered supernatant fraction of CM P2RX7 cells (Figure 23E). To conclude, it can be noted that there are factors in the filtered supernatant of CM P2RX7 cells, which most likely were not large apoptotic bodies that aid in contributing to improved antigen cross-presentation by BMDCs. We hypothesized that smaller vesicles or even nucleic acid molecules present in the filtered supernatant fraction might play a crucial role here.

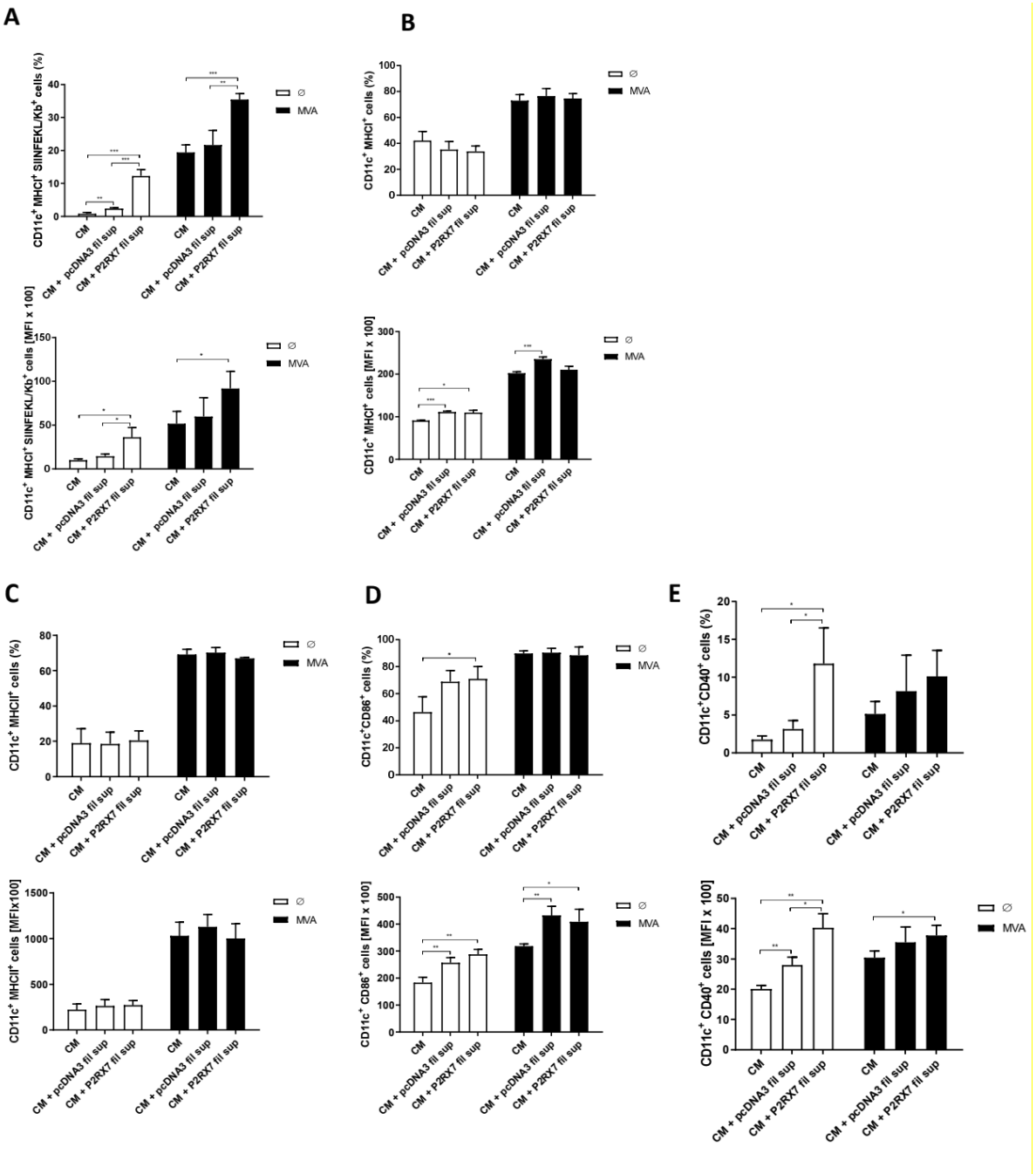

Figure 23: Filtered supernatant of CM P2RX7 affects SIINFEKL/H2-K^b expression of BMDCs. Mock- (Ø) or MVA-infected (MOI1, 20hpi) CM cells were co-cultured with either CM pcDNA3 or CM P2RX7-derived PUVA-inactivated filtered supernatant (0.2µm filter) (fil sup) fractions and BMDCs for 20h. (A) Expression of SIINFEKL/H2-K^b on the surface of BMDCs (upper graph) after 20h co-culture and the corresponding MFIs (bottom graph). (B) Expression of MHCI (total H2-K^b) on the surface of BMDCs after 20h co-culture and the corresponding MFI (bottom graph). (C) Expression of MHCII on the surface of BMDCs after 20h co-culture and the corresponding MFI (bottom graph). (D) Expression of CD86 on the surface of BMDCs after 20h co-culture and the corresponding MFI (bottom graph). (E) Expression of CD40 on the surface of BMDCs after 20h co-culture and the corresponding MFI (bottom graph). All data shown are representatives of n=3 independent experiments and shown as means ± SD. P values indicate statistical significance (P) with *P ≤ 0.05; **P ≤ 0.01; ***P ≤ 0.001.

7.5 STING pathway and Caspase-1 activity in CM P2RX7 cells

The STING pathway in CM P2RX7 was severely affected

A recent study has shown that STING in feeder cells is correlated with MVA antigen cross-presentation. It was demonstrated that absence of STING in feeder cells enhanced BMDCs-mediated antigen cross-presentation when co-cultured with these cells [66]. Therefore, the presence of STING in feeder cells was defined as rather hindering MVA cross-presentation. We thought to analyze the expression of *Sting* in CM feeder cells, as another possible pathway affected by the presence of functional P2RX7. Indeed, we demonstrated that the presence of functional P2RX7 in CM cells resulted in a significant reduction of *Sting* fold change as compared to CM or empty vector CM pcDNA3 control cells. *Sting* fold change after MVA infection in CM or CM pcDNA3 cells was increased over time with its maximum at 6hpi and subsequently decreased at 24hpi. However, fold change of *Sting* in CM P2RX7 cells remained constant over infection time with lowest expression at 24hpi (Figure 24A).

As previously stated, extracellular vesicles serve as transport vehicles for regulatory RNAs, or as shown in our study also of mRNA [113]. We thought to analyze the mRNA levels of *Sting* in these vesicles as well, as they might be indeed important information carriers to antigen-presenting cells. Consistent with the reduced protein amounts demonstrated by western blot analysis, we also detected significantly lower *Sting* mRNA levels in EVs of MVA-infected CM P2RX7 cells as compared to EVs of MVA-infected CM pcDNA3 or CM WT cells (Figure 24B). We also analyzed the mRNA levels of *Ifnb* and *Ifnar* in these EVs and detected significantly less transcripts in EVs of MVA-infected CM P2RX7 cells (Figure 24 C and D, respectively). *Ifnb* mRNA levels were, however, significantly higher in CM pcDNA3 cells than CM cells (Figure 24 C).

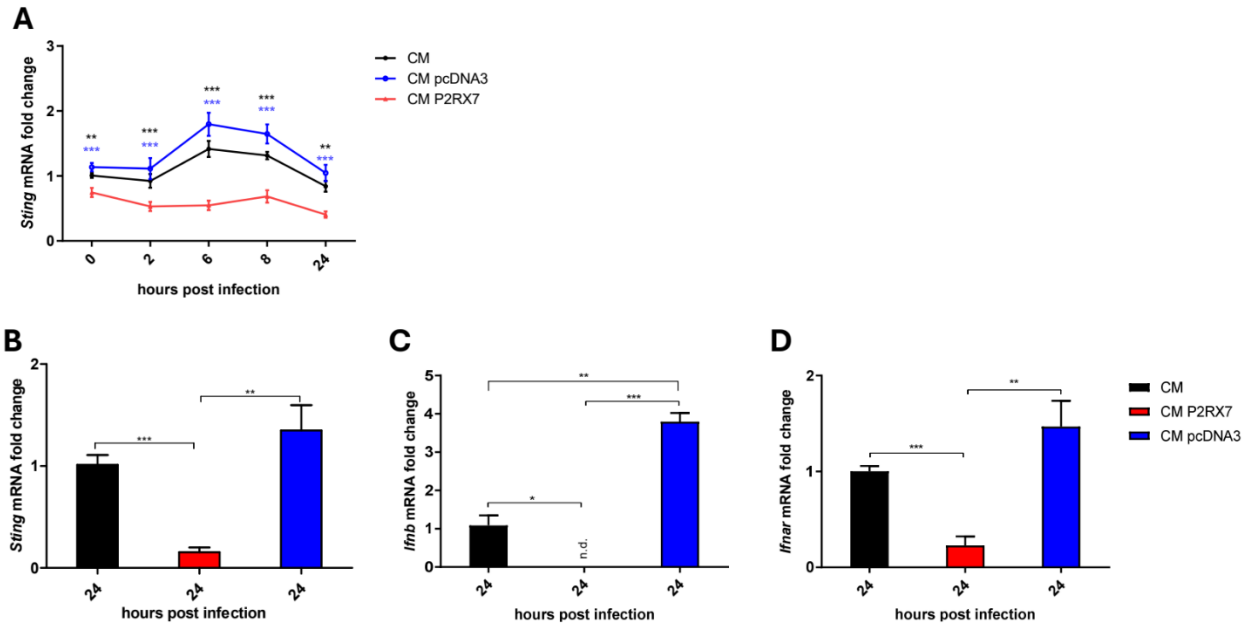

Figure 24: Expression of *Sting*, *Ifnb* and *Ifnar* in CM P2RX7 and their EVs is significantly reduced. (A) MVA-PK1L-Ova-infected (MOI1.5) CM cells (WT, pcDNA3 or P2RX7 transfected) were harvested at different time points (0h (1h at 4°C) to 24hpi). RNA was extracted and reverse transcribed to analyze *Sting* expression using ddCT, comparing each time point to the *18s* housekeeping gene expression and then to the 0h time point of *Sting* expression in CM cells. (B) CM, CM pcDNA3, CM P2RX7 cells were MVA-infected (MOI1.5) and EVs extracted after 24hpi. RNA was isolated, reverse transcribed and analyzed for expression of *Sting*, (C) *Ifnb* or (D) *Ifnar*, calculating the ddCT by comparison with the *18s* housekeeping gene and then the 24h time point of CM cells. Data are pooled from n=3 independent experiments and are shown as means ± SD. P values indicate statistical significance (P) with *P ≤ 0.05; **P ≤ 0.01; ***P ≤ 0.001.

Caspase-1 was active in CM P2RX7 cells

P2RX7 has extensively been described for its function on the activity of the canonical inflammasome. Activation of the P2X7 receptor is associated with the activation of the inflammasome consisting of the sensor molecule, the Caspase-1 and the ASC protein complex [164,165]. Until this point in the study, we have not considered the possible involvement of the canonical inflammasome during MVA antigen cross-presentation and have therefore analyzed the activity of the Caspase-1 in our CM cells, as well as the secretion of IL-18, a cytokine known to be released upon canonical inflammasome activation [166].

The Caspase-Glo 1 inflammasome assay, provided the Z-WEHD substrate, which could be cleaved by active Caspase-1 in the sample. The cleaved Z-WEHD was used as a substrate for luciferase, resulting in the generation of light (detected as relative light units (RLU)). We showed that presence of active P2RX7 in the context of MVA infection resulted in significant activation of Caspase-1 as compared to CM or CM pcDNA3 control cells. Mock-infected CM P2RX7 cells did not show activation of Caspase-1 (Figure 25A). As a consequence of Caspase-1 activation in the canonical inflammasome pathway, secretion of inflammatory

cytokines is described to occur [165]. We tested whether this was also true in our case since Caspase-1 seemed to be activated upon MVA infection in CM P2RX7 cells. However, we were not able to see a significant increase of IL-18 in the supernatant of CM P2RX7 cells as compared to CM or CM pcDNA3 cells, independently of MVA infection (Figure 25 B).

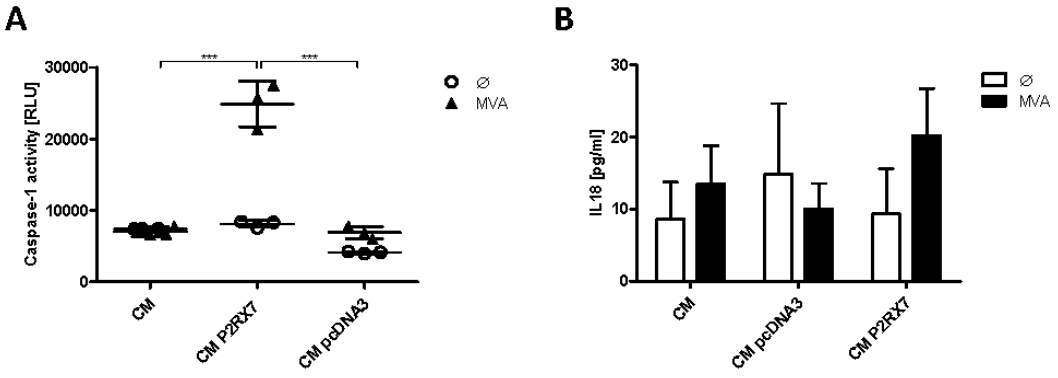

Figure 25: Caspase-1 activity but not IL-18 secretion is increased in MVA-infected CM P2RX7 cells. (A) Mock- (Ø) or MVA-PK1L-Ova-infected (MOI1, 20hpi) CM (WT, pcDNA3 or P2RX7 transfected) cells were tested for caspase-1 activity using the Caspase-Glo1 Inflammasome assay and plotted as RLU. (B) The supernatants of mock- or MVA-infected (MOI1, 20hpi) CM (WT, pcDNA3 or P2RX7 transfected) cells were used as material to determine secreted IL-18 by using the Mouse IL-18 ELISA Kit. Data are pooled from n=3 independent experiments and are shown as means ± SD. P values indicate statistical significance (P) with ***P ≤ 0.001.

7.6 Human HEK293 hP2RX7 and BALB/c-derived P2RX7 KO cells as feeders for MVA antigen cross-presentation

MVA-infected HEK293 hP2RX7 cells as feeders led to an increased SIINFEKL/H2-K^b surface expression on cross-presenting BMDCs when co-cultured

We wanted to confirm that the P2RX7-specific effects in CM feeder cells were not exclusive to this cell line, but are also present when using other cells bearing an active P2X7 receptor. Since the cross-presentation system limits us in the choice of feeder cells due to the requirement of MHC I mismatch, we were initially troubled in finding an appropriate testing cell line. The laboratory of Elena Adinolfi at the University of Ferrara supplied us with an established cell line transfected with the active human P2X7 receptor, hence the HEK293 hP2RX7 and its WT HEK293 counterpart.

We confirmed the presence of the P2RX7 protein in these cells as well as synthesis of the OVA protein upon MVA-Ova infection (Figure 26A).

We also confirmed activity of the P2X7 receptor by fluorometric analysis and showed that HEK293 cells transfected with hP2RX7 led to an increase in intracellular calcium upon Bz-ATP stimulus. MVA infection of HEK293 hP2RX7 cells reduced intracellular calcium increase slightly, whilst as expected, mock-transfected HEK293 cells did not show any intracellular calcium increase upon Bz-ATP stimulus (Figure 24B).

Additionally, we confirmed opening of the pore, leading to the entry of large molecules, as EtBr, in HEK293 hP2RX7 cells, confirming another P2RX7-specific feature. Here as well, MVA infection of HEK293 hP2RX7 cells reduced pore opening slightly (Figure 26C).

We also tested the presence of extracellular ATP in these cells and showed that active P2RX7 in these cells led to a significant increase in eATP as compared to HEK293 WT cells (Figure 26D).

As a final experiment, we used these cells as feeder cells, for our cross-presentation assay, substituting CM cells. We MVA-infected HEK293 or HEK293 hP2RX7 and co-cultured them with BMDCs to measure the surface expression of SIINFEKL on H2-K^b of BMDCs. Both feeder cell lines resulted in a high background expression of SIINFEKL/H2-K^b on the BMDCs´ surface. However, MVA-infected HEK293 hP2RX7 cells showed a significantly higher expression of SIINFEKL/H2-K^b complexes on the surface of BMDCs as compared to the HEK293-infected cells (Figure 26E).

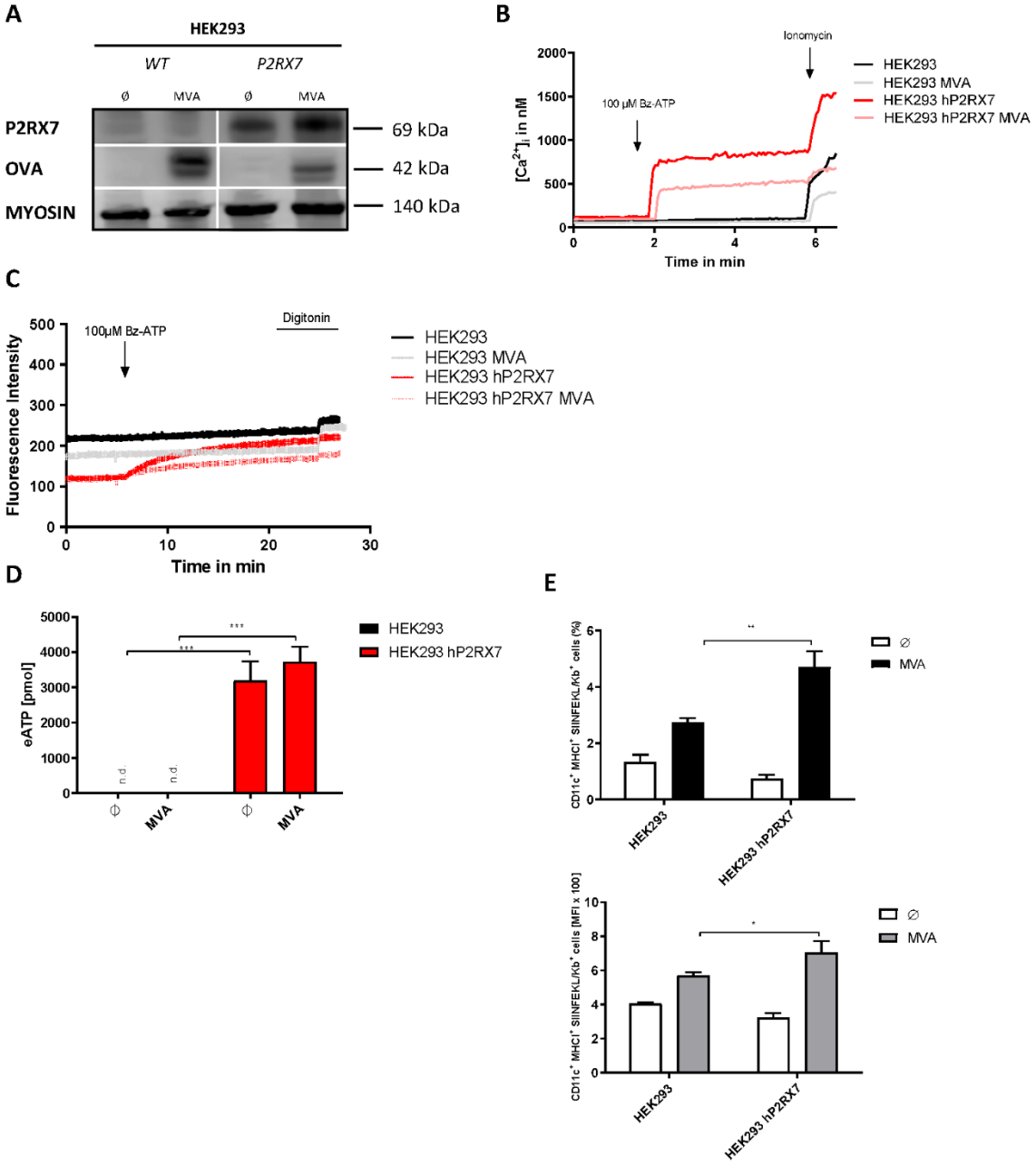

Figure 26: Presence of P2RX7 in HEK293 feeder cells confirms P2RX7-specific functions and increases SIINFEKL/H2-K^b surface expression in BMDCs. (A) Mock- (Ø) or MVA-PK1L-Ova-infected (MOI1) HEK293 cells (WT or hP2RX7 transfected) were harvested at 20hpi and proteins were isolated to test the presence of P2RX7, OVA and myosin as loading control. (B) HEK293 and HEK293 hP2RX7 cells were either mock- or MVA-infected (MOI1, 20hpi), harvested and stimulated with 100µM Bz-ATP and 1mM ionomycin to test the increase of intracellular calcium by fluorometric analysis. (C) HEK293 and HEK293 hP2RX7 cells were either mock- or MVA-PK1L-Ova-infected (MOI1, 20hpi), harvested and stimulated with 100µM Bz-ATP and 100µM digitonin at the indicated time points to test the pore opening by measuring the increase of fluorescence intensity by fluorometric analysis. (D) The supernatant of mock- or MVA-PK1L-Ova- infected (MOI1, 20hpi) of HEK293 (WT or hP2RX7) cells was used to assess concentrations of extracellular ATP using the Enliten Luciferase/luciferin reagent. (E) HEK293 or HEK293 hP2RX7 cells were either mock- or MVA-PK1L-Ova- infected (MOI1, 20hpi), PUVA inactivated and then co-cultured with BMDCs for 20h to assess the surface expression of SIINFEKL/H2-K^b complexes on BMDCs (upper graph) and the density of these complexes per cell (MFI) (bottom graph). Dara are pooled from n=3 independent experiments (except A n=1) and are shown as means ± SD. P values indicate statistical significance (P) with *P ≤ 0.05; **P ≤ 0.01; ***P ≤ 0.001.

BALB/c P2RX7 cells used as feeders did not show the expected P2RX7-specific phenotype during MVA antigen cross-presentation

To fully prove a functional system, we wanted to analyze cross-presentation capacity of BMDCs when co-cultured with P2RX7 KO cells as feeders. We kindly received bone marrow from Elena Adinolfi and Francesco di Virgilio from the University of Ferrara and generated BMDCs that we then used as mismatched feeder cells for our cross-presentation assay. We mock-or MVA-infected BALB/c WT or P2RX7 KO cells along with our CM cells as controls and co-cultured these with BMDCs. We showed that the absence of P2RX7 in BALB/c feeder cells co-cultured with BMDCs led to a significant increase in IFNγ and TNFα synthesis in B8-specific $CD8^+$ T cells. However, when BALB/c cells were used as feeder cells during cross-presentation assay, synthesis of IFNγ and TNFα was very low (Figure 27A). We additionally demonstrated that absence of P2RX7 in BALB/c feeder cells had no impact on the SIINFEKL/H2-K^b expression on the surface of BMDCs (Figure 27B). The STING pathway has been already published and confirmed to impact MVA-mediated cross-presentation [66]. We therefore analyzed the release of type I IFNs in BALB/c feeder cells and surprisingly realized that P2RX7 KO cells showed a significant reduction of mIFN-α2 and mIFN-ß production compared to the BALB/c WT counterpart (Figure 27C), possibly linking the STING pathway with CD8 T cell activation.

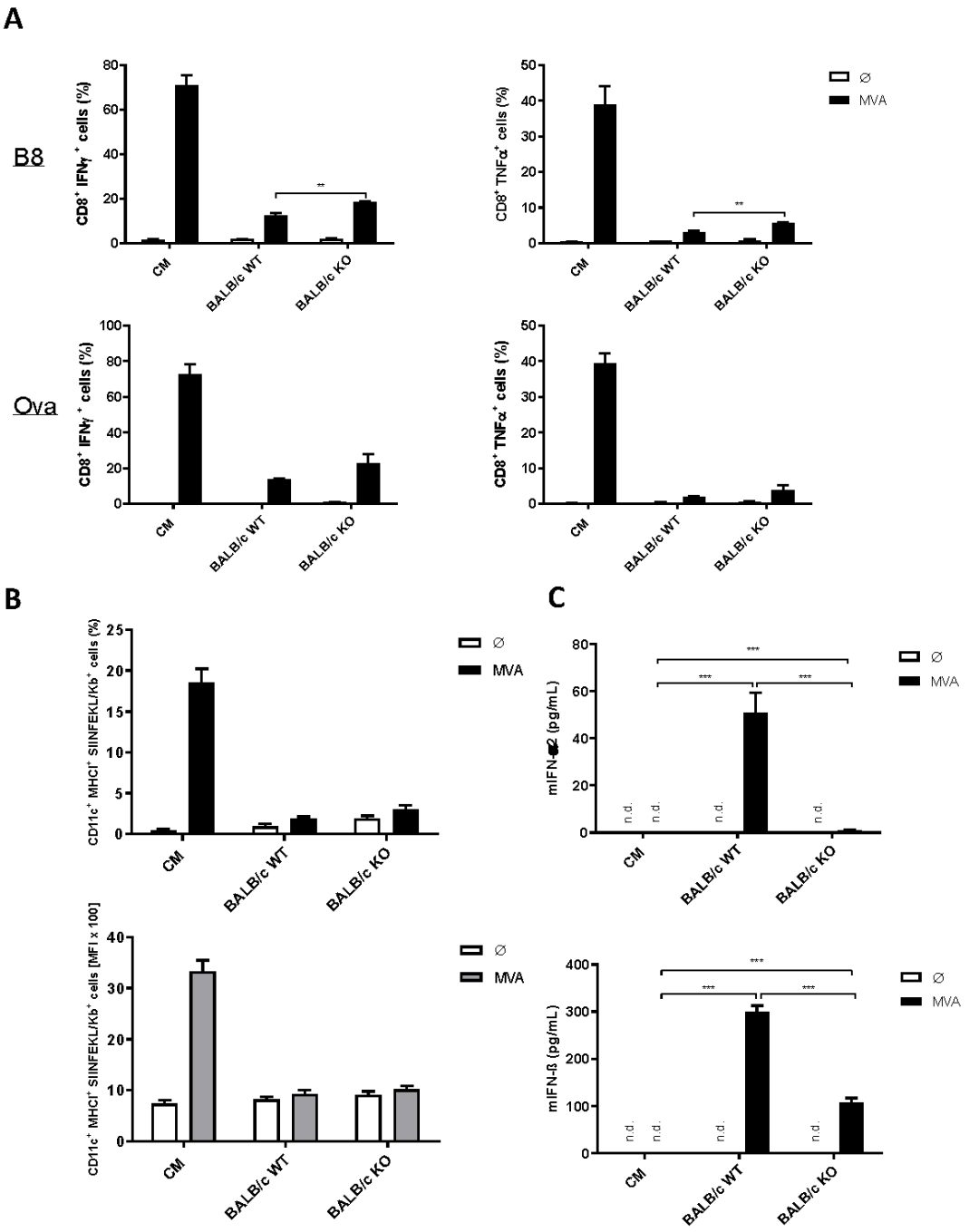

Figure 27: BALB/c P2RX7 KO BMDCs as feeders do not significantly alter the overall cross-presentation capacity of BMDCs. (A) Mock- (Ø) or MVA-PK1L-Ova-infected (MOI1, 20hpi) BALB/c-derived BMDC (either WT or P2RX7 KO) or CM cells (as controls) were PUVA inactivated and co-cultured with BMDCs (C57BL/6 background) for 20h. Thereafter, B8- (upper graphs) or Ova-specific (bottom graphs) $CD8^+$ T cells were added for 4h to assess INFγ (left graphs) or TNFα synthesis (right graphs). (B) Mock- or MVA-PK1L-Ova infected (MOI1, 20hpi) BALB/c BMDC (either WT or P2RX7 KO) or CM cells were PUVA inactivated and co-cultured with BMDCs (C57BL/6 background) for 20h to assess surface expression of SIINFEKL/H2-K^b on APCs (C57BL/6) (upper graph). The frequency SIINFEKL/H2-K^b complexes per cell was also calculated (MFI; bottom graph). (C) The supernatant of mock- or MVA-PK1L-Ova infected (MOI1, 20hpi) of BALB/c BMDC (WT or P2RX7 KO) or CM cells was used to determine the content of mIFN-α2 or mIFN-ß using the LumiKine Xpress mIFN-α2 or mIFN-ß 2.0 kits. Data are pooled from n=3 independent experiments (except (A) n=1) and are shown as means ± SD. P values indicate statistical significance (P) with **P ≤ 0.01; ***P ≤ 0.001.

7.7 Attempt of P2RX7 CRSIPR/Cas9 knockout in CM cells

CRISPR/Cas9 mediated off-side effects while attempting P2RX7 knockout in CM feeder cells led to an increased receptor activity

We have previously established that the surface P2X7 receptor in CM cells was not active. It has been demonstrated that functional P2RX7 is present in intracellular structures [89,90]. To exclude that intracellular P2X7 receptors in CM cells might impair processes that were important for subsequent MVA infection and alter their role as feeders during cross-presentation, we thought to create a P2RX7 knockout using the CRISPR/Cas9 technique. We selected a gRNA, which was predicted to be suitable for generating a functional knockout and used it to target a region in exon 1 of the *P2rx7* gene. Due to the lack of surface activity of P2RX7, we anticipated that the fluorometric assay was not a suitable assay to detect knockout of the receptor in CM cells. We therefore performed a western blot analysis and were surprised to see that the attempted knockout in CM cells (CM P2RX7 xKO) did not abolish P2RX7 protein synthesis bur rather increased it. Interestingly, CM P2RX7 xKO cells showed reduced production of OVA as compared to the CM WT cells after MVA-OVA infection (Figure 28A).

Fluorometric analysis demonstrated an increase in P2X7 surface receptor function, resulting in a significant increase in intracellular calcium upon Bz-ATP stimulus. This was independent of the MVA infection (Figure 28B).

In addition, we demonstrated the opening of the P2RX7-dependent pore, leading to the internalization of the test substance ethidium bromide and the subsequent increase in fluorescence intensity upon Bz-ATP stimulus in mock-infected CM P2RX7 xKO cells. Interestingly, pore opening was abrogated after MVA infection (Figure 28C).

It was previously published and we recently demonstrated that P2RX7 activity is correlated to the P2RX7-dependent release of extracellular vesicles [122,123]. Therefore, we either mock- or MVA-infected our CM cells (WT or CM P2RX7 xKO), stained with quinacrine, a nuclear stain, and PKH-26, a membrane dye, and visualized the cells during live confocal microscopy upon Bz-ATP stimulus. We detected secretion of EVs in the CM P2RX7 xKO cells but not in CM cells. EV secretion was enhanced when CM P2RX7 xKO cells were infected with MVA (Figure 28D).

We also showed that eATP levels in CM P2RX7 xKO MVA-infected cells were significantly reduced compared to CM MVA cells. As described above (Figure 17), infection with MVA led to a significant increase in eATP in CM WT cells (Figure 28E).

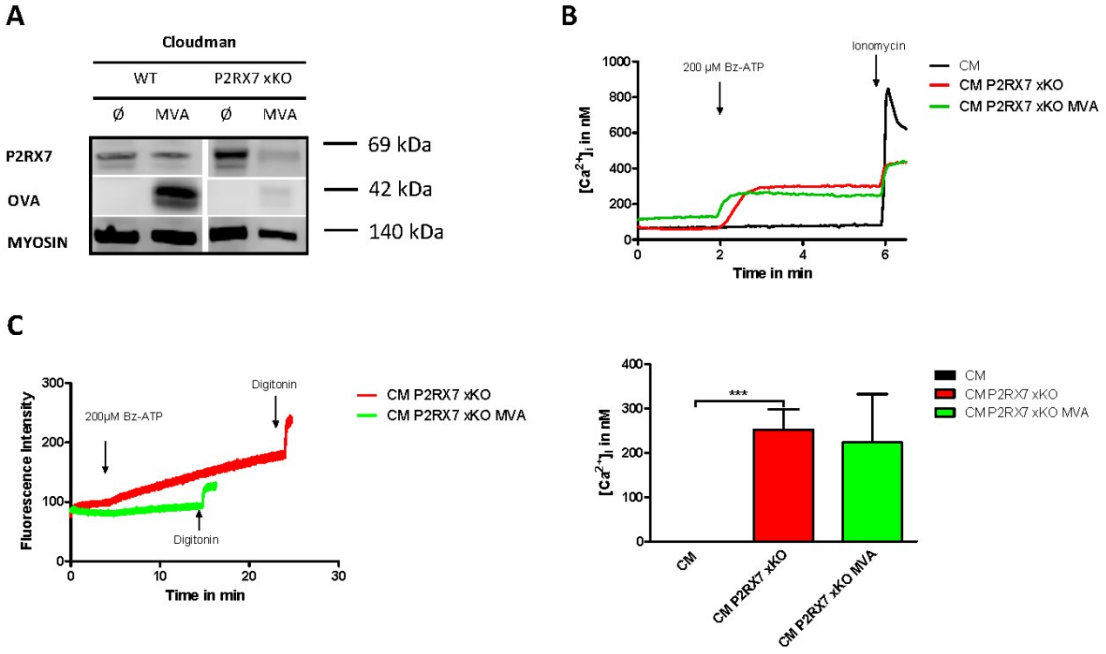
A
Cloudman
WT
P2RX7 xKO
Ø
MVA
Ø
MVA
P2RX7
OVA
MYOSIN
69 kDa
42 kDa
140 kDa
B
200 µM Bz-ATP
Ionomycin
CM
CM P2RX7 xKO
CM P2RX7 xKO MVA
[Ca2+]i in nM
Time in min
C
Digitonin
200µM Bz-ATP
Digitonin
CM P2RX7 xKO
CM P2RX7 xKO MVA
Fluorescence Intensity
Time in min
***
CM
CM P2RX7 xKO
CM P2RX7 xKO MVA
[Ca2+]i in nM

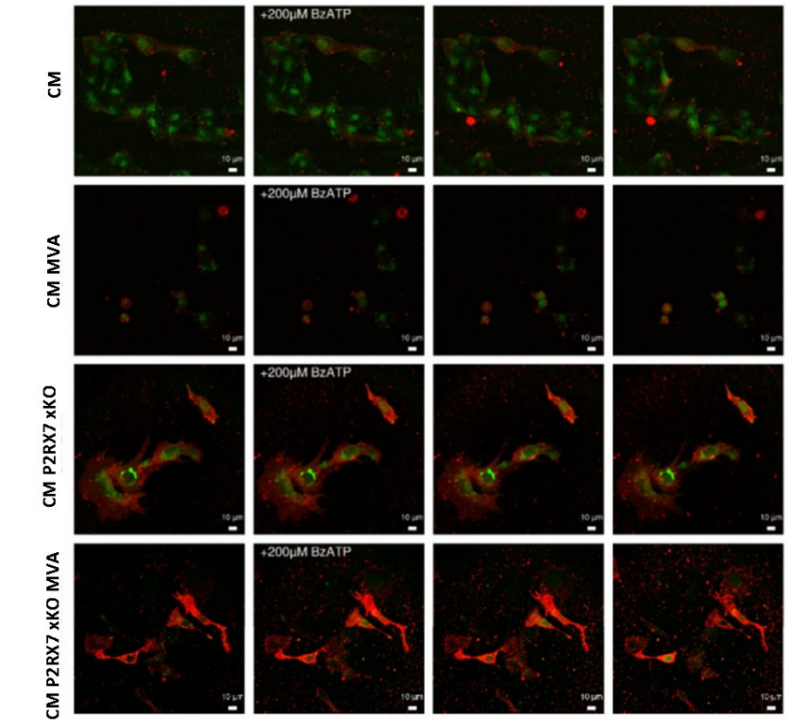
D
CM
CM MVA
CM P2RX7 xKO
CM P2RX7 xKO MVA
+200µM BzATP

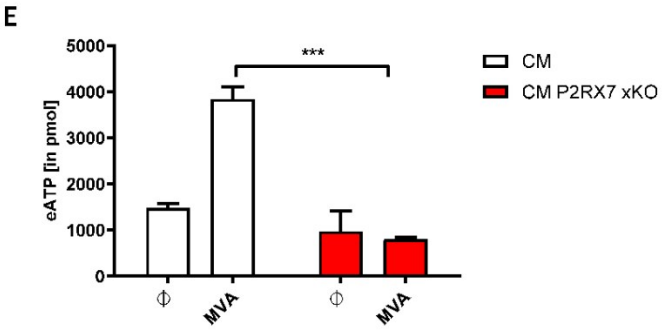
E
***
CM
CM P2RX7 xKO
eATP [in pmol]
Φ
MVA
Φ
MVA

Figure 28: Off-target effects due to failed CRISPR/Cas9-mediated P2RX7 KO in CM cells activates previously inactive P2X7 receptor. (A) CM cells were either not transduced (WT) or transduced with a lentivirus to generate the P2RX7 KO (P2RX7 xKO). Cells were mock- (Ø) or MVA-PK1L-Ova-infected (MOI1, 20hpi) to quantify P2RX7, OVA and Myosin as a control. (B) Mock- or MVA-infected (MOI1, 20hpi) CM or CM P2RX7 xKO cells were loaded with the fluorescent indicator FURA-2-AM (4µM) and then stimulated with 200µM Bz-ATP and 1mM ionomycin to measure intracellular calcium increase using fluorimetry (upper graph). Calculation of the delta from the peak to basal intracellular calcium influx (bottom graph). (C) Mock- or MVA-infected (MOI1, 20hpi) CM P2RX7 xKO cells were loaded with EtBr and then stimulated with 200µM Bz-ATP or 100µM digitonin to measure changes in fluorescence intensity due to P2RX7-specific pore opening. (D) CM (WT or P2RX7 xKO) cells were mock or MVA-infected (MOI1, 20hpi) and stained with quinacrine (visualizes nucleic acids) and PKH-26 (cell membrane dye) for live confocal imaging recording at 40x magnification. After 2min, cells were stimulated with 200µM Bz-ATP and EV release was visualized for a total of 20min. (E) CM or CM P2RX7 xKO were mock-or MVA-PK1L-Ova-infected at MOI1 for 20h and extracellular ATP was assessed in the medium using the Enliten Luciferase/luciferin reagent. Experiments shown are data from n=1 (A,C), n=2 (D) and n=3 (B,E) independent experiments as means ± SD. P values indicate statistical significance (P) ***P ≤ 0.001.

Viral gene and protein synthesis was impaired in CM P2RX7 xKO cells

Since the presence of the functional P2X7 receptor in CM cells altered viral gene expression, we thought to analyze the impact that the off-target effects due to the failed CRISPR/Cas9-mediated P2RX7 KO had on these cells. We first did a western blot analysis and compared synthesis of the model antigen OVA in CM and CM P2RX7 xKO cells (mock- or MVA-infected). For this purpose, we used three recombinant viral constructs, expressing *Ova* under the control of PK1L, an early poxviral promoter; P7.5, an early/late poxviral promoter; and P11, a late poxviral promoter [132,167].

We demonstrate that OVA protein could be detected as early as 4hpi in CM WT and CM P2RX7 xKO cells upon MVA-PK1L-Ova infection. However, it seems that OVA protein amounts were more abundant in CM cells than in CM P2RX7 xKO cells at 4hpi (Figure 29A, upper blot). Similarly, when CM cells were infected with MVA-P7.5-Ova, OVA protein was visible as early as 4hpi in CM cells, whilst protein synthesis was only detected at 8hpi in CM P2RX7 xKO cells. OVA protein in CM cells increased over infection time, however notably more in CM WT cells than in CM P2RX7 xKO cells (Figure 29A, middle blot). Finally, when infecting CM cells with an MVA expressing *Ova* under control of the late poxviral promoter P11, synthesis of OVA was shown as early as 8hpi in CM but not in CM P2RX7 xKO cells. OVA production was visible only at 24hpi in CM P2RX7 xKO cells and very weak as compared to the OVA synthesis in CM cells (Figure 29A bottom blot).

We also compared viral gene expression of *B8R, Ova* and *A19L* in CM and CM P2RX7 xKO cells. Consistent with the western blot results, both, the expression of *B8R*, an early MVA antigen and *Ova*, expressed under the control of the early PK1L promoter, started at 2hpi. Interestingly for both genes, expression remained up to eight times lower in the knockout as in CM cells. The highest *B8R* or *Ova* mRNA levels in CM P2RX7 xKO were reached between 6-8hpi, whilst maximal mRNA levels were reached at 4hpi in CM cells (Figure 29B, left and

middle graph). *A19L* expression, as predicted to be a late expressed antigen, started between 4 and 6hpi in CM WT cells, reaching its maximum expression at 8hpi and subsequently dropping the expression at 24hpi. In contrast to this, expression of *A19L* in CM P2RX7 xKO cells remained constantly very low, reaching its maximum at 24hpi (Figure 29B, right graph).

We wanted to exclude that the altered gene expression and protein synthesis were a consequence of reduced viral replication and therefore assayed this aspect by infecting CM and CM P2RX7 xKO cells with MVA and titrating the generated virions on MVA-permissive DF-1 cells. We showed that initially (0h) CM P2RX7 xKO cells showed an increased viral titer as compared to CM cells, which however diminished after time. In contrast to this, viral titer in CM cells decreased at 4hpi initially, but then rapidly increased to reach its maximum at 24hpi (Figure 29D).

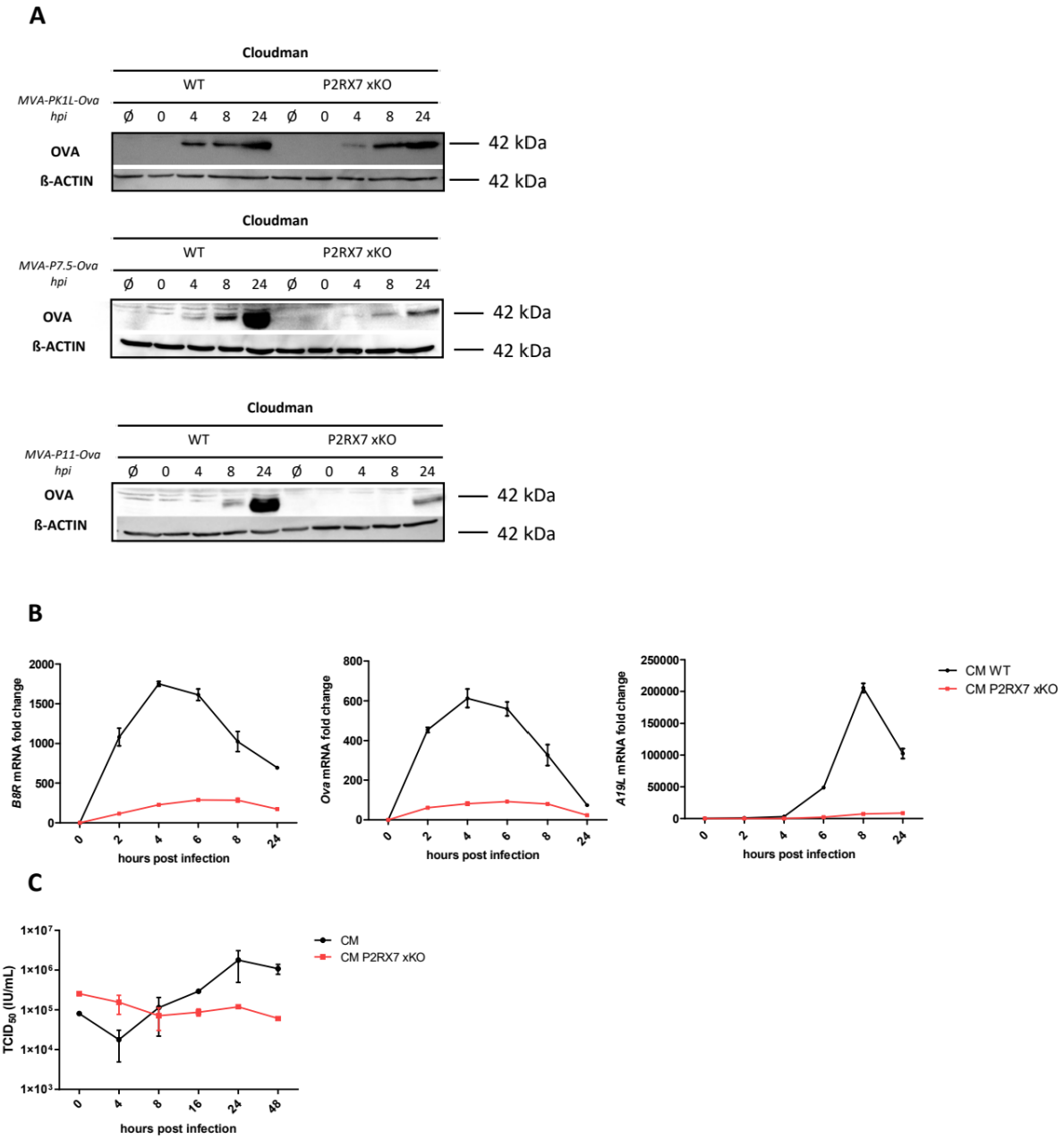

Figure 29: CM P2RX7 xKO cells show diminished viral gene expression and protein synthesis. (A) CM cells were either not transduced (WT), transduced with a lentivirus to generate the P2RX7 KO (P2RX7 xKO) cells and then mock- (Ø) or MVA-infected (MOI1, 0-24hpi) to test the presence of OVA and ß-ACTIN control protein. (Upper) MVA-PK1L-OVA, (middle) MVA-P7.5-OVA or (bottom) MVA-P11-OVA strains were used to infect CM cells. (B) Mock- or MVA-PK1L-Ova-infected (MOI1) CM or CM P2RX7 xKO cells were harvested at the indicated time points to isolate RNA, reverse transcribed and expression analysis of (left) *B8R*, (middle) *Ova* or (right) *A19L* were done. The ddCT values were calculated by normalization to the *18*s housekeeping gene control and the 0h time point of CM cells. (C) CM (WT or P2RX7 xKO) cells were infected with MVA-P7.5-GFP (MOI5) for the indicated time point (0h=1h at RT) and then harvested and prepared for back-titration on DF-1 cells. Cytopathic effect was determined one week post-experiment and tissue culture infectious dose ($TCID_{50}$) was calculated. Western blot experiments were performed for a total of n=1. (A) and expression and titration analyses for a total of n=2 (B,C) and are shown as means ± SD.

MVA-infected CM P2RX7 xKO cells led to a reduced cross-presentation when co-cultured with antigen-presenting cells

Since the main aim of this part of the study was to analyze the effect of the potential knockout in feeder cells during MVA antigen cross-presentation, we used these transduced feeders to be infected with MVA and then co-cultured with BMDCs and subsequently with $CD8^+$ T cells.

We assayed the synthesis of $CD8^+$ T cell activation markers in B8- or Ova-specific T cells and demonstrated that in the generated P2RX7 xKO cell line, even though the P2RX7 was fully functional (intracellular calcium increase and ethidium bromide pore opening) there was a significant reduction in IFNγ and TNFα production by B8- or Ova-specific $CD8^+$ T cells when co-cultured with BMDCs (Figure 30A). This effect was reflected in the expression of the SIINFEKL peptide on the H2-K^b of dendritic cells and the amount of complexes per cell (MFIs) when those were co-cultured with MVA-infected CM P2RX7 xKO cells (Figure 30B). We also saw a significant reduction in the synthesis of maturation markers, such as CD86 and CD40 on the surface of BMDCs, when co-cultured with MVA-infected CM P2RX7 xKO cells (Figure 30C).

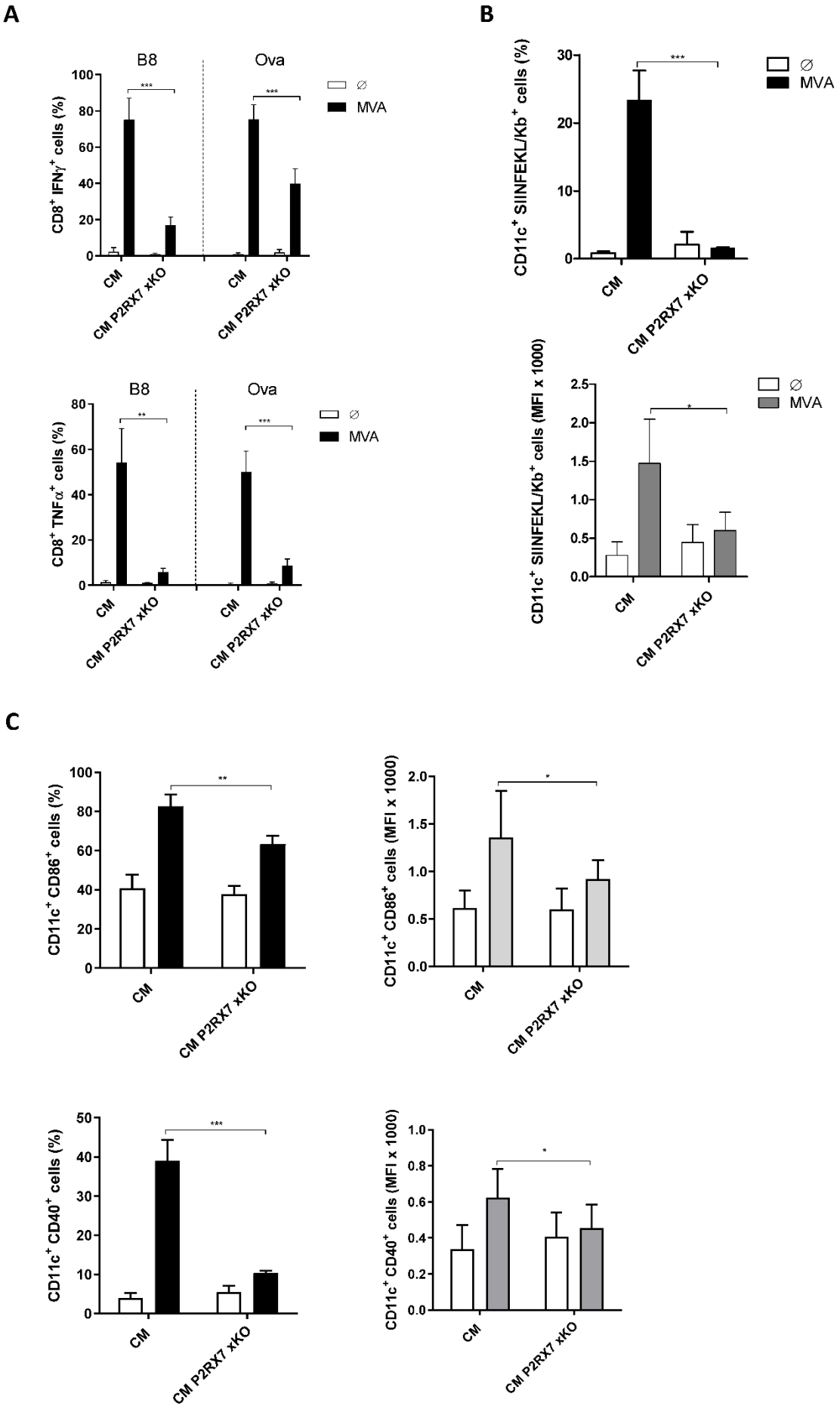
A
B8
Ova
∅
MVA
CD8+ IFNγ+ cells (%)
CD8+ TNFα+ cells (%)
CM
CM P2RX7 xKO
B
CD11c+ SIINFEKL/Kb+ cells (%)
CD11c+ SIINFEKL/Kb+ cells (MFI x 1000)
C
CD11c+ CD86+ cells (%)
CD11c+ CD86+ cells (MFI x 1000)
CD11c+ CD40+ cells (%)
CD11c+ CD40+ cells (MFI x 1000)

Figure 30: CRISPR/Cas9 treated feeder cells (CM P2RX7 xKO cells) offer a reduced cross-presentation capacity to BMDCs. (A) CM (WT or CM P2RX7 xKO) were infected with MVA-PK1L-Ova (MOI1) for 20h, harvested, PUVA inactivated and co-cultured with BMDCs (C57BL/6N background) for 20h. Cells were further co-cultured with B8-or Ova-specific $CD8^+$ T cells for 4h to assess IFNγ (upper graph) or TNFα (bottom graph) synthesis via flow cytometry. (B) Surface analysis of SIINFEKL/H2-K^b on the surface of BMDCs and the calculated amount of SIINFEKL/H2.K^b complexes per cell (MFI) (right) when co-cultured with MVA-infected CM or CM P2RX7 xKO cells. (C) Surface analysis of CD86 and CD40 maturation markers on BMDCs and the calculated markers per cell (MFI) (right graphs). Data are pooled from at least n=3 independent experiments and are shown as means ± SD. P values indicate statistical significance (P) with *P ≤ 0.05; **P ≤ 0.01; P***P ≤ 0.001.

CM P2RX7 xKO cells had an active STING-pathway

It was previously reported that absence of STING in feeder cells improved MVA-mediated antigen cross-presentation [66]. Therefore, since we saw a significant reduction in $CD8^+$ T cell activation markers when $CD8^+$ T cell were co-cultured with MVA-infected CM P2RX7 xKO cells and BMDCs, one of our first concerns was whether this specific pathway was altered in these feeder cells.

First, we performed a western blot analysis to assess the phosphorylation of STING and the downstream targets TBK1 and IRF3, indicating an active pathway. Indeed, we could detect strong activation of STING (p-STING), TBK1 (p-TBK1), and IRF3 (p-IRF3) in CM P2RX7 xKO cells infected with MVA starting from 6hpi. CM WT cells only showed low phosphorylation of TBK1 (p-TBK1) and no phosphorylation of STING (p-STING) (Figure 31A).

To confirm the activity of the STING-pathway, known to be responsible for the *de novo* synthesis of type I interferons, we tested the presence of mIFN-ß in the supernatant of mock- or MVA-infected CM cells [168,169]. We confirmed the release of mIFN-ß in CM P2RX7 xKO cells upon MVA infection, starting from 8hpi. Maximum mIFN-ß secretion was measured at 24 and 48hpi, reaching up to 350pg/ml. We did not detect mIFN-ß in mock- or MVA-infected CM cells (Figure 31B). We were also not able to detect any mIFN-α2 in neither CM P2RX7 xKO nor CM cells (data not shown).

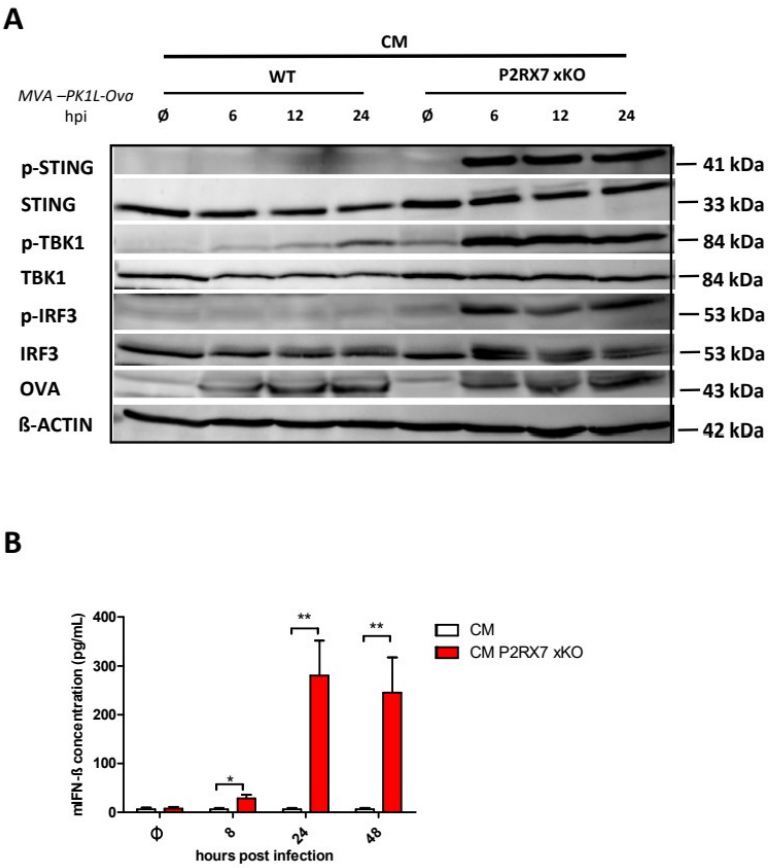

Figure 31: CM P2RX7 xKO cells secrete type I IFNs. (A) CM cells were either not transduced (WT) or transduced with a lentiviral Cas9 encoding vector to generate P2RX7 KO (P2RX7 xKO) cells and then mock- (Ø) or MVA-PK1L-Ova-infected (MOI1). The cells were harvested at the indicated time points and proteins were isolated to test the presence of STING, phosphorylated STING (p-STING), p-TBK1, TBK1, p-IRF3, IRF3, OVA and ß-ACTIN as control. (B) CM (WT or P2RX7 xKO) cells were infected with MVA-PK1L-Ova (MOI1) and the supernatants were harvested at the indicated time points to measure mIFN-ß using the LumiKine Xpress mIFN-ß 2.0 kit. Data are pooled from n=1 (A) or at least n=3 independent experiments (B) and are shown as means ± SD. P values indicate statistical significance (P) with *P ≤ 0.05; **P ≤ 0.01.

No mutations were detected in the selected gRNA region of the *P2rx7* exon 1

As previously shown, we observed off-target effects due to a failed CRISPR/Cas9-mediated P2RX7 KO. During the functional analysis of these cells, we saw an increase in intracellular calcium concentration, the pore opening and the secretion of EVs, all being indicative of a functional receptor. In addition to this, even though the receptor was functional, we saw a reduction in cross-presentation capacity when BMDCs were co-cultured with MVA-infected CM P2RX7 xKO cells. This concerned us, as with the transfection of CM cells with the active variant from BALB/c mice we saw a significant increase in the antigen cross-presentation capacity of BMDCs when co-cultured with MVA-infected CM P2RX7 cells. We also observed a completely different viral gene expression phenotype in these cells compared to CM P2RX7 xKO cells. We therefore wanted to investigate more closely, whether a direct off-target effect due to the CRISPR/Cas9 transduction occurred in our CM P2RX7 xKO cells as it is reported for this technique. It can occur that the Cas9 nuclease cleaves DNA regions similar to the gRNA region

that is supposed to be cut [170–173]. These regions do not have to be necessarily close to the gRNA region, but can also occur at long distances around the original region to be targeted by the gRNA. In addition to this, mutations due to the Cas9 cleaving in intronic regions can result in unspecific splicing variants of the protein, resulting in an erroneous protein that can be either misfolded or have another function [174,175].

We therefore sequenced the immediate region around the target gRNA in our CM P2RX7 xKO cells to check whether any mutation led to the phenotypical effects we observed using this cell line (Figure 32A, P2RX7 DNA transcript) and detected no mutation around the gRNA target region used for the CRISPR/Cas9 mediated knockout. The sequencing result is shown in Figure 32 B. We additionally sequenced the DNA around the transcript, including the beginning of each intron, downstream and upstream of exon 1, and were not able to detect any mutations as compared to the original P2RX7 sequence (Figure 32A, DNA around sequence). To exclude any other mutations in regions that we did not sequence resulted in a erroneous gRNA once transcribed and translated, we also sequenced the gRNA in reverse-transcribed cDNA of isolated RNA. We did not observe any mutations in this sequenced sample either (Figure 32A, gRNA in P2RX7 cDNA).

CpG islands are rich GC repeating regions within mammalian genomes that are described as epigenetic markers usually associated with the silencing of transcription due to methylation [176,177]. It has been described that CRISPR mediated modifications can lead to the alteration of these GC rich regions, therefore altering the transcriptome of the cell [178]. Since we were not able to detect any mutations in the region of interest, we thought to demonstrate that this region is rich in CpG islands and might therefore be prone to epigenetic modifications. The Sequence manipulation suite program allows detection of CpG rich regions, calculating as follows: “expected number of CpG dimers in a window is calculated as the number of 'C's in the window multiplied by the number of 'G's in the window, divided by the window length” [179]. An Obs/Exp ratio greater than 0.6 and the CpG content larger than 50% corresponds to an increased GC-rich area [180]. We performed a bioinfomatic analysis using the above-mentioned sequence manipulation suite [179] and detected an Obs/Exp ratio of 1.75 and a CpG content of 50.5% (Figure 32C).

We most likely observed an off-target effect in the CM P2RX7 xKO cells due to the CRISPR/Cas9 genome editing approach. Therefore, we stopped our research using these cells. We did not further investigate the methylation status, nor other signaling pathways in the CM P2RX7 xKO cells. Future attempts to generate an appropriate knockout are required to investigate P2RX7-specific functions in CM cells.

A

Sequencing sample	Result
P2RX7 DNA transcript	No mutations around gRNA
DNA around transcipt	No mutations
gRNA in P2RX7 cDNA	No mutations

B

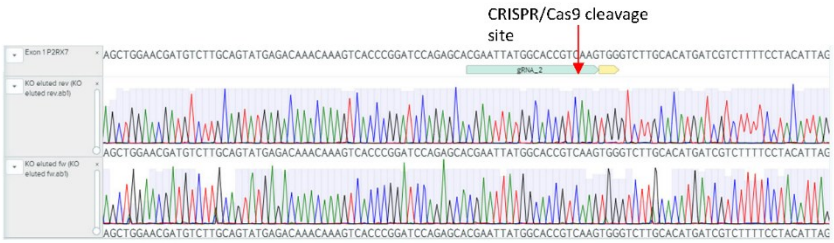

C

CpG Islands results

```
Results for 1200 residue sequence "Untitled" starting "taacatactt"

CpG island detected in region 32 to 231 (Obs/Exp = 1.75 and %GC = 50.50)

CpG island detected in region 33 to 232 (Obs/Exp = 1.75 and %GC = 50.50)
```

Figure 32: Sequencing of the exon 1 region of *P2rx7* in CM P2RX7 xKO cells shows no mutations. (A) DNA of CM P2RX7 xKO cells was isolated and sequenced (P2RX7 DNA transcript; DNA around transcript and RNA in P2RX7 cDNA) as depicted in the Materials and methods section. (B) Sequencing example of the gRNA targeted region in CM P2RX7 xKO cells and comparison to the *P2rx7* sequence. (C) Bioinformatic analysis to determine frequencies of CpG islands in exon 1 of P2RX7 using the Sequence manipulation suite from Bioinfomatics.com. All experiments or analyses shown were performed once.

8. Discussion

Originally, P2RX7 was thought to be a simple surface receptor, mediating ion fluxes upon agonistic activation. However, it was quickly acknowledged that P2RX7 functions go far beyond those initial considerations. Interestingly, despite the broad knowledge of P2RX7 functions, new research is still performed to this day to elucidate further and more ample roles of this purinergic receptor. Recently, P2X7 receptor function has been associated to the regulation of immune pathways. Little is known about the involvement of the P2X7 receptor during viral pathogenesis and during viral vaccine development, the latter being of high relevance for the scope of this study. MVA is one of the most potent viral vectors used in research and many studies only pinpoint the regulation of adaptive immune responses upon MVA infection. However, it has been demonstrated that innate triggers license feeder cells to activate BMCDs for cross-presentation of MVA antigens to subsequently activate $CD8^+$ T cells [66]. Following next generation sequencing analyses in this lab (Cornelia Barnowski, data not shown), we identified further candidates in MVA-infected feeder cells that were hypothesized to affect antigen cross-presentation, among which we focused on the purinergic receptor P2X7. Due to the limited knowledge of the role of P2RX7 in pathways participating in antigen generation and presentation, we aimed to explore various cellular machineries affected by P2RX7 that particularly focus on viral antigen processing and cross-presentation after MVA infection. This study aims to elucidate how MVA-mediated cross-presentation is regulated by feeder cells and how P2RX7 as an innate trigger in feeder cells influences these adaptive immune responses. Thus, our objective is to deepen the global understanding of how immune activation by viral vectors such as MVA can be optimized to possibly enhance immune responses and, as a consequence, advance future vaccine vector designs.

8.1 P2RX7 in CM feeder cells plays an important role during MVA infection

To investigate the role of the P2X7 receptor in feeder cells during MVA-mediated cross-presentation, we first aimed to analyze its surface function as a purinergic receptor. Since our established cross-presentation assay restricts us in the choice of feeder cells due to the MHCI mismatch requirement, we kept the S91 murine melanoma cell line as the most suitable and immunogenic feeder cells [181]. First, we measured the increase of intracellular calcium upon different stimuli. As expected, stimulus with concentrations from 200-800µM of Bz-ATP, a potent P2RX7 activator, did not lead to an increase in intracellular Ca^{2+}, independently of MVA infection (MOI1) (Figure 3A/B) [138]. This observed phenomenon can be corroborated with the fact that CM cells, deriving from the DBA mouse strain, have a less sensitive ATP variant of

P2RX7. It was published that cells from DBA mice have a natural mutation at position 451, where proline is exchanged with leucine, rendering the surface receptor function less sensitive to ATP stimuli [86,182]. We confirmed this altered allele by analyzing the sequence of this locus in the *P2rx7* gene of CM cells and compared it to the same locus in cells from C57BL/6 and BALB/c mice (Figure 3D). As previously published, cells from C57BL/6 also have the altered allele, unlike cells deriving from the BALB/c mouse strain, which harbor the original proline at position 451 [86]. Since we were not able to detect P2XR7 activation by calcium influx upon Bz-ATP stimuli, we thought to mimic cellular stress by infection with higher MOIs of 5 or 10. It was proposed that MVA infection induces apoptotic cell death and at the same time, leads to the release of high amounts of ATP, which might additionally serve to the Bz-ATP stimuli as P2RX7 agonists. Therefore, we conclude that viral infection poses a stress hazard to the cell initiating multiple pathways to overcome threat. As a consequence, the excess ATP can autocrinally stimulate P2RX7 [99,183,184]. However, even with potent cellular stress factors such as viral infection, as well as simultaneous stimuli with Bz-ATP, we were not able to detect intracellular calcium influx. Faulty loading of the fluorescent indicator FURA-2-AM can be excluded, as stimulation with the cell permeabilizing agent ionomycin increased $[Ca^{2+}]_i$ [139]. We therefore deduce that this surface receptor, even though it was already described to be less sensitive to ATP stimuli, seemed to be inactive in our CM cell line [82,86,99]. However, it was demonstrated that besides the activation with the known agonists Bz-ATP or ATP, P2RX7 can also be stimulated by ADP ribosylation of NAD, leading to an ATP-independent receptor opening. This process is mediated by ADP-ribosyltransferase and is a cell-specific phenomenon due to its absence in certain cell types [97]. For the purpose of this study, we focused on the role of ATP, which is considered to be the most relevant molecule involved in multiple cellular processes. Nonetheless, future research should include different agonists of the P2X7 receptor to study its activity in more detail [97,157].

Our focus lies on the understanding of the function of P2RX7 during MVA infection in CM feeder cells. However, it was proposed that P2RX7 activity can be affected by other purinergic receptors such as P2RX4. The gene for *P2rx4* is downstream of the *P2rx7* gene and shares approximately 47% similarity to *P2rx7*. The P2X4 receptor itself can also modulate P2RX7-dependent release of IL-1ß in macrophages [112,185]. NGS data showed differential expression of other purinergic receptors, including P2RX4 upon MVA infection (Cornelia Barnowski, data not shown). Therefore, we need to assess the possible activity of other purinergic receptors leading to the intracellular increase of Ca^{2+}, as they have been shown to be modulated during co-cultivation with gp120 (envelope glycoprotein) of HIV-1 [186]. As expected, stimulus with ATP led to the intracellular increase of Ca^{2+} in a dose-dependent manner, confirming our initial hypothesis that other purinergic receptors yet to be defined are also participating in calcium fluxes. Additionally, the response elicited after ATP stimuli strongly resembles the P2 (but not P2RX7) specific desensitizing effect, substantiating the function of

other surface receptors in CM cells (Figure 4A) [77]. This increase in intracellular Ca^{2+} derived from the presence of extracellular calcium molecules and not from intracellular calcium stores, distorting the experimental outcome (Figure 4B) [187].

Even though the original P2RX7 variant in CM cells did not show calcium channel function, we still hypothesized that P2RX7 played an important role in CM cells. CM cells with a functional form of P2RX7 from BALB/c mice showed, as expected, an intracellular Ca^{2+} increase [86,131]. Inhibition of the P2RX7 competitive inhibitor A740003 abolished the observed calcium increase, confirming the P2RX7 specific function upon transfection (Figure 5A) [78,94]. Interestingly, transfection of the P2RX7 also resulted in a significant increase of *P2rx7* expression in CM cells, as compared to CM WT or empty vector transfected cells. It seems that expression of *P2rx7* is generally kept low in the non-P2RX7 transfected cells and MVA infection resulted in a slight increase in expression. MVA infection in CM P2RX7 cells, however, seems to generally increase *P2rx7* expression after 2hpi. It is a known phenomenon that P2RX7, depending on cell type and immunological situation, can serve as either a pathogenic or beneficial receptor and, therefore, its expression is regulated accordingly [80,188–190]. In this case, it seems that low *P2x7* expression is crucial for these cells. In contrast, in the P2RX7 transfected cells, we observed an increase of up to 50 times in fold after MVA infection, indicating the active regulation of *P2rx7* due to viral infection (Figure 5B). Similarly, increased *P2rx7* expression upon mycobacterial infection in lung leukocytes *ex vivo* was also demonstrated, indicating a possible response mechanism to danger signals, such as ATP or infection *per se*, which could then result in autocrine stimulation [99,183,184,191]. However, since the transfected P2RX7 was under the control of a cytomegalovirus promoter, further studies are required to establish the regulation of the *P2rx7* expression by MVA infection. These results are the first in establishing the importance of a functional P2X7 receptor during poxviral infection.

We further analyzed the role of the receptor function after MVA infection and observed a significant increase of intracellular Ca^{2+} at 4hpi but not at 20hpi (Figure 6A/B), implying the importance of the P2RX7 during the early infection phases of MVA and fortifying the previously shown expression data. This effect could hint at a possible function of P2RX7 during viral gene expression. It was already shown that P2RX7 is crucial during human herpes virus 6 A entry or SARS-CoV-2 infection [192,193]. Another study also reinforces the potential role of hepatitis B virus entry into lung cells, demanding further research on purinergic receptor function during MVA entry [194].

It has been shown, that presence and strong activation of P2RX7 leads to the opening of the pore [77,110]. Interestingly, transfection of the CM cells with the active P2RX7 variant did not lead to the opening of the pore, independently of the additional MVA infection (20hpi) (Figure 6C). This could be considered beneficial, as pore opening can be associated with cell lysis,

which in turn could abrogate MVA antigen generation and subsequent cross-presentation [144]. In addition to this, the pore formation was described to occur only upon strong and prolonged activation of the P2X7 receptor, indicating that, under our tested circumstances, P2RX7 activity is regulated only to a limited degree [87,92,144]. Future studies should include the closer analysis of the pore at earlier MVA infection time points (such as 4hpi). However, as previously stated, pore opening is associated with cell lysis and therefore cell death, predicting a non functional pore during early stages of MVA infection as well.

As we were characterizing P2RX7-specific functions, we also tested the ability of P2RX7 to induce membrane blebbing, which we showed in CM P2RX7 cells in an MVA-dependent manner (Figure 7) [116]. In literature, P2RX7-dependent blebbing is described in models that do not necessarily involve infection or another specific trigger other than ATP [116,195]. Membrane blebs can result from the initiation of apoptotic pathways, which can develop into apoptotic bodies, components of the extracellular vesicle division. These, in turn, play an important function in the regulation of immune signaling, which will be discussed at a later time point [120,196,197]. Additionally, a prerequisite of membrane blebbing is the rearrangement of the actin cytoskeleton. This has been proposed to occur upon sphingomyelinase activation via P2RX7-dependent kinases [115,116,198,199]. In this regard, it was demonstrated that VACV, the parental strain of MVA, can also induce the activation of the MAPK and ERK cascade to mobilize actin dynamics, playing a crucial role during the different stages of viral infection [200,201]. Since we did not observe membrane blebbing and, hence, no visible cytoskeleton rearrangement in the presence of an active P2X7 receptor apart from MVA infection, we assume that both triggers, P2RX7 activity and MVA infection are required to induce cellular actin reorganization. Mercer and colleagues already stated that vaccinia virus exploits the exposure of phosphatidylserine on the viral membrane to induce apoptotic mimicry, as will be discussed at a later time point in more detail [202]. This suggests a possible mutual modulation of cellular processes by P2RX7 and the poxviral infection. Therefore, future studies should implement the analysis of cytoskeleton rearrangements and their modulation by P2RX7 during MVA-antigen generation.

In conclusion, we demonstrate that the surface P2X7 receptor in wildtype CM cells cannot be activated with low as well as with high Bz-ATP concentrations. Furthermore, induced stress factors, such as MVA infection, do not alter the sensitivity of the cells to P2RX7 channel opening. However, we could show that other purinergic receptors were active in CM cells and need further investigation as potential modulators of immune responses.

6.2 The functional P2RX7 in CM feeder cells strongly affects MVA-mediated cross-presentation by BMDCS and the synthesis of viral antigens

The focus of this study is to assess the implications that functional P2RX7 has on CM cells during MVA infection and subsequent cross-presentation by dendritic cells. We demonstrated that the presence of the ATP-sensitive P2RX7 variant in MVA-infected CM feeder cells resulted in significantly enhanced synthesis of IFNγ and TNFα in B8- or Ova-specific (only TNFα in the latter) $CD8^+$ T cells when co-cultured with BMDCs. It seems that the Ova-specific $CD8^+$ T cell line was more easily activated to produce cytokines, as we have previously shown with other experiments (Figure S9). We further measured the surface expression of the SIINFEKL peptide on the H2-K^b of BMDCs upon co-culture with MVA-infected CM cells (Figure 8). This assay is more sensitive in determining the importance of cross-presentation processes [203]. Consistent with the T cell assay, we observed a significant increase in SIINFEKL/H2-K^b surface expression on BMDCs when CM cells harbored the active P2RX7 and were infected with MVA. It is challenging to compare these results with current literature, as no research describing the role of P2RX7 in feeder cells for cross-presentation of antigens is available. However, many publications display the functions of P2RX7 in APCs and T cells for adaptive immune responses [110,190,204]. In this context, it was demonstrated that active P2RX7 in dendritic cells can lead to cross-dressing of preformed MHCI-SIINFEKL complexes from one dendritic cell to another [110]. We excluded, however, that this phenomenon occurred in our setup, as our feeder cells harbor a different MHCI haplotype than our APCs and T cells, therefore preventing antigen presentation upon cross-dressing of preformed MHCI-SIINFEKL molecules from CM cells. We also observed that the mere presence of P2RX7 in feeder cells led to a significant increase of MHCI on BMDCs. This is in contrast to current literature, as studies describe a reduction of MHCI in dendritic, Kupffer, or lung cells upon P2RX7 activation [110,205,206]. However, this data is not fully comparable to our study, as we employ CM cells as feeders and not APCs with an active P2RX7 receptor to analyze antigen presentation processes. We hypothesize that the observed increase in MHCI synthesis in dendritic cells being co-cultured with CM P2RX7 cells is mediated by multiple signals deriving from the feeder cell, one of these being the P2RX7-dependent secretion of cytokines, which might induce MHCI synthesis [141,207–209]. As expected, P2RX7-specific effects in MVA-infected CM cells were further corroborated when using the A740003 inhibitor (Figure 9) [93,210]. However, A740003 treatment of MVA-infected CM P2RX7 cells or mock-infected CM P2RX7 cells did not lead to a reduction IFNγ synthesis in $CD8^+$ T cells nor MHCI production in BMDCs, respectively, inferring the presence of an alternative P2X7 receptor-mediated pathway. It is noteworthy to mention that A740003 acts on the surface P2X7 receptor and is unlikely to permeate membrane structures. Consequently, possibly present intracellular P2RX7, which

might be involved in regulating APCs MHCI synthesis are not targeted by A740003 inhibition in this setup [89,90]. This is further corroborated by the fact that other maturation markers of APCs were also not affected upon A740003 treatment of MVA-infected CM P2RX7 feeder cells (Figure S1).

MVA as a viral vector allows for the expression of all classes of viral genes despite its replication deficiency in most mammalian cells [16,211]. Since we observed an increased antigen presentation capacity in BMDCs when co-cultured with MVA-infected CM P2RX7 cells, we initially thought that the presence of a functional purinergic receptor might alter the replication capacity of MVA, therefore increasing viral load and, as a consequence, viral protein amounts required for antigen cross-presentation. However, even though we initially observed a higher viral titer at 0hpi in CM P2RX7 cells titrated on DF-1 cells, the final viral output was similar to CM WT or CM pcDNA3 cells after 24hpi (Figure 10). It is well known that MVA can modulate the expression of cell surface receptors, therefore possibly facilitating its entry. In this regard, Laliberte and colleagues have proposed the requirement of different cellular proteins for poxviral cell attachment and entry in order to allow correct viral fusion with the cell membrane. Different cellular mechanisms have been described to be favorable for this process, such as membrane blebbing, cytoskeleton rearrangements and the function of certain protein kinases. Therefore, it could be that P2RX7 is directly involved in viral cell entry, as previously shown [82,107,111,195,199,212,213]. Indeed, it was demonstrated that the transfection of a functional P2X7 receptor in HEK293 cells confers phagocytosis capacity to these non-phagocytic cells. This activity was described to be ion-channel independent and was proposed to depend on the modulation of the cytoskeleton by P2RX7, possibly permitting viral entry [214,215]. Therefore, we first attributed the initially increased $TCID_{50}$ viral titer to a possible altered entry mechanism, other than micropinocytosis which usually takes place [213]. However, this would go along with an increased viral gene expression at early time points in CM P2RX7 cells, a phenomenon that we could not observe when analyzing *B8R*, *Ova* and *A19L* gene expression (Figure 11). As shown in the expression analyses above, we conclude that the presence of an active P2RX7 contributes to the altered MVA gene expression pattern and subsequent protein synthesis. To what extent these P2RX7-regulated phenomena affect antigen generation and subsequent antigen cross-presentation remains to be characterized. In addition to this, it also must be determined, whether the delayed time-expression pattern plays a crucial role for the improved antigen generation and subsequent cross-presentation, as delayed antigen availability was previously described to be important for improved cross-presentation [52]. For this purpose, cross-presentation analyses involving infection of the different feeder cells with MVA-vectors containing intermediate/late promoters could be used.

On the one hand, we hypothesize that the hijacking of MAPK/ERK signaling pathways by both poxvirus and P2RX7 plays a crucial role in the generation of adaptive immune responses, as

previously described. As a result, intracellular trafficking of certain proteins is possibly relevant for gene expression, viral DNA replication and subsequent antigen presentation [116,199,200,216]. On the other hand, it has been described that RNA regulation occurs on a different level than protein regulation, therefore allowing for a more controlled modulation under stressful conditions. This was shown in a study where different mammalian cell lines were treated with DTT, mimicking a stress factor and demonstrating the capacity of RNA levels to recover more promptly than protein levels, which were easily affected by misfolding stress [217,218]. This previous study, together with our experimental outcome in the increased mRNA expression level of viral genes in later time points but unaltered protein levels could indicate a potential role of mRNA during antigen cross-presentation processes, suggesting for the first time an alternative mechanism for activation of $CD8^+$ T cell responses. This will be addressed in more detail in a later section.

6.3 P2RX7 functionality in CM feeder cells affects energy metabolism and apoptosis signaling pathways

The duality of the P2X7 receptor has been extensively studied in the role of cell proliferative or cell death mechanisms [81,189,190]. Here, we investigated which effects the presence of a functional P2X7 receptor had in our model cell line (CM) and how this was affected by MVA infection. One of the described P2RX7 features is its involvement in initiating apoptosis, mediated by caspase activation and followed by cell blebbing. The exposure of phosphatidylserine residues on the cell surface is also controlled by P2RX7 activity [96,112,219]. We could demonstrate active Caspase-8 in both mock- and MVA-infected CM P2RX7 cells (Figure 13 A/B). This was accompanied by a large number of late apoptotic cells at 6hpi as well as in mock-infected CM P2RX7 cells. Interestingly, as compared to CM or CM pcDNA3 cells, CM P2RX7 MVA-infected cells showed a significantly lower amount of early apoptotic cells at 20hpi (Figure 13 C/D) as demonstrated by analysis of phosphatidylserine surface expression.

It is noteworthy that apoptosis of cells is a pre-requisite for antigen to be released so APCs can phagocyte and subsequently present it for the activation of $CD8^+$ T cells [48,52,220]. Besides this, phosphatidylserine flip is regarded as a “find-me” signal for phagocytic cells, facilitating engulfment and subsequent uptake of the structures. Interestingly, we have observed that even though CM P2RX7 cells (mock- or MVA-infected) presented typical apoptotic markers, such as Caspase-8 activation or phosphatidylserine flip, the cell morphology or immediate cell death was not necessarily affected. Indeed, cells bearing an active P2X7 receptor seemed to handle MVA infection better than CM or CM pcDNA3 cells

(Figure S3). This phenomenon was already described and results in the engagement of the immune system in a “silent” manner, stimulating pro-inflammatory processes without killing the cell itself. We hypothesize that P2RX7 engages these pseudo-apoptotic mechanisms to attract the attention of dendritic cells, e.g. by secretion of cytokines or exposure of “eat-me” signals, but at the same time allows for proper cell function to create optimal conditions for viral gene expression [189,221–224]. Additionally, it was shown in a VACV infection model, that infection was facilitated by “apoptotic-mimicry”, hence by engaging the phosphatidylserine residues on host cells to promote viral uptake [202,225].

These results are further fortified when analyzing the cellular metabolism in CM P2RX7 cells upon MVA infection. We demonstrated a significant increase in maximal respiration and spare capacity in mock- or MVA-infected CM P2XR7 cells, when compared to CM or CM pcDNA3 cells. Moreover, the extracellular acidification rate was also increased in CM P2RX7 cells, independently of the infection (Figure 15). These results indicate that CM P2RX7 cells can adapt to a higher energy demand, which under the circumstances in this study is mimicked by the MVA infection, by increasing ATP generation processes and creating a more favorable microenvironment for antigen generation and other processes triggering APCs activation [226]. Indeed, metabolic reprogramming in order to fit the needs of a viral infection has already been described during human cytomegalovirus infection [227,228]. This was further consolidated by the high presence of intracellular ATP in MVA-infected CM P2RX7 cells, as compared to MVA-infected CM or CM pcDNA3 cells (Figure 17A). The improved mitochondrial metabolism is directly attributed to the P2X7 surface receptor activity, as the influx of calcium leads to its entry into mitochondria and, as a consequence, increases its potential, leading to ATP synthesis and fitness of the cell, which we observed in this study [81]. Additionally, Sarti and colleagues have recalled the importance of the P2X7 receptor on the mitochondrial surface to be similarly involved in regulating mitochondrial metabolism [89]. VACV gene transcription was also shown to be highly dependent on ATP availability, possibly explaining the importance of a high ATP content in mock-infected CM P2RX7 cells [229,230]. The importance of mitochondria during MVA infection was further corroborated in a study analyzing DNA damage upon MVA infection, as a possible mechanism during microbial infection [223].

To correlate this finding with the described delayed, but increased viral gene expression in this study, it was shown that the VACV D10 decapping enzyme colocalized with mitochondria. It could be that the presence of P2RX7 on mitochondria might modulate and reduce the decapping function of VACV proteins and therefore hinder RNA decay [231]. The role of RNA during cross-presentation has to be further established, to determine whether the increased availability of RNA in feeder cells at later time points benefits cross-presentation mechanism.

In contrast to intracellular ATP contents, extracellular ATP in MVA-infected CM P2RX7 was either similar to CM or CM pcDNA3 cells under mild stress conditions (MOI1, 6hpi) (Figure

17B) or significantly lower when cells were MVA-infected with a higher MOI (Figure 16C) or for a longer period (Figure 17D). The fact that CM or CM pcDNA3 cells released higher amounts of ATP is most likely attributable to apoptotic processes occurring upon MVA infection [47,78,232]. It might also be described as a self-regulated protective mechanism against cell death in CM P2RX7 cells, as it has been shown that high ATP levels in active P2RX7-bearing cells tend to turn this receptor into a pro-apoptotic receptor [81]. In conclusion, ATP increase in CM or CM pcDNA3 is most likely apoptosis-dependent and could be triggered by MVA infection, whereas ATP levels in CM P2RX7 cells are rather regulated by purinergic receptor signaling as previously established [95]. Extracellular ATP levels in mock-infected CM P2RX7 cells were significantly higher at 6hpi (Figure 17 B/C). This hints at autocrine or paracrine stimulation of the P2X7 receptor, something that has already been described in the past [77,99]. Furthermore, another interesting phenomenon is worth mentioning in this section. Indeed, it was recently postulated that oxidative stress during VACV infection impairs early and late gene expression and subsequent virus production. VACV itself was shown to harbor viral redox proteins in lateral bodies to regulate reactive oxygen species (ROS) homeostasis in host cells [233]. In this regard, mitochondria serve as a buffering system for ROS production and modest ATP amounts activating P2X7 receptors have been shown to contribute to protective mitochondrial function [189,234–236]. It is likely that the P2X7 receptor in CM P2RX7 feeder cells aids to overcome infection as a stress factor, by improving mitochondrial function and removing harmful ROS, affecting overall cell function and in turn viral gene expression. It remains to be determined whether mitochondria-resident P2RX7 might also play a specific function in regards to ROS regulation and viral gene expression [89].

Due to variation in endogenous ATP levels as well as cell type-specific P2RX7 functions, it is challenging to describe the function of ATP in purinergic receptor downstream signaling [77,94]. ATP was shown to induce maturation of BMDCs, increasing MHCI and MHCII synthesis and resulting in stimulation of T cells [159]. Additionally, ATP has been described to play a crucial role in TAP-mediated peptide processing and transport, hypothesizing that released ATP from feeder cells could be phagocytosed by BMDCs and further used in these cells for antigen presentation to T cells [160]. We attempted to test the physiological function of extracellular ATP during the cross-presentation process, considering its potential importance as DAMP during antigen presentation. We initially hypothesized that ATP availability during co-culture with BMDCs was not the main mechanism by CM feeder cells to regulate antigen cross-presentation by BMDCs, as ATP amounts were different in the tested cell lines upon MVA infection. When adding apyrase to the co-culture of BMDCs and MVA-infected CM cells, we did not observe any significant changes in $CD8^+$ T cell activation as well as in the expression of SIINFEKL on the H2-K^b of BMDCs, confirming our initial theory (Figure 18). Even though these data were not consistent with the previously mentioned literature, we have to consider the specific experimental conditions, as the amount of apyrase used might

not be sufficient to hydrolyze ATP amounts, therefore not showing experimental differences. Moreover, by the addition of apyrase in the co-culture, we have to consider that ATP was possibly released by BMDCs, which might also affect cross-presentation. These results imply new aspects of P2RX7 signaling and the potential role of ATP during the initial stages of MVA infection in feeder cells. This should be assessed in a future study, possibly depleting ATP during viral infection of feeder cells. Nonetheless, other data also suggest that the presence of ATP can not only be attributed to improved antigen presentation but also to a diminished immune response, unveiling again the dual function of P2RX7 and ATP depending on the cell type [94,237,238]. Unlike previously described, with the current results we do not outline the released ATP as a “find-me” signal to engage phagocytes but assume that there must be other mechanisms to attract APC's attention in these feeder cells [239].

In another experiment in an attempt to characterize intracellular functions of P2RX7, we obtained an interesting finding. We found that in CM P2RX7 cells, MVA infection caused co-localization of P2RX7 structures with viral factories and the nucleus (Figure 16) [240]. It is not unusual that P2X7 receptors are found in intracellular compartments, such as mitochondria or nuclei [89,90]. It was surprising, however, that P2RX7 molecules were potentially found as oligomers around viral factories [77]. This phenomenon was observed for the first time in this study and could impact the cross-presentation capacity of APCs. These viral structures contain cell organelles such as mitochondria and may serve as a defense mechanism, serving as “hiding structures” [240]. It is possible that mitochondrial structures within viral factories allow direct access to ATP, a relevant molecule for viral transcription, therefore facilitating gene expression [229,241]. In addition, viral factories may serve as an immune defense mechanism employed by both VACV and MVA to avoid entry of late viral antigens into the cross-presentation pathway in APCs [132,242]. We hypothesize that a so far unappreciated mechanism of antigen generation in CM P2RX7 cells takes place, which needs to be further characterized. Since we have already observed that the expression kinetics of viral genes is delayed due to the presence of functional P2RX7, it could result in the sequestration of these “pseudo-late” genes in viral factories, preventing quick degradation and allowing the release of these at later time points, when more convenient for antigen presentation by dendritic cells. However, Tewalt and colleagues reported that early viral antigens are not sequestered in viral factories. Similarly, only late antigens, which are directed to compartments outside of viral factories, are cross-presented by virus-infected cells. This suggests that P2RX7 might somehow alter the localization of early viral antigens, redirecting them to viral factories - a result Tewalt and colleagues did not achieve, even when using early promoters with the originally late antigen [242]. Whether P2RX7 is directly involved in the release of these antigens into the cytoplasm and then into extracellular space or whether it serves as a mediator for release processes, remains to be determined. Nonetheless, the confocal experiments

should be considered with caution, as more P2XR7 structures were expected on the cell surface, hence requiring an improved methodology to visualize those.

These findings further strengthen the importance of intracellular P2RX7 structures and their role in antigen-generation processes, especially early during MVA infection. Thus, it is essential that in future studies the location of P2RX7 as well as its role at different time points of viral infection will be analyzed in more detail. Additionally, other cell death pathways, such as autophagy, should be analyzed as well, as they may be important for cross-presentation of melanoma antigens *in vitro* and *in vivo.* Their modulation has already been associated with P2RX7 activity [55,243,244]. Together with the potential role of ATP, further comprehensive ATP studies at different infection time points, along with assays with ATP in co-culture are necessary. As a first-time study, we also emphasize the relevance of feeder cells and purinergic signaling in the MVA infection model.

6.4 The secretome of CM P2RX7 cells is actively involved in improved MVA antigen cross-presentation

P2RX7 is involved in many signaling pathways in addition to its function as an ion channel. One of the most studied functions is the release of extracellular vesicles, which play a crucial role during inflammation [78,121]. This is mediated by the P2RX7-dependent action of the Src-kinase and subsequent p38 MAPK phosphorylation, inducing acid sphingomyelinase activation and subsequently microvesicle shedding [115]. In this chapter, we aimed to identify the functions and contents of these vesicles with a particular focus on their role for adaptive immune responses.

We first confirmed the P2RX7-dependent secretion of microvesicles in our P2RX7-transfected CM cells. Secretion was only visible when CM P2RX7 cells were infected with MVA, elucidating the possible importance of these vesicles during MVA infection. Minor amounts of vesicles were present in MVA-infected CM or CM pcDNA3 cells, possibly displaying the expected apoptotic cell structures described to be formed during MVA infection (Figure 19) [47,120]. Besides apoptotic bodies, microvesicles and exosomes are known to be formed by all types of cells, the latter two being described to be P2RX7-dependent [78,113,114]. We further aimed to investigate the viral transcriptome in these vesicles and isolated these structures as described in the Materials and Methods section. Using this methodology, we were able to discern the two bigger fractions, hence apoptotic bodies (P2RX7-independent and formed also by CM cells upon infection), as well as microvesicles (P2RX7-dependent and mainly formed by P2RX7-transfected CM cells). Of note, if one aimed to analyze the function of exosomes, an additional ultracentrifugation step is strictly required to obtain the smaller fraction and should

be analyzed in future studies. Each fraction has been described to have a specific content and employs different functions [47,120]. However, we demonstrated the presence of viral mRNA in extracellular vesicles of all MVA-infected cells (independent of the presence of active P2RX7). Interestingly we observed significantly higher mRNA levels of *B8R* in CM P2RX7 at 0hpi, suggesting the prompt release of mRNA in these vesicles and explaining the lower expression of the gene intracellularly, as shown above (Figure 20 A-C). This, however, needs to be further confirmed, by e.g. specifically inhibiting the vesicle release and subsequently analyzing *B8R* expression. In addition, the levels of OVA protein, the preferred antigenic source for cross-presentation, were comparable in EVs derived from all tested cell lines (Figure 20 D/E), indicating that P2RX7 in feeder cells employed a different mechanism to improve dendritic cells-mediated cross-presentation [52,245,246]. OVA protein levels were also not altered in the supernatant of MVA-infected CM P2RX7 as compared to CM or CM pcDNA3-infected cells (Figure 21 A/B). However, a higher amount of total protein release was visible in MVA-infected CM P2RX7 cells, hinting at the potential role of other secreted proteins for MVA-mediated cross-presentation (Figure 21C). It was already demonstrated that P2RX7 stimulation leads to the release of different protein subsets involved in cytoskeletal reorganization, protein binding and redox regulation in M1 macrophages [162]. Which role these or other proteins of the secretome during P2RX7 activation execute for cross-presentation needs to be further characterized.

We also analyzed the secretion of inflammatory cytokines in the supernatant of mock- or MVA-infected feeder cells. The active P2X7 receptor allowed CM cells to synthesize and release critical inflammatory mediators, such as KC, MCP-1, RANTES, IP-10 and IL-6. Even though the concentrations were still high upon MVA infection, infection *per se* slightly decreased the release in CM P2RX7 cells (except for IL-6, where a reversed effect was visible). A prolonged MVA infection led to an increase of cytokines released (Figure 21 D/E). Cytokine release in the presence of active P2RX7 has already been demonstrated in various studies [125,189]. This is mainly initiated upon P2RX7-dependent calcium influx and the activation of the Ca^{2+}-sensitive calcineurin phosphatase or MAPK kinases. As a consequence, transcription factors such as NFAT or CREB are activated and translocated into the nucleus to induce the synthesis of immune mediators, such as inflammatory cytokines or factors involved in cell development. One proposed mechanism by which P2RX7 regulates gene expression is the presence of consensus binding sites for CREB in promoter regions of P2RX7-controlled inflammatory genes [98,99,189,247–252]. The above mentioned observations with the secretion of IL-6 confirmed our initial hypothesis that both, MVA infection and P2RX7 activity, are involved in mitochondrial modulation. Brokatzky and colleagues have demonstrated a similar effect when infecting HeLa cells with MVA, confirming the infection-dependent contribution of the mitochondrial apoptosis pathway during infection [253]. Additionally, it has been previously reported that MVA infection led to the synthesis of MCP-1 (also CCL2) in leukocytes, KC (also

CXCL1) and RANTES (also CCL2) in murine lung fibroblasts, although we could only describe this effect in our feeder cells in the presence of a functional purinergic receptor [254,255]. IP-1ß (also CXC10) release after MVA infection was also shown by Pascutti and co-workers following MVA infection. However in our test system, secretion was enhanced by the presence of functional P2RX7 and significantly reduced after MVA infection. It has been described that type I IFNs play a role in the induction of this cytokine [256], which is in line with already published hypothesis that STING inhibits proper cross-presentation responses [66]. Furthermore, it should be considered that the presence of certain cytokines can induce the synthesis of other inflammatory mediators which we did not further characterize in this study [257]. All in all, these results indicate the functional importance of P2RX7 in the synthesis and release of proinflammatory mediators and highlight again the possible interplay between MVA infection and P2RX7 activity. Additionally, we postulate that the activation of downstream signaling pathways leading to the synthesis of the chemokines should also partly depend on intracellular P2X7 receptors, as treatment of these cells with P2RX7-specific inhibitor A740003 only incompletely restored CM WT chemokines levels (Figure S4), corroborating our hypothesis regarding functional intracellular P2RX7 structures.

It is proven that inflammatory cytokines as well as factors present in extracellular vesicles contribute to the regulation of adaptive immune responses [119,125,162,189]. Indeed, apoptotic vesicles of VACV-infected cells were highly efficient in cross-presenting VACV antigens [49]. We therefore aimed to investigate whether extracellular vesicle or supernatant fraction of CM cells (WT, pcDNA3 or P2RX7 transfected) had an impact on the cross-presentation ability of dendritic cells for the activation of $CD8^+$ T cells (Figure 22). As described above (Figure 22) we confirmed that the produced apoptotic bodies of MVA-infected CM cells, independently of P2RX7 activity, impacted cross-presentation ability of BMDCs (47). However we hypothesize, that other soluble factors (to be analyzed) that are present in the cellular fraction of P2RX7 active cells, are also responsible for the activation of BMDCs and the subsequent initiation of adaptive immune responses.

These released factors have a crucial impact in regulating immune responses and are hypothesized to contribute to the observed P2RX7-dependent improved cross-presentation by feeder cells. Apoptotic bodies are the largest within the extracellular vesicle portion. They not only contain cell debris, but may also act as antigen carriers for uptake by APCs. In this regard, the uptake of apoptotic vesicles resulted in the maturation of dendritic cells [118,258]. Another study postulated that Chikungunya virus can hide in apoptotic vesicles, therefore facilitating infection of neighboring cells. Even though in theory this phenomenon could also be possible in our assay, we exclude that this is the mechanism by which an increase in antigen cross-presentation by P2RX7 in feeder cells is achieved, as viral residues are inactivated with PUVA treatment before the co-culture of the feeder cells or different subcellular fractions with DCs

[119,120,254,259]. It was even reported that bystander DCs phagocytosed apoptotic vesicles more efficiently for subsequent cross-presentation of mycobacterial antigens [127]. To analyze whether apoptotic bodies released from CM P2RX7 cells have an additional impact on antigen cross-presentation, needs to be further characterized, e.g. by analyzing their amount and content in the tested cell lines.

One of the first studies analyzing extracellular vesicle portions proposed a substantial difference between apoptotic bodies and apoptotic blebs, the latter represent a smaller fraction of apoptotic bodies. We assume that microvesicles and exosomes that were described in this study are referred to as blebs nowadays. These were shown to derive from the membrane blebbing process and preferentially induce dendritic cell maturation and cytokine release, whereas apoptotic bodies did not result in a stimulatory effect, being in line with our postulated P2RX7-dependent EV release and its role in regulating adaptive immune responses [120,260]. We and others believe that besides the presence of antigens in P2RX7-dependent EVs and supernatants, the inflammatory proteins, ROS and ATP present in those structures play a leading role in the maturation and subsequent activation of DCs [78,121,189,261]. Besides this, EVs could serve as a protective depot for antigens, preventing quick degradation by cellular proteases which is a major requirement for successful antigen presentation [52,262]. The release of P2RX7-dependent vesicles could further favor our cross-presentation setup. We hypothesize that by capturing antigens, cytokines or other relevant factors for mediating the immune response in EVs, the dispersion and degradation of these molecules could be prevented, therefore allowing greater phagocytosis by APCs [78]. Even though we observed a higher MHCI synthesis in DCs co-cultured with mock-infected CM P2RX7 cells, we need to further analyze whether the phagocytosis activity in these cells is in general increased. Furthermore, we have already confirmed the presence of mRNA in vesicles, and hypothesize their potential role in antigen presentation. If degradation of these RNA molecules is prevented, one could even consider the translation of phagocytosed RNA molecules into protein in the APC as a novel mechanism for antigen cross-presentation [54,263,264].

The content of extracellular vesicles and supernatants from CM P2RX7 cells should be analyzed in more detail, as P2RX7 activity has been associated with the release of other proteins, potentially being involved in antigen presentation [54,111,162,265]. Recent studies have proposed the role of regulatory RNAs, such as microRNAs, in EVs induced by P2RX7 activity in the regulation of immune responses, cell growth and disease progression [113,266]. Due to its emerging functions and importance, miRNAs generated by active P2RX7 harboring cells during MVA infection should be analyzed in depth in the future.

Based on these results, we propose improved antigen presentation regulated by feeder cells synthetizing active P2RX7 which requires multilayered P2RX7 functionality in various intracellular downstream signaling pathways. For the first time in the field, we demonstrate that

multiple factors are required to induce feeder cell-derived stimuli to achieve improved cross-presentation of MVA antigens. We have endorsed the importance of cellular and extracellular (including supernatant) fractions of CM P2RX7 feeder cells for a superior cross-presentation capacity of MVA-produced antigens by BMDCs. Even though we have good reason to suggest a role of inflammatory cytokines and RNA molecules in CM P2RX7 cells to be partly responsible for improved immune responses, further research is necessary to investigate the mechanisms and further functions of these factors.

One major limitation of this experimental setup is the lack of vesicle quantification (amounts and size) as well as the analysis of other cytokines in the supernatant fraction. For future studies, one should consider the discrimination of the different extracellular vesicles as well as pursue a deeper analysis of their content. Additionally, the regulation of other cytokines in the presence of functional P2RX7 and their role during cross-presentation should be assessed in more depth.

6.5 Functional P2RX7 results in downregulation of members of the STING signaling pathway and in an inactive canonical-inflammasome pathway

The study of cross-presentation has gained researcher's attention since many years. Surprisingly, not much is known about how cross-presentation is initiated and how it can be modulated. Only recently this research group has published the importance of feeder cells in regulating cross-presentation processes. Barnowski and colleagues demonstrated that in the absence of STING in CM feeder cells the cross-presentation ability of DCs was significantly improved when co-cultured with MVA-infected CM *Sting* KO cells [66]. Another study also affirmed that the blockade of type I IFN signaling is a prerequisite for the effective immunogenicity and treatment of melanoma during recombinant VACV vaccination [267].

We therefore aimed to analyze this pathway in our CM feeder cell lines, to investigate the possible cross-talk between purinergic receptor and STING signaling. Interestingly, when CM cells harbored the active P2RX7, mRNA fold change of *Sting* remained significantly low in these cells, as when compared to CM or CM pcDNA3 upon MVA infection (Figure 24A). Similarly, the mRNA levels of *Sting*, *Ifnb* and *Ifnar* in the EV-fraction of CM P2RX7 was also significantly reduced in MVA-infected samples as compared to CM or CM pcDNA3 cells (Figure 24 B/C). This, on the one hand, confirms our initial hypothesis that P2RX7 activity modulates *Sting* mRNA levels in both the cellular fraction and the EV-fraction. On the other hand, it corroborates the assumption from Barnowski and co-workers [66], which states that down-regulation of the STING pathway in feeder cells plays a crucial role in subsequent cross-

presentation. The exact mechanism on how P2RX7 regulates *Sting* expression and, as a consequence, modulates adaptive immune responses, remains to be elucidated. One possible rationale could be the synthesis of miRNAs, which have been previously shown to be synthesized in the presence of an active P2X7 receptor [113]. In brief, miRNAs bind to their target mRNA and induce degradation of these molecules, inhibiting translation and are defined as a form of silencing mechanism [268]. Even though Pegoraro and colleagues have published a limited number of miRNAs to be significantly upregulated upon P2RX7 activation [113,266], many other miRNAs could be affected by the presence of P2RX7 depending on the condition analyzed (personal communication, Anna Pegoraro, University of Ferrara). It would therefore be of special relevance to assess the miRNA content in EVs upon MVA infection, to further study the effect of *Sting* silencing in feeder cells. Two studies postulated the presence of miR-576-3p or miR-181-a to be able to control *Sting* suppression [269,270]. In regards to this, another possibility on how STING-signaling could be controlled is by the transfer of STING into EVs, where it is easily degraded and as a consequence silences the immune response [271]. This in turn would explain the reduced mRNA levels of *Sting*, as well as *Ifnb* and *Ifnar* in our EVs, possibly explaining the abrogation of an autocrine stimulation of this pathway. It still remains to be determined, whether the higher fold change of *Ifnb* levels in MVA infected CM pcDNA3 EVs to CM EVs (Figure 24 B) was due to an unspecific effect caused by transfection of these cells with the pcDNA3 vector.

We have previously postulated the dual functions of P2RX7 activity, which has made understanding of this research area more complex. The regulation of calcium storage has already been described to be dependent on P2RX7 activity. At the same time, calcium was demonstrated to be crucial for the regulation of the STING signaling pathway. It was postulated that both, inhibitory as well as stimulatory Ca^{2+} signals are required to regulate STING activity and as a consequence also autophagic processes [77,272–274]. To which extent calcium signaling is crucial for the regulation of cross-presentation and how these ions specifically modulate STING activity and subsequent immune responses, remains to be elucidated in future studies [275,276].

Furthermore, we were curious to explore whether the P2X7 receptor was inducing the inflammasome pathway in our test system. The canonical inflammasome activity is assessed by determining Caspase-1 cleavage into its active form, as well as by measurement of secretion of IL-1ß or IL-18 cytokines [69,277]. Inflammasome activity during the modulation of adaptive immune responses displays controversial functions [278–280]. On the one hand, it has been described that inflammasome activity is beneficial for efficient cross-presentation of epithelial-derived antigens [280]. On the other hand, the expression of *Nlrp3* and *P2rx7* seems mutually regulated, resulting in a reduced *P2rx7* expression when *Nlrp3* was silenced [281]. How this impacts adaptive immune responses is still unknown. We could postulate from our

results that an non-functional canonical inflammasome in CM feeder cells, as demonstrated by the absence of IL-18 in the supernatant (Figure 25B), was essential for improved cross-presentation by DCs. However, we could demonstrate the cleavage of Caspase-1 into its active form in MVA-infected CM P2RX7 cells (Figure 25A), suggesting the involvement of this caspase in other inflammasome-independent pathways. Not much is known about the connection between Caspase-1 in the absence of IL-18 secretion, as we demonstrate in our study. It is hypothesized that even exosomes can regulate the activation of inflammasomes, e.g. by miRNAs [282]. We were not investigating the secretion of other inflammatory cytokines, such as IL-1ß in the supernatant or in EVs, supporting further research in this matter with relation to adaptive immune responses [283,284]. Unfortunately, current research about innate sensing regarding MVA is scarce. Most studies focus on the activity of the inflammasome in dendritic cells or *in vivo* studies and obliterate its possible role in feeder cells for cross-presentation processes *in vitro* [76,285,286]. However, we have to consider that most of these studies rely on the **retracted** publication from Delaloye and colleagues, who theorized the interaction between TLR-inflammasome-MVA signaling, questioning the data reliability and data availability to further study MVA in the inflammasome context [287].

Once again, we have demonstrated the duality of P2X7 receptor signaling, as it can lead to stimulatory effects, e.g. by activating Caspase-1, but at the same time to inhibitory signals, such as the downregulation of *Sting*. Even though these are two distinct pathways, further research to establish a possible cross-talk and function of the different pathways in adaptive immune responses is required. In the future, other inflammasome members should be assessed, too, to identify a possible involvement of P2X7-receptor signaling. NGS analyses in CM P2RX7 cells could ease the analyses of these possible cross-talking partners.

6.6 Further *in vitro* models analyzing P2RX7 functionality during cross-presentation of MVA antigens

It is important to prove the reproducibility of an established method or to corroborate the results e.g. the cross-presentation assay by using another cell line producing the functional P2RX7 as feeders. HEK293 cells do not harbor the P2X7 receptor, thus showing the functionality of only this receptor upon transfection [89,130]. We first proved that P2RX7-transfected HEK293 cells had a functional receptor (Figure 26 A-D). Interestingly, although present in minor amounts, we confirmed the importance of a functional P2X7 receptor in MVA-infected HEK293 feeder cells for improved SIINFEKL/H2-K^b expression by BMDCs (Figure 27E), corroborating our previous results with CM P2RX7 cells and reinforcing the cruciality of active P2RX7 as an innate trigger in regulating adaptive immune responses. Of note, it was difficult to find a suitable

feeder cell line to study cross-presentation, as due to the H2-K^b restricted $CD8^+$ T cell lines present in our laboratory, we are limited in the choice of feeder and antigen-presenting cells. Therefore, future studies would be urgently required to find an applicable feeder cell line that results in stronger adaptive immune responses. On the one hand, we can postulate that the presence of high eATP (up to three times more than for CM cells) in HEK293 hP2RX7 cells could have led to the lower activation of APCs, which could result in the reduced SIINFEKL/H2-K^b expression on BMDCs. High amounts of ATP can serve as DAMPs, consequently leading to a strong activation of P2RX7 receptors, instead of having a detrimental effect on the cell, inducing apoptotic cell death. Additionally, P2RX7 in HEK293 led to the opening of the pore, which resulted in the leakage of membrane structures and subsequent cell death [92,189,190]. Moreover, instable membrane structures (due to the pore opening) do not favor antigen generation upon MVA infection, resulting in the low observed expression of SIINFEKL molecules on the MHCI of BMDCs.

We further aimed to show that P2RX7 in feeder cells is crucial for improving adaptive immune responses. To achieve this, we used freshly generated BMDCs from the bone marrow of BALB/$c^{P2rx7-/-}$ (here referred to as BALB/c KO) mice as feeder cells for our cross-presentation assay. Interestingly, we observed the opposite effect as we were expecting, hence a slightly significant increase in B8-specific $CD8^+$ T cell activation by synthesis of IFNγ or TNFα (Figure 27A). The SIINFEKL/H2-K^b expression on the surface of dendritic cells, which is a more sensitive method in determining cross-presentation capacity, was not altered in the absence of P2RX7 in BALB/c feeder cells (Figure 27B). Even though the observed effect was minimal, we wanted to correlate this effect to the STING pathway and analyzed the secretion of type I IFNs in BALB/c feeder cells (Figure 27C). As expected, BALB/c P2RX7 KO cells released no mIFN-α2 and less mIFN-ß in the supernatant upon MVA infection as compared to BALB/c WT cells. This indicates once more the possible cross-talk between P2RX7 and STING signaling in feeder cells affecting cross-presentation responses upon MVA infection.

However, the potentially poor suitability of professional antigen-presenting cells to serve as feeder cells has to be considered as well [288]. These cells are known to be crucial as the link between innate and adaptive immune immunity, being characterized by their unique ability to phagocytose antigens, load them on MHC molecules and present them on their surface for the activation of T cells. As described in more detail above, depending on the antigen source, peptides are processed to be loaded on the MHCI or MHCII molecules, for the presentation to CD8 or CD4 T cells, respectively [289,290]. It was already described that depending on the cell status, P2RX7 functions can be differentially modulated, therefore a variable outcome in our setting for studying cross-presentation was also to be expected [188]. Even though we did not analyze the ATP levels in BALB/c feeder cells, representing a possible mechanism on how STING is activated, one might assume that these cells exhibited high amounts of eATP acting

on the surface P2X7 receptors and aiding in the transport of cGAMP into cells, subsequently activating STING, as previously postulated in a tumor model in macrophages [291].

All in all, to deepen the importance of P2RX7 in feeder cells, further cell lines with functional P2RX7 as well as suitable knockouts are required. Additionally, *in vivo* studies performed with appropriate knockout mice should be taken into consideration to further corroborate P2RX7-specific functions. Once again, due to cell-specific activity of P2RX7 , it remains challenging to investigate its role in immunologically relevant situations, such as viral infections or tumorigenesis.

6.7 *P2rx7* knockout in CM cells failed and almost completely abrogated MVA cross-presentation of dendritic cells

To corroborate our experimental results and to study the functions of the P2RX7, we thought to delete the *P2rx7* gene, even though it is not functional in cells from DBA mice [86]. A similar approach was used during the study of the inflammasome in my previously published master thesis, where a *P2rx7* knockout was described [292]. In this study, we aimed to further characterize the depletion of P2X7 receptor in feeder cells. Unexpectedly, instead of obtaining a knockout in our CM cells, we generated a cell line with a fully functional P2X7 receptor (CM P2RX7 xKO). Hence, CM P2RX7 xKO cells did not only have increased P2RX7 protein levels than CM WT cells (Figure 28A) but also a functional calcium channel (Figure 28B), a functional pore (as shown by ethidium bromide analyses) (Figure 28C) and even the release of extracellular vesicles (Figure 28D), all typical P2RX7-specific functions. Interestingly, OVA protein synthesis (under the control of different promoters: early and/or late) (Figure 28A/ 29A/B) as well as gene expression of early *Ova*, early *B8R* and late *A19L* was either delayed or reduced in CM P2RX7 xKO cells, respectively. At the same time, we could demonstrate a decrease in viral replication in CM P2RX7 xKO cells upon MVA infection. eATP levels remained very low in these cells, even after MVA infection (Figure 28E), similar to P2RX7-specific effects that we have observed above. Nevertheless, we wanted to analyze which phenotype these cells would have as feeders during cross-presentation. As expected, due to the reduced expression of early antigens, we saw a significant reduction in $CD8^+$ T cell activation as well as SIINFEKL/H2-K^b surface expression and maturation markers on BMDCs upon co-culture with MVA-infected CM P2RX7 xKO cells. This is interesting, as with the BALB/c variant of P2RX7 (functional variant) in CM cells we saw a delayed expression pattern as well, however, no abrogation of cross-presentation and similar viral replication after infection. Additionally, it was already postulated that excessive stimuli could lead to the opening of the pore, which we observe in CM P2RX7 xKO cells [92]. We therefore assume

that the results we observed are mainly due to the immediate induction of cell death due to the pore opening [144]. As a consequence, viral gene expression was delayed or completely aborted and failed to provide sufficient antigens to be phagocytosed by APCs.

Interestingly, the STING pathway in CM P2RX7 xKO cells was strongly activated, as demonstrated by the phosphorylation of STING, TBK1 and IRF3, as well as by the synthesis of mIFN-ß in these cells (Figure 31), confirming our initial hypothesis which was corroborated by our recent paper showing that an active STING pathway in feeder cells reduces cross-presentation capacities of dendritic cells [66]. However, since we could not generate a proper *P2rx7* knockout, we aborted further experiments to characterize the role of this receptor in these cells in this study.

To understand if a possible mutation on the DNA level has caused the observed phenotype, we have performed some sequencing as well as genomic analyses. It is well known that CRISPR/Cas9 mutagenesis can lead to the insertion-deletion (INDEL) mutations as well as to the synthesis of foreign gene products. This could result in the generation of new ribosomal entry sites and, as a consequence, the synthesis of protein-coding sequences or even new splice sites [174,293]. We partially excluded that these mutations occurred in our CM P2RX7 xKO cells, as we did not observe any mutations around the gRNA that was supposed to be targeted by the Cas9 nuclease, nor any mutations around the gRNA and in the reverse transcribed gRNA of the P2RX7 transcript (Figure 32 A/B). It remains to be determined, whether new splice initiation sites were added that resulted in the synthesis of a functional P2RX7. It must be stated that the *P2rx7* gene highly resembles the *P2rx4* gene. In addition to this, it was demonstrated that P2RX4 was also able to regulate P2RX7 function. This in turn opens the possibility that our CRISPR/Cas9 approach, due to the high sequence similarity of *P2rx4* to *P2rx7*, targeted the *P2rx4* sequence instead, possibly regulating the synthesis and function of the P2RX7 [77,112,185].

Interestingly, Shin and colleagues published that in epithelial cells the activity of P2RX7 is modulated by epigenetic processes, such as methylation [294]. Methylation is a regulation mechanism by which gene expression can be regulated, such as by silencing or activating them [295]. CRISPR/Cas9-mediated gene silencing is also described to affect methylation sites [178]. As described in this study, we observed CpG methylation regions in the *P2rx7* gene that could be targeted (Figure 32C). Therefore, we hypothesized that the CRISPR/Cas9 approach could have resulted in the addition of methylation sites, therefore regulating *P2rx7* gene expression and function in an uncontrolled manner. In this study, we did not further characterize the methylation pattern of the gene of interest. In the future, the methylation status of *P2rx7* in CM feeder cells and its impact on MVA-mediated antigen cross-presentation by BMDCs as well as other post-translational modifications should be further investigated.

For future approaches, a verified knockout obtained with a more suitable gRNA should be done. This knockout should be verified on the gene level, the protein level and the functional level, if possible. Unfortunately, the approach in this study did not lead to the expected knockout and the obtained results may most likely be explained by frequently occurring off-target effects during CRISPR/Cas9 mutagenesis.

6.8 Conclusion

MVA has been proven to be a highly efficient and safe viral vector, making it an excellent option for a promising vaccine candidate. Extensive research has indicated the significance of poxviral antigens for cross-presentation, contributing to a significant portion of $CD8^+$ T cell responses. Currently, the research on innate immune triggers on feeder cells, known to play a crucial role in stimulating T cell responses via cross- presentation, is scarce. It is of high relevance to improve MVA as a vaccine candidate due to its outstanding performance to be quickly modified and generated when emerging diseases have to be prevented [18–20]. We have found that an ATP-sensitive P2X7 receptor (derived from BALB/c mice) in MVA-infected CM feeder cells significantly enhanced BMDC-mediated antigen cross-presentation. We assume that the above mentioned observations were due to the P2RX7-specific effects induced in CM feeder cells. These effects involved more than apoptotic mechanisms, which were already acknowledged to be crucial for modulating immune responses upon MVA infection. In addition to apoptotic bodies, P2RX7-bearing cells secreted other extracellular vesicles, such as microvesicles or exosomes, as well as potent inflammatory cytokines, which seemed to contribute to enhanced cross-presentation, possibly by triggering downstream inflammatory cascades. Until now we have also hypothesized, that altered RNA content in these vesicles affected cross-presentation. We also suggest that an improved microenvironment in CM feeder cells, e.g. by enhanced energy metabolism and higher intracellular ATP concentrations, is associated with the enhanced antigen-presentation by BMDCs. We suppose that this could affect cell fitness and as a consequence how viral antigens are produced. Another mechanism could be the modulation of the expression of viral antigens. We believe that the delayed antigen production, is be beneficial for cross-presentation. Whether this is because of the trapping of antigens in viral factories or the release of mRNA in extracellular vesicles, preventing pre-mature degradation, needs to be studied in more detail in future research. Our hypothesis on how cross-presentation is aided by the P2X7 receptor in feeder cells is summarized in Figure 33.

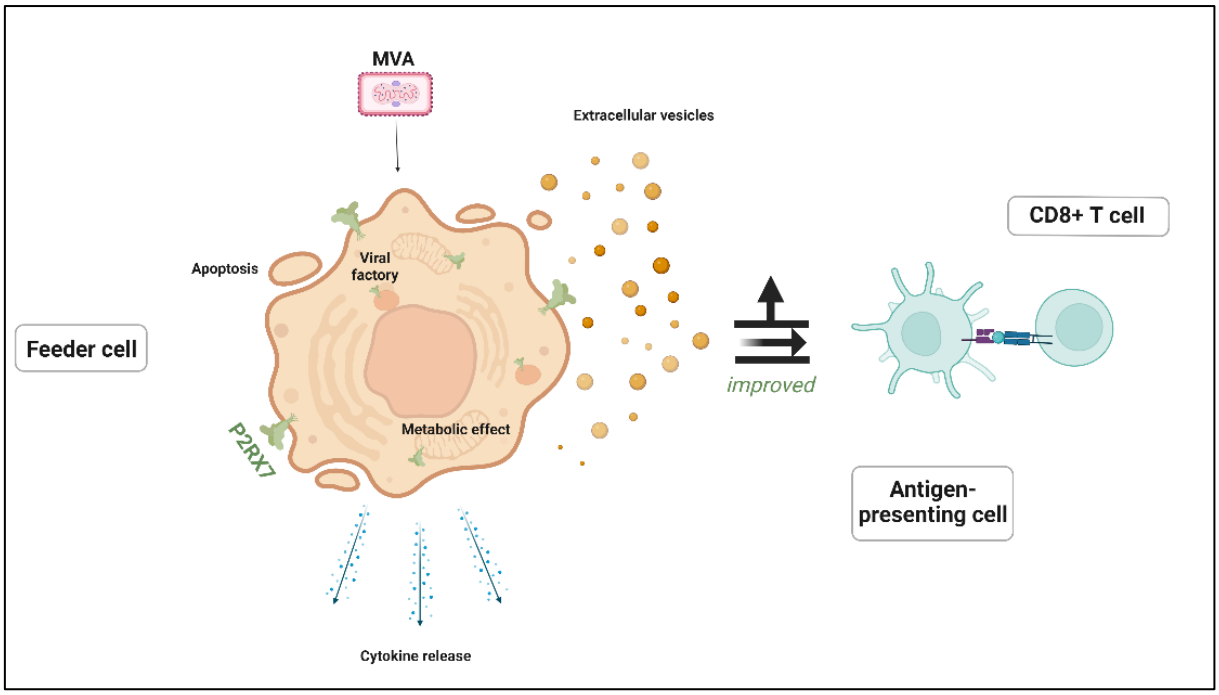

Figure 33: Mechanisms activated by functional P2RX7 in Cloudman feeder cells for MVA-mediated cross-presentation by antigen-presenting cells. Upon transfection of CM cells with the functional P2RX7 variant from BALB/c mice, we observed various P2RX7-mediated effects in these cells. Upon transfection and MVA infection, cells released inflammatory cytokines as well as extracellular vesicles. The contents of this extracellular fraction could be fundamental for the fate of cross-presentation. At the same time, functional P2RX7 harboring cells also showed the presence of the P2X7 receptors intracellularly, more precisely on viral factories. In addition, CM cells bearing the active P2RX7 also exhibited apoptosis-like features and a higher energy metabolism. We assume that all these mechanisms induced by the presence of the BALB/c P2RX7 in feeder cells are responsible for the improved antigen cross-presentation by antigen-presenting cells, which in turn could activate $CD8^+$ T cells more efficiently. This Figure was created using Biorender.com.

In conclusion, we have demonstrated that innate triggers in infected feeder cells are critical for the induction of MVA-mediated cross-presentation and subsequent T cell activation. With this study, we have expanded the knowledge about P2RX7 functions in feeder cells upon MVA infection and, for the first time, associated its important role with cross-presentation. We hypothesize that P2RX7 is not a solo player in regulating adaptive immune responses, but strongly cross-communicates with other members of the innate immune system as well as with cell-associated factors responsible for antigen production during MVA infection. These key findings were recently published and highlight the most significant aspects of P2RX7 signaling [296]. However, future studies will require comprehensive analyses of P2RX7 interaction partners in feeder cells and how these influence MVA-mediated cross-presentation.

9. References

[1] García-Arriaza J, Esteban M. Enhancing poxvirus vectors vaccine immunogenicity. Hum Vaccin Immunother 2014;10:2235. https://doi.org/10.4161/HV.28974.

[2] Moss Bernard. Poxviridiae: The viruses and their replication. In: Knipe DM, Howley PM, editors. Fields Virology, Philadelphia: Lippincott WIlliams & Wilkins; 2007, p. 2905–46.

[3] Fenner F. Portraits of viruses: the poxviruses. Intervirology 1979;11:137–57. https://doi.org/10.1159/000149027.

[4] Baxby D. Poxviruses. Medical Microbiology 1996.

[5] Sakhatskyy P, Wang S, Zhang C, Chou TH, Kishko M, Lu S. Immunogenicity and protection efficacy of subunit-based smallpox vaccines using variola major antigens. Virology 2008;371:98–107. https://doi.org/10.1016/J.VIROL.2007.09.029.

[6] Riedel S. Edward Jenner and the history of smallpox and vaccination. Proc (Bayl Univ Med Cent) 2005;18:21. https://doi.org/10.1080/08998280.2005.11928028.

[7] History of Smallpox | Smallpox | CDC n.d. https://www.cdc.gov/smallpox/history/history.html (accessed October 16, 2023).

[8] Wilkinson L. Princes and peasants. Smallpox in history. Med Hist 1984;28:441.

[9] Willis NJ. Edward Jenner and the eradication of smallpox. Scott Med J 1997;42:118–21. https://doi.org/10.1177/003693309704200407.

[10] Moss B. Genetically engineered poxviruses for recombinant gene expression, vaccination, and safety. Proc Natl Acad Sci U S A 1996;93:11341. https://doi.org/10.1073/PNAS.93.21.11341.

[11] Baxby D. The origins of vaccinia virus. J Infect Dis 1977;136:453–5. https://doi.org/10.1093/INFDIS/136.3.453.

[12] Stickl H, Hochstein-Mintzel V. [Intracutaneous smallpox vaccination with a weak pathogenic vaccinia virus (“MVA virus”)]. Munch Med Wochenschr 1971;113:1149–53.

[13] Mayr A, Munz E. [Changes in the vaccinia virus through continuing passages in chick embryo fibroblast cultures]. Zentralbl Bakteriol Orig 1964;195:24–35.

[14] Antoine G, Scheiflinger F, Dorner F, Falkner FG. The complete genomic sequence of the modified vaccinia Ankara strain: comparison with other orthopoxviruses. Virology 1998;244:365–96. https://doi.org/10.1006/VIRO.1998.9123.

[15] Stickl H, Hochstein-Mintzel V, Mayr A, Huber HC, Schäfer H, Holzner A. [MVA vaccination against smallpox: clinical tests with an attenuated live vaccinia virus strain (MVA) (author’s transl)]. Dtsch Med Wochenschr 1974;99:2386–92. https://doi.org/10.1055/S-0028-1108143.

[16] Mayr A, Stickl H, Müller HK, Danner K, Singer H. [The smallpox vaccination strain MVA: marker, genetic structure, experience gained with the parenteral vaccination and behavior in organisms with a debilitated defence mechanism (author’s transl)]. Zentralbl Bakteriol B 1978;167:375–90.

[17] Blanchard TJ, Alcami A, Andrea P, Smith GL. Modified vaccinia virus Ankara undergoes limited replication in human cells and lacks several immunomodulatory

proteins: implications for use as a human vaccine. Journal of General Virology 1998;79:1159–67. https://doi.org/https://doi.org/10.1099/0022-1317-79-5-1159.

[18] Drexler I, Heller K, Wahren B, Erfle V, Sutter G. Highly attenuated modified vaccinia virus Ankara replicates in baby hamster kidney cells, a potential host for virus propagation, but not in various human transformed and primary cells. J Gen Virol 1998;79 (Pt 2):347–52. https://doi.org/10.1099/0022-1317-79-2-347.

[19] Stittelaar KJ, Kuiken T, De Swart RL, Van Amerongen G, Vos HW, Niesters HGM, Van Schalkwijk P, Van Der Kwast T, Wyatt LS, Moss B, Osterhaus ADME. Safety of modified vaccinia virus Ankara (MVA) in immune-suppressed macaques. Vaccine 2001;19:3700–9. https://doi.org/10.1016/S0264-410X(01)00075-5.

[20] Drexler I, Staib C, Sutter G. Modified vaccinia virus Ankara as antigen delivery system: how can we best use its potential? 2004. https://doi.org/10.1016/j.copbio.2004.09.001.

[21] Staib C, Drexler I, Sutter G. Construction and isolation of recombinant MVA. Methods Mol Biol 2004;269:77–100. https://doi.org/10.1385/1-59259-789-0:077.

[22] Gomez C, Najera J, Krupa M, Esteban M. The Poxvirus Vectors MVA and NYVAC as Gene Delivery Systems for Vaccination Against Infectious Diseases and Cancer. Curr Gene Ther 2008;8:97–120. https://doi.org/10.2174/156652308784049363.

[23] Verheust C, Goossens M, Pauwels K, Breyer D. Biosafety aspects of modified vaccinia virus Ankara (MVA)-based vectors used for gene therapy or vaccination. Vaccine 2012;30:2623–32. https://doi.org/10.1016/J.VACCINE.2012.02.016.

[24] Tscherne A, Hendrik Schwarz J, Rohde C, Kupke A, Kalodimou G, Limpinsel L, Okba NMA, Bošnjak B, Sandrock I, Odak I, Halwe S, Sauerhering L, Brosinski K, Liangliang N, Duell E, Jany S, Freudenstein A, Schmidt J, Werner A, Serra MG, Klüver M, Guggemos W, Seilmaier M, Wendtner CM, Förster R, Haagmans BL, Becker S, Sutter G, Volz A. Immunogenicity and efficacy of the COVID-19 candidate vector vaccine MVA-SARS-2-S in preclinical vaccination. Proc Natl Acad Sci U S A 2021;118. https://doi.org/10.1073/PNAS.2026207118.

[25] Bronte V, Carroll MW, Goletz TJ, Wang M, Overwijk WW, Marincola F, Rosenberg SA, Moss B, Restifo NP. Antigen expression by dendritic cells correlates with the therapeutic effectiveness of a model recombinant poxvirus tumor vaccine. Proc Natl Acad Sci U S A 1997;94:3183–8. https://doi.org/10.1073/PNAS.94.7.3183.

[26] Goldstein N, Bockstal V, Bart S, Luhn K, Robinson C, Gaddah A, Callendret B, Douoguih M. Safety and Immunogenicity of Heterologous and Homologous 2-Dose Regimens of Adenovirus Serotype 26- and Modified Vaccinia Ankara-Vectored Ebola Vaccines: A Randomized, Controlled Phase 1 Study. J Infect Dis 2022;226:595–607. https://doi.org/10.1093/INFDIS/JIAA586.

[27] Sebastian S, Gilbert SC. Recombinant modified vaccinia virus Ankara-based malaria vaccines. Expert Rev Vaccines 2016;15:91–103. https://doi.org/10.1586/14760584.2016.1106319.

[28] Tameris MD, Hatherill M, Landry BS, Scriba TJ, Snowden MA, Lockhart S, Shea JE, McClain JB, Hussey GD, Hanekom WA, Mahomed H, McShane H. Safety and efficacy of MVA85A, a new tuberculosis vaccine, in infants previously vaccinated with BCG: a randomised, placebo-controlled phase 2b trial. Lancet 2013;381:1021. https://doi.org/10.1016/S0140-6736(13)60177-4.

[29] Gómez CE, Nájera JL, Perdiguero B, García-Arriaza J, Sorzano COS, Jiménez V, González-Sanz R, Jiménez JL, Muñoz-Fernández MA, Quirós JCLB de, Guardo AC,

García F, Gatell JM, Plana M, Esteban M. The HIV/AIDS Vaccine Candidate MVA-B Administered as a Single Immunogen in Humans Triggers Robust, Polyfunctional, and Selective Effector Memory T Cell Responses to HIV-1 Antigens. J Virol 2011;85:11468. https://doi.org/10.1128/JVI.05165-11.

[30] Kastenmuller W, Gasteiger G, Gronau JH, Baier R, Ljapoci R, Busch DH, Drexler I. Cross-competition of CD8+ T cells shapes the immunodominance hierarchy during boost vaccination. J Exp Med 2007;204:2187–98. https://doi.org/10.1084/jem.20070489.

[31] Wong YC, Croft S, Smith SA, Lin LCW, Cukalac T, La Gruta NL, Drexler I, Tscharke DC. Modified Vaccinia Virus Ankara Can Induce Optimal CD8(+) T Cell Responses to Directly Primed Antigens Depending on Vaccine Design. J Virol 2019;93. https://doi.org/10.1128/jvi.01154-19.

[32] Coulibaly S, Brühl P, Mayrhofer J, Schmid K, Gerencer M, Falkner FG. The nonreplicating smallpox candidate vaccines defective vaccinia Lister (dVV-L) and modified vaccinia Ankara (MVA) elicit robust long-term protection. Virology 2005;341:91–101. https://doi.org/10.1016/J.VIROL.2005.06.043.

[33] Earl PL, Americo JL, Wyatt LS, Eller LA, Whitbeck JC, Cohen GH, Eisenberg RJ, Hartmann CJ, Jackson DL, Kulesh DA, Martinez MJ, Miller DM, Mucker EM, Schamblin JD, Zwiers SH, Huggins JW, Jahrting PB, Moss B. Immunogenicity of a highly attenuated MVA smallpox vaccine and protection against monkeypox. Nature 2004;428:182–5. https://doi.org/10.1038/NATURE02331.

[34] Ramírez JC, Gherardi MM, Esteban M. Biology of attenuated modified vaccinia virus Ankara recombinant vector in mice: virus fate and activation of B- and T-cell immune responses in comparison with the Western Reserve strain and advantages as a vaccine. J Virol 2000;74:923–33. https://doi.org/10.1128/JVI.74.2.923-933.2000.

[35] Gómez CE, Rodríguez D, Rodríguez JR, Abaitua F, Duarte C, Esteban M. Enhanced CD8+ T cell immune response against a V3 loop multi-epitope polypeptide (TAB13) of HIV-1 Env after priming with purified fusion protein and booster with modified vaccinia virus Ankara (MVA-TAB) recombinant: a comparison of humoral and cellular immune responses with the vaccinia virus Western Reserve (WR) vector. Vaccine 2001;20:961–71. https://doi.org/10.1016/S0264-410X(01)00389-9.

[36] Caminero F, Iqbal Z, Tadi P. Histology, Cytotoxic T Cells. StatPearls 2023.

[37] Banchereau J, Steinman RM. Dendritic cells and the control of immunity. Nature 1998 392:6673 1998;392:245–52. https://doi.org/10.1038/32588.

[38] Liu L, Chavan R, Feinberg MB. Dendritic cells are preferentially targeted among hematolymphocytes by Modified Vaccinia Virus Ankara and play a key role in the induction of virus-specific T cell responses in vivo. BMC Immunol 2008;9:15. https://doi.org/10.1186/1471-2172-9-15.

[39] Rock KL, Shen L. Cross-presentation: underlying mechanisms and role in immune surveillance. Immunol Rev 2005;207:166–83. https://doi.org/10.1111/j.0105-2896.2005.00301.x.

[40] Newton K, Dixit VM. Signaling in Innate Immunity and Inflammation. Cold Spring Harb Perspect Biol 2012;4. https://doi.org/10.1101/CSHPERSPECT.A006049.

[41] Chaplin DD. Overview of the Immune Response. J Allergy Clin Immunol 2010;125:S3. https://doi.org/10.1016/J.JACI.2009.12.980.

[42] Tscharke DC, Croft NP, Doherty PC, La Gruta NL. Sizing up the key determinants of the CD8+ T cell response. Nature Reviews Immunology 2015 15:11 2015;15:705–16. https://doi.org/10.1038/nri3905.

[43] Eickhoff S, Brewitz A, Gerner MY, Klauschen F, Komander K, Hemmi H, Garbi N, Kaisho T, Germain RN, Kastenmüller W. Robust Anti-viral Immunity Requires Multiple Distinct T Cell-Dendritic Cell Interactions. Cell 2015;162:1322–37. https://doi.org/10.1016/j.cell.2015.08.004.

[44] Shen X, Wong SBJ, Buck CB, Zhang J, Siliciano RF. Direct Priming and Cross-Priming Contribute Differentially to the Induction of CD8+ CTL Following Exposure to Vaccinia Virus Via Different Routes. The Journal of Immunology 2002;169:4222–9. https://doi.org/10.4049/JIMMUNOL.169.8.4222.

[45] Gasteiger G, Kastenmuller W, Ljapoci R, Sutter G, Drexler I. Cross-priming of cytotoxic T cells dictates antigen requisites for modified vaccinia virus Ankara vector vaccines. J Virol 2007;81:11925–36. https://doi.org/10.1128/JVI.00903-07.

[46] Reits E, Griekspoor A, Neijssen J, Groothuis T, Jalink K, Van Veelen P, Janssen H, Calafat J, Drijfhout JW, Neefjes J. Peptide Diffusion, Protection, and Degradation in Nuclear and Cytoplasmic Compartments before Antigen Presentation by MHC Class I. Immunity 2003;18:97–108. https://doi.org/10.1016/S1074-7613(02)00511-3.

[47] Chahroudi A, Garber DA, Reeves P, Liu L, Kalman D, Feinberg MB. Differences and similarities in viral life cycle progression and host cell physiology after infection of human dendritic cells with modified vaccinia virus Ankara and vaccinia virus. J Virol 2006;80:8469–81. https://doi.org/10.1128/JVI.02749-05.

[48] Albert ML, Sauter B, Bhardwaj N. Dendritic cells acquire antigen from apoptotic cells and induce class I-restricted CTLs. Nature 1998;392:86–9. https://doi.org/10.1038/32183.

[49] Larsson M, Fonteneau J-F, Somersan S, Sanders C, Bickham K, Thomas EK, Mahnke K, Bhardwaj N. Efficiency of cross presentation of vaccinia virus-derived antigens by human dendritic cells n.d. https://doi.org/10.1002/1521-4141.

[50] Iborra S, Izquierdo HM, Martinez-Lopez M, Blanco-Menendez N, Reis e Sousa C, Sancho D. The DC receptor DNGR-1 mediates cross-priming of CTLs during vaccinia virus infection in mice. J Clin Invest 2012;122:1628–43. https://doi.org/10.1172/JCI60660.

[51] Sigal LJ, Crotty S, Andino R, Rock KL. Cytotoxic T-cell immunity to virus-infected non-haematopoietic cells requires presentation of exogenous antigen. Nature 1999;398:77–80. https://doi.org/10.1038/18038.

[52] Embgenbroich M, Burgdorf S. Current Concepts of Antigen Cross-Presentation. Front Immunol 2018;9. https://doi.org/10.3389/fimmu.2018.01643.

[53] Neijssen J, Herberts C, Drijfhout JW, Reits E, Janssen L, Neefjes J. Cross-presentation by intercellular peptide transfer through gap junctions. Nature 2005;434:83–8. https://doi.org/10.1038/NATURE03290.

[54] Arina A, Tirapu I, Alfaro C, Rodríguez-Calvillo M, Mazzolini G, Inogés S, López A, Feijoo E, Bendandi M, Melero I. Clinical implications of antigen transfer mechanisms from malignant to dendritic cells: Exploiting cross-priming. Exp Hematol 2002;30:1355–64. https://doi.org/https://doi.org/10.1016/S0301-472X(02)00956-6.

[55] Li Y, Wang LX, Yang G, Hao F, Urba WJ, Hu HM. Efficient cross-presentation depends on autophagy in tumor cells. Cancer Res 2008;68:6889–95. https://doi.org/10.1158/0008-5472.CAN-08-0161.

[56] Boukhebza H, Bellon N, Limacher JM, Inchauspé G. Therapeutic vaccination to treat chronic infectious diseases: Current clinical developments using MVA-based vaccines. Hum Vaccin Immunother 2012;8:1746. https://doi.org/10.4161/HV.21689.

[57] Guzman E, Cubillos-Zapata C, Cottingham MG, Gilbert SC, Prentice H, Charleston B, Hope JC. Modified Vaccinia Virus Ankara-Based Vaccine Vectors Induce Apoptosis in Dendritic Cells Draining from the Skin via both the Extrinsic and Intrinsic Caspase Pathways, Preventing Efficient Antigen Presentation. J Virol 2012;86:5452. https://doi.org/10.1128/JVI.00264-12.

[58] Jung S, Unutmaz D, Wong P, Sano GI, De Los Santos K, Sparwasser T, Wu S, Vuthoori S, Ko K, Zavala F, Pamer EG, Littman DR, Lang RA. In vivo depletion of CD11c+ dendritic cells abrogates priming of CD8+ T cells by exogenous cell-associated antigens. Immunity 2002;17:211–20. https://doi.org/10.1016/S1074-7613(02)00365-5.

[59] Schulz O, Reis E Sousa C. Cross-presentation of cell-associated antigens by CD8α+ dendritic cells is attributable to their ability to internalize dead cells. Immunology 2002;107:183. https://doi.org/10.1046/J.1365-2567.2002.01513.X.

[60] Norbury CC, Basta S, Donohue KB, Tscharke DC, Princiotta MF, Berglund P, Gibbs J, Bennink JR, Yewdell JW. CD8+ T cell cross-priming via transfer of proteasome substrates. Science (1979) 2004;304:1318–21. https://doi.org/10.1126/science.1096378.

[61] Serna A, Ramirez MC, Soukhanova A, Sigal LJ. Cutting Edge: Efficient MHC Class I Cross-Presentation during Early Vaccinia Infection Requires the Transfer of Proteasomal Intermediates between Antigen Donor and Presenting Cells. The Journal of Immunology 2003;171:5668–72. https://doi.org/10.4049/JIMMUNOL.171.11.5668.

[62] Pfeifer JD, Wick MJ, Roberts RL, Findlay K, Normark SJ, Harding C V. Phagocytic processing of bacterial antigens for class I MHC presentation to T cells. Nature 1993 361:6410 1993;361:359–62. https://doi.org/10.1038/361359a0.

[63] Gros M, Amigorena S. Regulation of Antigen Export to the Cytosol During Cross-Presentation. Front Immunol 2019;10:41. https://doi.org/10.3389/fimmu.2019.00041.

[64] Mbongue JC, Nieves HA, Torrez TW, Langridge WHR. The role of dendritic cell maturation in the induction of insulin-dependent diabetes mellitus. Front Immunol 2017;8:229424. https://doi.org/10.3389/FIMMU.2017.00327/BIBTEX.

[65] Ghosh M, Shapiro LH. In vitro Ag Cross-presentation and in vivo Ag Cross-presentation by Dendritic Cells in the Mouse. Bio Protoc 2012;2:e305. https://doi.org/10.21769/BIOPROTOC.305.

[66] Barnowski C, Ciupka G, Tao R, Jin L, Busch DH, Tao S, Drexler I. Efficient Induction of Cytotoxic T Cells by Viral Vector Vaccination Requires STING-Dependent DC Functions. Front Immunol 2020;11:1458. https://doi.org/10.3389/fimmu.2020.01458.

[67] Ma Z, Ni G, Damania B. Innate Sensing of DNA Virus Genomes. Annu Rev Virol 2018;5:341–62. https://doi.org/10.1146/ANNUREV-VIROLOGY-092917-043244.

[68] Ma F, Li B, Yu Y, Iyer SS, Sun M, Cheng G. Positive feedback regulation of type I interferon by the interferon-stimulated gene STING. EMBO Rep 2015;16:202–12. https://doi.org/10.15252/EMBR.201439366.

[69] Martínez-Banaclocha H, Pelegrín P. Detection of Inflammasome Activation by P2X7 Purinoceptor Activation by Determining ASC Oligomerization. Methods Mol Biol 2020;2041:335–43. https://doi.org/10.1007/978-1-4939-9717-6_25.

[70] Kong H, Zhao H, Chen T, Song Y, Cui Y. Targeted P2X7/NLRP3 signaling pathway against inflammation, apoptosis, and pyroptosis of retinal endothelial cells in diabetic retinopathy. Cell Death & Disease 2022 13:4 2022;13:1–13. https://doi.org/10.1038/s41419-022-04786-w.

[71] Karmakar M, Katsnelson MA, Dubyak GR, Pearlman E. Neutrophil P2X7 receptors mediate NLRP3 inflammasome-dependent IL-1β secretion in response to ATP. Nature Communications 2016 7:1 2016;7:1–13. https://doi.org/10.1038/ncomms10555.

[72] Dai P, Wang W, Cao H, Avogadri F, Dai L, Drexler I, Joyce JA, Li XD, Chen Z, Merghoub T, Shuman S, Deng L. Modified Vaccinia Virus Ankara Triggers Type I IFN Production in Murine Conventional Dendritic Cells via a cGAS/STING-Mediated Cytosolic DNA-Sensing Pathway. PLoS Pathog 2014;10. https://doi.org/10.1371/JOURNAL.PPAT.1003989.

[73] Waibler Z, Anzaghe M, Ludwig † Holger, Akira S, Weiss S, Sutter G, Kalinke U. Modified Vaccinia Virus Ankara Induces Toll-Like Receptor-Independent Type I Interferon Responses. J Virol 2007;81:12102–10. https://doi.org/10.1128/JVI.01190-07.

[74] Zhong C, Liu F, Hajnik RJ, Yao L, Chen K, Wang M, Liang Y, Sun J, Soong L, Hou W, Hu H. Type I Interferon Promotes Humoral Immunity in Viral Vector Vaccination. J Virol 2021;95. https://doi.org/10.1128/JVI.00925-21/ASSET/9A82E02F-23E5-4FE5-8238-9AF1F07378F9/ASSETS/IMAGES/LARGE/JVI.00925-21-F006.JPG.

[75] Heery C, Pico-Navarro C, Adams T, Bauman L, Medina J, Hinterberger M, Heiseke A, Lauterbach H, Hochrein H. Novel applications of MVA to improve outcomes in immunooncology. Annals of Oncology 2019;30:i3. https://doi.org/10.1093/annonc/mdz027.002.

[76] Sagoo P, Garcia Z, Breart B, Lemaître F, Michonneau D, Albert ML, Levy Y, Bousso P. In vivo imaging of inflammasome activation reveals a subcapsular macrophage burst response that mobilizes innate and adaptive immunity. Nat Med 2016;22:64–71. https://doi.org/10.1038/NM.4016.

[77] North RA. Molecular physiology of P2X receptors. Physiol Rev 2002;82:1013–67. https://doi.org/10.1152/physrev.00015.2002.

[78] Lombardi M, Gabrielli M, Adinolfi E, Verderio C. Role of ATP in Extracellular Vesicle Biogenesis and Dynamics. Front Pharmacol 2021;12:654023. https://doi.org/10.3389/fphar.2021.654023.

[79] Gu BJ, Zhang WY, Bendall LJ, Chessell IP, Buell GN, Wiley JS. Expression of P2X(7) purinoceptors on human lymphocytes and monocytes: evidence for nonfunctional P2X(7) receptors. Am J Physiol Cell Physiol 2000;279:C1189-97. https://doi.org/10.1152/ajpcell.2000.279.4.C1189.

[80] Burnstock G, Knight GE. Cellular Distribution and Functions of P2 Receptor Subtypes in Different Systems. Int Rev Cytol, vol. 240, Academic Press; 2004, p. 31–304. https://doi.org/https://doi.org/10.1016/S0074-7696(04)40002-3.

[81] Adinolfi E, Callegari MG, Ferrari D, Bolognesi C, Minelli M, Wieckowski MR, Pinton P, Rizzuto R, Di Virgilio F. Basal activation of the P2X7 ATP receptor elevates mitochondrial calcium and potential, increases cellular ATP levels, and promotes serum-independent growth. Mol Biol Cell 2005;16:3260–72. https://doi.org/10.1091/mbc.e04-11-1025.

[82] Bartlett R, Stokes L, Sluyter R. The P2X7 receptor channel: recent developments and the use of P2X7 antagonists in models of disease. Pharmacol Rev 2014;66:638–75. https://doi.org/10.1124/pr.113.008003.

[83] Nuttles LC, Dubyakj GR. Differential Activation of Cation Channels and Non-selective Pores by Macrophage P2, Purinergic Receptors Expressed in Xenopus Oocytes*. Journal of Biological Chemistry 1994;269:13988–96. https://doi.org/10.1016/S0021-9258(17)36744-3.

[84] P2rx7 - P2X purinoceptor 7 - Mus musculus (Mouse) | UniProtKB | UniProt n.d. https://www.uniprot.org/uniprotkb/Q9Z1M0/entry (accessed October 20, 2023).

[85] Smart ML, Gu B, Panchal RG, Wiley ¶ § § J, Cromer B, Williams DA, Petrou S, Vincent' S. P2X7 Receptor Cell Surface Expression and Cytolytic Pore Formation Are Regulated by a Distal C-terminal Region* 2002. https://doi.org/10.1074/jbc.M211094200.

[86] Adriouch S, Dox C, Welge V, Seman M, Koch-Nolte F, Haag F. Cutting edge: a natural P451L mutation in the cytoplasmic domain impairs the function of the mouse P2X7 receptor. J Immunol 2002;169:4108–12. https://doi.org/10.4049/jimmunol.169.8.4108.

[87] Surprenant A, Rassendren F, Kawashima E, North RA, Buell G. The Cytolytic P2Z Receptor for Extracellular ATP Identified as a P2X Receptor (P2X7). Science (1979) 1996;272:735–8. https://doi.org/10.1126/SCIENCE.272.5262.735.

[88] Di Virgilio F. The P2Z purinoceptor: an intriguing role in immunity, inflammation and cell death. Immunol Today 1995;16:524–8. https://doi.org/10.1016/0167-5699(95)80045-X.

[89] Sarti AC, Vultaggio-Poma V, Falzoni S, Missiroli S, Giuliani AL, Boldrini P, Bonora M, Faita F, Di Lascio N, Kusmic C, Solini A, Novello S, Morari M, Rossato M, Wieckowski MR, Giorgi C, Pinton P, Di Virgilio F. Mitochondrial P2X7 Receptor Localization Modulates Energy Metabolism Enhancing Physical Performance. Function 2021;2. https://doi.org/10.1093/function/zqab005.

[90] Atkinson L, Milligan CJ, Buckley NJ, Deuchars J. An ATP-gated ion channel at the cell nucleus. Nature 2002;420:42. https://doi.org/10.1038/420042A.

[91] Yegutkin GG. Nucleotide- and nucleoside-converting ectoenzymes: Important modulators of purinergic signalling cascade. Biochim Biophys Acta 2008;1783:673–94. https://doi.org/10.1016/J.BBAMCR.2008.01.024.

[92] Di Virgilio F, Pizzo P, Zanovello P, Bronte V, Collavo D. Extracellular ATP as a possible mediator of cell-mediated cytotoxicity. Immunol Today 1990;11:274–7. https://doi.org/10.1016/0167-5699(90)90111-L.

[93] Allsopp RC, Dayl S, Dayel A Bin, Schmid R, Evans RJ. Mapping the allosteric action of antagonists A740003 and A438079 reveals a role for the left flipper in ligand sensitivity at P2X7 receptorss. Mol Pharmacol 2018;93:553–62. https://doi.org/10.1124/MOL.117.111021/-/DC1.

[94] Burnstock G. Purine and pyrimidine receptors. Cell Mol Life Sci 2007;64:1471–83. https://doi.org/10.1007/S00018-007-6497-0.

[95] Amores-Iniesta J, Barberà-Cremades M, Martínez CM, Pons JA, Revilla-Nuin B, Martínez-Alarcón L, Di Virgilio F, Parrilla P, Baroja-Mazo A, Pelegrín P. Extracellular ATP Activates the NLRP3 Inflammasome and Is an Early Danger Signal of Skin Allograft Rejection. Cell Rep 2017;21:3414–26. https://doi.org/10.1016/j.celrep.2017.11.079.

[96] Orioli E, De Marchi E, Giuliani AL, Adinolfi E. P2X7 Receptor Orchestrates Multiple Signalling Pathways Triggering Inflammation, Autophagy and Metabolic/Trophic Responses. Curr Med Chem 2017;24:2261–75. https://doi.org/10.2174/0929867324666170303161659.

[97] Seman M, Adriouch S, Scheuplein F, Krebs C, Freese D, Glowacki G, Deterre P, Haag F, Koch-Nolte F. NAD-induced T cell death: ADP-ribosylation of cell surface proteins by ART2 activates the cytolytic P2X7 purinoceptor. Immunity 2003;19:571–82. https://doi.org/10.1016/S1074-7613(03)00266-8.

[98] Macian F. NFAT proteins: key regulators of T-cell development and function. Nat Rev Immunol 2005;5:472–84. https://doi.org/10.1038/nri1632.

[99] Yip L, Woehrle T, Corriden R, Hirsh M, Chen Y, Inoue Y, Ferrari V, Insel PA, Junger WG. Autocrine regulation of T-cell activation by ATP release and P2X7 receptors. FASEB J 2009;23:1685–93. https://doi.org/10.1096/FJ.08-126458.

[100] Viola JPB, Carvalho LDS, Fonseca BPF, Teixeira LK. NFAT transcription factors: from cell cycle to tumor development. Braz J Med Biol Res 2005;38:335–44. https://doi.org/10.1590/S0100-879X2005000300003.

[101] Buchholz M, Ellenrieder V. Cell Cycle An Emerging Role for Ca2+/Calcineurin/NFAT Signaling in Cancerogenesis An Emerging Role for Ca 2+ /Calcineurin/NFAT Signaling in Cancerogenesis. Cell Cycle 2007;6:16–9. https://doi.org/10.4161/cc.6.1.3650.

[102] Moon H, Na HY, Chong KH, Kim TJ. P2X7 receptor-dependent ATP-induced shedding of CD27 in mouse lymphocytes. Immunol Lett 2006;102:98–105. https://doi.org/10.1016/J.IMLET.2005.08.004.

[103] Gu B, Bendall LJ, Wiley JS. Adenosine Triphosphate–Induced Shedding of CD23 and L-Selectin (CD62L) From Lymphocytes Is Mediated by the Same Receptor but Different Metalloproteases. Blood 1998;92:946–51. https://doi.org/10.1182/BLOOD.V92.3.946.

[104] Garbers C, Jänner N, Chalaris A, Moss ML, Floss DM, Meyer D, Koch-Nolte F, Rose-John S, Scheller J. Species specificity of ADAM10 and ADAM17 proteins in interleukin-6 (IL-6) trans-signaling and novel role of ADAM10 in inducible IL-6 receptor shedding. J Biol Chem 2011;286:14804–11. https://doi.org/10.1074/JBC.M111.229393.

[105] Lin C, Ren S, Zhang L, Jin H, Sun J, Zuo Y. Extracellular ATP induces CD44 shedding from macrophage-like P388D1 cells via the P2X7 receptor. Hematol Oncol 2012;30:70–5. https://doi.org/10.1002/HON.1008.

[106] Pupovac A, Foster CM, Sluyter R. Human P2X7 receptor activation induces the rapid shedding of CXCL16. Biochem Biophys Res Commun 2013;432:626–31. https://doi.org/10.1016/J.BBRC.2013.01.134.

[107] Adinolfi E, Callegari MG, Cirillo M, Pinton P, Giorgi C, Cavagna D, Rizzuto R, Di Virgilio F. Expression of the P2X7 receptor increases the Ca2+ content of the endoplasmic reticulum, activates NFATc1, and protects from apoptosis. J Biol Chem 2009;284:10120–8. https://doi.org/10.1074/jbc.M805805200.

[108] Costa-Junior HM, Marques-da-Silva C, Vieira FS, Moncao-Ribeiro LC, Coutinho-Silva R. Lipid metabolism modulation by the P2X7 receptor in the immune system and during the course of infection: new insights into the old view. Purinergic Signal 2011;7:381–92. https://doi.org/10.1007/s11302-011-9255-6.

[109] Saéz PJ, Vargas P, Shoji KF, Harcha PA, Lennon-Duméni AM, Saéz JC. ATP promotes the fast migration of dendritic cells through the activity of pannexin 1 channels and P2X7 receptors. Sci Signal 2017;10. https://doi.org/10.1126/SCISIGNAL.AAH7107/SUPPL_FILE/AAH7107_SM.PDF.

[110] Barrera-Avalos C, Briceno P, Valdes D, Imarai M, Leiva-Salcedo E, Rojo LE, Milla LA, Huidobro-Toro JP, Robles-Planells C, Escobar A, Di Virgilio F, Moron G, Sauma D, Acuna-Castillo C. P2X7 receptor is essential for cross-dressing of bone marrow-derived dendritic cells. IScience 2021;24:103520. https://doi.org/10.1016/j.isci.2021.103520.

[111] Kim M, Jiang LH, Wilson HL, North RA, Surprenant A. Proteomic and functional evidence for a P2X7 receptor signalling complex. EMBO J 2001;20:6347–58. https://doi.org/10.1093/EMBOJ/20.22.6347.

[112] Kopp R, Krautloher A, Ramirez-Fernandez A, Nicke A. P2X7 Interactions and Signaling - Making Head or Tail of It. Front Mol Neurosci 2019;12:183. https://doi.org/10.3389/fnmol.2019.00183.

[113] Pegoraro A, De Marchi E, Ferracin M, Orioli E, Zanoni M, Bassi C, Tesei A, Capece M, Dika E, Negrini M, Di Virgilio F, Adinolfi E. P2X7 promotes metastatic spreading and triggers release of miRNA-containing exosomes and microvesicles from melanoma cells. Cell Death Dis 2021;12:1088. https://doi.org/10.1038/s41419-021-04378-0.

[114] Ruan Z, Delpech JC, Venkatesan Kalavai S, Van Enoo AA, Hu J, Ikezu S, Ikezu T. P2RX7 inhibitor suppresses exosome secretion and disease phenotype in P301S tau transgenic mice. Mol Neurodegener 2020;15:1–14. https://doi.org/10.1186/S13024-020-00396-2/FIGURES/6.

[115] Bianco F, Perrotta C, Novellino L, Francolini M, Riganti L, Menna E, Saglietti L, Schuchman EH, Furlan R, Clementi E, Matteoli M, Verderio C. Acid sphingomyelinase activity triggers microparticle release from glial cells. EMBO J 2009;28:1043–54. https://doi.org/10.1038/emboj.2009.45.

[116] Pfeiffer ZA, Aga M, Prabhu U, Watters JJ, Hall DJ, Bertics PJ. The nucleotide receptor P2X7 mediates actin reorganization and membrane blebbing in RAW 264.7 macrophages via p38 MAP kinase and Rho. J Leukoc Biol 2004;75:1173–82. https://doi.org/10.1189/JLB.1203648.

[117] Van Niel G, D'Angelo G, Raposo G. Shedding light on the cell biology of extracellular vesicles. Nature Reviews Molecular Cell Biology 2018 19:4 2018;19:213–28. https://doi.org/10.1038/nrm.2017.125.

[118] Caruso S, Poon IKH. Apoptotic Cell-Derived Extracellular Vesicles: More Than Just Debris. Front Immunol 2018;9:1486. https://doi.org/10.3389/fimmu.2018.01486.

[119] Lindenbergh MFS, Stoorvogel W. Antigen Presentation by Extracellular Vesicles from Professional Antigen-Presenting Cells. Annu Rev Immunol 2018;36:435–59. https://doi.org/10.1146/annurev-immunol-041015-055700.

[120] Battistelli M, Falcieri E. Apoptotic Bodies: Particular Extracellular Vesicles Involved in Intercellular Communication. Biology (Basel) 2020;9. https://doi.org/10.3390/biology9010021.

[121] Pizzirani C, Ferrari D, Chiozzi P, Adinolfi E, Sandona D, Savaglio E, Di Virgilio F. Stimulation of P2 receptors causes release of IL-1beta-loaded microvesicles from human dendritic cells. Blood 2007;109:3856–64. https://doi.org/10.1182/blood-2005-06-031377.

[122] Ferrari D, Pizzirani C, Adinolfi E, Lemoli RM, Curti A, Idzko M, Panther E, Di Virgilio F. The P2X7 receptor: a key player in IL-1 processing and release. J Immunol 2006;176:3877–83. https://doi.org/10.4049/JIMMUNOL.176.7.3877.

[123] MacKenzie A, Wilson HL, Kiss-Toth E, Dower SK, North RA, Surprenant A. Rapid Secretion of Interleukin-1β by Microvesicle Shedding. Immunity 2001;15:825–35. https://doi.org/10.1016/S1074-7613(01)00229-1.

[124] Yáñez-Mó M, Siljander PRM, Andreu Z, Zavec AB, Borràs FE, Buzas EI, Buzas K, Casal E, Cappello F, Carvalho J, Colás E, Cordeiro-Da Silva A, Fais S, Falcon-Perez JM, Ghobrial IM, Giebel B, Gimona M, Graner M, Gursel I, Gursel M, Heegaard NHH, Hendrix A, Kierulf P, Kokubun K, Kosanovic M, Kralj-Iglic V, Krämer-Albers EM, Laitinen S, Lässer C, Lener T, Ligeti E, Line A, Lipps G, Llorente A, Lötvall J, Manček-Keber M, Marcilla A, Mittelbrunn M, Nazarenko I, Nolte-'t Hoen ENM, Nyman TA, O'Driscoll L, Olivan M, Oliveira C, Pállinger É, Del Portillo HA, Reventós J, Rigau M, Rohde E, Sammar M, Sánchez-Madrid F, Santarém N, Schallmoser K, Ostenfeld MS, Stoorvogel W, Stukelj R, Van Der Grein SG, Helena Vasconcelos M, Wauben MHM, De Wever O. Biological properties of extracellular vesicles and their physiological functions. J Extracell Vesicles 2015;4:1–60. https://doi.org/10.3402/JEV.V4.27066.

[125] Cocucci E, Racchetti G, Meldolesi J. Shedding microvesicles: artefacts no more. Trends Cell Biol 2009;19:43–51. https://doi.org/10.1016/J.TCB.2008.11.003.

[126] Al-Nedawi K, Meehan B, Micallef J, Lhotak V, May L, Guha A, Rak J. Intercellular transfer of the oncogenic receptor EGFRvIII by microvesicles derived from tumour cells. Nat Cell Biol 2008;10:619–24. https://doi.org/10.1038/NCB1725.

[127] Schaible UE, Winau F, Sieling PA, Fischer K, Collins HL, Hagens K, Modlin RL, Brinkmann V, Kaufmann SHE. Apoptosis facilitates antigen presentation to T lymphocytes through MHC-I and CD1 in tuberculosis. Nature Medicine 2003 9:8 2003;9:1039–46. https://doi.org/10.1038/nm906.

[128] Giri PK, Schorey JS. Exosomes derived from M. Bovis BCG infected macrophages activate antigen-specific CD4+ and CD8+ T cells in vitro and in vivo. PLoS One 2008;3. https://doi.org/10.1371/JOURNAL.PONE.0002461.

[129] Lo Cicero A, Stahl PD, Raposo G. Extracellular vesicles shuffling intercellular messages: for good or for bad. Curr Opin Cell Biol 2015;35:69–77. https://doi.org/10.1016/J.CEB.2015.04.013.

[130] Adinolfi E, Cirillo M, Woltersdorf R, Falzoni S, Chiozzi P, Pellegatti P, Callegari MG, Sandona D, Markwardt F, Schmalzing G, Di Virgilio F. Trophic activity of a naturally occurring truncated isoform of the P2X7 receptor. FASEB J 2010;24:3393–404. https://doi.org/10.1096/fj.09-153601.

[131] Adinolfi E, Raffaghello L, Giuliani AL, Cavazzini L, Capece M, Chiozzi P, Bianchi G, Kroemer G, Pistoia V, Di Virgilio F. Expression of P2X7 receptor increases in vivo tumor growth. Cancer Res 2012;72:2957–69. https://doi.org/10.1158/0008-5472.CAN-11-1947.

[132] Tao S, Tao R, Busch DH, Widera M, Schaal H, Drexler I. Sequestration of Late Antigens Within Viral Factories Impairs MVA Vector-Induced Protective Memory CTL Responses. Front Immunol 2019;10:2850. https://doi.org/10.3389/fimmu.2019.02850.

[133] Oseroff C, Kos F, Bui HH, Peters B, Pasquetto V, Glenn J, Palmore T, Sidney J, Tscharke DC, Bennink JR, Southwood S, Grey HM, Yewdell JW, Sette A. HLA class I-restricted responses to vaccinia recognize a broad array of proteins mainly involved in virulence and viral gene regulation. Proc Natl Acad Sci U S A 2005;102:13980–5. https://doi.org/10.1073/pnas.0506768102.

[134] Rötzschke O, Falk K, Stevanovic S, Jung G, Walden P, Rammensee H-G. Exact prediction of a natural T cell epitope. Eur J Immunol 1991;21:2891–4. https://doi.org/https://doi.org/10.1002/eji.1830211136.

[135] Lohr V, Rath A, Genzel Y, Jordan I, Sandig V, Reichl U. New avian suspension cell lines provide production of influenza virus and MVA in serum-free media: studies on growth, metabolism and virus propagation. Vaccine 2009;27:4975–82. https://doi.org/10.1016/J.VACCINE.2009.05.083.

[136] Concordet J-P, Haeussler M. CRISPOR: intuitive guide selection for CRISPR/Cas9 genome editing experiments and screens. Nucleic Acids Res 2018;46:W242–5. https://doi.org/10.1093/nar/gky354.

[137] Martínez M, Martínez NA, Silva WI. Measurement of the Intracellular Calcium Concentration with Fura-2 AM Using a Fluorescence Plate Reader. Bio Protoc 2017;7. https://doi.org/10.21769/BIOPROTOC.2411.

[138] Young MT, Pelegrin P, Surprenant A. Amino Acid Residues in the P2X7 Receptor that Mediate Differential Sensitivity to ATP and BzATP. Mol Pharmacol 2007;71:92–100. https://doi.org/10.1124/MOL.106.030163.

[139] Faria RX, Reis RAM, Casabulho CM, Alberto AVP, De Farias FP, Henriques-Pons A, Alves LA. Pharmacological properties of a pore induced by raising intracellular Ca2+. Am J Physiol Cell Physiol 2009;297. https://doi.org/10.1152/AJPCELL.00476.2008.

[140] Adriouch S, Scheuplein F, Bähring R, Seman M, Boyer O, Koch-Nolte F, Haag F. Characterisation of the R276A gain-of-function mutation in the ectodomain of murine P2X7. Purinergic Signal 2009;5:151–61. https://doi.org/10.1007/S11302-009-9134-6.

[141] Di Virgilio F, Dal Ben D, Sarti AC, Giuliani AL, Falzoni S. The P2X7 Receptor in Infection and Inflammation. Immunity 2017;47:15–31. https://doi.org/10.1016/j.immuni.2017.06.020.

[142] Werner P, Seward EP, Buell GN, North RA. Domains of P2X receptors involved in desensitization. Proc Natl Acad Sci U S A 1996;93:15485. https://doi.org/10.1073/PNAS.93.26.15485.

[143] Bergamin LS, Capece M, Salaro E, Sarti AC, Falzoni S, Pereira MSL, Bastiani MA De, Scholl JN, Battastini AMO, Virgilio F Di, Bergamin L, Scussel cia, Capece M, Salaro E, Sarti AC, Falzoni S, Pereira MS, Leivas fani, De Bastiani MA, nio, Scholl JN, Battastini AMO, Di Virgilio F. Role of the P2X7 receptor in in vitro and in vivo glioma tumor growth. Oncotarget 2019;10:4840–56. https://doi.org/10.18632/ONCOTARGET.27106.

[144] Virginio C, Mackenzie A, North RA, Surprenant A. Kinetics of cell lysis, dye uptake and permeability changes in cells expressing the rat P2X7 receptor. J Physiol 1999;519 Pt 2:335–46. https://doi.org/10.1111/J.1469-7793.1999.0335M.X.

[145] Mellman I, Steinman RM. Dendritic cells: specialized and regulated antigen processing machines. Cell 2001;106:255–8. https://doi.org/10.1016/S0092-8674(01)00449-4.

[146] Garber DA, O'Mara LA, Zhao J, Gangadhara S, An IC, Feinberg MB. Expanding the Repertoire of Modified Vaccinia Ankara-Based Vaccine Vectors via Genetic Complementation Strategies. PLoS One 2009;4. https://doi.org/10.1371/JOURNAL.PONE.0005445.

[147] Satheshkumar PS, Weisberg AS, Moss B. Vaccinia Virus A19 Protein Participates in the Transformation of Spherical Immature Particles to Barrel-Shaped Infectious Virions. J Virol 2013;87:10700. https://doi.org/10.1128/JVI.01258-13.

[148] Shen L, Sigal LJ, Boes M, Rock KL. Important role of cathepsin S in generating peptides for TAP-independent MHC class I crosspresentation in vivo. Immunity 2004;21:155–65. https://doi.org/10.1016/j.immuni.2004.07.004.

[149] Segawa K, Nagata S. An Apoptotic 'Eat Me' Signal: Phosphatidylserine Exposure. Trends Cell Biol 2015;25:639–50. https://doi.org/https://doi.org/10.1016/j.tcb.2015.08.003.

[150] Poon IKH, Hulett MD, Parish CR. Molecular mechanisms of late apoptotic/necrotic cell clearance. Cell Death Differ 2010;17:381–97. https://doi.org/10.1038/cdd.2009.195.

[151] Cavalcante GC, Schaan AP, Cabral GF, Santana-Da-Silva MN, Pinto P, Vidal AF, Ribeiro-Dos-Santos Â. A Cell's Fate: An Overview of the Molecular Biology and Genetics of Apoptosis. International Journal of Molecular Sciences 2019, Vol 20, Page 4133 2019;20:4133. https://doi.org/10.3390/IJMS20174133.

[152] Borges da Silva H, Beura LK, Wang H, Hanse EA, Gore R, Scott MC, Walsh DA, Block KE, Fonseca R, Yan Y, Hippen KL, Blazar BR, Masopust D, Kelekar A, Vulchanova L, Hogquist KA, Jameson SC. The purinergic receptor P2RX7 directs metabolic fitness of long-lived memory CD8+ T cells. Nature 2018;559:264–8. https://doi.org/10.1038/s41586-018-0282-0.

[153] Ferrick DA, Neilson A, Beeson C. Advances in measuring cellular bioenergetics using extracellular flux. Drug Discov Today 2008;13:268–74. https://doi.org/https://doi.org/10.1016/j.drudis.2007.12.008.

[154] Plitzko B, Loesgen S. Measurement of Oxygen Consumption Rate (OCR) and Extracellular Acidification Rate (ECAR) in Culture Cells for Assessment of the Energy Metabolism. Bio Protoc 2018;8. https://doi.org/10.21769/BIOPROTOC.2850.

[155] Yetkin-Arik B, Vogels IMC, Nowak-Sliwinska P, Weiss A, Houtkooper RH, Van Noorden CJF, Klaassen I, Schlingemann RO. The role of glycolysis and mitochondrial respiration in the formation and functioning of endothelial tip cells during angiogenesis. Scientific Reports 2019 9:1 2019;9:1–14. https://doi.org/10.1038/s41598-019-48676-2.

[156] Pike Winer LS, Wu M. Rapid Analysis of Glycolytic and Oxidative Substrate Flux of Cancer Cells in a Microplate. PLoS One 2014;9:109916. https://doi.org/10.1371/JOURNAL.PONE.0109916.

[157] Di Virgilio F, Giuliani AL, Vultaggio-Poma V, Falzoni S, Sarti AC. Non-nucleotide Agonists Triggering P2X7 Receptor Activation and Pore Formation. Front Pharmacol 2018;9. https://doi.org/10.3389/FPHAR.2018.00039.

[158] De Marchi E, Orioli E, Pegoraro A, Sangaletti S, Portararo P, Curti A, Colombo MP, Di Virgilio F, Adinolfi E. The P2X7 receptor modulates immune cells infiltration, ectonucleotidases expression and extracellular ATP levels in the tumor microenvironment. Oncogene 2019;38:3636–50. https://doi.org/10.1038/s41388-019-0684-y.

[159] Furuta K, Onishi H, Ikada Y, Masaki K, Tanaka S, Kaito C. ATP and its metabolite adenosine cooperatively upregulate the antigen-presenting molecules on dendritic cells leading to IFN-γ production by T cells. Journal of Biological Chemistry 2023;299:104587. https://doi.org/10.1016/j.jbc.2023.104587.

[160] Karttunen JT, Trowsdale J, Lehner PJ. Antigen presentation: TAP dances with ATP. Current Biology 1999;9:R820–4. https://doi.org/10.1016/s0960-9822(99)80499-0.

[161] Clark G, Brown KA, Tripathy MK, Roux SJ. Recent Advances Clarifying the Structure and Function of Plant Apyrases (Nucleoside Triphosphate Diphosphohydrolases). International Journal of Molecular Sciences 2021, Vol 22, Page 3283 2021;22:3283. https://doi.org/10.3390/IJMS22063283.

[162] de Torre-Minguela C, Barbera-Cremades M, Gomez AI, Martin-Sanchez F, Pelegrin P. Macrophage activation and polarization modify P2X7 receptor secretome influencing the inflammatory process. Sci Rep 2016;6:22586. https://doi.org/10.1038/srep22586.

[163] Kaczmarek-Hájek K, Lörinczi E, Hausmann R, Nicke A. Molecular and functional properties of P2X receptors--recent progress and persisting challenges. Purinergic Signal 2012;8:375–417. https://doi.org/10.1007/s11302-012-9314-7.

[164] Latz E, Xiao TS, Stutz A. Activation and regulation of the inflammasomes. Nature Reviews Immunology 2013 13:6 2013;13:397–411. https://doi.org/10.1038/nri3452.

[165] Cassel SL, Sutterwala FS. Sterile inflammatory responses mediated by the NLRP3 inflammasome. Eur J Immunol 2010;40:607. https://doi.org/10.1002/EJI.200940207.

[166] Chan AH, Schroder K. Cytokines Focus: Inflammasome signaling and regulation of interleukin-1 family cytokines. J Exp Med 2020;217. https://doi.org/10.1084/JEM.20190314.

[167] Alharbi NK. Poxviral promoters for improving the immunogenicity of MVA delivered vaccines. Hum Vaccin Immunother 2019;15:203. https://doi.org/10.1080/21645515.2018.1513439.

[168] Liu S, Cai X, Wu J, Cong Q, Chen X, Li T, Du F, Ren J, Wu YT, Grishin N V., Chen ZJ. Phosphorylation of innate immune adaptor proteins MAVS, STING, and TRIF induces IRF3 activation. Science (1979) 2015;347. https://doi.org/10.1126/SCIENCE.AAA2630/SUPPL_FILE/LIU.SM.REVISION.1.PDF.

[169] Sun Z, Hornung V. cGAS–STING signaling. Current Biology 2022;32:R730–4. https://doi.org/10.1016/j.cub.2022.05.027.

[170] Guo C, Ma X, Gao F, Guo Y. Off-target effects in CRISPR/Cas9 gene editing. Front Bioeng Biotechnol 2023;11. https://doi.org/10.3389/FBIOE.2023.1143157/FULL.

[171] Wang H, La Russa M, Qi LS. CRISPR/Cas9 in Genome Editing and Beyond. Annu Rev Biochem 2016;85:227–64. https://doi.org/10.1146/ANNUREV-BIOCHEM-060815-014607.

[172] Hsu PD, Scott DA, Weinstein JA, Ran FA, Konermann S, Agarwala V, Li Y, Fine EJ, Wu X, Shalem O, Cradick TJ, Marraffini LA, Bao G, Zhang F. DNA targeting specificity

of RNA-guided Cas9 nucleases. Nat Biotechnol 2013;31:827–32. https://doi.org/10.1038/NBT.2647.

[173] Fu YW, Dai XY, Wang WT, Yang ZX, Zhao JJ, Zhang JP, Wen W, Zhang F, Oberg KC, Zhang L, Cheng T, Zhang XB. Dynamics and competition of CRISPR-Cas9 ribonucleoproteins and AAV donor-mediated NHEJ, MMEJ and HDR editing. Nucleic Acids Res 2021;49:969–85. https://doi.org/10.1093/NAR/GKAA1251.

[174] Tuladhar R, Yeu Y, Tyler Piazza J, Tan Z, Rene Clemenceau J, Wu X, Barrett Q, Herbert J, Mathews DH, Kim J, Hyun Hwang T, Lum L. CRISPR-Cas9-based mutagenesis frequently provokes on-target mRNA misregulation. Nat Commun 2019;10. https://doi.org/10.1038/S41467-019-12028-5.

[175] Zhang Q, Fu Y, Thakur C, Bi Z, Wadgaonkar P, Qiu Y, Xu L, Rice MK, Zhang W, Almutairy B, Chen F. CRISPR-Cas9 gene editing causes alternative splicing of the targeting mRNA. Biochem Biophys Res Commun 2020;528:54. https://doi.org/10.1016/J.BBRC.2020.04.145.

[176] Deaton AM, Bird A. CpG islands and the regulation of transcription. Genes Dev 2011;25:1010. https://doi.org/10.1101/GAD.2037511.

[177] Blackledge NP, Klose RJ. CpG island chromatin: A platform for gene regulation. Epigenetics 2011;6:147. https://doi.org/10.4161/EPI.6.2.13640.

[178] Farris MH, Texter PA, Mora AA, Wiles M V., Mac Garrigle EF, Klaus SA, Rosfjord K. Detection of CRISPR-mediated genome modifications through altered methylation patterns of CpG islands. BMC Genomics 2020;21. https://doi.org/10.1186/S12864-020-07233-2.

[179] Stothard P. The sequence manipulation suite: JavaScript programs for analyzing and formatting protein and DNA sequences. Biotechniques 2000;28. https://doi.org/10.2144/00286IR01.

[180] Gardiner-Garden M, Frommer M. CpG islands in vertebrate genomes. J Mol Biol 1987;196:261–82. https://doi.org/10.1016/0022-2836(87)90689-9.

[181] Peter I, Mezzacasa A, LeDonne P, Dummer R, Hemmi S. Comparative analysis of immunocritical melanoma markers in the mouse melanoma cell lines B16, K1735 and S91-M3. Melanoma Res 2001;11:21–30. https://doi.org/10.1097/00008390-200102000-00003.

[182] BARISHAK R, WELLINGS SR, SIEGEL B V. Cytologic Studies of Cultured Cells of the Cloudman S-91 Mouse Melanoma. Am J Pathol 1961;38:371.

[183] Santiago-Carvalho I, Almeida-Santos G de, Bomfim CCB, Souza PC de, Silva JCS e., Melo BMS de, Amaral EP, Cione MVP, Lasunskaia E, Hirata MH, Alves-Filho JCF, Nakaya HI, Alvarez JM, D'Império Lima MR. P2x7 Receptor Signaling Blockade Reduces Lung Inflammation and Necrosis During Severe Experimental Tuberculosis. Front Cell Infect Microbiol 2021;11:672472. https://doi.org/10.3389/FCIMB.2021.672472/BIBTEX.

[184] Soare AY, Freeman TL, Min AK, Malik HS, Osota EO, Swartz TH. P2RX7 at the Host-Pathogen Interface of Infectious Diseases. Microbiol Mol Biol Rev 2021;85. https://doi.org/10.1128/mmbr.00055-20.

[185] Pérez-Flores G, Lévesque SA, Pacheco J, Vaca L, Lacroix S, Pérez-Cornejo P, Arreola J. The P2X7/P2X4 interaction shapes the purinergic response in murine

macrophages. Biochem Biophys Res Commun 2015;467:484–90. https://doi.org/10.1016/J.BBRC.2015.10.025.

[186] Zhao S, Zhou Y, Fan Y, Gong Y, Yang J, Yang R, Li L, Zou L, Xu X, Li G, Liu S, Zhang C, Li G, Liang S. Involvement of purinergic 2X4 receptor in glycoprotein 120-induced pyroptosis in dorsal root ganglia. J Neurochem 2019;151:584–94. https://doi.org/10.1111/JNC.14850.

[187] Bagur R, Rgy Hajnó Czky G. Molecular Cell Review Intracellular Ca 2+ Sensing: Its Role in Calcium Homeostasis and Signaling 2017. https://doi.org/10.1016/j.molcel.2017.05.028.

[188] Marques-da-Silva C, Chaves MM, Rodrigues JC, Corte-Real S, Coutinho-Silva R, Persechini PM. Differential modulation of ATP-induced P2X7-associated permeabilities to cations and anions of macrophages by infection with Leishmania amazonensis. PLoS One 2011;6:e25356. https://doi.org/10.1371/journal.pone.0025356.

[189] Adinolfi E, Pizzirani C, Idzko M, Panther E, Norgauer J, Di Virgilio F, Ferrari D. P2X(7) receptor: Death or life? Purinergic Signal 2005;1:219–27. https://doi.org/10.1007/s11302-005-6322-x.

[190] Rissiek B, Haag F, Boyer O, Koch-Nolte F, Adriouch S. P2X7 on Mouse T Cells: One Channel, Many Functions. Front Immunol 2015;6:204. https://doi.org/10.3389/fimmu.2015.00204.

[191] Salles ÉM de, Menezes MN de, Siqueira R, Silva HB da, Amaral EP, Castillo-Méndez SI, Cunha I, Cassado A dos A, Vieira FS, Olivieri DN, Tadokoro CE, Alvarez JM, Coutinho-Silva R, D'Império-Lima MR. P2X7 receptor drives Th1 cell differentiation and controls the follicular helper T cell population to protect against Plasmodium chabaudi malaria. PLoS Pathog 2017;13:e1006595. https://doi.org/10.1371/JOURNAL.PPAT.1006595.

[192] Pegoraro A, Bortolotti D, Marci R, Caselli E, Falzoni S, De Marchi E, Di Virgilio F, Rizzo R, Adinolfi E. The P2X7 Receptor 489C>T Gain of Function Polymorphism Favors HHV-6A Infection and Associates With Female Idiopathic Infertility. Front Pharmacol 2020;11:96. https://doi.org/10.3389/fphar.2020.00096.

[193] Lécuyer D, Nardacci R, Tannous D, Gutierrez-Mateyron E, Deva Nathan A, Subra F, Di Primio C, Quaranta P, Petit V, Richetta C, Mostefa-Kara A, Del Nonno F, Falasca L, Marlin R, Maisonnasse P, Delahousse J, Pascaud J, Deprez E, Naigeon M, Chaput N, Paci A, Saada V, Ghez D, Mariette X, Costa M, Pistello M, Allouch A, Delelis O, Piacentini M, Le Grand R, Perfettini J-L. The purinergic receptor P2X7 and the NLRP3 inflammasome are druggable host factors required for SARS-CoV-2 infection. Front Immunol 2023;14. https://doi.org/10.3389/FIMMU.2023.1270081.

[194] Taylor JM, Han Z. Purinergic receptor functionality is necessary for infection of human hepatocytes by hepatitis delta virus and hepatitis B virus. PLoS One 2010;5. https://doi.org/10.1371/JOURNAL.PONE.0015784.

[195] Verhoef PA, Estacion M, Schilling W, Dubyak GR. P2X7 receptor-dependent blebbing and the activation of Rho-effector kinases, caspases, and IL-1 beta release. J Immunol 2003;170:5728–38. https://doi.org/10.4049/JIMMUNOL.170.11.5728.

[196] Golia MT, Gabrielli M, Verderio C. P2X7 Receptor and Extracellular Vesicle Release. International Journal of Molecular Sciences 2023, Vol 24, Page 9805 2023;24:9805. https://doi.org/10.3390/IJMS24129805.

[197] Brassart B, Da Silva J, Donet M, Seurat E, Hague F, Terryn C, Velard F, Michel J, Ouadid-Ahidouch H, Monboisse JC, Hinek A, Maquart FX, Ramont L, Brassart-Pasco S. Tumour cell blebbing and extracellular vesicle shedding: key role of matrikines and ribosomal protein SA. British Journal of Cancer 2019 120:4 2019;120:453–65. https://doi.org/10.1038/s41416-019-0382-0.

[198] Hodges RR, Vrouvlianis J, Shatos MA, Dartt DA. Characterization of P2X7 Purinergic Receptors and Their Function in Rat Lacrimal Gland. Invest Ophthalmol Vis Sci 2009;50:5681–9. https://doi.org/10.1167/IOVS.09-3670.

[199] Amstrup J, Novak I. P2X7 receptor activates extracellular signal-regulated kinases ERK1 and ERK2 independently of Ca2+ influx. Biochemical Journal 2003;374:51. https://doi.org/10.1042/BJ20030585.

[200] Andrade AA, Silva PNG, Pereira ACTC, De Sousa LP, Ferreira PCP, Gazzinelli RT, Kroon EG, Ropert C, Bonjardim CA. The vaccinia virus-stimulated mitogen-activated protein kinase (MAPK) pathway is required for virus multiplication. Biochem J 2004;381:437–46. https://doi.org/10.1042/BJ20031375.

[201] De Magalhães JC, Andrade AA, Silva PNG, Sousa LP, Ropert C, Ferreira PCP, Kroon EG, Gazzinelli RT, Bonjardim CA. A mitogenic signal triggered at an early stage of vaccinia virus infection: implication of MEK/ERK and protein kinase A in virus multiplication. J Biol Chem 2001;276:38353–60. https://doi.org/10.1074/JBC.M100183200.

[202] Mercer J, Helenius A. Vaccinia virus uses macropinocytosis and apoptotic mimicry to enter host cells. Science (1979) 2008;320:531–5. https://doi.org/10.1126/science.1155164.

[203] Pennock ND, White JT, Cross EW, Cheney EE, Tamburini BA, Kedl RM. T cell responses: naïve to memory and everything in between. Adv Physiol Educ 2013;37:273. https://doi.org/10.1152/ADVAN.00066.2013.

[204] Mutini C, Falzoni S, Ferrari D, Chiozzi P, Morelli A, Baricordi OR, Collo G, Ricciardi-Castagnoli P, Di Virgilio F. Mouse dendritic cells express the P2X7 purinergic receptor: characterization and possible participation in antigen presentation. J Immunol 1999;163:1958–65.

[205] Toki Y, Takenouchi T, Harada H, Tanuma S, Kitani H, Kojima S, Tsukimoto M. Extracellular ATP induces P2X7 receptor activation in mouse Kupffer cells, leading to release of IL-1β, HMGB1, and PGE2, decreased MHC class I expression and necrotic cell death. Biochem Biophys Res Commun 2015;458:771–6. https://doi.org/10.1016/j.bbrc.2015.02.011.

[206] Di Virgilio F, Tang Y, Sarti AC, Rossato M. A rationale for targeting the P2X7 receptor in Coronavirus disease 19. Br J Pharmacol 2020;177:4990–4. https://doi.org/10.1111/BPH.15138.

[207] Shao X, Guha S, Lu W, Campagno KE, Beckel JM, Mills JA, Yang W, Mitchell CH. Polarized Cytokine Release Triggered by P2X7 Receptor from Retinal Pigmented Epithelial Cells Dependent on Calcium Influx. Cells 2020;9. https://doi.org/10.3390/CELLS9122537.

[208] Ikeda M, Minota S, Kano S. Regulation of MHC Class I Expression by Inflammatory Cytokines in Rat Mesangial Cells. Nephron 1997;76:90–5. https://doi.org/10.1159/000190146.

[209] Raval A, Puri N, Rath PC, Saxena RK. Cytokine regulation of expression of class I MHC antigens. Exp Mol Med 1998;30:1–13. https://doi.org/10.1038/EMM.1998.1.

[210] Honore P, Donnelly-Roberts D, Namovic MT, Hsieh G, Zhu CZ, Mikusa JP, Hernandez G, Zhong C, Gauvin DM, Chandran P, Harris R, Medrano AP, Carroll W, Marsh K, Sullivan JP, Faltynek CR, Jarvis MF. A-740003 [N-(1-{[(cyanoimino)(5-quinolinylamino) methyl]amino}-2,2-dimethylpropyl)-2-(3,4-dimethoxyphenyl)acetamide], a novel and selective P2X7 receptor antagonist, dose-dependently reduces neuropathic pain in the rat. J Pharmacol Exp Ther 2006;319:1376–85. https://doi.org/10.1124/jpet.106.111559.

[211] Altenburger W, Süter CP, Altenburger J. Partial deletion of the human host range gene in the attenuated vaccinia virus MVA. Arch Virol 1989;105:15–27. https://doi.org/10.1007/BF01311113/METRICS.

[212] Leite Pereira A, Jouhault Q, Marcos Lopez E, Cosma A, Lambotte O, Le Grand R, Lehmann MH, Tchitchek N. Modulation of Cell Surface Receptor Expression by Modified Vaccinia Virus Ankara in Leukocytes of Healthy and HIV-Infected Individuals. Front Immunol 2020;11:2096. https://doi.org/10.3389/fimmu.2020.02096.

[213] Laliberte JP, Weisberg AS, Moss B. The Membrane Fusion Step of Vaccinia Virus Entry Is Cooperatively Mediated by Multiple Viral Proteins and Host Cell Components. PLoS Pathog 2011;7:e1002446. https://doi.org/10.1371/journal.ppat.1002446.

[214] Gu BJ, Saunders BM, Jursik C, Wiley JS. The P2X7-nonmuscle myosin membrane complex regulates phagocytosis of nonopsonized particles and bacteria by a pathway attenuated by extracellular ATP. Blood 2010;115:1621–31. https://doi.org/10.1182/blood-2009-11-251744.

[215] Sobhy H. A comparative review of viral entry and attachment during large and giant dsDNA virus infections. Arch Virol 2017;162:3567. https://doi.org/10.1007/S00705-017-3497-8.

[216] Renukaradhya GJ, Khan MA, Shaji D, Brutkiewicz RR. Vesicular stomatitis virus matrix protein impairs CD1d-mediated antigen presentation through activation of the p38 MAPK pathway. J Virol 2008;82:12535–42. https://doi.org/10.1128/JVI.00881-08.

[217] Cheng Z, Teo G, Krueger S, Rock TM, Koh HW, Choi H, Vogel C. Differential dynamics of the mammalian mRNA and protein expression response to misfolding stress. Mol Syst Biol 2016;12:855. https://doi.org/10.15252/msb.20156423.

[218] Perl K, Ushakov K, Pozniak Y, Yizhar-Barnea O, Bhonker Y, Shivatzki S, Geiger T, Avraham KB, Shamir R. Reduced changes in protein compared to mRNA levels across non-proliferating tissues. BMC Genomics 2017;18:305. https://doi.org/10.1186/s12864-017-3683-9.

[219] Sluyter R, Shemon AN, Wiley JS. P2X(7) receptor activation causes phosphatidylserine exposure in human erythrocytes. Biochem Biophys Res Commun 2007;355:169–73. https://doi.org/10.1016/J.BBRC.2007.01.124.

[220] Matheoud D, Perié L, Hoeffel G, Vimeux L, Parent I, Marañón C, Bourdoncle P, Renia L, Prevost-Blondel A, Lucas B, Feuillet V, Hosmalin A. Cross-presentation by dendritic cells from live cells induces protective immune responses in vivo. Blood 2010;115:4412–20. https://doi.org/10.1182/BLOOD-2009-11-255935.

[221] Shlomovitz I, Speir M, Gerlic M. Flipping the dogma - Phosphatidylserine in non-apoptotic cell death. Cell Communication and Signaling 2019;17. https://doi.org/10.1186/s12964-019-0437-0.

[222] Mackenzie AB, Young MT, Adinolfi E, Surprenant A. Pseudoapoptosis induced by brief activation of ATP-gated P2X7 receptors. J Biol Chem 2005;280:33968–76. https://doi.org/10.1074/jbc.M502705200.

[223] Brokatzky D, Dörflinger B, Haimovici A, Weber A, Kirschnek S, Vier J, Metz A, Henschel J, Steinfeldt T, Gentle IE, Häcker G. A non-death function of the mitochondrial apoptosis apparatus in immunity. EMBO J 2019;38. https://doi.org/10.15252/embj.2018100907.

[224] Borisenko GG, Matsura T, Liu SX, Tyurin VA, Jianfei J, Serinkan FB, Kagan VE. Macrophage recognition of externalized phosphatidylserine and phagocytosis of apoptotic Jurkat cells--existence of a threshold. Arch Biochem Biophys 2003;413:41–52. https://doi.org/10.1016/s0003-9861(03)00083-3.

[225] Ichihashi Y, Oie M. The activation of vaccinia virus infectivity by the transfer of phosphatidylserine from the plasma membrane. Virology 1983;130:306–17. https://doi.org/https://doi.org/10.1016/0042-6822(83)90085-5.

[226] Mahmoudabadi G, Milo R, Phillips R. Energetic cost of building a virus. Proc Natl Acad Sci U S A 2017;114:E4324–33. https://doi.org/10.1073/PNAS.1701670114/SUPPL_FILE/PNAS.1701670114.SD03.XLSX.

[227] Munger J, Bajad SU, Coller HA, Shenk T, Rabinowitz JD. Dynamics of the cellular metabolome during human cytomegalovirus infection. PLoS Pathog 2006;2:e132. https://doi.org/10.1371/journal.ppat.0020132.

[228] Chambers JW, Maguire TG, Alwine JC. Glutamine metabolism is essential for human cytomegalovirus infection. J Virol 2010;84:1867–73. https://doi.org/10.1128/jvi.02123-09.

[229] Kates JR, McAuslan BR. Poxvirus DNA-dependent RNA polymerase. Proc Natl Acad Sci U S A 1967;58:134. https://doi.org/10.1073/PNAS.58.1.134.

[230] Munyon W, Paoletti E, Grace JT. RNA polymerase activity in purified infectious vaccinia virus. Proc Natl Acad Sci U S A 1967;58:2280–7. https://doi.org/10.1073/PNAS.58.6.2280.

[231] Cao S, Molina JA, Cantu F, Hernandez C, Yang Z. A Poxvirus Decapping Enzyme Colocalizes with Mitochondria To Regulate RNA Metabolism and Translation and Promote Viral Replication. MBio 2022;13. https://doi.org/10.1128/MBIO.00300-22.

[232] Elliott MR, Chekeni FB, Trampont PC, Lazarowski ER, Kadl A, Walk SF, Park D, Woodson RI, Ostankovich M, Sharma P, Lysiak JJ, Harden TK, Leitinger N, Ravichandran KS. Nucleotides released by apoptotic cells act as a find-me signal to promote phagocytic clearance. Nature 2009;461:282–6. https://doi.org/10.1038/nature08296.

[233] Bidgood SR, Samolej J, Novy K, Collopy A, Albrecht D, Krause M, Burden JJ, Wollscheid B, Mercer J. Poxviruses package viral redox proteins in lateral bodies and modulate the host oxidative response. PLoS Pathog 2022;18:e1010614. https://doi.org/10.1371/journal.ppat.1010614.

[234] Zelentsova AS, Deykin A V., Soldatov VO, Ulezko AA, Borisova AY, Belyaeva VS, Skorkina MY, Angelova PR. P2X7 Receptor and Purinergic Signaling: Orchestrating Mitochondrial Dysfunction in Neurodegenerative Diseases. ENeuro 2022;9. https://doi.org/10.1523/ENEURO.0092-22.2022.

[235] Giorgi C, Marchi S, Pinton P. The machineries, regulation and cellular functions of mitochondrial calcium. Nat Rev Mol Cell Biol 2018;19:713–30. https://doi.org/10.1038/S41580-018-0052-8.

[236] Subramaniam SR, Chesselet MF. Mitochondrial dysfunction and oxidative stress in Parkinson's disease. Prog Neurobiol 2013;106–107:17–32. https://doi.org/10.1016/J.PNEUROBIO.2013.04.004.

[237] La Sala A, Sebastiani S, Ferrari D, Di Virgilio F, Idzko M, Norgauer J, Girolomoni G. Dendritic cells exposed to extracellular adenosine triphosphate acquire the migratory properties of mature cells and show a reduced capacity to attract type 1 T lymphocytes. Blood 2002;99:1715–22. https://doi.org/10.1182/BLOOD.V99.5.1715.

[238] Baroja-Mazo A, Barberà-Cremades M, Pelegrín P. P2X7 receptor activation impairs exogenous MHC class I oligopeptides presentation in antigen presenting cells. PLoS One 2013;8:e70577. https://doi.org/10.1371/journal.pone.0070577.

[239] Grassi F, De Ponte Conti B. The P2X7 Receptor in Tumor Immunity. Front Cell Dev Biol 2021;9:694831. https://doi.org/10.3389/fcell.2021.694831.

[240] Novoa RR, Calderita G, Arranz R, Fontana J, Granzow H, Risco C. Virus factories: associations of cell organelles for viral replication and morphogenesis. Biol Cell 2005;97:147–72. https://doi.org/10.1042/BC20040058.

[241] Broyles SS, Moss B. DNA-dependent ATPase activity associated with vaccinia virus early transcription factor. Journal of Biological Chemistry 1988;263:10761–5. https://doi.org/10.1016/s0021-9258(18)38036-0.

[242] Tewalt EF, Grant JM, Granger EL, Palmer DC, Heuss ND, Gregerson DS, Restifo NP, Norbury CC. Viral sequestration of antigen subverts cross presentation to CD8(+) T cells. PLoS Pathog 2009;5:e1000457. https://doi.org/10.1371/journal.ppat.1000457.

[243] Takenouchi T, Nakai M, Iwamaru Y, Sugama S, Tsukimoto M, Fujita M, Wei J, Sekigawa A, Sato M, Kojima S, Kitani H, Hashimoto M. The activation of P2X7 receptor impairs lysosomal functions and stimulates the release of autophagolysosomes in microglial cells. J Immunol 2009;182:2051–62. https://doi.org/10.4049/jimmunol.0802577.

[244] Young CNJ, Sinadinos A, Lefebvre A, Chan P, Arkle S, Vaudry D, Gorecki DC. A novel mechanism of autophagic cell death in dystrophic muscle regulated by P2RX7 receptor large-pore formation and HSP90. Autophagy 2015;11:113–30. https://doi.org/10.4161/15548627.2014.994402.

[245] Colbert JD, Cruz FM, Rock KL. Cross-presentation of exogenous antigens on MHC I molecules. Curr Opin Immunol 2020;64:1. https://doi.org/10.1016/J.COI.2019.12.005.

[246] Blander JM. Regulation of the Cell Biology of Antigen Cross-Presentation. Annu Rev Immunol 2018;36:717–53. https://doi.org/10.1146/annurev-immunol-041015-055523.

[247] Hemenway CS, Heitman J. Calcineurin. Structure, function, and inhibition. Cell Biochem Biophys 1999;30:115–51. https://doi.org/10.1007/BF02737887.

[248] Wen AY, Sakamoto KM, Miller LS. The Role of the Transcription Factor CREB in Immune Function. J Immunol 2010;185:6413. https://doi.org/10.4049/JIMMUNOL.1001829.

[249] Hogan PG, Chen L, Nardone J, Rao A. Transcriptional regulation by calcium, calcineurin, and NFAT. Genes Dev 2003;17:2205–32. https://doi.org/10.1101/GAD.1102703.

[250] Gavala ML, Pfeiffer ZA, Bertics PJ. The nucleotide receptor P2RX7 mediates ATP-induced CREB activation in human and murine monocytic cells. J Leukoc Biol 2008;84:1159–71. https://doi.org/10.1189/JLB.0907612.

[251] Mayr B, Montminy M. Transcriptional regulation by the phosphorylation-dependent factor CREB. Nature Reviews Molecular Cell Biology 2001 2:8 2001;2:599–609. https://doi.org/10.1038/35085068.

[252] Aga M, Watters JJ, Pfeiffer ZA, Wiepz GJ, Sommer JA, Bertics PJ. Evidence for nucleotide receptor modulation of cross talk between MAP kinase and NF-kappa B signaling pathways in murine RAW 264.7 macrophages. Am J Physiol Cell Physiol 2004;286. https://doi.org/10.1152/AJPCELL.00417.2003.

[253] Brokatzky D, Häcker G. Mitochondria: intracellular sentinels of infections. Med Microbiol Immunol 2022;211:161–72. https://doi.org/10.1007/s00430-022-00742-9.

[254] Lehmann MH, Kastenmuller W, Kandemir JD, Brandt F, Suezer Y, Sutter G. Modified Vaccinia Virus Ankara Triggers Chemotaxis of Monocytes and Early Respiratory Immigration of Leukocytes by Induction of CCL2 Expression. J Virol 2009;83:2540–52. https://doi.org/10.1128/JVI.01884-08.

[255] Price PJR, Luckow B, Torres-Domínguez LE, Brandmüller C, Zorn J, Kirschning CJ, Sutter G, Lehmann MH. Chemokine (C-C Motif) Receptor 1 Is Required for Efficient Recruitment of Neutrophils during Respiratory Infection with Modified Vaccinia Virus Ankara. J Virol 2014;88:10840. https://doi.org/10.1128/JVI.01524-14.

[256] Pascutti MF, Rodríguez AM, Falivene J, Giavedoni L, Drexler I, Gherardi MM. Interplay between Modified Vaccinia Virus Ankara and Dendritic Cells: Phenotypic and Functional Maturation of Bystander Dendritic Cells. J Virol 2011;85:5532. https://doi.org/10.1128/JVI.02267-10.

[257] Shiratori M, Tozaki-Saitoh H, Yoshitake M, Tsuda M, Inoue K. P2X7 receptor activation induces CXCL2 production in microglia through NFAT and PKC/MAPK pathways. J Neurochem 2010;114:810–9. https://doi.org/10.1111/j.1471-4159.2010.06809.x.

[258] Fehr EM, Spoerl S, Heyder P, Herrmann M, Bekeredjian-Ding I, Blank N, Lorenz HM, Schiller M. Apoptotic-cell-derived membrane vesicles induce an alternative maturation of human dendritic cells which is disturbed in SLE. J Autoimmun 2013;40:86–95. https://doi.org/10.1016/J.JAUT.2012.08.003.

[259] Krejbich-Trotot P, Denizot M, Hoarau J, Jaffar-Bandjee M, Das T, Gasque P. Chikungunya virus mobilizes the apoptotic machinery to invade host cell defenses. FASEB J 2011;25:314–25. https://doi.org/10.1096/FJ.10-164178.

[260] Fransen JH, Hilbrands LB, Ruben J, Stoffels M, Adema GJ, van der Vlag J, Berden JH. Mouse dendritic cells matured by ingestion of apoptotic blebs induce T cells to produce interleukin-17. Arthritis Rheum 2009;60:2304–13. https://doi.org/10.1002/art.24719.

[261] Di Mambro T, Pellielo G, Agyapong ED, Carinci M, Chianese D, Giorgi C, Morciano G, Patergnani S, Pinton P, Rimessi A. The Tricky Connection between Extracellular Vesicles and Mitochondria in Inflammatory-Related Diseases. Int J Mol Sci 2023;24. https://doi.org/10.3390/IJMS24098181.

[262] Ho NI, Camps MG, Garcia-Vallejo JJ, Bos E, Koster AJ, Verdoes M, van Kooyk Y, Ossendorp F. Distinct antigen uptake receptors route to the same storage compartments for cross-presentation in dendritic cells. Immunology 2021;164:494–506. https://doi.org/10.1111/IMM.13382.

[263] McCullough KC, Bassi I, Démoulins T, Thomann-Harwood LJ, Ruggli N. Functional RNA delivery targeted to dendritic cells by synthetic nanoparticles. Ther Deliv 2012;3:1077–99. https://doi.org/10.4155/TDE.12.90/ASSET/IMAGES/LARGE/FIGURE4.JPEG.

[264] Boczkowski D, Nair SK, Snyder D, Gilboa E. Dendritic cells pulsed with RNA are potent antigen-presenting cells in vitro and in vivo. J Exp Med 1996;184:465. https://doi.org/10.1084/JEM.184.2.465.

[265] Cueto FJ, Del Fresno C, Sancho D. DNGR-1, a Dendritic Cell-Specific Sensor of Tissue Damage That Dually Modulates Immunity and Inflammation. Front Immunol 2019;10:3146. https://doi.org/10.3389/fimmu.2019.03146.

[266] Guo J, Yang P, Li YF, Tang JF, He ZX, Yu SG, Yin HY. MicroRNA: Crucial modulator in purinergic signalling involved diseases. Purinergic Signal 2023;19:329–41. https://doi.org/10.1007/s11302-022-09840-y.

[267] Riding RL, Richmond JM, Fukuda K, Harris JE. Type I interferon signaling limits viral vector priming of CD8(+) T cells during initiation of vitiligo and melanoma immunotherapy. Pigment Cell Melanoma Res 2021;34:683–95. https://doi.org/10.1111/pcmr.12935.

[268] MacFarlane L-A, Murphy PR. MicroRNA: Biogenesis, Function and Role in Cancer. Curr Genomics 2010;11:537. https://doi.org/10.2174/138920210793175895.

[269] Barber GN. Sting: infection, inflammation and cancer. Nat Rev Immunol 2015;15:760–71. https://doi.org/10.1038/NRI3921.

[270] Bustos MA, Yokoe T, Shoji Y, Kobayashi Y, Mizuno S, Murakami T, Zhang X, Sekhar SC, Kim SM, Ryu S, Knarr M, Vasilev SA, DiFeo A, Drapkin R, Hoon DSB. MiR-181a targets STING to drive PARP inhibitor resistance in BRCA- mutated triple-negative breast cancer and ovarian cancer. Cell Biosci 2023;13. https://doi.org/10.1186/S13578-023-01151-Y.

[271] Liang J, Yin H. STAM transports STING oligomers into extracellular vesicles, down-regulating the innate immune response. J Extracell Vesicles 2023;12:e12316. https://doi.org/10.1002/jev2.12316.

[272] Mathavarajah S, Salsman J, Dellaire G. An emerging role for calcium signalling in innate and autoimmunity via the cGAS-STING axis. Cytokine Growth Factor Rev 2019;50:43–51. https://doi.org/10.1016/j.cytogfr.2019.04.003.

[273] Joshi B, Joshi JC, Mehta D. Regulation of cGAS Activity and Downstream Signaling. Cells 2022;11. https://doi.org/10.3390/cells11182812.

[274] Kwon D, Sesaki H, Kang SJ. Intracellular calcium is a rheostat for the STING signaling pathway. Biochem Biophys Res Commun 2018;500:497–503. https://doi.org/10.1016/j.bbrc.2018.04.117.

[275] Bendz H, Marincek BC, Momburg F, Ellwart JW, Issels RD, Nelson PJ, Noessner E. Calcium signaling in dendritic cells by human or mycobacterial Hsp70 is caused by contamination and is not required for Hsp70-mediated enhancement of cross-

presentation. J Biol Chem 2008;283:26477–83. https://doi.org/10.1074/JBC.M803310200.

[276] Shumilina E, Huber SM, Lang F. Ca2+ signaling in the regulation of dendritic cell functions. Am J Physiol Cell Physiol 2011;300. https://doi.org/10.1152/AJPCELL.00039.2011.

[277] Pelegrin P. P2X7 receptor and the NLRP3 inflammasome: Partners in crime. Biochem Pharmacol 2021;187. https://doi.org/10.1016/J.BCP.2020.114385.

[278] Evavold CL, Kagan JC. How Inflammasomes Inform Adaptive Immunity. J Mol Biol 2018;430:217–37. https://doi.org/10.1016/J.JMB.2017.09.019.

[279] Deets KA, Vance RE. Inflammasomes and adaptive immune responses. Nat Immunol 2021;22:412–22. https://doi.org/10.1038/S41590-021-00869-6.

[280] Deets KA, Doyle RN, Rauch I, Vance RE. Inflammasome activation leads to cDC1-independent cross-priming of CD8 T cells by epithelial cell-derived antigen. Elife 2021;10. https://doi.org/10.7554/ELIFE.72082.

[281] Salaro E, Rambaldi A, Falzoni S, Amoroso FS, Franceschini A, Sarti AC, Bonora M, Cavazzini F, Rigolin GM, Ciccone M, Audrito V, Deaglio S, Pelegrin P, Pinton P, Cuneo A, Di Virgilio F. Involvement of the P2X7-NLRP3 axis in leukemic cell proliferation and death. Sci Rep 2016;6:26280. https://doi.org/10.1038/srep26280.

[282] Noonin C, Thongboonkerd V. Exosome-inflammasome crosstalk and their roles in inflammatory responses. Theranostics 2021;11:4436. https://doi.org/10.7150/THNO.54004.

[283] Bianco F, Pravettoni E, Colombo A, Schenk U, Möller T, Matteoli M, Verderio C. Astrocyte-derived ATP induces vesicle shedding and IL-1 beta release from microglia. J Immunol 2005;174:7268–77. https://doi.org/10.4049/JIMMUNOL.174.11.7268.

[284] Qu Y, Franchi L, Nunez G, Dubyak GR. Nonclassical IL-1 beta secretion stimulated by P2X7 receptors is dependent on inflammasome activation and correlated with exosome release in murine macrophages. J Immunol 2007;179:1913–25. https://doi.org/10.4049/jimmunol.179.3.1913.

[285] Hickman HD. Illuminating inflammasome activity in vivo. Nat Med 2016;22:22. https://doi.org/10.1038/NM.4026.

[286] Climent N, Guerra S, García F, Rovira C, Miralles L, Gómez CE, Piqué N, Gil C, Gatell JM, Esteban M, Gallart T. Dendritic Cells Exposed to MVA-Based HIV-1 Vaccine Induce Highly Functional HIV-1-Specific CD8+ T Cell Responses in HIV-1-Infected Individuals. PLoS One 2011;6:e19644. https://doi.org/10.1371/JOURNAL.PONE.0019644.

[287] Delaloye J, Roger T, Steiner-Tardivel QG, Le Roy D, Knaup Reymond M, Akira S, Petrilli V, Gomez CE, Perdiguero B, Tschopp J, Pantaleo G, Esteban M, Calandra T. Innate immune sensing of modified vaccinia virus Ankara (MVA) is mediated by TLR2-TLR6, MDA-5 and the NALP3 inflammasome. PLoS Pathog 2009;5:e1000480. https://doi.org/10.1371/journal.ppat.1000480.

[288] Ciupka G. Role of innate immune triggers for the induction of poxviral T cell responses. Heinrich-Heine-University, 2019.

[289] Stagg AJ, Knight SC. Antigen-presenting Cells. ELS 2001. https://doi.org/10.1038/NPG.ELS.0000903.

[290] Koszinowski UH, Reddehase MJ, Jonjic S. The role of CD4 and CD8 T cells in viral infections. Curr Opin Immunol 1991;3:471–5. https://doi.org/10.1016/0952-7915(91)90005-L.

[291] Zhou Y, Fei M, Zhang G, Liang WC, Lin W, Wu Y, Piskol R, Ridgway J, McNamara E, Huang H, Zhang J, Oh J, Patel JM, Jakubiak D, Lau J, Blackwood B, Bravo DD, Shi Y, Wang J, Hu HM, Lee WP, Jesudason R, Sangaraju D, Modrusan Z, Anderson KR, Warming S, Roose-Girma M, Yan M. Blockade of the Phagocytic Receptor MerTK on Tumor-Associated Macrophages Enhances P2X7R-Dependent STING Activation by Tumor-Derived cGAMP. Immunity 2020;52:357-373 e9. https://doi.org/10.1016/j.immuni.2020.01.014.

[292] Longo Y. Impact of inflammasome activation on cross-presentation of viral antigens after MVA infection. Heinrich-Heine-University, 2020.

[293] Kosicki M, Allen F, Steward F, Tomberg K, Pan Y, Bradley A. Cas9-induced large deletions and small indels are controlled in a convergent fashion. Nature Communications 2022 13:1 2022;13:1–11. https://doi.org/10.1038/s41467-022-30480-8.

[294] Shin YH, Kim M, Kim N, Choi SK, Namkoong E, Choi SY, Lee JH, Cha S, Park K. Epigenetic alteration of the purinergic type 7 receptor in salivary epithelial cells. Biochem Biophys Res Commun 2015;466:704–10. https://doi.org/10.1016/j.bbrc.2015.09.095.

[295] Menezo Y, Clement P, Clement A, Elder K. Methylation: An Ineluctable Biochemical and Physiological Process Essential to the Transmission of Life. Int J Mol Sci 2020;21:1–13. https://doi.org/10.3390/IJMS21239311.

[296] Longo Y, Mascaraque SM, Andreacchio G, Werner J, Katahira I, De Marchi E, Pegoraro A, Lebbink RJ, Köhrer K, Petzsch P, Tao R, Di Virgilio F, Adinolfi E, Drexler I. The purinergic receptor P2X7 as a modulator of viral vector-mediated antigen cross-presentation. Front Immunol 2024;15. https://doi.org/10.3389/FIMMU.2024.1360140.

10. Supplementary Figures

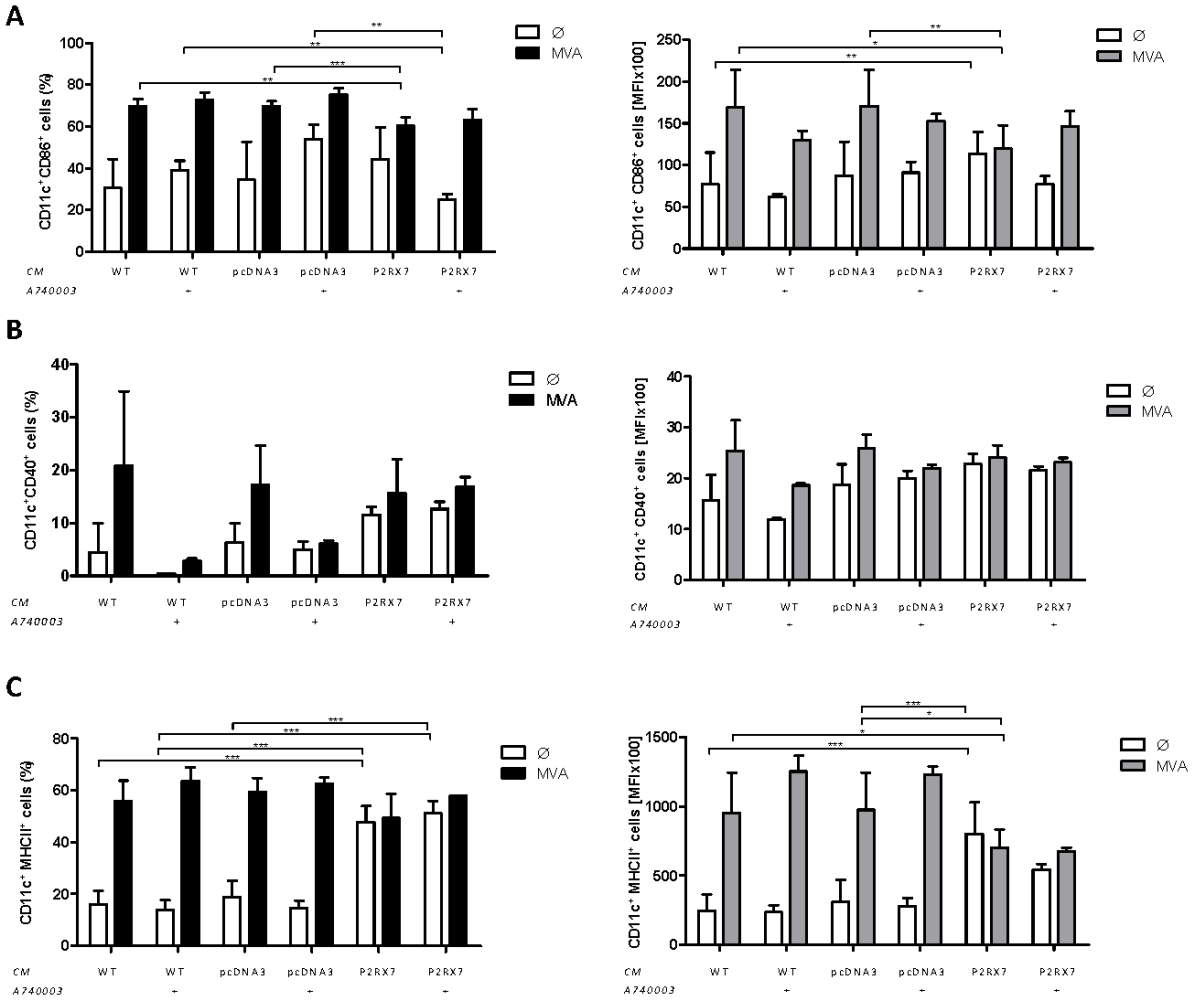

Figure S1: Maturation of BMDCs is not altered when co-cultured with A740003-treated CM P2RX7 cells. CM (WT, pcDNA3- or P2RX7-transfected) were untreated or pre-treated for 1h with 20µM A740003. Cells were then either mock-(Ø) or MVA-PK1L-Ova-infected (MOI1, 20hpi), harvested, washed, PUVA-treated and then co-cultured with BMDCs, previously generated from bone marrow cells grown in GM-CSF. Left image depicts the frequency (in %) and the right image the MFI of (A) CD86 (B) CD40 and (C) MHCII. The synthesis was determined using flow cytometry. Data are pooled from at least n=3 independent experiments and are shown as means ± SD. P values indicate statistical significance (P) with *P ≤ 0.05; **P ≤ 0.01; P***P ≤ 0.001.

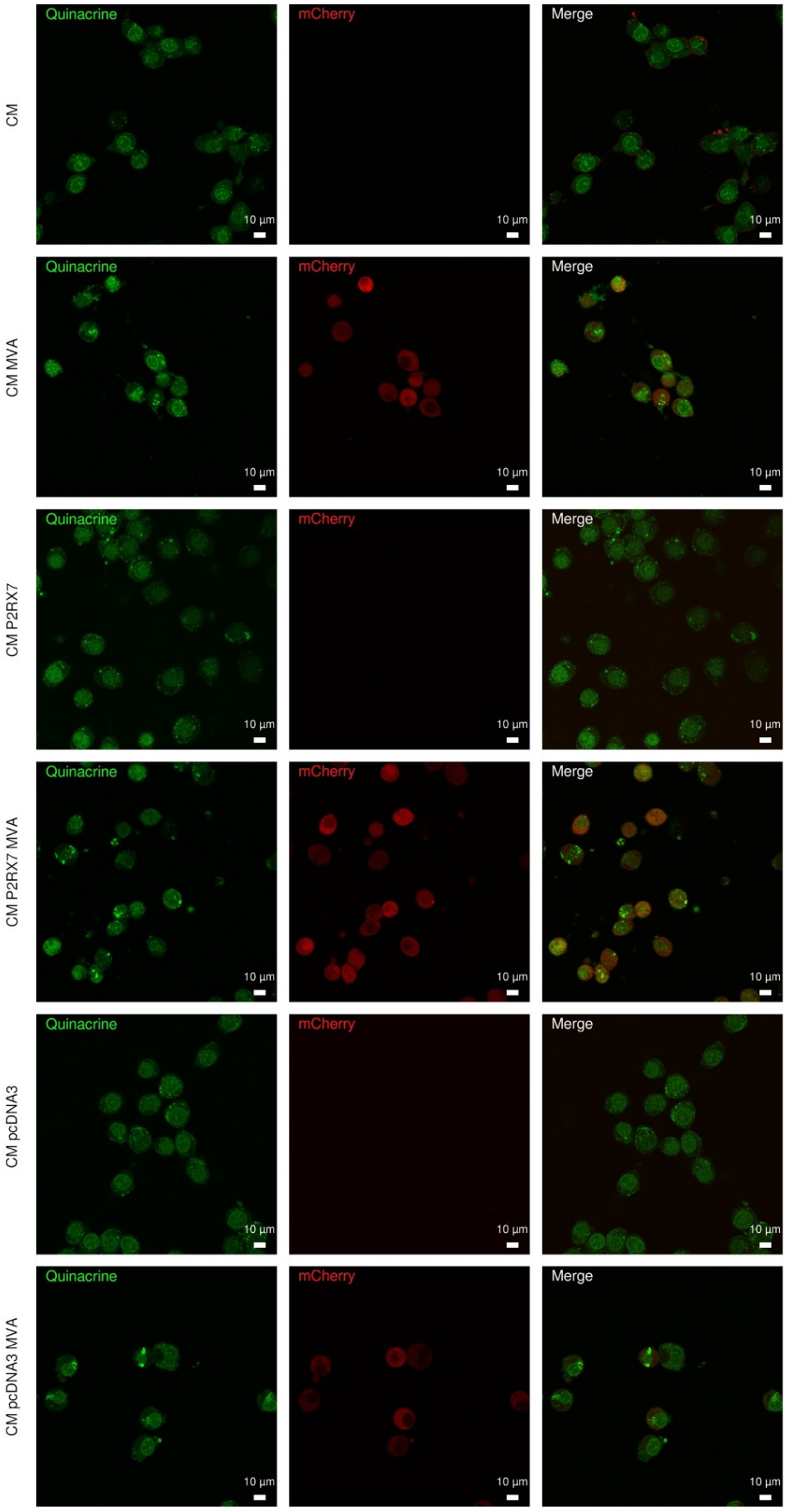
CM
CM MVA
CM P2RX7
CM P2RX7 MVA
CM pcDNA3
CM pcDNA3 MVA
Quinacrine
mCherry
Merge
10 µm

Figure S2: MVA infection of CM cells. CM (WT, pcDNA3- or P2RX7-transfected) were either mock- or MVA-PK1L-mCherry-Ova-infected (MOI1, 20hpi) as indicated. Red fluorescent OVA protein fused to mCherry was synthetized and nucleic acids were stained with 2µM quinacrine (green color). Cells were then visualized at 40x magnification. Images are from one biological experiment. The first row displays images highlighting nucleic acids. The second row images reveal the red fluorescent OVA-mCherry protein. The third row represents merged images, combining the nucleic acid stain with the fluorescent OVA-mCherry protein.

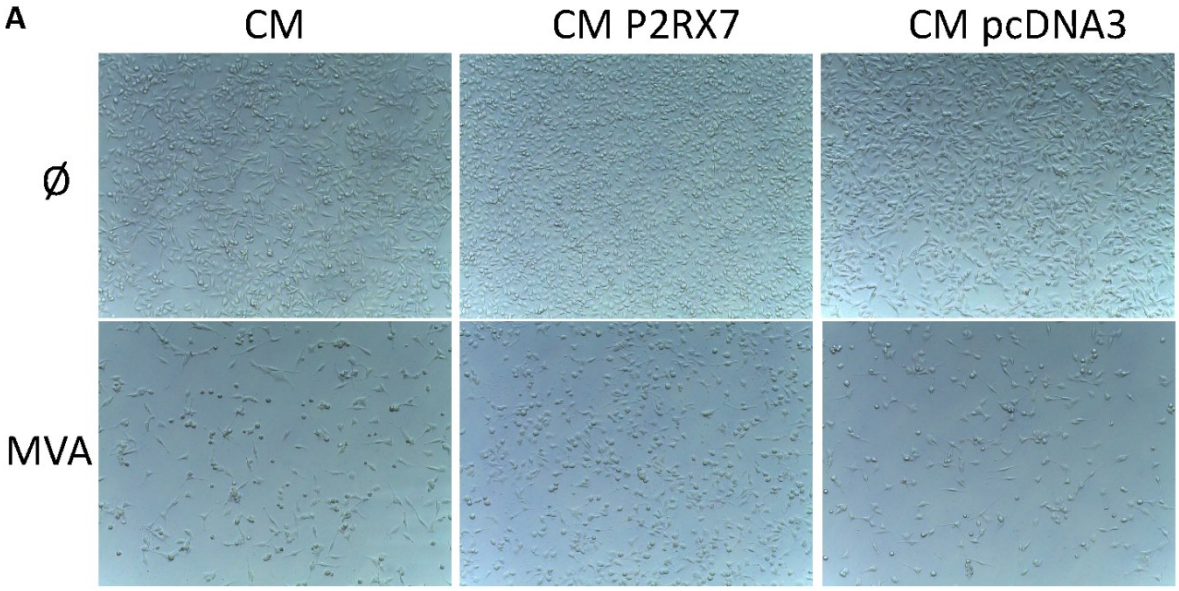

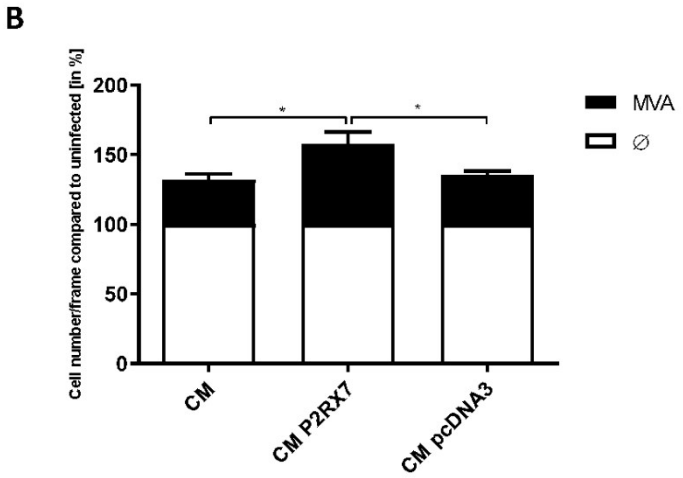

Figure S3: MVA-infected CM P2XR7 cells show less mortality than CM or CM pcDNA3 cells. CM (WT, pcDNA3- or P2RX7-transfected) were either mock-(Ø) or MVA-PK1L-Ova-infected (MOI1, 20hpi). (A) Representative microscopic pictures. (B) Cells of each cell type (WT, pcDNA3- or P2RX7-transfected) were counted within a comparable area and normalized to the respective mock-infected cells. Data are pooled from n=3 independent experiments and shown as means ± SD. P values indicate statistical significance (P) with *P ≤ 0.05.

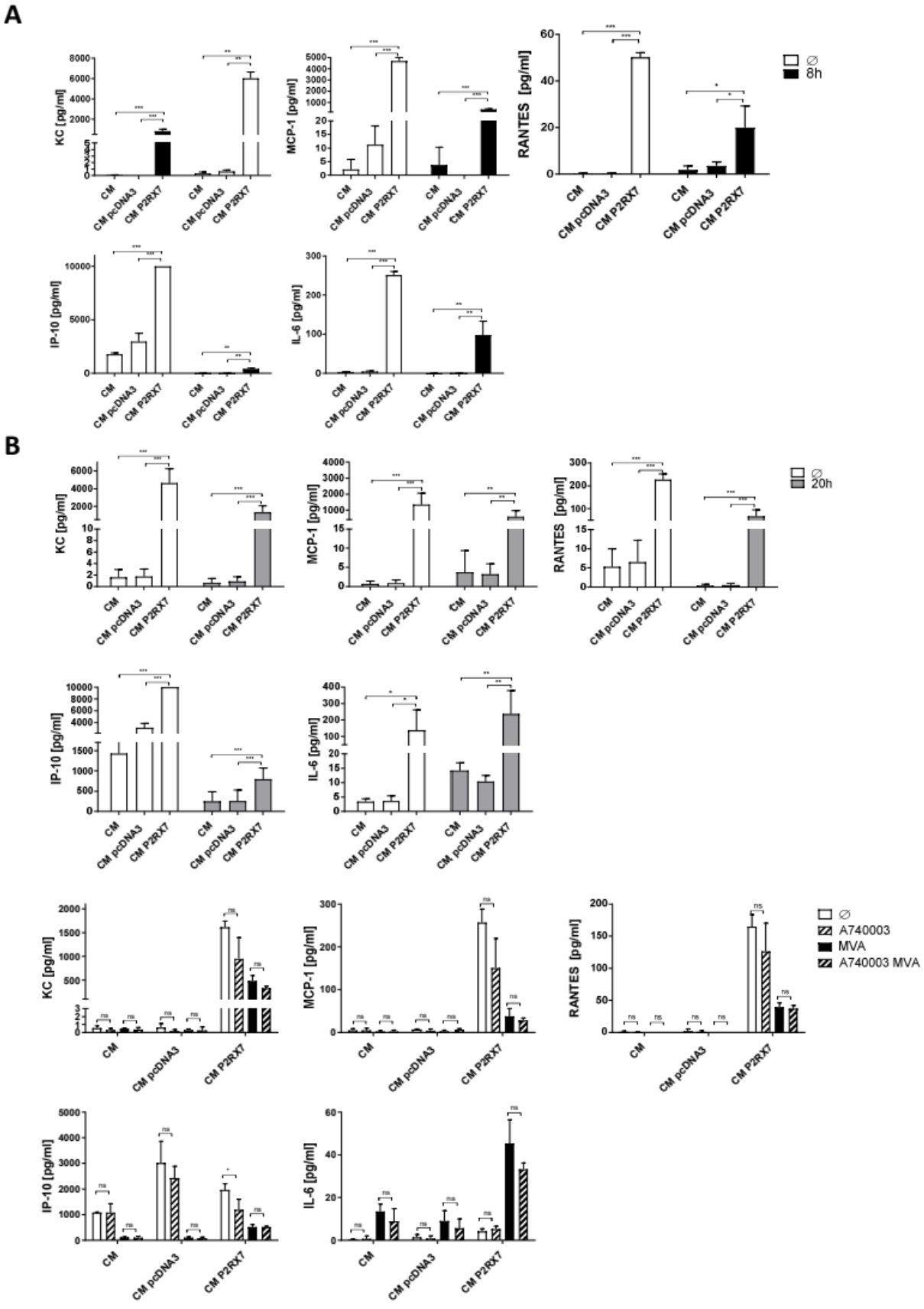
A
KC [pg/ml]
MCP-1 [pg/ml]
RANTES [pg/ml]
IP-10 [pg/ml]
IL-6 [pg/ml]
∅
8h
CM
CM pcDNA3
CM P2RX7
B
20h
C
A740003
MVA
A740003 MVA
ns

Figure S4: Chemokine secretion from CM P2RX7 is significantly altered and is only partially rescued to CM phenotype upon A740003 treatment. CM, empty vector pcDNA3- (CM pcDNA3) or P2RX7-transfected cells (CM P2RX7) were mock (Ø) or MVA-PK1L-Ova-infected (MOI1). The supernatant was used to detect the presence of chemokines using the Legendplex Mouse Anti-Virus Response panel 13-plex after (A) 8hpi or (B) 24hpi. (C) CM, CM pcDNA3 or CM P2RX7 were pre-treated with 20µM A740003 for 1h and then mock or MVA-PK1L-Ova-infected (MOI1 for 20h). The supernatant was used to detect the presence of chemokines using the Legendplex Mouse Anti-Virus Response panel 13-plex. All data shown are pooled from at least n=3 independent experiments and shown as means ± SD. P values indicate statistical significance (P) with **P ≤ 0.01; ***P ≤ 0.001.

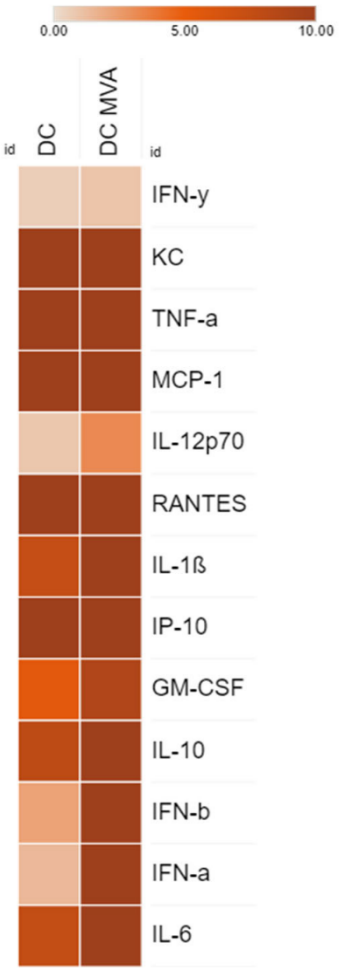

Figure S5: Chemokine secretion from mock- and MVA-infected BMDCs. BMDCs were mock (DC)- or MVA-PK1L-OVA-infected (DC MVA) for 20hpi at MOI1. After infection, the supernatant was harvested and used to determine cytokine levels using the Legendplex Mouse Anti-Virus Response panel 13-plex. The heat map is a representative figure of pooled data from from n=3 independent experiments.

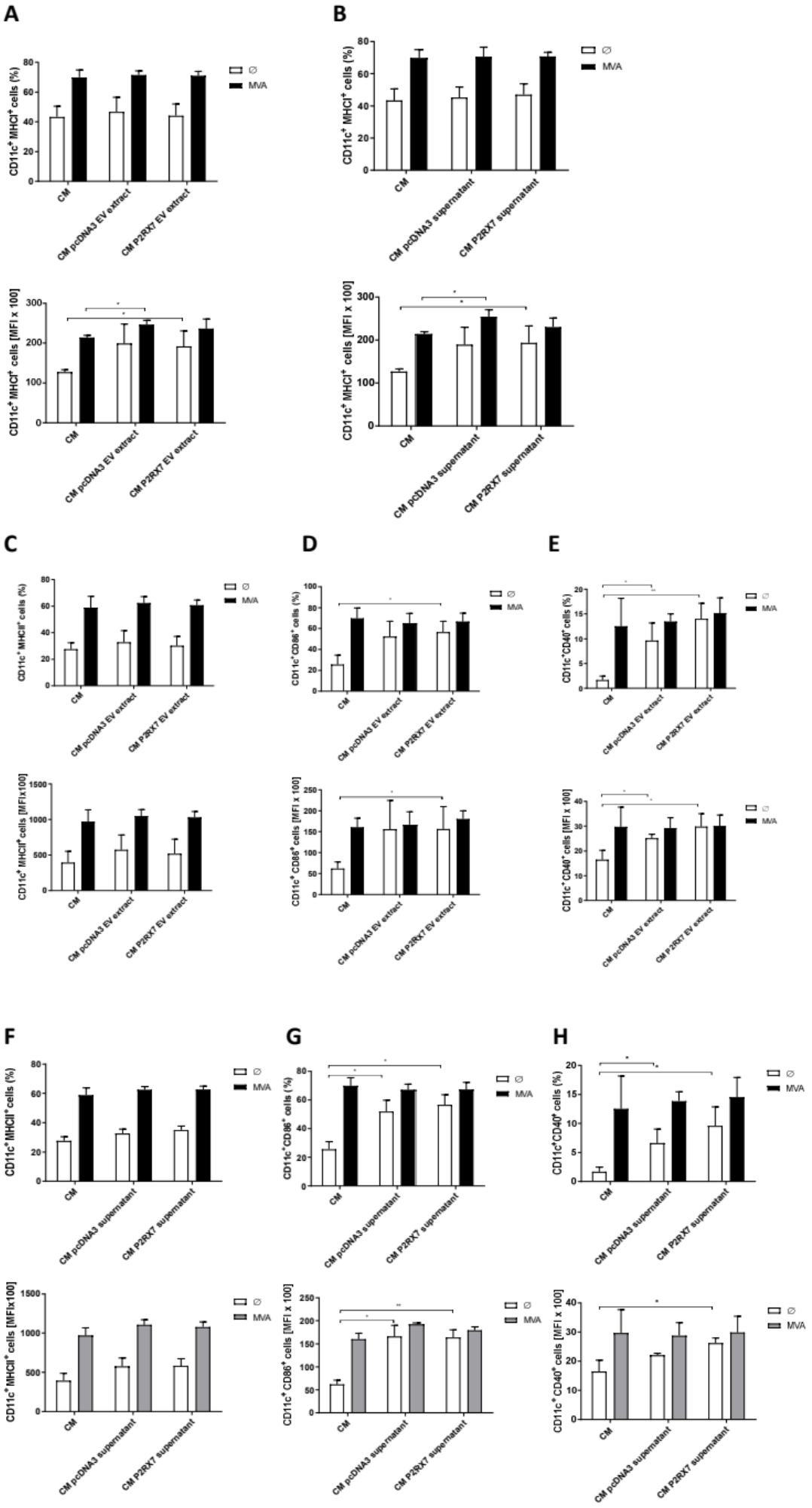
A
B
C
D
E
F
G
H
∅
MVA
CM
CM pcDNA3 EV extract
CM P2RX7 EV extract
CM pcDNA3 supernatant
CM P2RX7 supernatant
CD11c+ MHCI+ cells (%)
CD11c+ MHCI+ cells [MFI x 100]
CD11c+ MHCII+ cells (%)
CD11c+ MHCII+ cells [MFIx100]
CD11c+CD86+ cells (%)
CD11c+ CD86+ cells [MFI x 100]
CD11c+CD40+ cells (%)
CD11c+ CD40+ cells [MFI x 100]

Figure S6: Maturation of BMDCs is not significantly altered when co-cultured with EVs and supernatant-fractions of CM P2RX7 cells. CM pcDNA3 or CM P2RX7-transfected cells were MVA-PK1L-Ova-infected (20hpi). For the extraction of the EV-fraction, cells were infected at MOI1.5. For the isolation of the supernatant fraction cells were infected at MOI1. The isolated EV-fraction or supernatant fraction were PUVA inactivated and added to the co-culture of either mock- (Ø) or MVA-PK1L-OVA-infected (MOI1, 20hpi) CM and BMDCs for 20h. Upper graph depicts the frequency (in %) and the lower graph the MFI of the indicated fractions of (A/B) MHCI on BMDCS (C/F) MHCII (D/G) CD86 on BMDCs(E/H) CD40 on BMDCs. Data are pooled from at least n=3 independent experiments and shown as means ± SD. P values indicate statistical significance (P) with *P ≤ 0.05; **P ≤ 0.01.

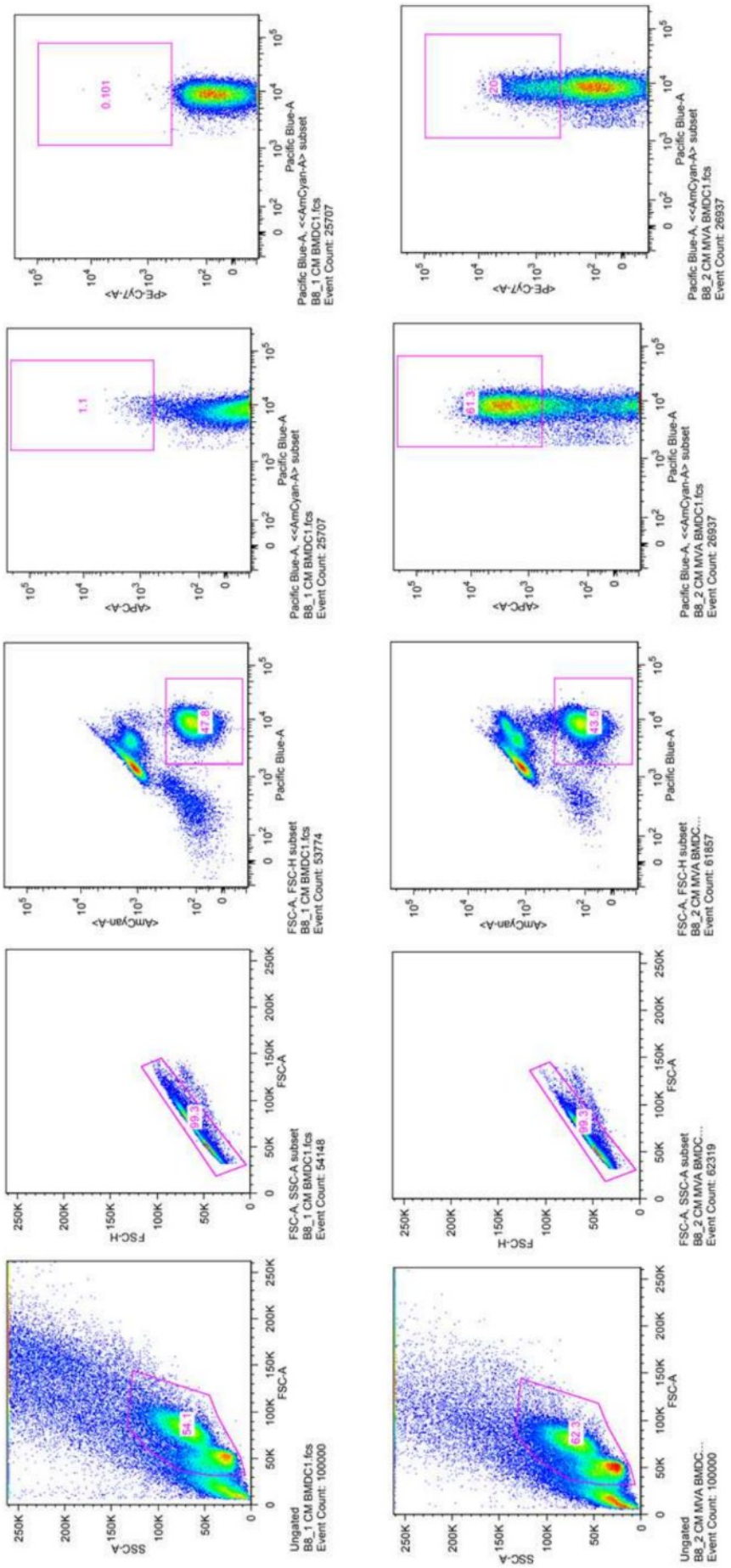

Figure S7: Gating strategy used for the analysis of B8-specific CD8⁺ T cell activation. A cell population reflecting T cells was first selected and then cell duplets were excluded. CD8⁺ (Pacific blue) and AmCyan⁻ (alive) cells were selected. These cells were then either selected for IFNγ⁺ (APC⁺) or TNFα⁺ (PE-Cy7⁺) cells. Images show Mock (left images) or MVA-PK1L-OVA (MOI1, 20hpi) (right images) CM cells were co-cultured with BMDCs for 20h and then with B8 specific CD8⁺ T cells for 4h.

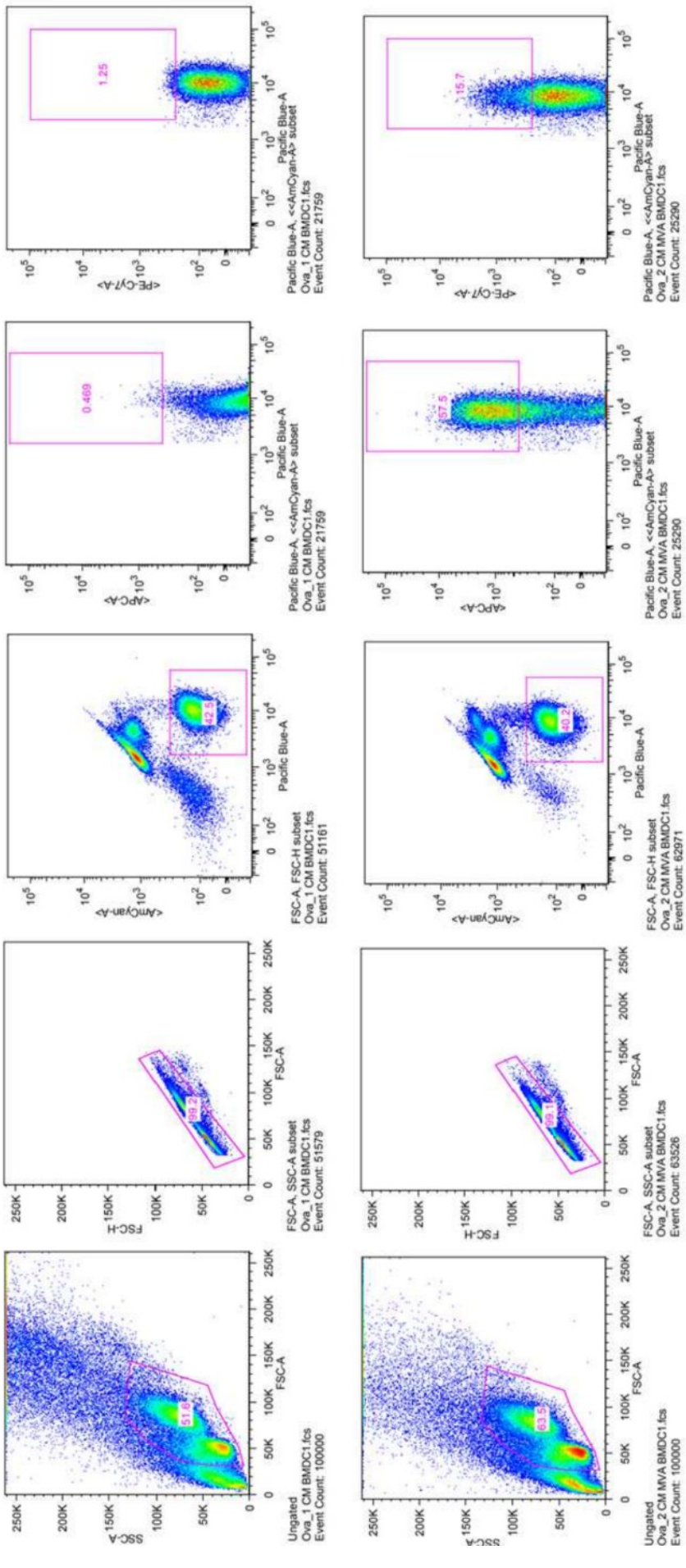

Figure S8: Gating strategy used for the analysis of Ova-specific CD8⁺ T cell activation. A cell population reflecting T cells was first selected and then cell duplets were excluded. CD8⁺ (Pacific blue) and AmCyan⁻ (alive) cells were selected. These cells were then either selected for IFNγ⁺ (APC⁺) or TNFα⁺ (PE-Cy7⁺) cells. Images show Mock (left images) or MVA-PK1L-OVA (MOI1, 20hpi) (right images) CM cells were co-cultured with BMDCs for 20h and then with B8 specific CD8⁺ T cells for 4h.

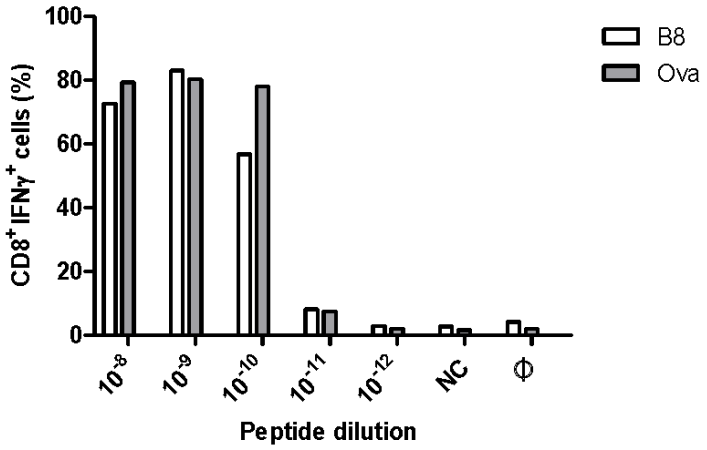

Figure S9: Peptide activation assay after weekly restimulation of CD8⁺ T cells. CD8⁺ T cells were weekly restimulated as described in the Materials and Methods section. After at least two restimulations, DC2.4 cells were loaded with different concentrations of peptides (10^{-8}-10^{-12}) or negative control (NC control cells were incubated with the lowest dilution of the opposite peptide and for the Ø- control cell were incubated with medium). These cells were co-cultured with either B8- or Ova-specific CD8⁺ T cells in the presence of 1.25µg/ml BFA for 4h. Activation of cells was assessed by measurement of IFNγ synthesis after ICS by flow cytometry analysis. This experiment was performed once for quality control after T cells had been thawed.

11. Acknowledgements

I am deeply grateful to my first supervisor, Prof. Ingo Drexler, for giving me the opportunity to pursue my PhD in his lab. Under your guidance and expertise throughout these years, I have learned to push myself beyond my limits and to always strive for excellence.

I would also like to thank my second supervisor Prof. Julia Frunzke for agreeing to take over the overseeing of my project. I appreciated your availability during this time.

Another thanks goes to the RTG1949 for the provided funds. A heartfelt thank you to their coordinator Eva for doing an excellent job managing the program and for always being accessible to us.

Additionally, I would like to express my gratitude to Prof. Elena Adinolfi and her team, Elena and Anna, for the warm welcome in their lab and for providing me with more than just the technical and theoretical knowledge I was seeking during my laboratory rotation.

I would also like to particularly thank the other members of the AG Drexler, Ronny, Sha, Gara, Jana, Annika, Annia and Angelina, for offering their immediate support when required. Furthermore, I would like to thank Cornelia, for her mentoring and for introducing me to this project. A special thanks goes to Giuseppe, who helped me tackle difficult problems with his knowledge of the matter. Another extraordinary recognition goes to Sara, who during and after the PhD has always been there to encourage me, by either staying late nights in the lab with me or by just providing emotional backup whenever needed.

Besides this I consider myself fortunate to have had my siblings and close friends with me all along, motivating and providing me with some time off. Amy, Kevin, Dennis, Fernanda, Arlen, Hannah and Sahar, thank you for always being there.

I am also indebted to my parents, who have always advocated me in my career path and have always believed in me. Grazie Mamma e Papà, finalmente c`è l´ho fatta!

Lastly, I want to express my appreciation to my husband, Vincenzo. I am extremely grateful for your unwavering support and company, especially during those early and late nights of my studies.

“Last but not least, I wanna thank me
I wanna thank me for believing in me
I wanna thank me for doing all this hard work
I wanna thank me for having no days off
I wanna thank me, for never quitting”

Snoop Dogg, 2019

Thank you!

12. Declaration

I hereby declare that I wrote this thesis solely by myself under the guidance of the “Good Scientific practice” prepositions of the Heinrich-Heine-University Düsseldorf. Except when stated otherwise, the work presented is entirely my own and submitted for the degree of Dr.rer.nat.

Düsseldorf, _____

Ylenia Longo